Stanford University Petroleum Research Institute
Stanford, California 94305

TEMPERATURE EFFECTS ON OIL-WATER RELATIVE PERMEABILITIES FOR UNCONSOLIDATED SANDS

SUPRI TR-35

By

Arshad H. Sufi, Henry J. Ramey, Jr. and William E. Brigham

Work Performed for the Department of Energy
Under Contract No. DE-AC03-81SF11564

August 1982

ACKNOWLEDGEMENTS

Financial support during the course of this work was provided by the Department of Energy through the Stanford University Petroleum Research Institute, under Contract No. DE-AC03-81SF11564.

ABSTRACT

This study presents an experimental investigation of temperature effects on relative permeabilities of oil-water systems in unconsolidated sands. In the past, various reasons have been given for observed temperature dependence of relative permeabilities. With increasing use of thermal recovery methods, it becomes important to understand the principles governing these effects. The fluids used in this study were refined mineral oil and distilled water.

A rate sensitivity study was done on residual oil saturation (S_{or}) and oil and water relative permeabilities (k_{ro}, k_{rw}). Results indicate no effect on S_{or} with flooding velocity between 3.947 cm/hr.(flowrate = 20 cc/hr) and 19.735 cm/hr.(flowrate = 78.941 cc/hr). No change in k_{ro} was observed with flowrate while k_{rw} was substantially lower at smaller flow rates, indicating major capillary end effects under these conditions. Above a velocity of 47.365 cm/hr.(flowrate = 240 cc/hr), no rate effect was observed. Conducting rate sensitivity studies at 150 °F, again indicated the curves to be rate-independent above velocities of 47.365 cm/hr. Experiments to determine relative permeability curves were subsequently conducted at 78.941 cm/hr.(flowrate = 400 cc/hr.)

The temperature sensitivity study of relative permeabilities was conducted in three parts. The first was to investigate changes in S_{or} with temperature where the cores were 100% saturated with oil at the

start of the waterflood. Runs were terminated when the water-cut exceeded 99.8%. For these experiments, S_{or} decreased from 0.31 at 70°F to 0.09 at 250°F.

Second, changes in S_{or} with temperature were studied when connate water was present at the start of the waterflood. The same S_{or} values were obtained here as for the case with no initial water. These two sets of runs show that changes in S_{or} with temperature are independent of possible changes in the irreducible water saturation (S_{wi}).

The third part continued the floods for a longer time until the water-cut was virtually 100%. Under these conditions, little change in S_{or} was observed with temperature; (0.11 at 70°F and 0.085 at 186°F). For runs at 70°F, 20% additional oil was produced beyond a water-cut of 99.8%. This is due to the nature of the fractional flow curve which has a long "tail" for large viscosity ratios.

"Practical" S_{or} decreases with temperature due to a change in the shape of the fractional flow curve. This phenomenon can explain many results of previous studies on temperature dependence of relative permeabilities. The actual residual saturations show negligible change with temperature. In cases where floods were conducted to completion, the same relative permeabilities were obtained at different temperatures.

Temperature effects on irreducible water saturations were studied. A small increase in irreducible water saturation was observed upon increasing the temperature. However, the same magnitude of change was observed by changing the flowrate. Upon increasing the oil flowrate, immediate water production was observed from the core indicating a change in the capillary end effect. By comparing the change in

irreducible water saturation with rate and temperature, it was determined that the change was caused mainly by a change in the viscous force across the core.

A study on viscous instabilities was also verformed. This verified the existence of viscous fingers during Waterflooding. It was also observed that tubing volume after the core could cause fingering, resulting in lower apparent breakthrough oil recoveries.

TABLE OF CONTENTS

	Page
ACKNOWLEDGEMENTS	ii
ABSTRACT	iii
TABLE OF CONTENTS	vi
LIST OF FIGURES	x
1. INTRODUCTION	1
2. THEORY	3
3. LITERATURE SURVEY	13
4. EXPERIMENTAL EQUIPMENT AND PROCEDURE	32
4.1 FLUID INTAKE	33
4.2 FLUID FLOW	35
4.3 CORE HOLDER	39
4.4 PRESSURE MONITORING	42
4.5 OIL ANALYSIS	45
4.6 CONFINING PRESSURE	52
4.7 CORE CLEANING	54
4.8 COMPLETE SYSTEM	54

Page

4.9 PROCEDURE AND EXPERIMENTS 56

5 ANALYSIS OF DATA 60

6 RESULTS AND DISCUSSION 63

6.1 RATE EFFECT ON BUCKLEY–LEVERETT FRONT 63

6.2 VISCOUS INSTABILITIES 73

6.3 TEMPERATURE EFFECTS ON RESIDUAL OIL SATURATION 80

6.4 TEMPERATURE EFFECTS ON IRREDUCIBLE WATER SATURATION 85

6.5 TEMPERATURE EFFECTS ON RELATIVE PERMEABILITY CURVES 93

6.6 INTERDEPENDENCE OF END–POINT SATURATIONS 95

7. CONCLUSIONS 98

8. RECOMMENDATIONS FOR FURTHER WORK 101

9. NOMENCLATURE 104

10. REFERENCES 107

11. APPENDICES 112

APPENDIX A-1. DERIVATION AND APPLICATION OF THE JONES-ROSZELLE GRAPHICAL TECHNIQUE TO CALCULATE RELATIVE PERMEABILITIES BY THE DYNAMIC DISPLACEMENT METHOD 113

APPENDIX A–2 LISTING OF COMPUTER PROGRAM TO CALCULATE 127

Page

	RELATIVE PERMEABILITY CURVES BY THE JONES-ROSZELLE GRAPHICAL TECHNIQUE	
APPENDIX B-1	PLOTS OF OIL AND WATER RELATIVE PERMEABILITY CURVES	135
APPENDIX B-2	PLOTS OF OIL AND WATER PERMEABILITY RATIO CURVES	147
APPENDIX B-3	TABLES OF RELATIVE PERMEABILITIES AND PERMEABILITY RATIOS	160
APPENDIX B-4	TABLES AND PLOTS OF RECOVERY DATA FROM THE EXPERIMENTS	172
APPENDIX B-5	TABLES AND PLOTS OF RELATIVE INJECTIVITY DATA FROM THE EXPERIMENTS	197
APPENDIX B-6	TABLES AND PLOTS OF FRACTIONAL FLOW DATA	220
APPENDIX B-7	TABLES OF DATA FROM EXPERIMENTS STUDYING CHANGES IN IRREDUCIBLE WATER SATURATIONS	245
APPENDIX B-8	TABLES OF DATA FROM EXPERIMENTS STUDYING VISCOUS FINGERING	249
APPENDIX B-9	TABLES OF DATA FROM EXPERIMENTS STUDYING RESIDUAL OIL SATURATION	252
APPENDIX C-1	DETAILED SCHEMATIC DIAGRAM OF THE EXPERIMENTAL EQUIPMENT	255
APPENDIX C-2	SCHEMATIC DIAGRAMS OF COMPONENTS OF THE CORE HOLDER	258

		Pane
APPENDIX C-3	SCHEMATIC DIAGRAM OF THE PHOTO-CELL ASSEMBLY	263
APPENDIX C-4	WIRING DIAGRAM OF THE ELECTRONIC GATE	265
APPENDIX C-5	SCHEMATIC DIAGRAM OF CAPACITANCE PROBE	268

LIST OF FIGURES

		Page
Fig. 2.1	Forces Acting at Interfaces of Immiscible Fluids on Solid Surface	6
Fig. 2.2	Water Entrapment During Capillary Drainage	8
Fin. 2.3	Drainage and Imbibition Capillary Pressure Curves	9
Fin. 2.4	Pore Size Distribution Curve Showing Relative Locations of the End Point Saturations	11
Fig. 4.1	Schematic of Fluid Intake System	34
Fig. 4.2	Schematic of Oil and Water Flow Lines	36
Fig. 4.3	Working Mechanism of Four-Way Switching Valve	38
Fig. 4.4	Schematic of Core Holder	40
Fig. 4.5	Pressure Monitoring Equipment	43
Fin. 4.6	Photoelectric Oil Counter	46
Fig. 4.7	Calibration of Oil Production Photocell	48
Fig. 4.8	Fluid Metering and Collection Apparatus	49
Fig. 4.9	Modified Fluid Collection and Metering Apparatus	51
Fig. 4.10	Confining Pressure Apparatus	53
Fig. 4.11	Simplified Schematic of Complete System	55
Fig. 6.1	Residual Oil Saturation Vs Flowrate (Temp = 70°F)	65
Fig. 6.2	Computed Oil and Water Relative Permeabilities Vs Water Saturation for Several Flooding Rates (Temperature = 70°F)	66
Fig. 6.3	Effect of Waterflooding Rate on the Shape of the Bucklev-Leverett Front	67
Fig. 6.4	Saturation and Pressure Distribution in a Core with Capillary End Effects During Waterflooding	69
Fig. 6.5	Residual Oil Saturation Vs Flowrate (Temp = 150°F)	70

		Page
Fig. 6.6	Computed Oil and Water Relative Permeabilities Vs Water Saturation for Several Flooding Rates (Temperature = 150°F)	71
Fig. 6.7	Breakthrough Oil Recovery Vs Flowrate for Oil Saturated Cores (Temperature = 70°F)	74
Fie;. 6.8	Breakthrough Oil Recovery Vs Flowrate for Different Exit Flow Line Volumes (T = 70°F)	75
Fig. 6.9	Breakthrough Oil Recovery Vs Exit Tubing Volume for a Flowrate of 60 cc/hr (Temperature = 70°F)	77
Fig. 6.10	Displaced Phase Recovery Vs Viscosity Ratio (Mungan, September 1966)	79
Fig. 6.11	Residual Oil Saturation Vs Temperature for Waterfloods Terminated at 99^+ % Water Cut	81
Fig. 6.12	Residual Oil Saturation Vs Temperature for Waterfloods Carried to Completion	82
Fig. 6.13	Water Fractional Flow Vs Water Saturation for Waterfloods at Several Temperatures	84
Fig. 6.14	Apparent Irreducible Water Saturation Vs Temperature	87
Fig. 6.15	Irreducible Water Saturation Vs Oil Flowrate at Room Temperature	88
Fig. 6.16	Saturation Profile at the Completion of an Oil Flood for "bo Different Flooding Rates, Showing the Effect on the Capillary End Effect	89
Fig. 6.17	Trapped Water in a Water-Wet Porous Medium	90
Fig. 6.18	Irreducible Water Saturation Vs Viscous Force	92
Fig. 6.19	Oil and Water Relative Permeabilities Vs Water Saturation at "bo Different Temperatures (S_{wi}=0)	94
Fig. 6.20	Oil and Water Relative Permeability Curves Vs Water Saturation for "bo Different Initial Water Saturations (T = 70°F)	96

1. INTRODUCTION

The aim of this study is to identify and explain temperature effects on oil-water relative permeabilities in unconsolidated sands. Temperature effects have been studied extensively in the past. As a result, various explanations have been provided that are often contradictory. Hence, the objectives of this study are to answer the following questions:

A. Is there a temperature effect on oil-water relative permeabilities in unconsolidated sands?
B. Is the temperature effect confined near the end point saturations or does it effect the entire flow region?
C. If there is a temperature effect, what causes it?

To answer these questions, an understanding of multiphase flow through porous media is necessary. These concepts are reviewed in Section 2. The reasons for undertaking this study concern enhanced oil recovery.

Enhanced oil recovery processes have become increasingly popular in recent years. One of the major oil recovery methods is thermal recovery. In steam injection, oil is heated and mobilized by injected steam. Some steam condenses, resulting in simultaneous flow of steam,

hot water and heated oil. In combustion oil recovery, the same phenomenon occurs due to vaporization of water and formation of water during the combustion process. In modeling thermal recovery processes, knowledge of the fundamentals of multiphase flow is essential. Relative permeability curves are important in describing multiphase flow through porous media. Hence, an understanding of temperature effects on relative permeability curves will yield insight into changes in flow characteristics during steam flooding or in-situ combustion. This will allow better planning of thermal projects and a means to compute performance once a field is under thermal drive.

2. THEORY

Single phase flow through porous media is a complex process. On a microscopic scale, reservoir rocks consist of a multitude of differently sized, arbitrarily connected flow channels. Although porosity represents the pore volume, rock permeability is primarily controlled by pore throat openings. The equation that expresses single phase fluid flow through a porous medium is Darcy's law:

$$q = -\frac{k\,A\,dP}{\mu\,dx} \tag{2.1}$$

In this equation, q is the volumetric flowrate of the fluid, A the cross-sectional area, μ the fluid viscosity, and dp/dx the pressure gradient. The term k, which is the constant of proportionality, is the absolute permeability of the porous medium. This term describes the conglomeration of tortuous microscopic paths through which the fluid must flow.

Darcy's law can be extended to multiphase flow with the absolute permeability replaced by the effective permeability to a particular fluid:

$$q_i = -\frac{k_i\,A\,dP_i}{\mu_i\,dx} \tag{2.2}$$

where q_i is the volumetric flowrate of fluid i, μ_i its viscosity and dp_i/dx the pressure gradient in that fluid. The term k_i is the effective permeability to fluid i and is related to the absolute permeability by:

$$k_i = k \; k_{ri} \tag{2.3}$$

where k_{ri} is the relative permeability to fluid i and decreases from one to zero as the fluid saturation decreases. This is due to the lower cross-sectional area available for flow as saturation decreases and to the development of more tortuous flow paths. Relative permeability is, however, a non-linear function of fluid saturation for immiscible flow through a porous medium. This non-linearity arises from competing forces within the porous media. Hence, in order to comprehend relative permeability behavior, it is necessary to understand these forces.

The forces of primary interest are viscous and capillary forces. Depending on the density difference between fluids, gravitational forces can be significant in certain reservoirs. Most experiments to determine relative permeabilities, however, are scaled to minimize gravity forces. Thus, this section concentrates on the other two forces which can dominate in experimental work on multiphase flow through a porous medium.

Viscous Forces: For a fluid flowing through a circular tube, the flow equation for laminar flow is given by Poiseuille's law:

$$q = \frac{\pi \quad r^4 \Delta p}{8 \quad \mu \quad L} \tag{2.4}$$

where q is the volumetric flowrate, r the radius of the flow channel, μ the fluid viscosity, L the length of the flow channel, and dp the pressure drop across the channel. Although pores are not circular tubes, a comparison can be made to conclude that flow of a fluid through a pore channel will result in a pressure gradient across it. As will be shown later, the magnitude of the pressure gradient can alter the direction of flow of a particular fluid within the pores.

Capillary force: This is a force that exists due to the presence of immiscible fluid interfaces and solid surfaces. Since it occurs due to interaction between different surfaces, it is perhaps helpful to first consider surface interactions.

When two immiscible fluids are in contact with each other, the interface has a finite energy associated with it. This is due to the presence of molecules having different chemical properties on either side of the interface. A similar interfacial energy exists for fluids contacting solids. The force per unit length on the interface is defined as the interfacial tension between the two fluids or the fluid and the solid. It is expressed in dynes/cm or mN/m. These interfacial tensions are responsible for the formation of drops of fluids on solid surfaces. Such a situation is shown in Fig. 2.1. Here, a drop of water, fluid A, is present on a solid surface and surrounded by oil, fluid B. For the drop to be stable, the sum of the horizontal forces must equal zero. This yields:

$$\sigma_{BA} \cos\theta = \sigma_{BS} - \sigma_{AS} \tag{2.5}$$

where σ is the interfacial tension between the various surfaces, and s denotes the solid surface. The angle θ in the above equation is defined as the contact angle of the system and, by convention, is always measured through the denser phase. For an oil-water-solid system, if θ is much less then 90°, the surface is considered water-wet, and oil-wet if θ is much greater then 90°. Neutral wettability exists in between.

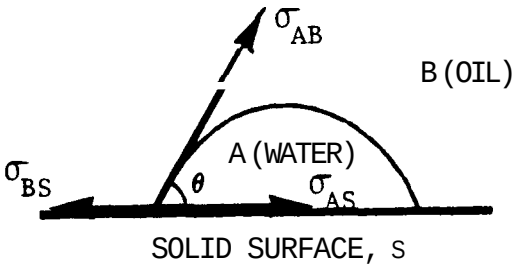

Fig. 2.1 FORCES ACTING AT INTERFACES OF IMMISCIBLE, FLUIDS ON SOLID SURFACE

When immiscible fluids contact each other in the presence of solid surfaces, a pressure difference develops between the fluids. This pressure difference is capillary pressure and is defined as:

$$p_c = p_{nw} - p_w \tag{2.6}$$

where p_{nw} is the pressure in the non-wetting phase, and p_w the pressure in the wetting phase.

In natural porous media, immiscible fluids contact each other on irregularly curved grain surfaces. The resulting expression for the

capillary pressure in spherically packed beads was given by Plateau (1863–1866):

$$p_c = \sigma \left(\frac{1}{R_1} + \frac{1}{R_2} \right) \tag{2.7}$$

where σ is the interfacial tension between the fluid pair involved and R_1 and R_2 are the principal radii of curvature of the interface. These radii are difficult to measure. Hence, a mean radius, as defined by:

$$\frac{1}{R_m} = \frac{1}{R_1} + \frac{1}{R_2} = \frac{2 \cos\theta}{r_t} \tag{2.8}$$

is used in the capillary pressure equation. This results in the final form of the capillary pressure equation, which is:

$$p_c = \frac{2 \sigma \cos\theta}{r_t} \tag{2.9}$$

From this equation, it is clear that interfacial tension, wettability, pore size and capillary pressure are interrelated. However, one can treat capillary pressure as the final result of the combination of the other parameters. Now consider the effect of capillary pressure on the movement of fluids through a porous medium.

Consider a water–wet core, initially saturated with water as shown in Fig. 2.2a. It is surrounded by oil which, in this case, is the non–wetting phase. The oil is indicated by the dotted area on the right of each diagram. The water is the open space. If the pressure in both phases equals p_0, no oil will enter the core. The water saturation in the core, S_w, then equals 1. This is shown by point A on Fig. 2.3,

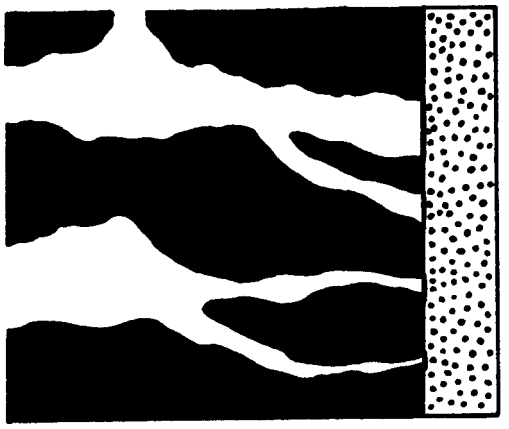

Fig. 2.2a

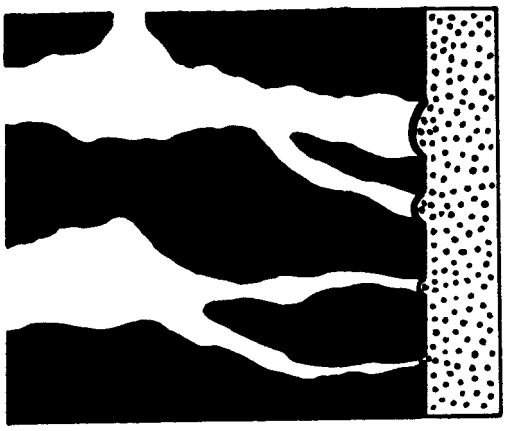

Fig. 2.2b

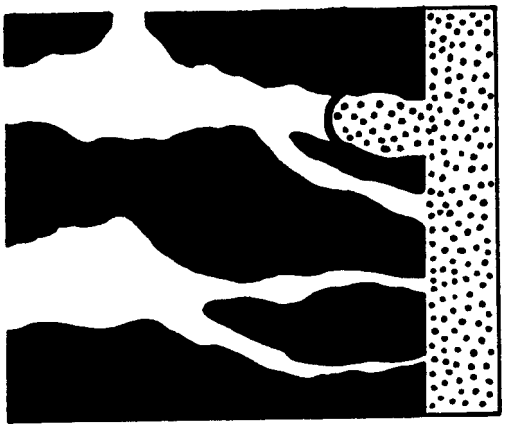

Fig. 2.2c

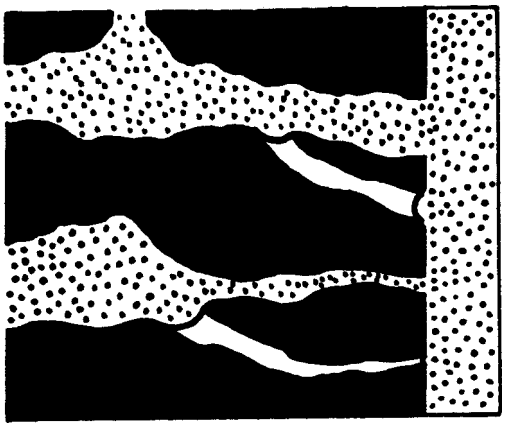

Fig. 2.2d

OIL

WATER

Fig. **2.2** WATER ENTRAPMENT DURING CAPILLARY DRAINAGE

which is a capillary pressure curve for this system. Suppose the pressure in the oil phase is increased to p_1. This will cause the interfaces on all inlet pores to bend inward as shown in Fig 2.2b. Due to the indentation, the water saturation within the core drops slightly below me. At that point, the capillary pressure equals $p_1 - p_0$. This condition is represented by point B on Fig. 2.3. Upon increasing the pressure in the oil phase further, a level will occur when the oil will move into the largest opening (least capillary pressure). This will drop the saturation within the core significantly. The condition at this point is depicted by Fig. 2.2c, and corresponds to point C on Fig.2.3. Extrapolating the curve back to $S_w=1$ (point F) corresponds to the pore entry pressure for the system. Further increase in the oil pressure will result in the invasion of smaller pores as shown in Fig. 2.2d. Notice however, that now the pore adjacent to the large one initially invaded has oil at both entrances. This results in trapping of water in this pore. On the capillary pressure curve, Fig. 2.3, the situation is represented by point D. Eventually, after all the pores that can be invaded contain oil, further increases in the oil pressure will cause no change

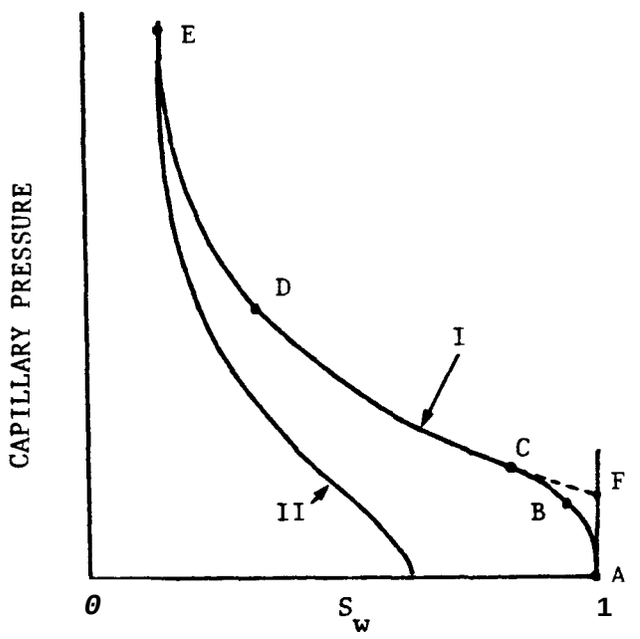

Fig. 2.3 DRAINAGE AND IMBIBITION CAPILLARY PRESSURE CURVES

in the saturation (beyond a compression of the trapped water). The capillary pressure curve then rises rapidly as shown by point E in Fig. 2.3. The entire process has now defined a drainage capillary pressure curve. The water saturation at point E is comprised entirely of water trapped in pores due to capillary forces on all pore entrances. This water saturation is known as the irreducible water saturation, S_{wi}.

If the pressure in the oil phase is now reduced, water will flow back by capillary suction or imbibition. The capillary pressure curve defined by this process however, will be lower then the first one due to a hysteresis effect. This is shown by curve II in Fig. 2.3. A point will be reached at which further reduction in the oil pressure will cause no more water to enter the core. The oil saturation at this point is known as the residual oil saturation, S_{or}, and the curve defined by the process is known as the imbibition capillary pressure curve.

An interesting point is that the smallest pores need not necessarily contain the residual wetting phase saturation. This is apparent from Fig. 2.2d, where water is trapped in the pore adjacent to the large pore while a smaller pore has had water displaced from it. The general tendency will be, however, to have the residual wetting phase saturation in the smaller pores. Following this logic, consider Fig. 2.4. This shows a normal pore size distribution for a particular core. Curve I represents the number of pores that will contain the wetting fluid at conditions of residual wetting fluid saturation. Conversely, curve II represents the number of pores that will contain the non-wetting fluid at conditions of residual non-wetting fluid saturation. Some overlap of curves I and II is possible, suggesting interdependence of the end point saturations.

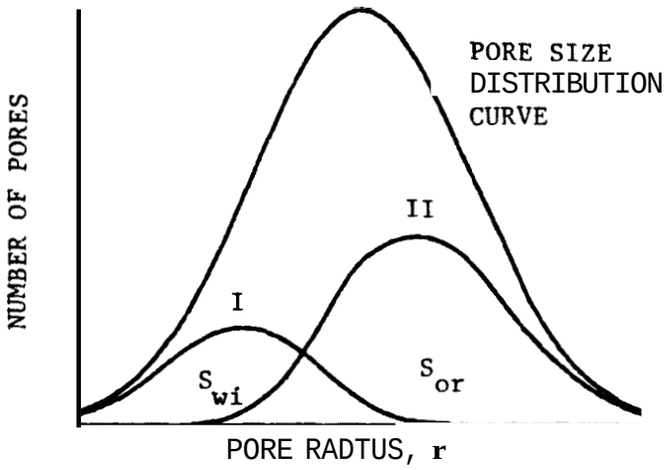

Fig. 2.4 PORE SIZE DISTRIBUTION CURVE SHOWING RELATIVE LOCATIONS OF THE END POINT SATURATIONS

In the displacement procedure considered so far, only capillary forces were considered. Consider the core as described by point E in Fig. 23. The trapped water is due to an equilibrium of capillary forces at all the entrances to the pores containing the water. Upon flowing the oil, however, an extra pressure drop due to viscous forces is imposed across each segment of the trapped water. Depending on the magnitude of this viscous force, some of the trapped water may be mobilized. Hence, end point saturations as obtained from displacement rum may differ somewhat from those obtained from capillary pressure measurements.

Now, with the understanding of forces governing multiphase flow through porous media, the effects of temperature on the flow behavior can be analyzed. Increasing temperature causes a reduction in liquid viscosities, thereby changing the viscous forces in the core. Further, interfacial tension and wettabilftp are usually functions of temperature. At the same time, thermal grain expansion may cause slight changes in pore geometries. All these effects can combine to alter capillary pressures within pores if the temperature is altered. So, an analysis of the data from this study must be made in light of the

interaction between viscous and capillary forces.

There are two standard techniques for measuring relative permeabilities. One is known as steady-state, and the other as dynamic displacement. The former consists of injecting both fluids into a core at a fixed ratio and rate and measuring pressure drop and saturation when both have stabilized. Dynamic displacement, as the name implies, consists of displacing one fluid by another and measuring produced fluid ratios and pressure drops as they change. The former technique can require a long time to reach equilibrium, while the displacement method can often yield relative permeabilities quickly. Hence, the unsteady state dynamic displacement method has been used in this study.

Before discussing the various effects of temperature on relative permeability curves, it might be appropriate to consider the past work in this area. The body of literature present is large and an effort has been made to limit the discussion to works that shed light on multiphase flow of fluids through porous media.

3. LITERATURE SURVEY

Relative permeability is a measure of the ability of a porous medium to conduct fluid when more then one fluid is present. Relative permeability curves are used in flow calculations to match reservoir production and pressure response. The curves may be dependent on fluid saturation, fluid distribution within the pores, capillary pressure, saturation history, wettability, viscosity, pore geometry and pore size distribution, interfacial tension, temperature, pressure and flow-rate. There are a number of agreements and contradictions present in the literature on the subject of relative permeability. It is the purpose of this study to identify which parameters play a significant role in multiphase flow through porous media with a special emphasis on temperature effects.

Temperature effects on relative permeability have generated considerable interest and speculation in recent years. This interest is due to the increasing importance of thermal recovery processes. Most of the studies that have been made on this subject agree on the physical effect of temperature on relative permeabilities. Agreement, however, is not found on the reasons for these changes. To understand the changes that may cause temperature effects, it is necessary to review the various parameters that have been studied to date.

One of the first experiments on immiscible fluid displacements was

conduct by Hassler et al. *(1936).* Using sandstone cores, they studied the effect of oil viscosity on recovery characteristics for air displacing oil. By analogy with a tubular capillary model, they explained empirical expressions for the decrease of oil saturation with displacing time. They did not report residual oil saturations associated with their displacements. Botset *(1940)* conducted experiments on water-gas relative permeabilities and observed residual water saturations for gas displacing water. He found this saturation to be about *15 %* of pore space for unconsolidated sands, and about *25* % for consolidated ones.

Leverett and Lewis *(1940)* conducted three-phase experiments to attempt to understand flow mechanisms in porous media. Their conclusions were that water surrounds sand grains (presuming water is the wetting phase) at all times, while oil exists as a continous web or network around and between the water covered sand grains. As water saturation increases, water appears first as rings around the point of contact of the sand grains. These rings then coalesce upon further increase in water saturation. The authors also speculated that gas tends to occupy the central portions of intergrain spaces.

Leverett *(1940)* studied capillary behavior in porous solids. His study was from a thermodynamic viewpoint considering the sand grains as spheres with the water and oil having a curved interface. He also introduced the concept of the "boundary effect" in flow experiments due to capillary forces. He pointed out that upon leaving the core, the wetting phase has a tendency to be held back due to a discontinuity in the capillary forces. This causes a buildup in the wetting phase saturation and a subsequent decrease in the non-wetting phase

permeability near the outlet. The entire process results in an additional pressure drop that would not be present in a reservoir where this effect should be negligibly small.

Perhaps the most fundamental work in the area of oil displacement was by Buckley and Leverett **(1941)**. They introduced the concept of fractional flow. Their equation could be used to compute the performance of linear displacements given relative permeabilities and viscosity ratios. The mathematical derivation resulted in a triple value of water saturation at some planes in the invaded region for a waterflood initially at irreducible water saturation. The physical interpretation of the triple saturation was the formation of a shock front, the position of which was determined by a material balance. The authors discussed the effect of viscosity, initial fluid saturation, and capillary and gravitational effects on this type of displacement.

Cardwell **(1959)** investigated the meaning of the triple value in the Buckley-Leverett theory and concluded that it occurred because the equations in the theory lost their mathematical significance before the triple point was reached. Using a simulator, Fayers and Sheldon **(1959)** verified that the Buckley-Leverett triple value does not occur if the capillary term is included in the analysis. They also observed that gravity and capillary pressures affect the Buckley-Leverett profile at low flow rates only. This leads to the concept of scaling which will be considered subsequently.

Welge **(1952)** initially presented a method for calculating relative permeability ratio curves using the Buckley-Leverett frontal advance theory. He illustrated the method by solving a gas-drive problem using production data. He showed that the method was equally applicable in

cases of waterfloods. His work was extended by Johnson, Bossler and Naumann (1958) to calculate individual relative permeabilities as a function of displacing phase saturations. Their calculation technique required oil production data as well as changes in relative injectivity with water injected. This method was reused in a novel manner by Jones and Roszelle (1978) to solve for relative permeabilities using a graphical technique. This technique is easier and more straightforward to use than the origional Johnson, Bossler and Naumann method. It has thus been used in this study for the calculation of relative permeabilities from waterflooding experiments. A detailed description of the Jones and Roszelle technique is presented in Appendix A.1.

Scaling was first studied for linear waterfloods by Rapoport and Leas (1953). Working with oil wet cores, they were able to show that the flood "stabilized" above a certain scaling parameter. Their scaling parameter, derived mathematically, was $Lv\mu_w$. When oil breakthrough recovery was graphed versus this parameter, the recovery increased with increasing $Lv\mu_w$ until the latter reached a value of approximately 2 (cm^2 cp/min). Increasing $Lv\mu_w$ beyond two showed no further change in breakthrough recovery. They maintained that the stabilized point was unique to the core and should be determined experimentally to establish a minimum rate above which the flood had to be conducted.

Jones-Parra and Calhoun (1953) reused the data of Rapoport and Leas and presented another approach to stability criterion. However, their theoretical calculations did not match the experimental data very well. They claimed the reason for the deviation was that they had used steady-state relative permeabilities and static capillary data to represent a dynamic displacement process. Their approach provides an

estimate of the breakover $Lv\mu_w$ from a capillary pressure curve alone. This can be useful in designing a flooding experiment.

Kyte and Rapoport (1958) conducted experiments to study waterflooding and end effects in a water-wet porous medium. They observed that the stability behavior for a water-wet core was similar to an oil-wet core. The difficulty was to observe the stable point experimentally. When water reaches the outlet end, it is held back by capillarity in a water-wet core. This results in an apparent increased breakthrough recovery. They used phenolphthalein dried on the outlet face of the core to indicate the moment of water arrival at that face. This was accomplished by injecting a small amount of ammonia along with the water. When the ammonia solution contacted the phenolphthalein, it produced a sharp coloration that was observed through a lucite end plate. In this manner, they observed that the water arrival efficiency of water-wet cores increased for increasing $Lv\mu_w$ up to a certain point, beyond which it remained constant. This matched the behavior of the breakthrough recovery for oil wet cores where water arrival and water breakthrough occur simultaneously. However, water breakthrough recovery for water-wet cores was almost constant over all values of the scaling coefficient. It thus becomes difficult to determine the breakover value of the scaling coefficient in normal waterfloods conducted on water-wet cores. One method is to use the breakover point observed by Kyte and Rapoport in their water arrival curve. This gives a value of $LV\mu_w$ of 1.0 (cm^2 cp/min) for water-wet cores. Care should be taken, however, in using this value for cores having different wettabilities.

Douglas and Wagner (1958) and Hovanessian and Payers (1961) were among others who performed simulation studies of the Buckley-Leverett

frontal advance theory including capillary and gravity effects. Their observations indicated that at low rates, the front was smeared. Once the rate was increased beyond a certain point, the front stabilized into the form predicted by Buckley-Leverett theory. Their results match well with the stability criteria of Rapoport and Leas (1953). The simulation studies also showed water saturation increasing sharply near the outlet end of the core. This is the "end effect" first noted by Leverett (1940).

The core saturation profiles obtained from numerical models were experimentally verified by Bentsen and Saeedi (1981) using a technique based on microwave attenuation. Their results also showed the dependence of stabilized flow on the viscosity ratio. Profiles for displacements at favorable viscosity ratios gave stable fronts at much lower flowrates than those displacements at unfavorable viscosity ratios. For high flowrates and unfavorable viscosity ratios, they again observed non Buckley-Leverett saturation profiles. They attributed this to viscous fingering, which is a phenomenon that can occur during displacement of a more viscous fluid by a less viscous one.

Viscous fingering was first studied by van Meurs (1957). Using finely powdered glass as a porous medium, he observed viscous fingers when the oil-water viscosity ratio was 80, while a sharp front formed for a unit viscosity ratio. In a discussion of this paper, Perkins (1957) pointed out that glass beads might not represent a wettability condition of any practical interest. Later, van Meurs and van der Poel (1958) presented a theoretical description of viscous fingering. They compared their equations with experimental data and were able to obtain good agreement. Their results show that for viscosity ratios above 100,

the water cut increases rapidly after breakthrough. Even though ultimate recovery is the same, it would require substantially larger throughputs to attain this recovery for more viscous oils. This could affect laboratory experiments which are generally terminated after the water cut attains some predetermined high value.

Chuoke et al. **(1959)** studied instabilities using two kinds of models. In the first, oil was displaced by water-glycerine solutions in the space between parallel glass plates. The second model consisted of the same plates except that crushed glass was used to pack the space between the plates. For the first system, the instabilities had clearly defined and smooth shapes, while irregularities in the fingers were observed when the crushed glass was present. For either case, a necessary condition for instability was that the mobility of the displacing fluid be higher then that of the displaced fluid. Further, for a higher viscosity oil being displaced, the fingers seemed to be smaller. These smaller fingers were also observed when the interfacial tension was lowered. This matched well with the theory they presented. However, the study indicated that it would be difficult to scale laboratory experiments properly in cases of fingering. In such cases, laboratory experiments would generally exhibit higher recoveries than the prototypes.

In direct contrast to this, Rachford ***(1964)*** concluded that water wet laboratory models, when scaled by the criterion of Rapoport and Leas were also correctly scaled for frontal instabilities. Using perturbation theory, he showed that parallel plate models do not correlate well with two-dimensional waterfloods in porous media. The study also indicated that flow velocity had only a minor influence on

the onset of instability, and though recovery decreased for a more adverse viscosity ratio, the instabilities did not necessarily become more severe as they did in solvent and parallel plate models.

Perkins and Johnston (1969) studied capillary effects on immiscible fingering. Their results showed that packed models tend to suppress instabilities to a much greater extent than do parallel plate models. High rates induced viscous fingers along the inlet and the entire width of the model. The fingers tended to "break down" into graded saturation zones a certain distance into the model, which the authors claimed was a result of crossflow of the phases perpendicular to the direction of gross fluid movement. Another important observation was that a single entry port into a core could result in an initial finger which would bypass considerable oil on either side.

Croissant (1970), through physical observations, showed that the width of instabilities increased with increasing capillary forces. Hagoort (1974) observed , as had Chouke et al. (1959), that fingering occurred for shock front mobility ratios greater than one. However, he showed that for instabilities to occur, the wavelength of the instabilities had to be smaller then the canal width.

Extending the work of Chouke et al. (1959), Peters and Flock (1979) were able to develop a dimensionless number which could predict the onset of instability in a porous medium. Their analysis was based on a piston-like displacement. However, based on experimental results, they claimed the analysis adequately described Buckley-Leverett displacement as well. Further, even though instabilities occured for both water-wet and oil-wet porous media, oil-wet media had a tendency to produce the fingers at lower rates than water-wet media. Their experiments

indicated a sharp decrease in breakthrough recovery above a critical value of the dimensionless number.

As mentioned before, Bentsen and Saeedi (1981) observed non Buckley-Leverett saturation profiles at high flowrates. They attributed this to viscous fingering. The main instabilities occurred near the inlet of the core. This matches well with the earlier observations of Perkins and Johnston (1969). An interesting conclusion of Bentsen and Saeedi's work was that instabilities occurred before the Rapoport and Leas (1953) stability criteria had been satisfied for their system. This leads to the problem of selecting a rate for laboratory measurements of relative permeabilities of viscous oils. If the rate is too low, the Buckley-Leverett front may not develop. On the other hand, viscous fingering can occur at high rates. Kyte and Rapoport (1958) showed in their paper that for fingering, oil recovery deviated from the Buckley-Leverett profile by only a small amount near breakthrough. If this is the case, it may not be a problem to run displacement experiments at high rates. However, at high rates, viscous forces dominate within the pores. This may not be the case in reservoir waterflooding.

Geffen et al. (1951) performed experiments investigating factors affecting relative permeability measurements. They recognized the problem of end effects and observed that three core sections could be placed end to end and steady-state relative permeabilities measured. The pressure drop could be controlled so that the end effects would be confined to the first and third core sections. Then, the pressure drop across the middle section would yield true relative permeability curves. They also observed that instead of being a single valued

function of saturation, relative permeability also depended upon saturation history. This was because the saturation history affected the saturation distribution of the fluids within the pore space. They also showed that relative permeabilities are not affected by the physical properties of the fluids involved as long as wettability remained constant. Further, in waterflooding a gas-saturated core, they found residual gas saturations as high as **15** to **50** percent. This was a much higher value then the critical gas saturations which ranged from one to eleven percent.

Osoba et al. **(1951)** compared the various relative permeability measuring techniques and concluded that oil permeability curves obtained using the Penn state (steady-state), single core dynamic, and gas drive methods gave comparable results. The Hassler method gave oil relative permeability curves that were consistantly lower then those produced by the other methods.

Richardson et al. **(1952)** studied factors influencing relative permeabilities. Their observations were that existing steady-state relative permeability measuring techniques all measured correct relative permeabilities. Further, for these experiments, the influence of boundary effects could be predicted using equations of fluid flow. Dynamic displacement experiments on short cores were found to give higher values of relative permeability to oil and gas.

Levine **(1954)** observed that relative permeabilities depend on the direction of saturation change. At the same time, relative permeabilities were not observed to be dependent on 'fluid viscosity. Naar et al. **(1962)** did experimental work to indicate that a difference in flow characteristics existed between flow through consolidated rock

and unconsolidated porous media. For unconsolidated cores, the non-wetting imbibition relative permeability curve lay above the drainage curve, while their relative positions were reversed for consolidated porous media. They raised the point that sand pack relative permeabilities might not be representative of field reservoirs. Artificial cementation of the sand packs was suggested as a means of providing porous media that would more closely represent multiphase flow characteristics of reservoirs.

Contrary to the conclusions presented by Richardson et al. **(1952),** Owens et al. **(1956)** observed that dynamic relative permeability measuring techniques gave results that were compatible with steady-state results. The advantage of the dynamic method was the shorter time involved and the ease of performing the experiment.

Theoretically, dynamic and steady-state methods should give the same set of relative permeability curves. They represent the effective permeability to either fluid at a particular gross saturation. However, on a pore level, there can be a considerable difference in the actual flow and trapping mechanism. In steady-state experiments, for any phase that is left in the pores, replenishing fluid is available because both fluids are injected simultaneously into the core. This generally results in distinct channels of flow for each fluid. In dynamic methods, trapped oil will occur in pockets that have been bypassed. To understand the physics of multiphase flow through porous media, one must consider forces existing within the pores.

Flow can be controlled within the pores by viscous forces in some cases, while capillary forces may dominate in others. Capillary forces are related to the rock wettability, and the fluids' interfacial

tension. Viscous forces depend on the viscosities of the fluids present in the core. The effects of these parameters have been studied extensively. Trieber et al. (1972) showed that oil reservoir wettability can range from strongly water-wet to strongly oil-wet, and that there is no apparent correlation between reservoir wettability and temperature or API gravity of the crude oil present in the reservoir.

Kyte et al. (1961) observed that rock samples tend to be more water-wet at reservoir conditions than at surface conditions. Their conclusion was based on the fact that core samples showing intermediate wettability at surface conditions were found to be strongly water-wet and to waterflood more effectively at reservoir conditions. This may be connected to temperature effects and will be discussed later.

Bobek et al. (1958) showed oil recoveries from water-wet rock were 15 % higher then from oil-wet rock. They pointed out wettability changes that could occur in coring water-wet reservoir rocks using oil-based muds. Further, they observed that weathering of fresh water-wet cores would frequently cause the grain surface to become oil-wet.

Newcombe et al. **(1955)** studied effects of changing wettability, interfacial tension and rate on recovery from prepared unconsolidated sand columns. They concluded that wettability was important in controlling the effects interfacial tension and rate had on recovery. For water-wet systems, oil recovery increased with an increase in interfacial tension while the opposite effect was observed for an oil-wet system. For low viscosity ratio oil-water systems, recovery increased with rate up to a point beyond which it stabilized. The stabilizing rate for neutral wettability systems was lower then that for either oil-wet or water-wet systems. On the other hand, recovery was

found to decrease with rate if the oil viscosity was high. This may be related to viscous fingering.

Donaldson et al. (1966) studied viscosity and wettability effects on oil-water relative permeabilities. Their results indicated that viscosity changes had no effect on relative permeabilities while wettability changes did. The oil and water relative permeabilities could be changed independently by treating the oil-brine-rock systems with selective fluids. They agreed with previous work in that cleaning reservoir cores often resulted in a reduction in water-wetness.

Mungan (1964) showed that wettability reversal from oil-wet to water-wet conditions resulted in increased oil recovery. However, he observed no increase in recovery if water-wet cores were changed to cores having neutral wettability. This would indicate that wettability changes would have to be considerable to affect oil recovery. Mungan (February, 1966) observed that preserved oil-wet cores from a reservoir became water-wet upon exposure to air. Saturating the cores with crude and aging for two weeks restored the original wettability. For oil-wet cores, reversing the wettability resulted in recovery of 11 to 15 % more of the initial oil in place when waterflooding. Mungun (September, 1966) conducted further experiments to study interfacial tension, wettability and viscosity effects on oil recovery. For the displacement of a non-wetting phase by a wetting phase, recovery increased by 6 % pore volume upon a reduction in interfacial tension from 40 to 0.5 dyne/cm. Similar changes were observed for displacement of a wetting phase by a non-wetting phase. Wettability reversal, from a non-wetting displacing phase to a wetting displacing phase, resulted in increased recovery. The amount of the increase in recovery was larger for a higher displaced

to displacing phase viscosity ratio. Mungun also observed an increase in oil recovery on decreasing the oil-water viscosity ratio. The major part of the increase occurred near a viscosity ratio of one. The breakthrough curves obtained resemble those of Peters and Flock (1979) who used them to indicate the onset of instability due to viscous fingering.

Wagner and Leach (1966) used an interesting approach to study low interfacial tension displacements. They used a binary mixture of methane-n-pentane and, at any given pressure, used the equilibrium liquid as the displaced phase and the equilibrium vapor as the displacing phase. By increasing the equilibrium pressure to near the critical pressure of the binary system, they obtained extremely low interfacial tensions between the displaced and displacing fluids. Their results indicated that displacement efficiency could be greatly increased by decreasing the interfacial tension below some low value. For the core used, this interfacial tension value was 0.07 dynes/cm. There is some question as to how much mass transfer occurred between the flowing phases due to pressure variation within the core.

Taber (1969) conducted experiments to determine the conditions under which residual oil could be mobilized. He found that the discontinous, non-wetting phase saturation (residual oil) was a unique function of the capillary number, N_{ca}, which is the ratio between the viscous to capillary forces, $\Delta p/L\sigma$. Here Ap is the pressure drop across the system, L the core length and a the interfacial tension. For Berea sandstone samples, a significant quantity of oil was recovered if the value of the capillary number exceeded 5.0 [(psi/ft)/(dynes/cm)]. Taber indicated that the capillary number could be increased either by

increasing the flooding rate or by decreasing the interfacial tension. Surface-active agents were suggested as a means of reducing the interfacial tensions in waterfloods.

Du Prey **(1973)** also observed the dependence of residual saturations, both wetting and non-wetting, on the capillary number. He found higher relative permeabilities and lower residual saturations for both fluids with larger capillary numbers. Viscosity ratio was seen to have an influence on relative permeability curves.

Abrams **(1975)** included a viscosity ratio term and the capillary number to obtain a unique recovery curve for sandstone cores. The parameter used was $(V\mu_w/\sigma)/(\mu_w/\mu_o)^{0.4}$. The shape of the curve obtained for limestone was distinctly different from the response for various sandstone cores. This might be attributed to the generally more hetrogenous nature of limestone.

Rate effects had been studied extensively by then, but emphasis was placed more on the Rapoport and Leas stability criteria then on possible effects on ultimate recovery. To this extent, Merliss et al. **(1955)** noted that gas-oil relative permeabilities were independent of flowrate once capillary end effects had been overcome. The same conclusions were drawn by Sandberg et al. **(1956)** in studying oil-water systems. Taber's results however, would indicate some effect on relative permeability curves when approaching the residual oil saturation. This was indeed observed by Labastie et al. **(1980)** using semi-permeable membranes to measure pressures separately in both the oil and water phases. Their study was on oil-water systems and indicated that the water relative permeability was independent of flowrate, being truncated at the residual oil saturation. The oil relative permeability however, did

change with flowrate near the residual oil saturation.

Recognizing the complexity of relating the role of viscous and capillary forces in waterflooding, Batycky et al. (1980) suggested a technique to obtain displacement relative permeabilities at rates comparable to reservoir waterfloods. By stopping flow in the cores for a certain period to establish capillary equilibrium and then restarting, they obtained the extra pressure drop caused by the outlet end effect. It is possible, however, that capillary equilibrium might not be achieved due to a hysteresis in the capillary pressure curve. In such a case, the accuracy of the technique may be questionable.

In dealing with temperature effects on relative permeability curves, it is important to recognize that a number of the parameters mentioned in the preceeding can change with temperature. Specifically, temperature can alter viscosities, viscosity ratios, wettability, interfacial tension, and pore throat openings. These in turn, can effect the magnitude of end effects, viscous fingering, and the ratio of viscous to capillary forces within the pores. Added to this are possible rock-fluid interactions that may occur at high temperatures. Many studies agree on the effects of temperature on relative permeabilities. There is, however, considerable difference in the reasons given for these temperature effects.

The study of temperature effects on relative permeability gained in importance in the mid 1950's. Wilson (1956) observed no effect of temperature on relative permeability. The reason given for not observing any change was that the viscosity ratio of the fluids used had a minimal change with temperature. Kyte et al.(1961) observed better recoveries at reservoir conditions than at room temperature. They

attributed this to wettability effects claiming that temperature made the rock more water-wet, Edmonson (1965) found a reduction in residual oil saturation in consolidated sandstone cores upon increasing temperature. He used water with two refined oils and two crude oils and observed the same trend of residual oil saturation for all the fluid pairs.

Poston et al. (1970) presented results of experiments studying temperature effects on residual saturations. Their cores consisted of two different types of unconsolidated sand and the fluids used were water and refined oils. Three refined oils having viscosities of 600, 99 and 80 cp at 70°F were used with water to obtain end point saturations. An increase of 8% in irreducible water saturation was observed for a temperature increase from 70°F to 280°F. They also observed a hysteresis of 5% after each cycle of heating to 280°F and down to 70°F. Their waterfloods were stopped at a water-oil ratio of 100:1 which gave a "practical" residual oil saturation that decreased with temperature. For the 600 cp oil-water system, the residual oil saturation dropped from 39% at 70°F to 15% at 280°F. The corresponding change for the 80 cp oil-water system was from 22% to 11%. Once again, a 5% hysteresis was observed following each heating cycle. As a result of these end-point saturation changes, the oil relative permeability curve was shifted in the direction of higher water saturation. The relative permeability to water was found to be higher at higher temperatures. The reason for these changes was given as an increase in the water wetness of the sand with temperature.

Combarnous and Pavan (1968) explained reductions they found in residual oil saturations through changes in viscosity ratio. Davidson

(1969) explained similar results he obtained through changes in interfacial properties. His permeability ratio curves were insensitive to temperature in the mid-saturation range and only deviated at the ends.

Sinnokrot et al. (1971) conducted capillary pressure measurements on consolidated cores at elevated temperatures. They used three different types of sandstones and a limestone for their experiments. Their results indicated a 10% increase in irreducible water saturation upon increasing the temperature from 70°F to 300°F for the sandstone cores. They postulated that this was due to an increase in water-wetness of sandstones at higher temperatures. No change in irreducible water saturation was observed with temperature for the limestone core. A difference in behavior of sandstone and limestone cores was also observed by Abrams (1975) while studying residual oil saturations as a function of capillary number.

Lo and Mungan (1972) conducted steady-state measurements of relative permeability at elevated temperature. First, they used viscous refined oil-water systems and observed an increase in irreducible water saturation and a decrease in the residual oil saturation upon increasing temperature. In these cases, the viscosity ratio of the oil-water systems used dropped significantly with temperature. Next, they used a tetradecane-water system which had minimal change in viscosity ratio with temperature. For this set of runs, they observed no temperature effects on irreducible water saturation and residual oil saturation. Their conclusion was that viscosity ratio affected relative permeability curves. For the viscous oil-water systems used, increasing temperature caused an increase in the relative permeability to oil and a higher rate

of increase in the relative permeability to water with increasing water saturation.

Weinbrandt et al. (1975) presented results showing temperature effects on water-oil relative permeabilities. They used consolidated sandstone cores and obtained 15% increase in irreducible water saturation on increasing the temperature from 75°F to 175°F. The corresponding decrease in residual oil was from 36X to 18%. The relative permeabilities they obtained were shifted towards increasing water saturation because of the above mentioned changes. They also accepted the explanation of increased water-wetness for the observed temperature dependance of relative permeabilities.

Sanyal et al. (1975) suggested that the changes in the end-point saturations might be caused by expansion of the rock matrix with temperature. This expansion, although small, could effect pore throat openings substantially, thereby altering ratios of viscous to capillary forces within the pores. Counsil (1979) reported results of steam-water and nitrogen-water relative permeabilities at different temperatures. He artifically cemented his sandpacks to more closely resemble reservoir rock. His results indicated no change in either end point saturations or gas-water relative permeabilities with temperature.

The preceeding works done on factors affecting multiphase flow through porous media serve as a basis for this research. In many cases, temperature has been seen to affect relative permeabilities. As is evident however, various explanations have been presented to explain these changes. It is the purpose of this research to identify and explain temperature effects on relative permeabilities of oil-water systems.

4. EXPERIMENTAL EQUIPMENT AND PROCEDURE

This section presents a description of the equipment used and the procedure followed in this study. First, the equipment is described and then procedures given for the experiments.

The description has been divided into several sections. Their headings depict the purpose of that particular part of the equipment. These sections are:

1. fluid intake,
2. fluid flow,
3. core holder,
4. pressure monitoring,
5. oil analysis,
6. confining pressure,
7. core cleaning,
8. complete system, and
9. procedure for experiments

Separate flow diagrams for each section are provided. The important features of the entire system are then combined and presented in one section. A complete detailed diagram of the equipment is presented in Appendix C-1

4.1 Fluid intake

This part of the experimental apparatus loads the pumps for discharge to the rest of the system. A schematic of the intake assembly is presented in Fig *4.1.* The pump is a model 2248/49 WIII Ruska constant rate pump. It has two cylinders, each having a capacity of 500 cc. The pump can work in two modes. In the first mode, one cylinder discharges while the other fills. This mode can be used for contiuous discharge of a single fluid. In the second mode both cylinders discharge simultaneously at the same rate. However, by changing gear sizes within the pump, it is possible to discharge at different rates from each cylinder. In the present study, the pump was used in the second mode with both cylinders discharging at the same rate. One cylinder was used to discharge oil and the other water. The pump has 28 discharge speeds, ranging from 5 cc/hr to 1120 cc/hr.

Charging the cylinders in Ruska pumps is generally accomplished by the suction created as the piston moves back. The water cylinder is filled in this manner. The suction line is connected to a vessel containing distilled, de-mineralized water.

The oil cylinder could not be filled in the same manner because the oil has a viscosity of 220 cp at 70" F. This high viscosity prevents easy flow of oil into the cylinder by suction. Hence, a different arrangement shown in Fig. 4.1, was constructed which fills an oil charge cylinder with the oil. The filling is accomplished by first pulling a vacuum on the charge cylinder. Oil is poured in from the funnel at the top. The vacuum in the charge cylinder sucks the oil in through the short tubing. When the cylinder is full of oil, nitrogen pressure is

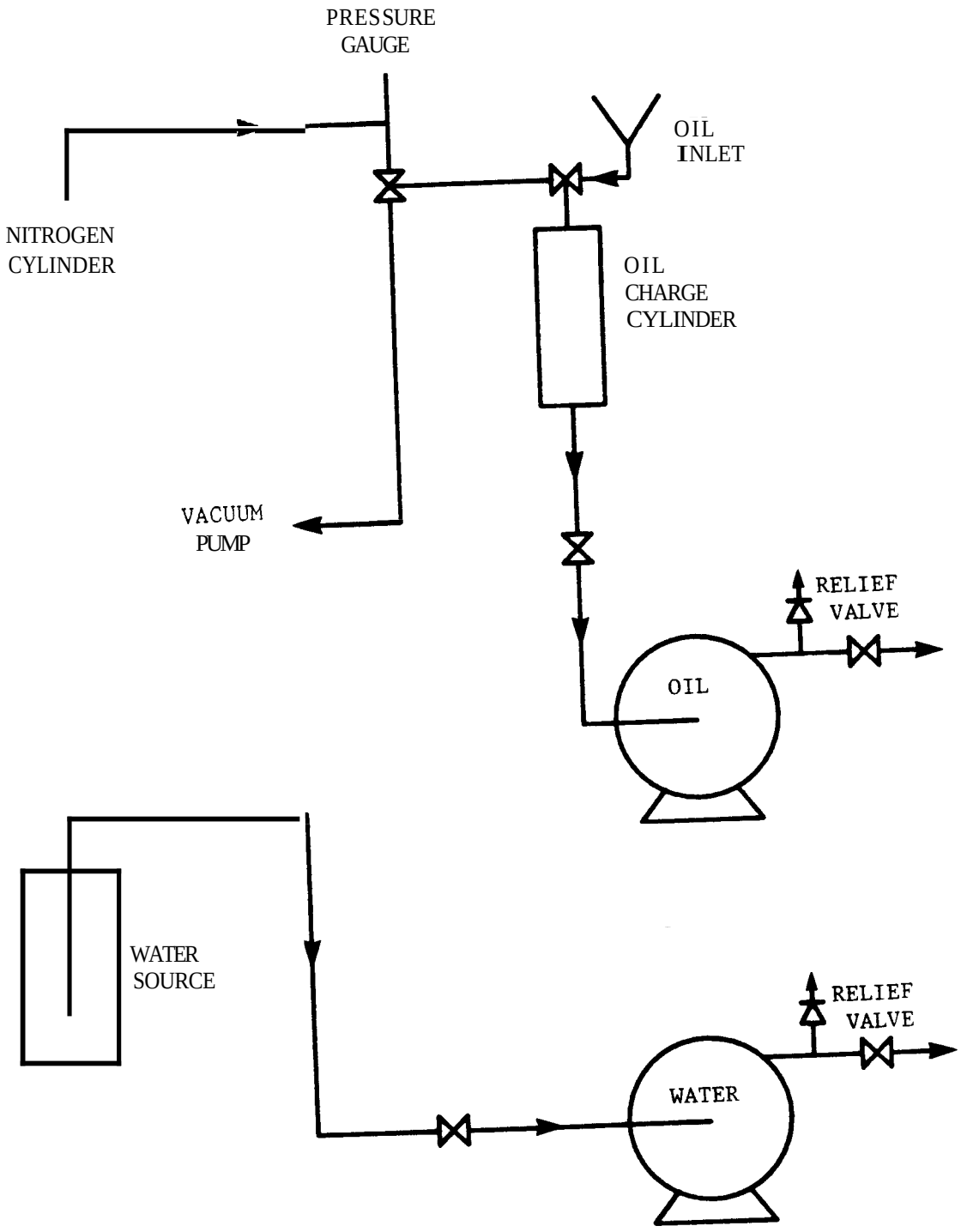

Fig. 4.1 SCHEMATIC OF FLUID INTAKE SYSTEM

applied. This is accomplished by means of a three-way valve that can direct the line from the charge cylinder either to the nitrogen source or to the vacuum pump. The pressurized oil is then allowed to flow into the oil cylinder of the Ruska pump. The volume of the charge cylinder is 1000 cc which is twice as large as that of the pump cylinder. Hence, the pump cylinder can be completely filled without having to reload the charge cylinder. Once the pump cylinder is filled, the valve connecting it to the charge cylinder is closed. The oil is then ready to be injected into the system. Relief valves set at 2200 psi are placed in the outlet line to prevent accidental damage to the cylinders. The pump cylinders are of 316 stainless steel and rated to pressures of 2800 psi.

This method for loading the oil cylinder has proved to be time efficient. From the cylinders, the fluids flow in separate lines into the rest of the system. The part of the system described next consists of the lines that transmit fluids to and from the core.

4.2 Fluid flow

The schematic of the fluid flow lines is shown in Fig. 4.2. All the tubing used in the equipment to transmit fluid is 1/8 in. OD (0.085 in. ID) stainless steel. From the cylinders of the Ruska pump, separate flow lines are provided to transmit oil and water into the rest of the system. The water line leaves the water cylinder of the Ruska pump and passes through filters to prevent impurities from entering the core. Two 7 micron filters are connected in parallel, and flow can be directed through either by means of a three-way valve. Two filters are provided in case one plugs during an experiment. The outlets from these filters

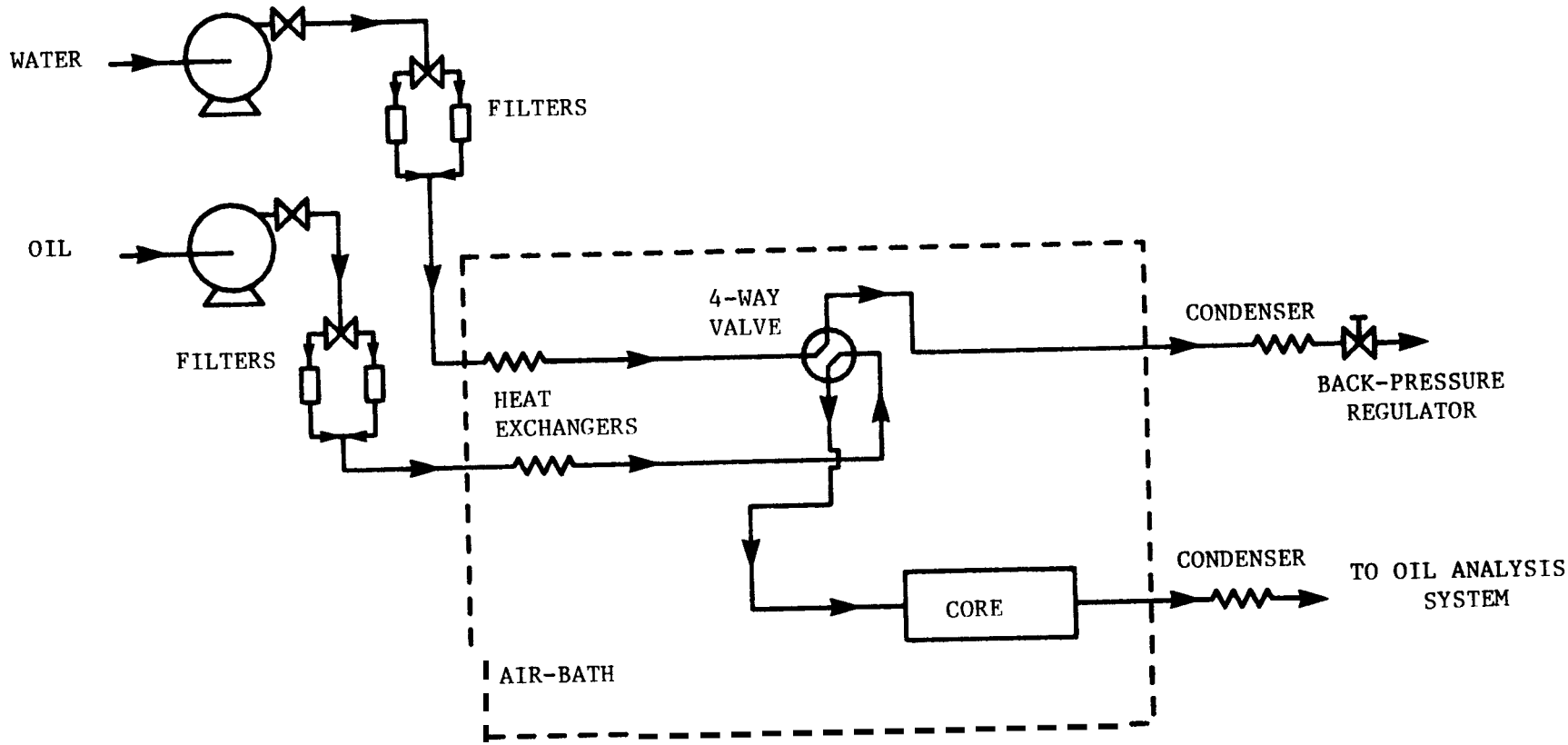

Fig c 2 SCHEMATIC OF OIL AND WATER FLOW LINES

connect into a single flow tube which enters an air bath (Blue M, Model POM-140601). This air bath is capable of maintaining a constant temperature up to 650°F with a stability of ±0.2°F.

Upon entering the air bath, the fluid enters a heat exchanger. This heat exchanger is a coiled length (20 ft) of 1/8 in. OD stainless steel tubing, and is used to heat the incoming fluid to the temperature of the air bath. Once the fluid leaves the heat exchanger, it flows through a 6 ft long, small inside diameter (0.049 in.) tubing (1/8" OD) which acts as a capillary tube viscometer. The pressure drop is measured by means of pressure taps at both the upstream and downstream ends of the flow tube. The viscometer is used to measure the viscosity of the fluid at the temperature of the air bath. From the viscometer, the flow enters a four-way switching valve.

Fluid flows from the oil cylinder of the Ruska pump into the other inlet of the four-way valve. As can be seen from Fig. 4.2, the oil flows through a similar arrangement as the water. The length of the heating coil is the same as for the water line. The inside diameter of the capillary tube viscometer, however, is larger than for the water line due to the higher viscosity of the oil.

The four-way valve has two inlets and two outlets. The valve used in this experiment (Valco, Model LV-4-HTA-HC) is rated at 500 psi at 570°F. The principle behind the switching valve can be seen in Fig. 4.3. In the normal position, one fluid enters through port a and leaves through port c, while the other flow channel is through ports b and d. When the valve is switched, however, the flow channels are reversed. This results in fluid that is entering through port a leaving through port d, while fluid that enters through port b leaves through port c.

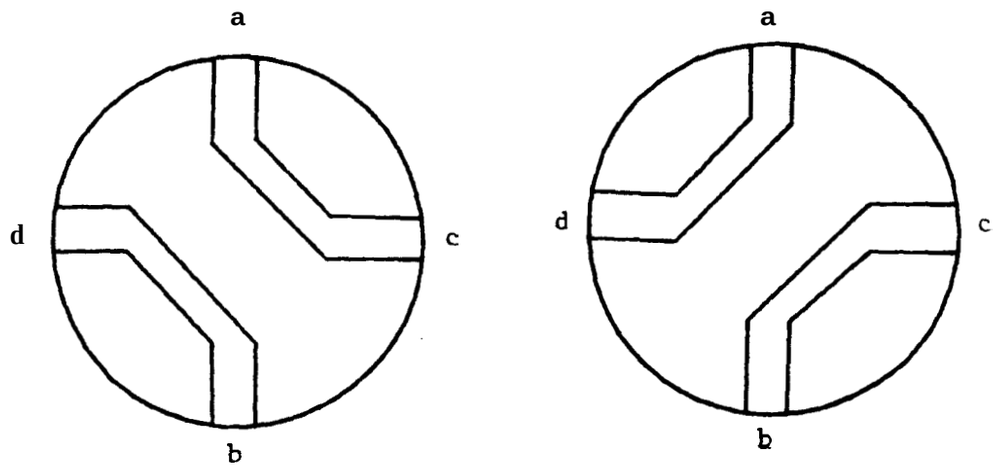

Fig. 4.3 WORKING MECHANISM OF FOUR-WAY SWITCHING VALVE

This valve essentially switches the source of flow into the core. It has a long handle that extends outside the air bath enabling the switch to be made without opening the air bath.

One of the outlets from the four-way valve directly leaves the air bath. This fluid is then cooled by passing through a condenser. Following the condenser, the line is connected to a spring-loaded, back-pressure regulator (Grove, Model *26-1727-24-014)* This is an adjustable regulator capable of holding a back pressure set between 0 to 500 psig.

The other outlet from the four-way valve enters the core. Fluid leaving the core goes out of the air bath, through a condenser, and into the oil analysis assembly. Pressure taps are provided to obtain pressures at both the upstream and downstream end of the cote. The exact location of these pressure taps is explained in the next section which presents the design of the core holder.

4.3 Core Holder

The core holder was designed for the specific purpose of conducting displacement experiments on unconsolidated sand packs. A schematic of the core holder is shown in Fig 4.4. A detailed diagram of the core holder is presented in Appendix C-2. The porous medium, which is clean Ottowa sand, mesh 170–200, is housed in a thick walled (1/8th in. wall thickness) stainless steel sleeve. End plugs press against the sand on either end of the sleeve. These end plugs are referred to as the inlet and outlet end plugs based on the direction of fluid flow. Between the face of each of the end plugs and the sand is a metal screen (mesh 400) which prevents sand movement. The inlet end plug has three entrances. One is used as a flow inlet and another, on the same flow path, is used as the upstream pressure tap. A third inlet is used to direct cleaning fluids into the core. Leakage is prevented between the end plugs and the sleeve by two O–rings on each end plug. The actual sealing is provided by the O–ring further from the sand. The second O–ring is provided to prevent sand from reaching the first O–ring. The outlet end plug has a straight 3/16 in. hole through which a 1/16 in. stainless steel tube is inserted close to the sand face. This tube provides the downstream pressure tap, while the annular flow channel around it provides the outlet for fluid from the core.

The faces of the end plugs adjacent to the sand have a cobweb of grooves machined into them. This is to diffuse the flow near the ends of the sand pack. Further, the main flow line within the plugs diverges into six flow channels, thereby providing seven inlets onto the sand face and the same number of outlets. The design of fluid entry ports in

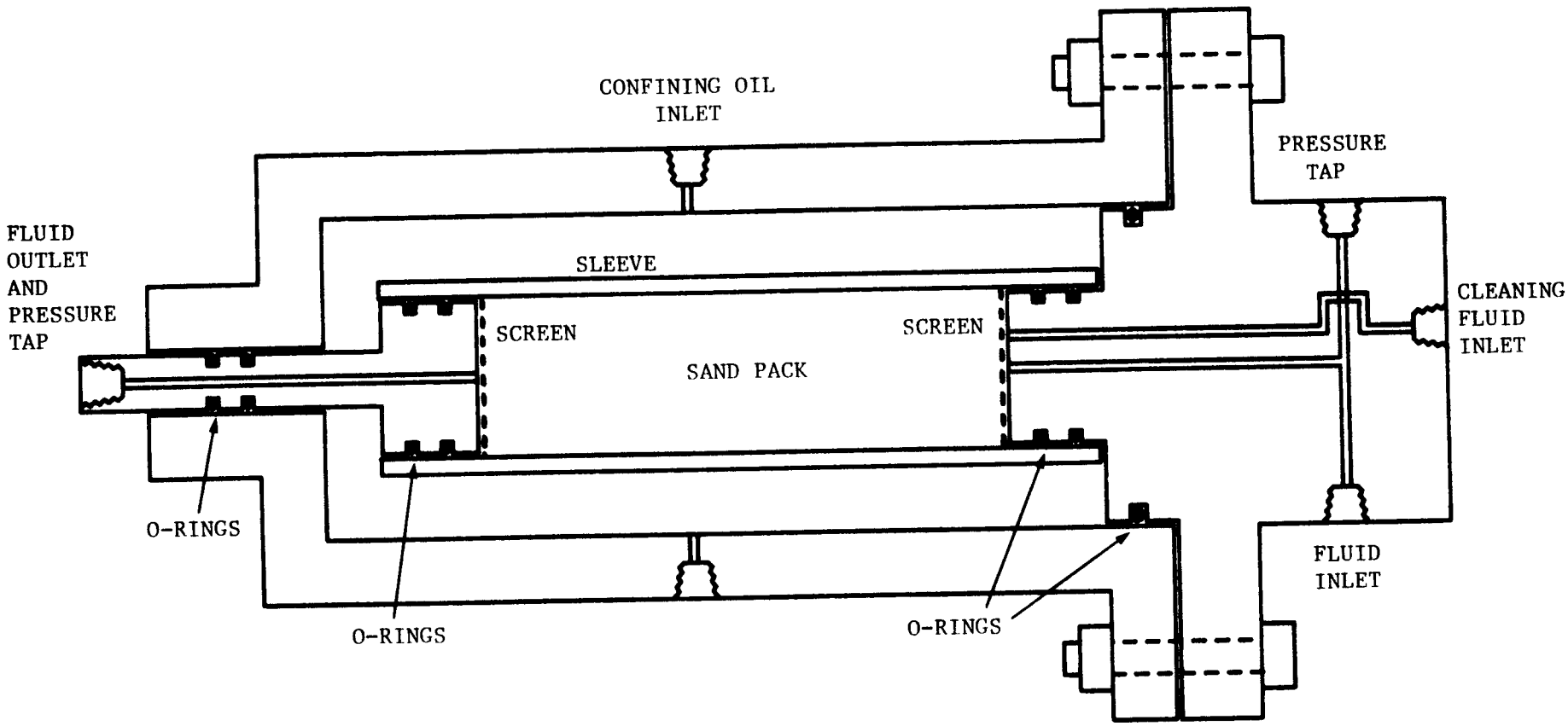

Fig. 4.4 SCHEMATIC OF CORE HOLDER

the end plugs is important. The sand is water-wet, the metal oil-wet. During an oil flood, oil will have a tendency to be held back from entering the core. In this case, the diverging flow lines will work effectively. During a waterflood, however, water will reach the sand face via the central flow channel first. When it does, capillary forces will suck it into the core. In this case, the effectiveness of the diverging flow lines is minimized. No simple way is known to compensate for this problem other than to have a large number of parallel flow lines into the core. This complicates the design of the core holder somewhat. This study used the core holder with the seven inlets and outlets. Results show the effect of the core design on diffuse flow at the sand face to be minimal.

Originally, the channel now used for the cleaning fluid was planned for the upstream pressure tap. This created a capillary pressure difference at the screen next to the sand due to a film of oil which covered the inlet to the tap. The only place where this film would not be present is directly in front of the central flow channel. Hence, to prevent an additional pressure effect in the pressure drop measurements, the pressure tap was connected directly to the main flow line.

The entire assembly of the sleeve and two end plugs fits inside the core-holder shell. The chamber between the shell and the sleeve contains the confining fluid. The confining pressure is only transmitted axially to the sand. This is done by means of the outlet end plug which is allowed to slide. Due to the difference in areas, however, the sand experiences a pressure which is 70 % of the chamber pressure. The end plug provides an axial pressure, and presses unconsolidated sand against the inside of the sleeve. The reaction from

the sleeve then results in a radial confining pressure. The purpose of the confining pressure is to simulate some sort of overburden pressure. Leakage of the confining fluid is again prevented by O-rings between the end plugs and the core holder shell. This core holder was pressure checked to 10,000 psi confining pressure, and a temperature of 400°F. The temperature limit is a result of the Viton O-rings in the holder.

The upstream and downstream pressure taps are connected to differential pressure transducers. The assembly that monitors the differential pressure, along with the transducer calibration network, is described in the next section.

4.4 Pressure Monitoring

Figure 4.5 shows the configuration of the pressure transducers (Celesco, Models P7D and KP15) used to monitor differential pressure. Due to the large difference in the viscosity of the oil and water used in these experiments, pressure drop in the core varied from 0.25 psi to 360 psi, depending on the saturation in the core. Hence, a set of five transducers was used to monitor the pressure drop across the core. These are hooked up in parallel and have ranges of 500, 100, 25, 5 and 1 psi. Using the appropriate transducer, high accuracy can be achieved for all pressure drops.

One side of the transducers connects to the upstream pressure tap of the core and the other side to the downstream tap. A loop is provided around each transducer. This loop, if activated, provides the same pressure (downstream pressure) to both sides of the transducer

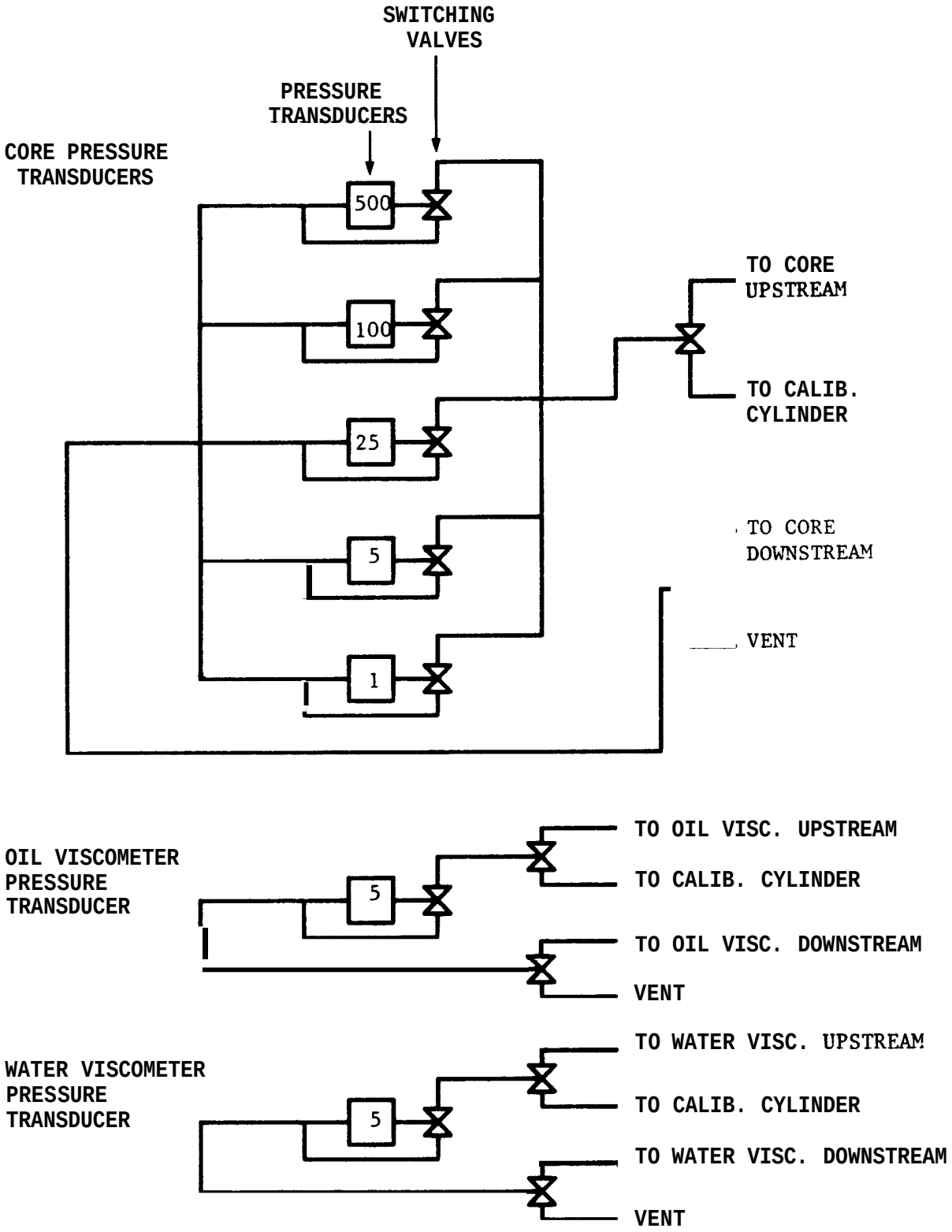

Fig. *4.5* PRESSURE MONITORING EQUIPMENT

plate. The loop can be activated by means of a three-way switching valve as shown in the diagram. If the valve connects to the upstream pressure tap, the transducer reads the pressure drop. When the valve position is switched, a net zero pressure differential is imposed across the transducer plate. This provides a convenient means of checking the zero setting of the transducer. It also provides a safeguard against over pressuring transducer plates.

Figure 4.5 shows the pressure monitoring manifold connections to a calibration cylinder. This enables the transducers to be calibrated without disconnecting them. A three-way valve is capable of connecting the transducers to the calibration nitrogen cylinder instead of the upstream pressure line. Another valve vents the downstream side of the transducers. Two Heise gauges, with ranges of 0-30 psi and 0-1000 psi, are also connected to the calibration cylinder. These gauges provide a standard against which the transducers are calibrated.

Also shown in Fig. 4.5 are the transducers across the capillary tube viscometers in the oil and water flow lines. For each viscometer, a single transducer with a range of 0-5 psi is used. These transducers are also connected to the calibration line.

Output from the transducers is sent to demodulators. The demodulators convert the signal from the transducers to a 0-10 volt output. The demodulators are connected to digital voltmeters and a strip chart recorder. The latter provides a continous record of the pressure drop. The other parameter required to determine relative permeabilities is the oil produced from the core. A variety of oil analyzing methods have been used in this experiment. These are described next.

4.5 Oil Analysis

A photoelectric cell has been used to measure oil production from the core. (This cell was donated by ARCO Oil & Gas Co.). Figure 4.6 shows a diagram of the cell and the electronic equipment that enables measurement of oil production. A detailed diagram of the photocell is presented in Appendix C-3. The cell assembly consists of a steel frame which provides a bracket for a thick-walled glass capillary tube with an inside diameter of 0.0040 in. The assumption made in using this technique is that oil and water flow as distinct slugs through the tube. This is a reasonable assumption considering the pure fluids and clean porous medium used in this study. A ceramic block is mounted across the glass tube. The diagram also shows a cross-section of the block. On one side is a light emitting diode (LED) which projects through an opening into the glass tube. The light then travels through the tube and fluid within, being detected by a photoelectric cell at the other end of the block. Due to the different refractive indices of oil and water, the intensity of the light reaching the photocell is higher for oil in the tube than for water. The output from the cell is connected to an electronic gate which is, in turn, connected to a frequency counter set at 1000 Hz. The gate compares the voltage output from the cell against a set threshold voltage. If the cell voltage is higher, it activates the counter, stopping only when the cell voltage drops below the threshold voltage. The value of the threshold voltage can be set at any desired value by means of a variable resister. By setting the voltage between the voltages obtained from the cell for oil and water flow, the counter can be made to operate only when oil flows

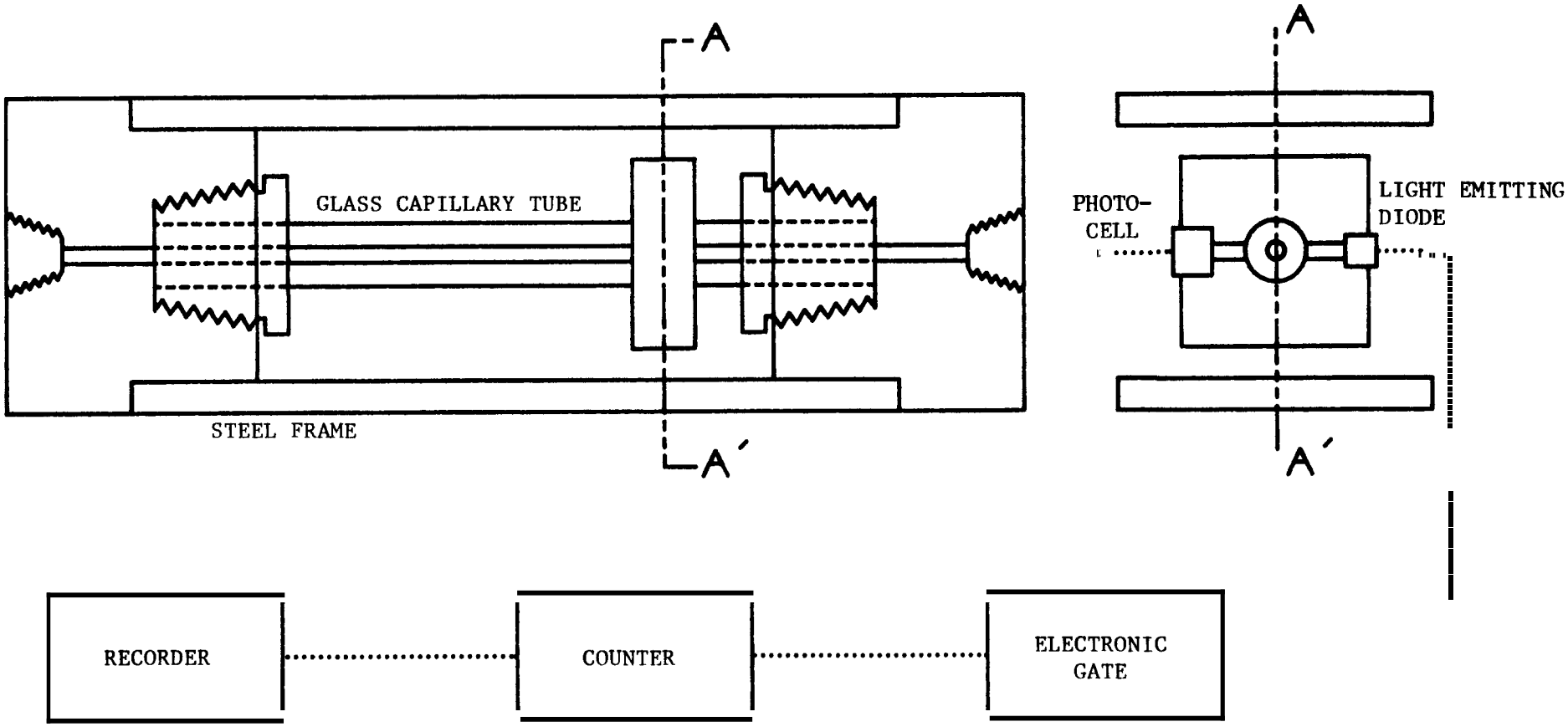

Fig 6 PHOTOELECTRIC OIL COUNTER

through the tube. The counter then indicates the time for which oil has been flowing in the tube. For a constant flow rate, this is proportional to the volume of oil produced from the core. The output from the counter is connected to a strip chart recorder which provides a continuous record of oil produced. A switch is also provided on the gate which reverses its output. In that mode, the frequency counter is activated when the cell voltage drops below the set voltage. This mode is used to monitor water production during an oil flood. A circuit diagram of the gate is provided in Appendix C-4.

Runs were made prior to the experiment to determine the effectiveness of this technique. Figure 4.7 presents a comparison of the output from the cell against material balance measurements conducted by weighing the produced fluids. As can be seen, excellent agreement was observed.

Figure 4.8 shows the flow path beyond the photocell. Fluid from the core passes from the air-bath, and through a condenser before entering the glass photocell tube. Upon leaving the cell, the fluid is collected in a pressure bomb. This consists of a 500 cc steel cylinder which is pressurized with nitrogen to the required back pressure for the flow system. As the multi-phase liquid enters the bomb, nitrogen is bled through a relief valve to maintain constant pressure. When the cylinder is full, fluid can be drained from the bottom. The fluid collected provides a material balance check for the photocell measurements.

It was observed during the course of the experiments that the photocell failed to detect oil produced from the core near the end of the waterflood. Oil must flow as a slug through the photocell to be

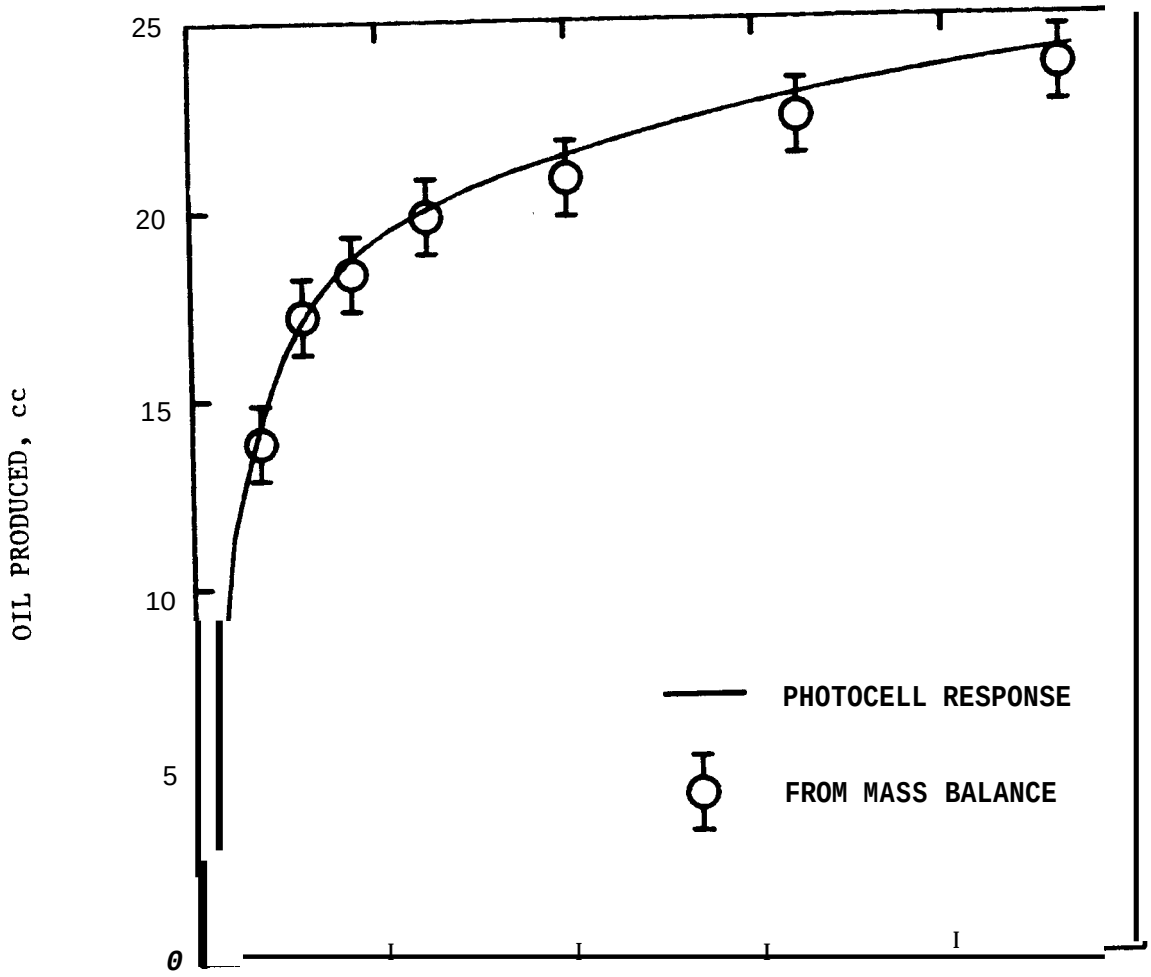

Fig. 4.7 CALIBRATION OF OIL PRODUCTION PHOTOCELL

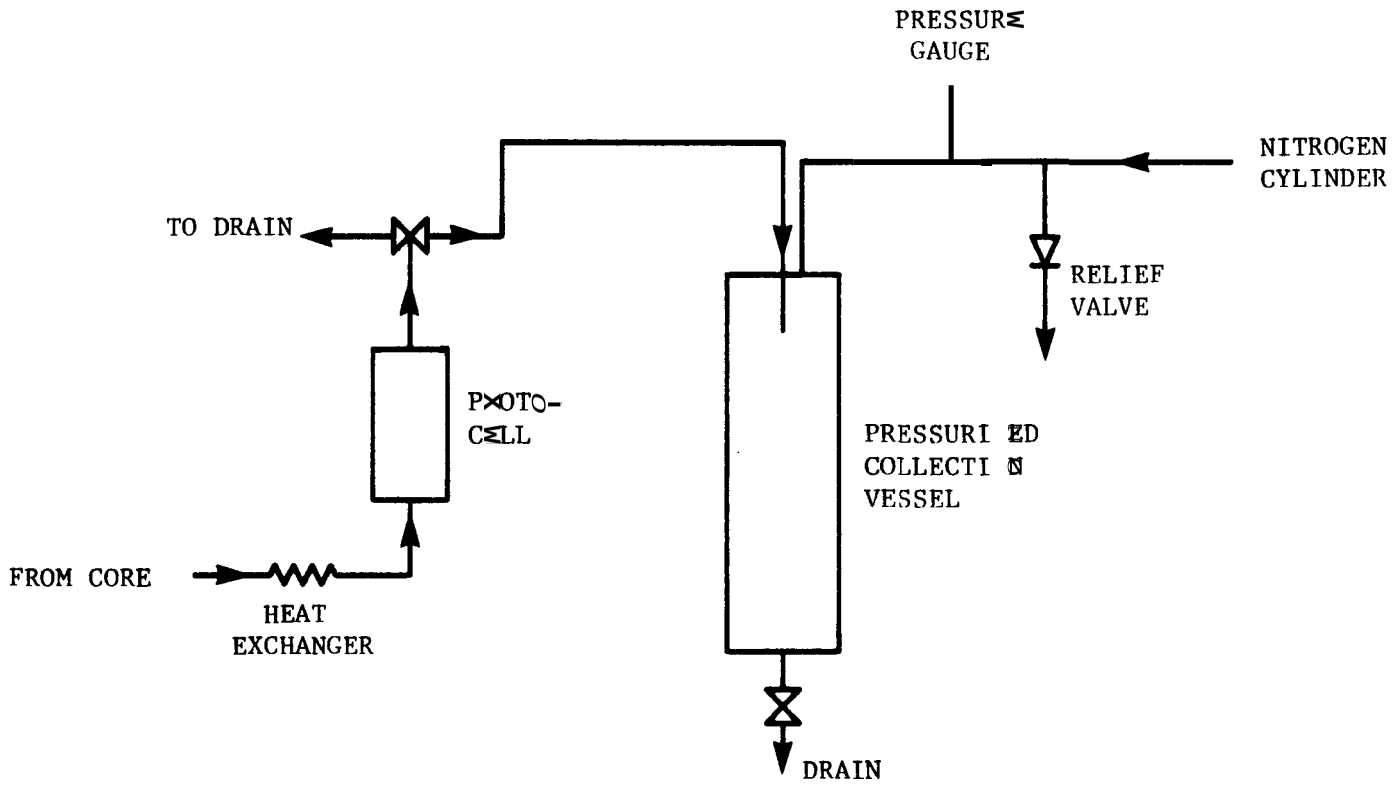

Fig. 4.8 FLUID METERING AND COLLECTION APPARATUS

detected by the cell. However, towards the end of a waterflood, oil is produced from the core in small droplets which are carried in water and pass through the tube without touching the sides. In these cases, the cell does not detect enough voltage increase to activate the counter. So, even though oil is being produced, the ouput on the chart recorder indicates conditions of residual oil saturation within the core.

To overcome this problem, the system shown in Fig. 4.9 was constructed. The output from the photocell tube passes through a three-way switching valve into one of two glass cylinders. These cylinders are thick-walled and graduated. During a waterflood, the oil-collecting column is initially filled with water. The two-phase mixture flows in from the bottom. The oil, being lighter than the water, floats to the top. Water flows out from another outlet at the bottom, through two other three-way valves to a backpressure regulator. If the first of these two valves is reversed, the column discharge will begin from the top. In this case, oil will be pushed out from the column. This position can be used to reset the water level before starting a waterflood. The second three-way valve can direct flow either to the regulator or a drain.

The water collection column for an oilflood is identical to the oil collection column. The only difference is that the working position of the valves is such that the two phases enter from the bottom, and oil is removed from the top. At the start of the oil flood, the column is full of oil. Once again, valve positions can be reversed to re-set the fluid levels within the column before the start of an experiment.

This equipment enables visual determination of oil production from the core. As long as oil bubbles appear and float upwards, the core is

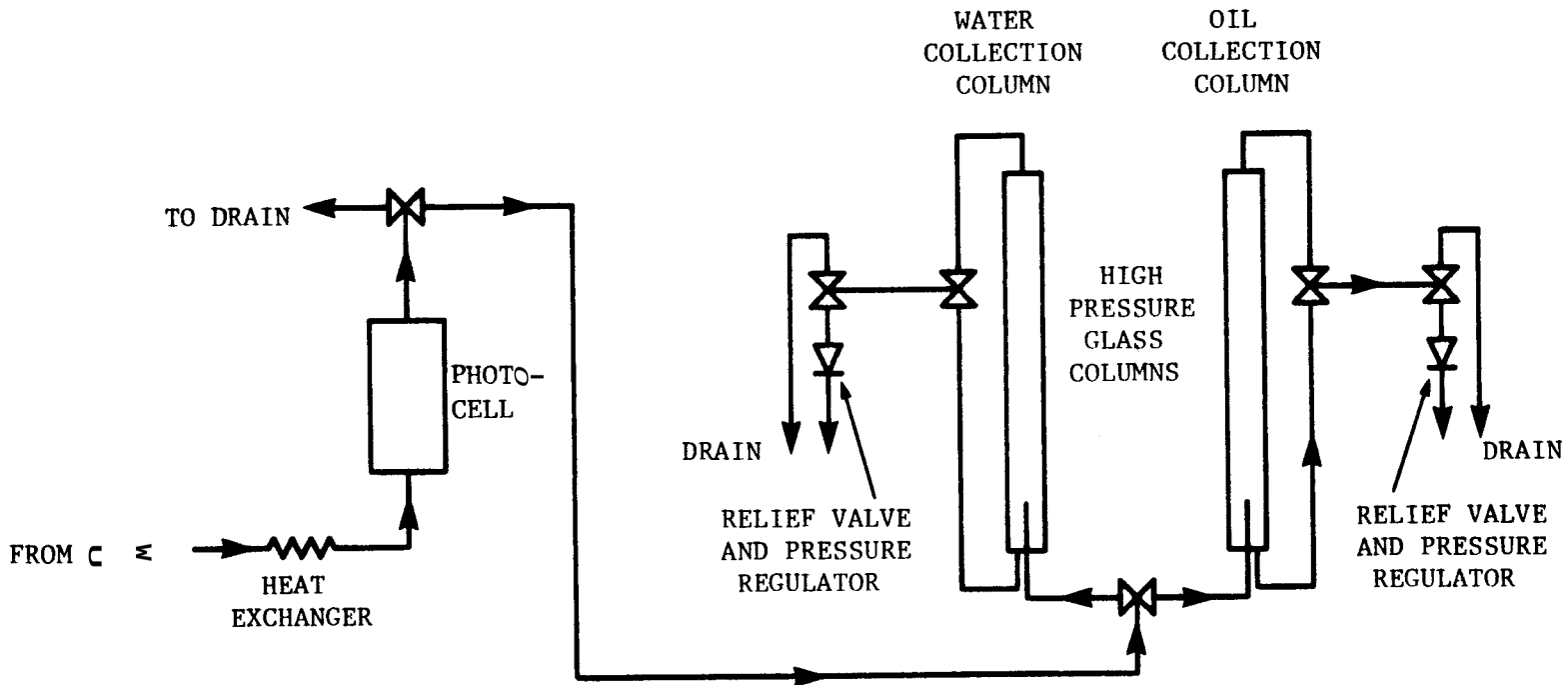

Fig C 9 MODIFIED FLUID COLLECTION AND METERING APPARATUS

not at residual oil saturation. This system was used in the later part of the study to determine accurate oil saturations near the end of the displacements.

4.6 Confining Pressure

The core is subjected to a confining pressure which simulates overburden pressure. This is done by pumping a confining fluid into the chamber around the core as described in Section 4.4. The fluid is pressurized by means of a hand pump (Enerpac, Model K22.005). A schematic of the confining fluid system is shown in Fig. 4.10. The pump draws oil from a reservoir and pushes it into the system. The valves indicated on the confining fluid lines are special high pressure valves rated to 45,000 psi. The pump is rated to 10,000 psi. Pressure taps are taken from the line going to the core. One of these goes to a high pressure gauge. This gauge then indicates the confining pressure in the chamber around the sleeve housing the sandpack. Another pressure tap goes to a pressure relief valve. This valve is used when heating the core. During heating, the confining oil expands. The relief valve then bleeds the excess oil and maintains the confining pressure. In the experiments, this valve was set at 3500 psi. The sliding end plug transmitted 70% of this pressure resulting in an axial confining pressure of 2450 psi on the sandpack. Radial confining pressure, resulting from a reaction from the walls of the sleeve, was present but its value could not be measured.

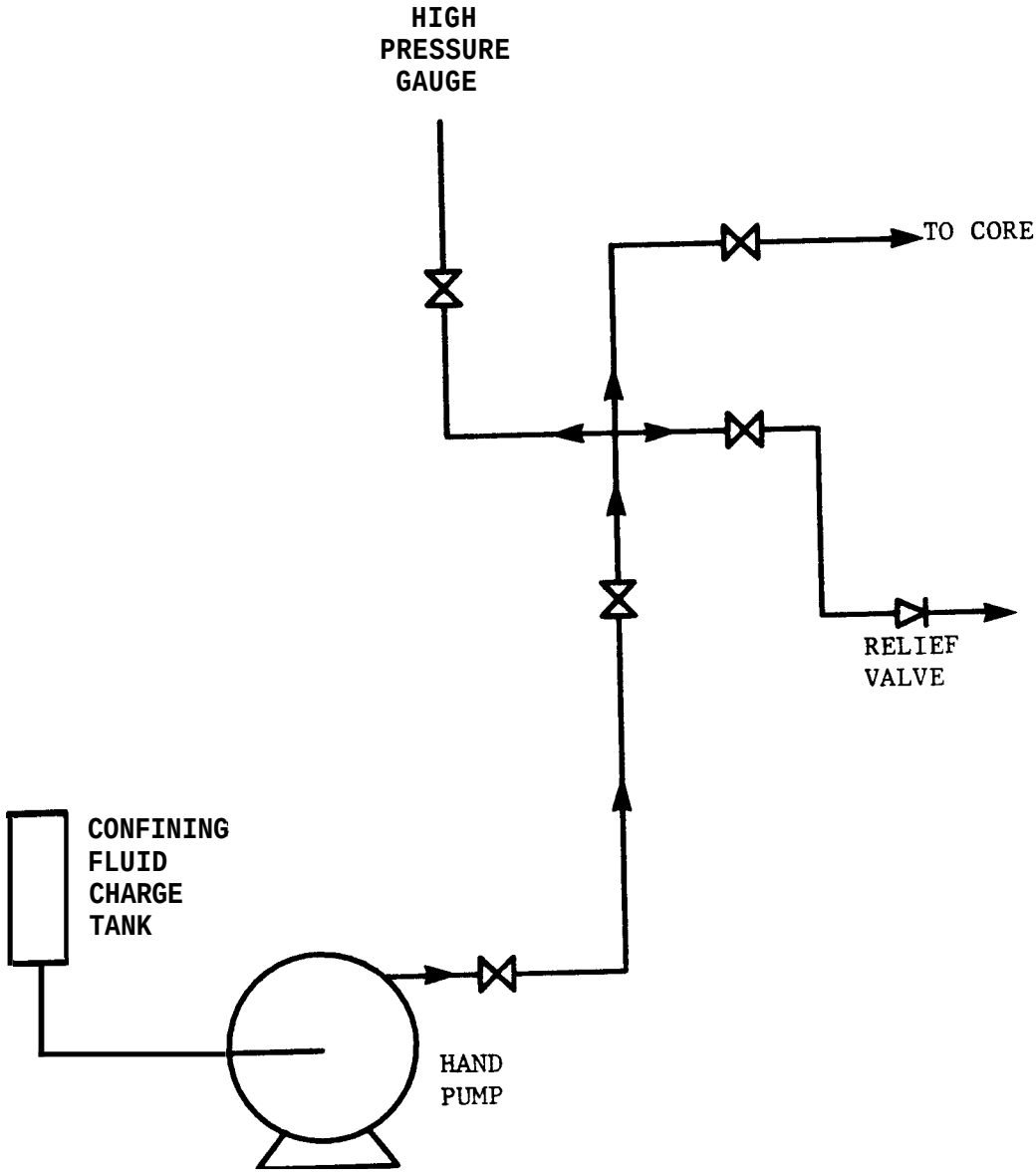

Fig. 4.10 CONFINING PRESSURE APPARATUS

4.7 Core Cleaning

After each run, the core was cleaned by a series of miscible displacements. In removing an oil-water mixture, mineral spirits were first used to flush the oil. Then, iso-propyl alcohol, which is miscible with both water and mineral spirits, was used to displace the fluids within the core. Following this, acetone was used to displace the alcohol. The final displacement was to flush the acetone with water. This resulted in a 100% water saturated core. If 100% oil saturation was required at the start of an experiment, the cleaning sequence was reversed. A Pulsafeeder pump (Lapp, Model 5KH32KG651AX) was used for the cleaning fluids. The location of the pump and the line connecting to the core is shown in Fig 4.11.

4.8 Complete System

Figure 4.11 shows a schematic of the entire system. This diagram shows how the various sections of the apparatus are connected. A vacuum pump is installed to evacuate the oil and water flow lines. The vacuum pump is also connected to the transducer tap lines and the outlet from the core. In this manner, all lines to and from the core can be evacuated.

Temperature is monitored within the system by means of Iron-Constantan (J-type) thermocouples installed in the flow lines. (Constantan is a Copper-Nickel alloy) The locations of the thermocouples are as follows:

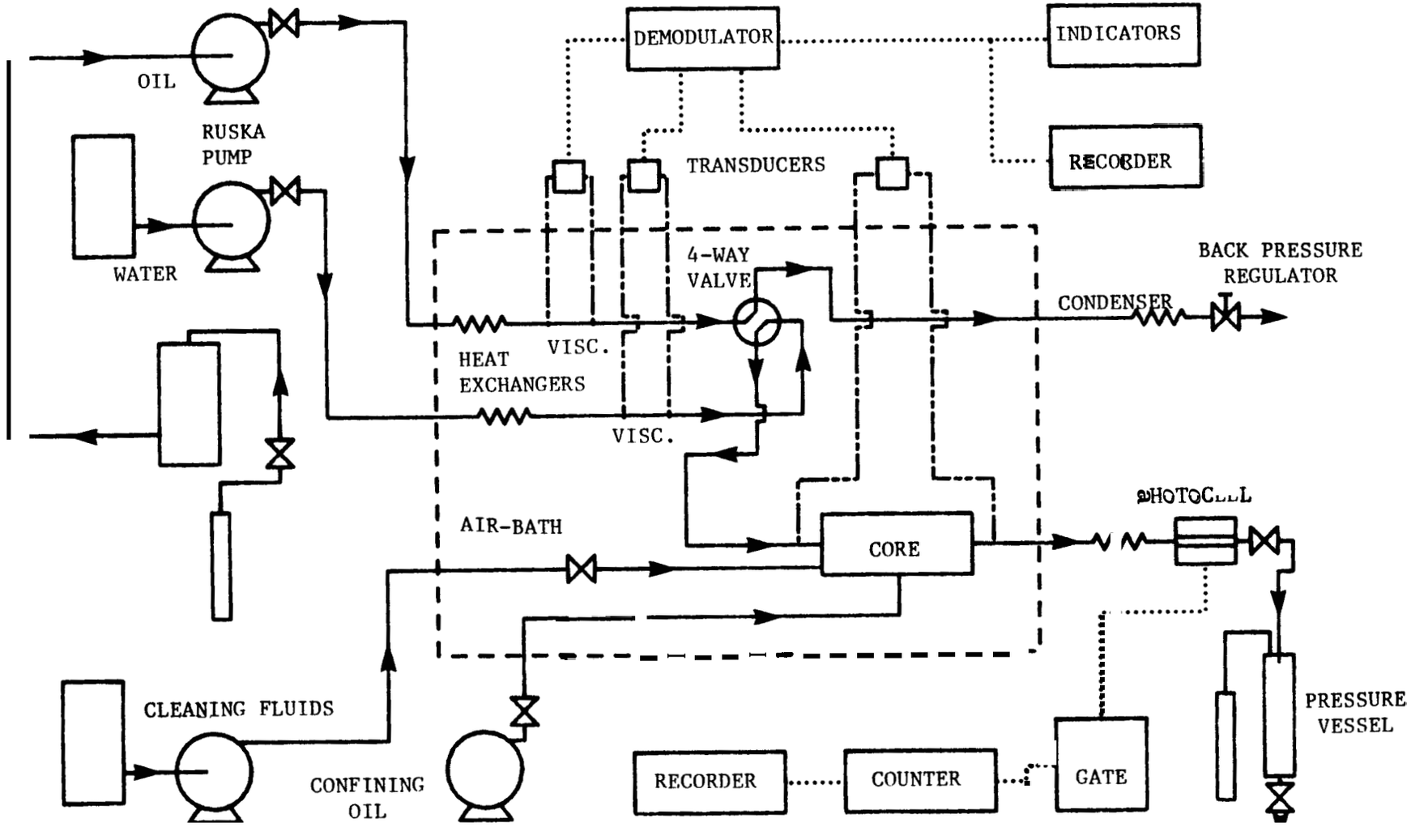

Fig. 4.11 SIMPLIFIED SCHEMATIC OF COMPLETE SYSTEM

1. after the heating coils in the oil and water lines,
2. at the inlet of the core,
3. at the outlet of the core, and
4. between the condenser and the photocell.

The thermocouples are connected to a IO-channel digital temperature indicator (Omega, model 2176 A-J). The temperature indicator is used to indicate when isothermal conditions have been reached.

This concludes the description of the equipment used in this study. The next section presents the procedure followed in performing the experiments.

4.9 Procedure and Experiments

Displacement experiments were conducted on Ottowa sand packs. The properties of the porous media and the fluids used are presented In Table 4.1. Cores were initially 100% saturated with water with the photocell assembly set to monitor water production. Both pistons of the Ruska pump were started at the desired flooding rate. At this point, water flowed through the four-way valve into the core. The pressure drop across the core was continuously recorded on the chart recorder. The oil left the four-way valve to the spring-loaded regulator. The regulator was adjusted until the pressures at the switching valve were the same in both the water and oil lines. The four-way valve was then switched to allow oil to flow into the core. After the switch, the water cylinder of the Ruska pump was stopped. The tubing and fitting (dead) volume between the four-way valve and the core was 1.50 cc.

When the oil reached the sand face, a sharp increase in the

Table 4.1

PROPERTIES OF POROUS MEDIUM AND FLUIDS

Porous medium properties:

porous medium is Ottawa sand (mesh 170-200)

permeability, k = 5.3 darcys

porosity, ϕ = 0.394 cm

length, L = 17.8 cm

diameter, d = 2.54 cm

Fluid properties:

Oil used is Kaydol (equivalent to Chevron #15)

viscosity at 70°F = 220 cp

density at 70°F = 0.878 gm/cc

water used is distilled and demineralized

viscosity at 70°F = 0.97 cp

density at 70°F = 1.00 gm/cc

pressure drop was noted. The sudden increase corresponds to the capillary entrance pressure of the oil/water/sand system. As oil injection was continued, the pressure drop increased. The appropriate transducer was used to monitor the pressure drop. For the high viscosity oil used, oil displacement of water was essentially piston-like. As a result, the pressure drop increased until breakthrough and then remained constant. Four pore volumes of oil were injected to ensure that irreducible water saturation was reached. Once irreducible water saturation was obtained, the water cylinder of the Ruska pump was restarted. Once again, the spring-loaded regulator was adjusted to match pressures in the oil and water lines upstream of the four-way valve. The pressure drop at this stage was the initial pressure drop used in calculating relative injectivities. Once the four-way valve was switched and waterflooding initiated, the pressure decreased steadily. A record of this pressure drop was used to calculate the individual relative permeabilities.

During an oil flood, the produced water was measured. By material balance, the core saturation was determined. Then, at the start of a water flood, the cell assembly was set to monitor oil production. As oil was produced from the core, the cell provided a trace of oil production versus time on the chart recorder. The dead volume of the flow lines from the core was 6.4 cc. This, together with the dead volume of the flow lines into the core, was subtracted from the produced oil during the material balance calculations. A record of the saturation history was used to determine the permeability ratios.

In the later part of the study when the vertical glass columns were used in conjunction with the photocell, both the inlet four-way valve

and outlet three-way valve were operated simultaneously. In this case, a visual record of the oil produced was kept throughout the life of the flood.

The next section presents the equations used for computing the relative permeabilities. The technique is based on the method presented by Jones and Roszelle (1978).

5. ANALYSIS OF DATA

This study calculates relative permeabilities from dynamic displacement experiments. Each run is performed at a constant rate. During a run, the pressure drop and oil produced are recorded continously as functions of time. This section presents the equations used to compute relative permeability from the test data using the Jones-Roszelle *(1978)* graphical technique. Derivation of these equations is presented in Appendix A-1.

By measuring oil produced as a function of pore volumes of water injected, W_i, the change in the average saturation within the core, $\bar{S}_w - S_{wi}$, can be calculated and graphed. If a tangent is drawn to this curve, the point of tangency corresponds to the change in average water saturation, while the intercept for $W_i = 0$ corresponds to the change in outlet face saturation, $S_{w2} - S_{wi}$. The oil cut at the outlet face, f_{o2}, is then calculated from:

$$W_i \, f_{o2} = \bar{S}_w - S_{w2} \tag{5.1}$$

Knowing f_{o2}, permeability ratio can be calculated from the equation

$$\frac{k_{ro}}{k_{rw}} = \left(\frac{\mu_o}{\mu_w}\right)\left(\frac{f_{o2}}{1 - f_{o2}}\right) \tag{5.2}$$

The permeability ratio obtained from Eq. 5.2 corresponds to the outflow face saturation, S_{w2}.

The individual relative permeabilities can be calculated by using the pressure drop data. The parameter used is relative injectivity defined by:

$$\frac{1}{I_r} = \frac{(\Delta p/q)}{(\Delta p/q)_i} \tag{5.3}$$

where I_r is the relative injectivity, AP the pressure drop, and q the flowrate at that time. The subscript i refers to conditions at the start of the flood.

To analyze the data, $1/I_r$ is graphed vs W_i. A tangent to the resulting curve has an intercept with the y-axis, $1/I_0$, given by:

$$\frac{1}{I_0} = \frac{f_{o2}}{k_{ro2}} \tag{5.4}$$

where k_{ro2} is the relative permeability to oil at the outlet face saturation. In Eq. 5.4, the values of I_0 and f_{o2} corresponding to the same W_i are used and k_{rw2} is obtained by combining results from Eqs. 5.2 and 5.4.

When W_i becomes large, drawing tangents and extrapolating to the ordinate may cause large errors in calculations. For large W_i, both the saturation change and the relative injectivity can be graphed versus $1/W_i$. The tangent to the saturation curve will now result in an intercept, S_w^*. This intercept can be related to the outlet face saturation by:

$$S_w^* = 2\,\bar{S}_w - S_{w2} \tag{5.5}$$

Similarly, the corresponding tangent on the relative injectivity vs $1/W_i$ curve intersects the ordinate at $1/I_r^*$. This intercept is related to k_{ro2} through:

$$\frac{f_{o2}}{k_{ro2}} = \frac{2}{I_r} - \frac{1}{I_r^*} \tag{5.6}$$

Equations *5.5* and *5.6* permit accurate determination of relative permeabilities towards the end of the flood.

A computer program has been written to perform the graphical computations. A listing of this program is provided in Appendix A-2.

6. RESULTS AND DISCUSSION

The results are presented in six sections, each studying a separate parameter as outlined by the heading. These sections are:

1 rate effects on Buckley-Leverett front

2 viscous instabilities

3 temperature effects on residual oil saturation

4 temperature effects on irreducible water saturation

5 temperature effects on relative permeability curves

6 interdependence of end-point saturations

Discussions and explanations of the results are given for the observed trends. When possible, other works showing similar results are cited.

6.1 Rate Effects on Buckley-Leverett Front

The front stability criterion of Rapoport and Leas (1953) indicates waterfloods should be conducted above a minimum rate as governed by the scaling factor, $Lv\mu_w$. However, due to a holdup of the wetting phase, water, experimental determination of this minimum rate is not easy. In this study, another method was used in which relative permeability curves were obtained at different rates. Theoretically, relative permeabilities are independent of flowrate. Cores, initially saturated

with oil, were waterflooded to residual oil saturation. These floods were conducted at velocities of 3.947, 19.735, 47.365 and 78.941 cm/hr (flowrates of 20, 100, 240 and 400 cc/hr). Figure 6.1 shows room temperature residual oil saturations as a function of flowrate. (Data for residual oil saturation is presented in Appendix B-9). Within experimental error, no change was observed. However, as shown by Fig. 6.2, a definite trend was observed in the relative permeability curves generated from these runs. (The data from which the relative permeability curves were constructed is presented graphically in Appendix B-1 and in tabular form in Appendix B-3). Although the relative permeabilities for oil remained relatively unchanged, the water relative permeability curves were lower at 20 and 100 cc/hr, only becoming rate-independent above 240 cc/hr. It was assumed that 240 cc/hr indicates the minimum rate for front stability required by the Rapoport and Leas theory. This technique of determining a stable rate for waterflooding is an original finding of this study.

Two physical interpretations of the effect of flow rate are obvious. The first concerns capillary smearing of the front at low flowrates. This can be visualized from Fig. 6.3 which shows hypothetical saturation profiles at two different rates. At a high rate a shock front, as dictated by Buckley-Leverett theory, will form as shown in Fig. 6.3a. However, once the velocity is reduced below a critical value, capillary forces dominate viscous pressure gradients and pull water ahead of the advancing water front. This causes the smeared saturation profile shown in Fig. 6.3b. Such a situation could result in significantly different fluid distributions within a core at different rates. These differences may cause changes in pressure drop across the

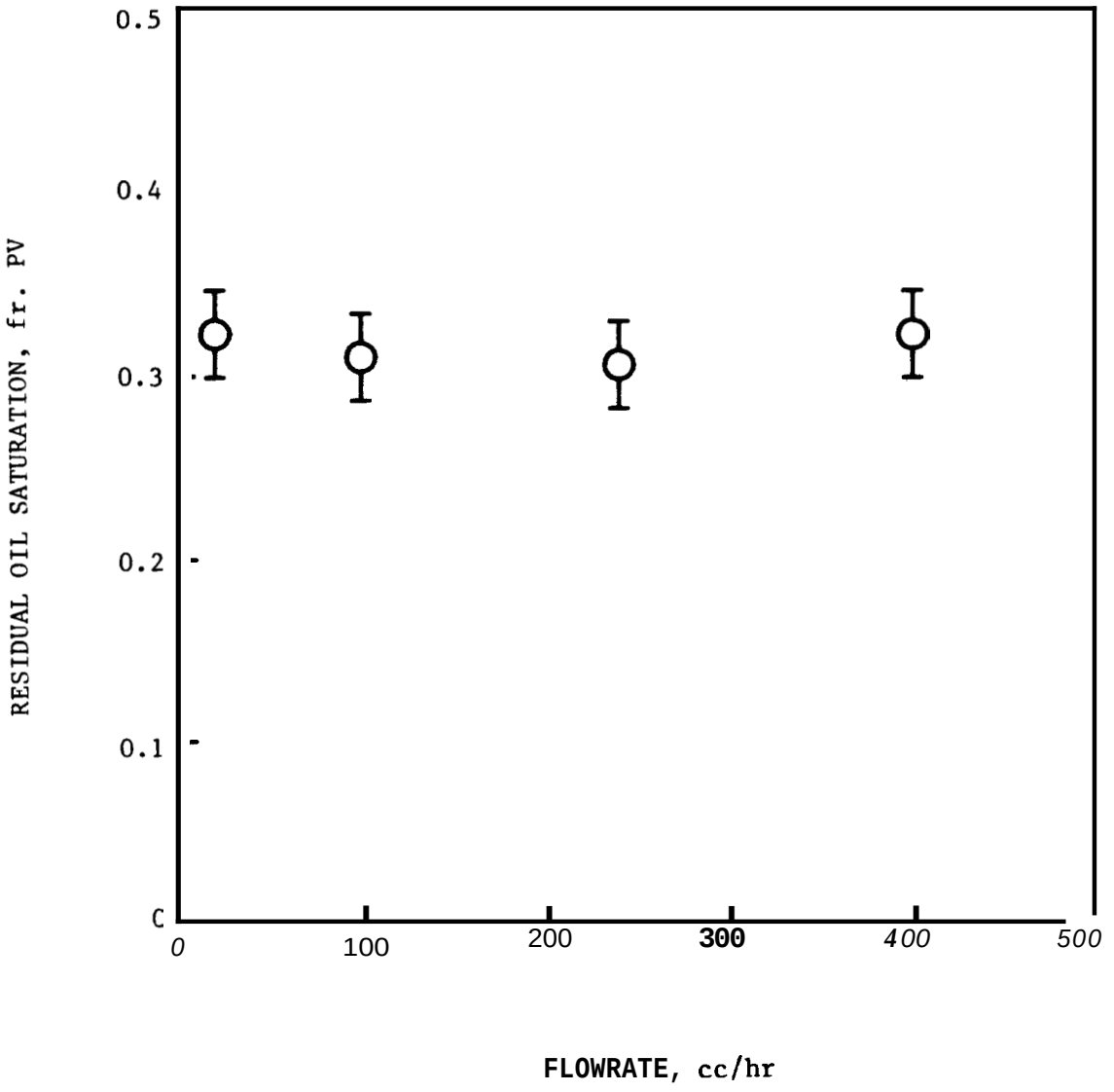

Fig. 6.1 RESIDUAL OIL SATURATION VS FLOWRATE (TEMPERATURE = 70°F)

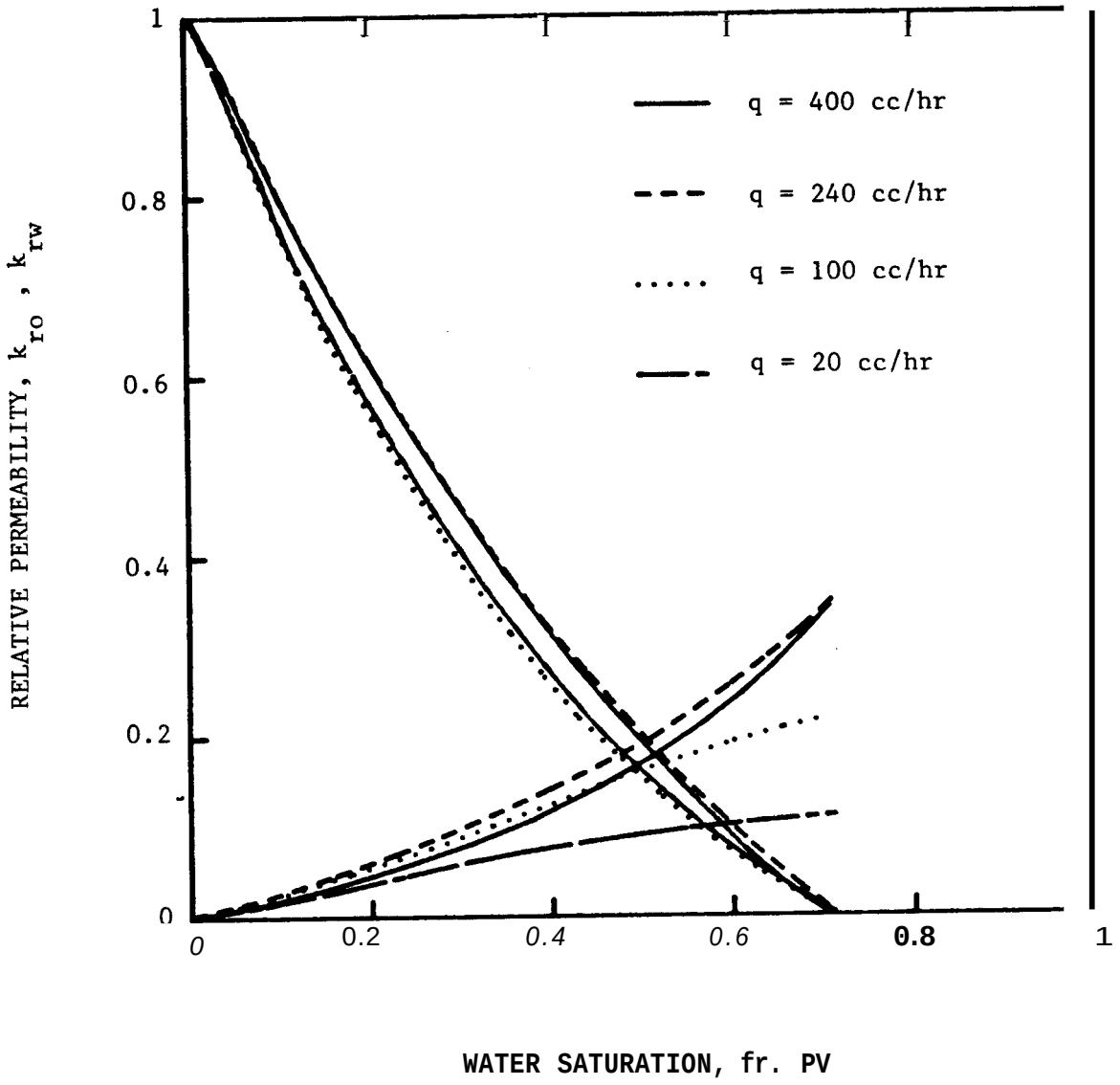

Fig. 6.2 COMPUTED OIL AND WATER RELATIVE PERYEABILITIES VS WATER SATURATION FOR SEVERAL FLOODING RATES (TEMPERATURE = 70°F)

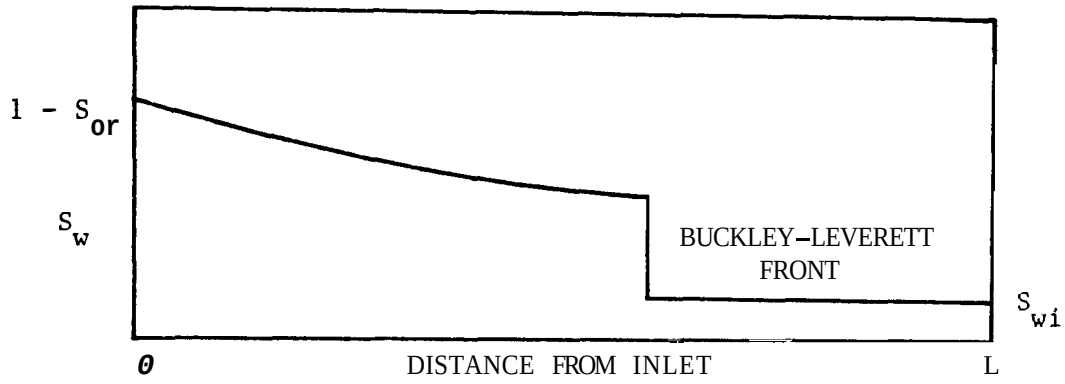

Fig. 6.3a WATERFLOODING AT A HIGH RATE

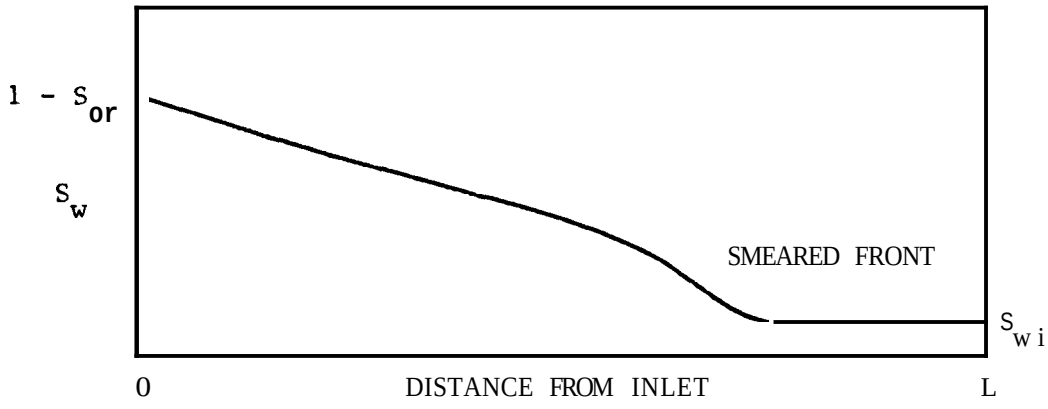

Fig. 6.3b WATERFLOODING AT A LOW RATE

Fig. **6.3** EFFECT OF WATERFLOODING RATE ON THE SHAPE OF THE BUCKLEY–LEVERETT FRONT

core which could result in an apparent rate dependence of the relative permeability curves.

A second explanation of the observed behavior centers around the capillary end effect. During a water flood on a water wet core, the saturation at the outflow face remains near the residual oil saturation. This buildup of the wetting phase saturation causes an additional pressure drop near the outflow face as a result of lower permeability to oil, as shown in Fig. 6.4. At low velocities, the pressure drop caused by this saturation buildup, Δp_l, can be a major portion of the total pressure drop, Δp. Increasing the velocity can result in two changes. First, the length of the zone affected by the end effect may decrease due to higher viscous forces. Second, the total pressure drop, Δp, increases more than the increase in Δp_l. Hence, the percentage contribution from the end effect decreases. This behavior matches results published by Hadley and Handy (1956). The decreased contribution of Δp_l at increased rates could yield the rate-dependent curves of Fig. 6.2. Above 240 cc/hr, the contribution from the end effect may be negligible, resulting in further insensitivity to flow rate.

A similar sensitivity analysis was done at 150" F. Three different rates of 20, 240 and 400 cc/hr were used. Fig. 6.5 shows residual oil saturation as a function of flow rate. Once again, no significant change in residual oil saturation was observed with rate, within experimental error. There was a large apparent decrease in residual oil saturation (compare Fig. 6.1 with Fig. 6.5) with temperature which will be discussed in Section 6.3. The relative permeability curves again showed rate dependence below 240 cc/hr as shown in Fig. 6.6.

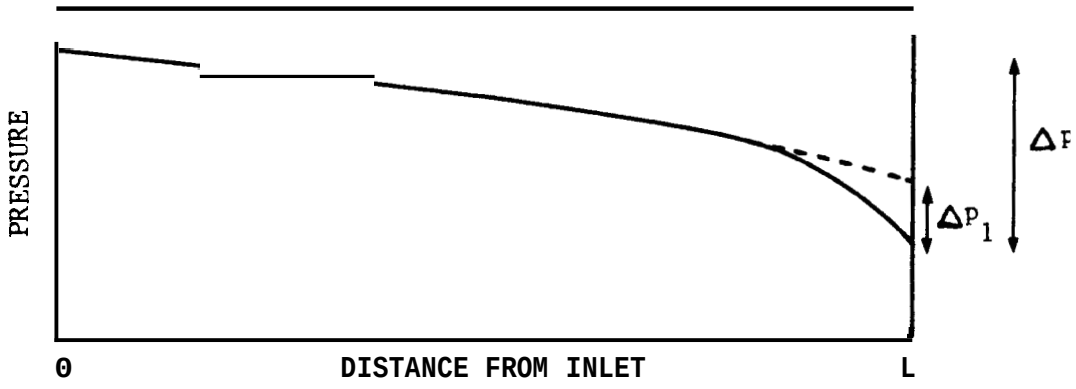

Fig. 6.4a PRESSURE DISTRIBUTION IN CORE WITH OUTLET END EFFECT

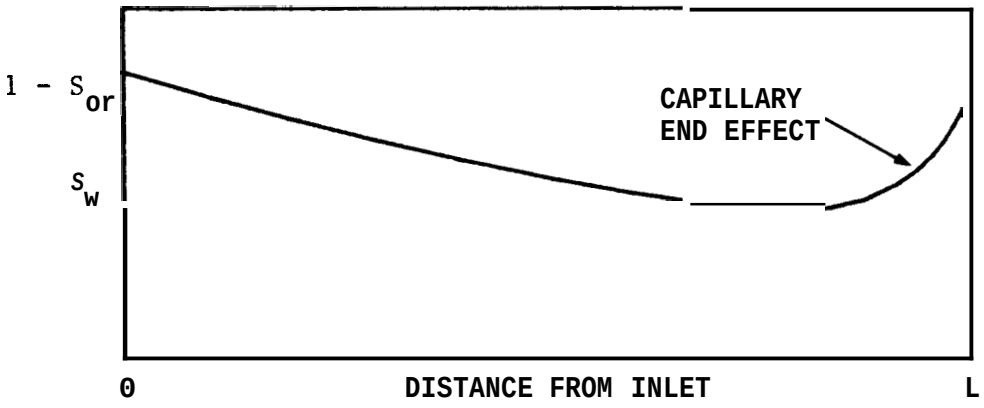

Fig. 6.4b SATURATION DISTRIBUTION IN CORE WITH OUTLET END EFFECT

Fig. 6.4 SATURATION *AND* PRESSURE DISTRIBUTIONS IN A CORE WITH CAPILLARY END EFFECTS DURING WATERFLOODING

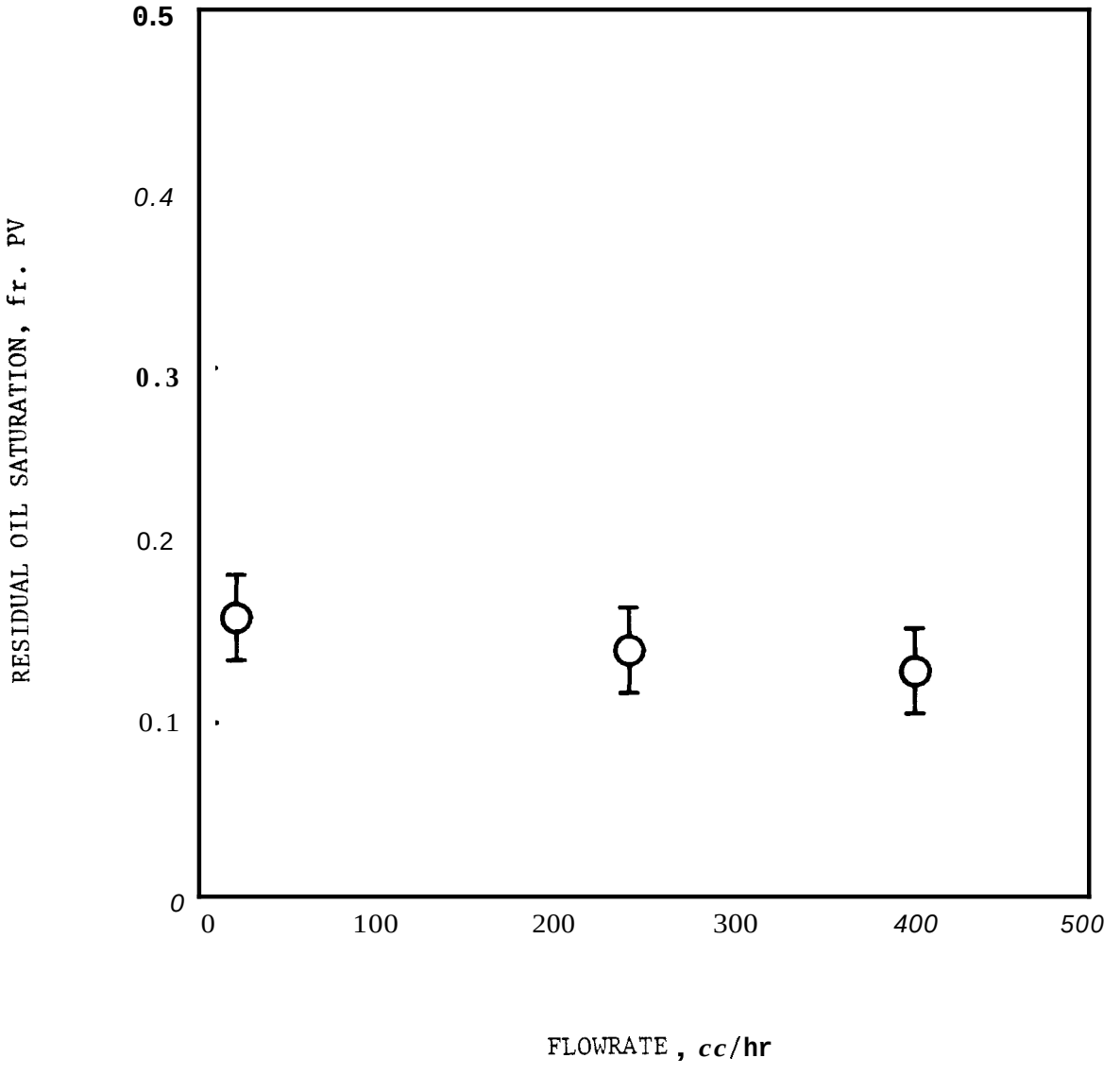

Fig. 6.5 RESIDUAL OIL SATURATION VS FLOWRATE (TEMPERATURE = 150°F)

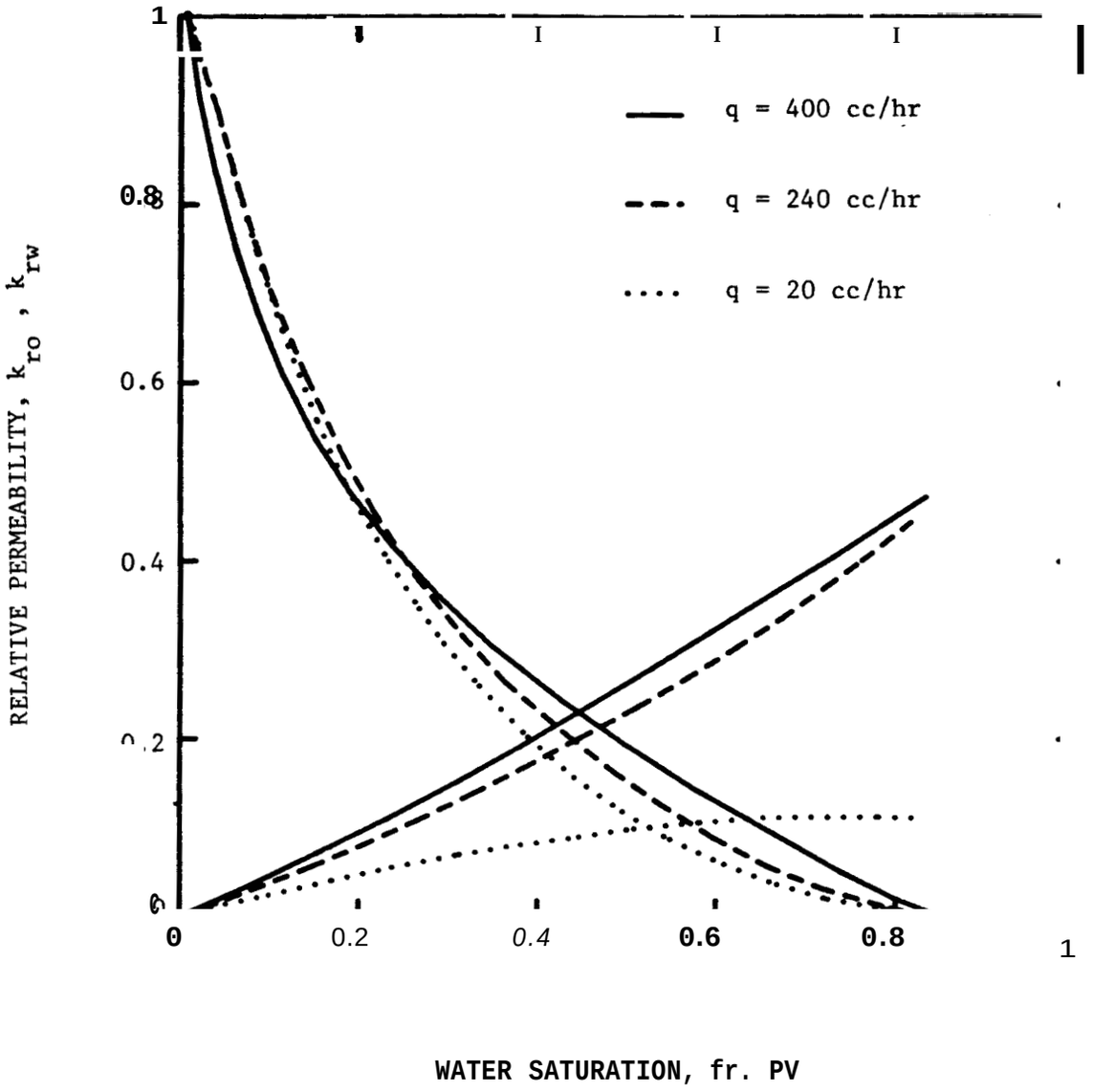

Fig. 6.6 COMPUTED OIL AND WATER RELATIVE PERMEABILITIES VS WATER SATURATION FOR SEVERAL FLOODING RATES (TEMPERATURE = 150°F)

On the assumption that the rate dependence is caused by the Rapoport and Leas stability criterion, a range for the minimum scaling coefficient for Buckley-Leverett displacement can be derived. Room temperature floods at 100 cc/hr resulted in a lower water relative permeability than at 240 cc/hr. At 100 cc/hr, the value of the scaling coefficient, $LV\mu_w$, was 5.85 cm^2-cp/min. At 150°F, a flow rate of 240 cc/hr corresponds to a scaling coefficient of 5.97 cm^2-cp/min. The 100 cc/hr run at room temperature showed rate dependence while the 240 cc/hr run at 150°F did not. This would indicate that the critical value of $LV\mu_w$ is between 5.85 cm^2-cp/min and 5.97 cm^2-cp/min. Hence, for floods to 200°F, 400 cc/hr was used as a waterflooding rate. At 200°F, water viscosity is 0.303 cp, resulting in a scaling coefficient of 7.09 cm^2-cp/min for a flowrate of 400 cc/hr. This value was above the 5.97 cm^2.cp/min apparently corresponding to a stable flood.

The minimum scaling coefficient may be determined by oilflooding a water-saturated core. However, for a 220 cp oil, the flow rate would have to be less than about 1 cc/hr to permit unstable flow. The pump used in this experiment has a minimum flow rate of 5 cc/hr which made this technique impossible. However, this method is suggested here as a possible means of determining the minimum scaling coefficient value. If this method was used, it would be necessary to assume that the minimum scaling coefficient value is the same for a waterflood as for an oilflood.

In waterflooding viscous oils, unstable flow may occur due to viscous fingering. The next section presents results identifying rates above which this phenomenon occurred during the experiment.

6.2 Viscous Instabilities

Instabilities were first suspected due to strange recovery versus time profiles seen immediately following breakthrough. Some holdup within the exit tubing from the core was also suspected. Experiments were made to identify at which rates instabilities develop in the core. By varying tubing lengths from the core, the magnitude of instabilities within the tubing was also estimated.

The first set of runs consisted of waterfloods on an oil-saturated core. The efflux passed through 10.2 cc tubing volume after leaving the core. Figure 6.7 shows breakthrough oil recovery vereus flooding rate. The recovery remained constant as flowrate increased to 100 cc/hr, beyond which, oil recovery decreased sharply. However, above 400 cc/hr, the breakthrough oil recovery remained constant again. This behavior has also been observed by Peters and Flock (1979). The sharp decrease in oil recovery occurs when viscous fingers develop and grow in the system. There is holdup of the wetting phase. However, the fingers build up sufficient water saturation to flow out before the water front reaches the outlet face. The theory presented by Peters and Flock indicates that as flowrate is increased, a few large fingers develop first. Further increase of the rate causes more, smaller fingers to develop. Above 400 cc/hr, the face becomes "saturated" with the fingers and breakthrough recovery stabilizes.

To study the effect of fingering within the exit tubing after the core, the same set of experiments were conducted with the exit tubing volume reduced to 2.4 cc. The points obtained for these runs are graphed on Fig. 6.8. A trend similar to that observed on Fig. 6.7 is

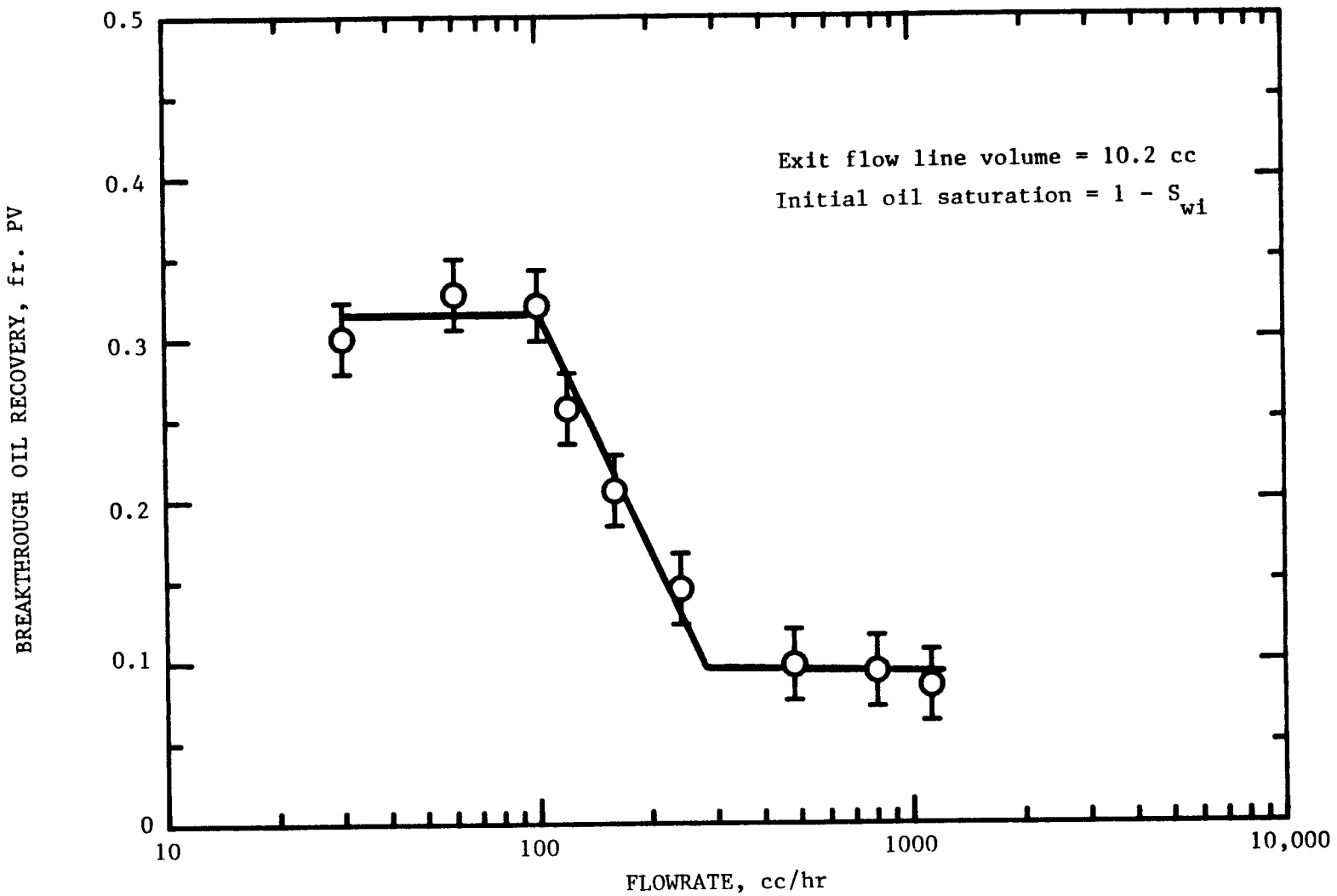

Fig. 6.7 BREAKTHROUGH OIL RECOVERY VS FLOWRATE FOR OIL SATURATED CORES (TEMPERATURE = $70^{o}F$)

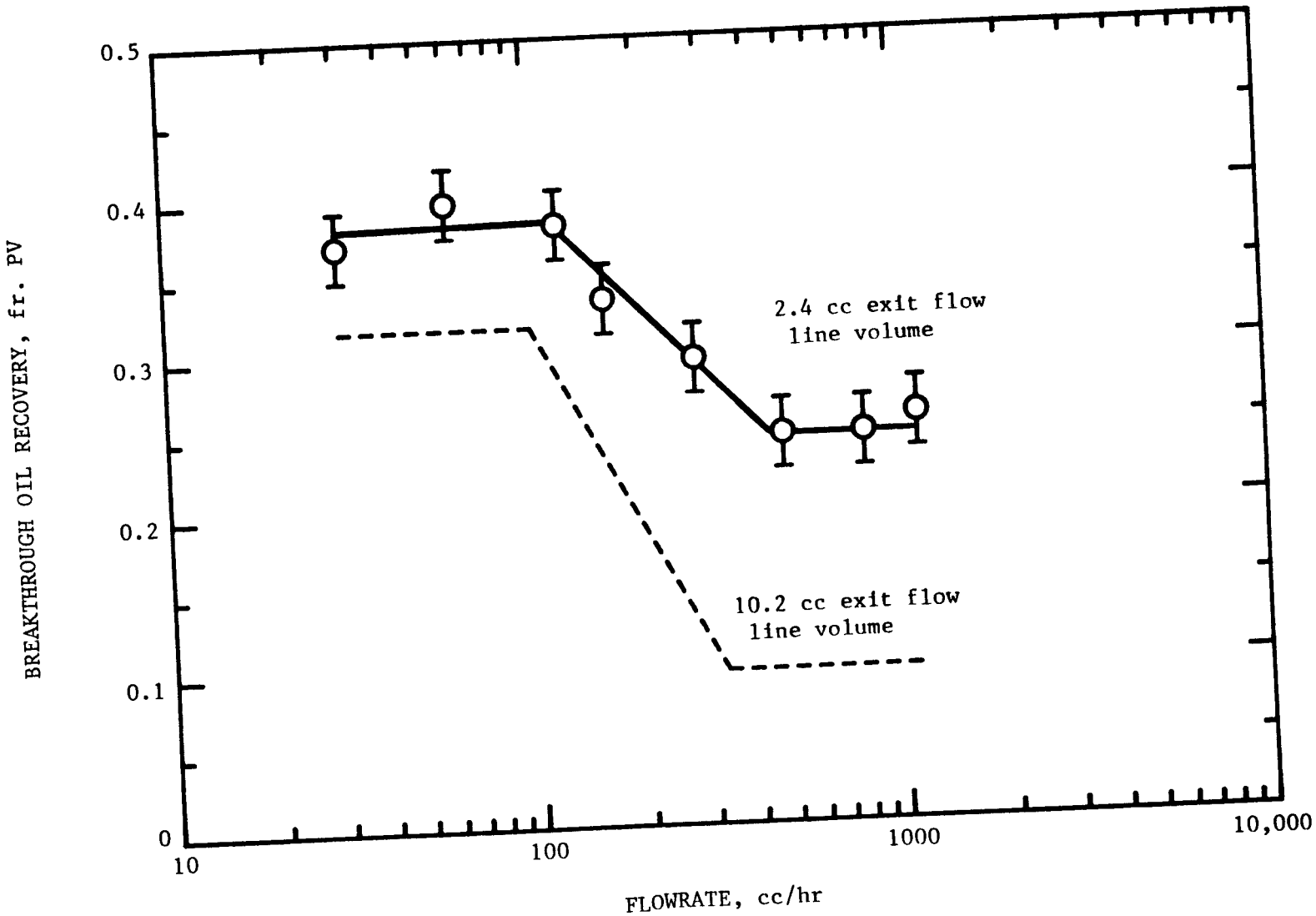

Fig. 6.8 BREAKTHROUGH OIL RECOVERY VS FLOWRATE FOR DIFFERENT EXIT FLOW LINE VOLUMES (T = 70°F)

evident with some important differences. In comparison with runs for the 10.2 cc exit flow line volume, shown by the dashed line, the breakthrough oil recoveries are consistently higher. This indicate that the exit flow tubing causes fingering no matter what the flowrate. Again, a decrease in breakthrough oil recovery was observed with an increase in flowrate. However, the magnitude of the decrease was smaller for the smaller exit flow line volume.

Another run was conducted with an exit tubing volume of 6.0 cc. The breakthrough oil recoveries for the three tubing volumes at a flowrate of 60 cc/hr are presented in Fig. 6.9. A linear trend is apparent. Extrapolation of the data to a zero tubing volume yields a breakthrough oil recovery of 42% of pore volume.

This part of the study raises two interesting points. The first is that the tubing downstream of the core may cause fingering of water after breakthrough, resulting in erroneous breakthrough recoveries. The volume of tubing after the core is subtracted from the volume of oil produced in determining saturations within the core. If part of the oil is bypassed in the tubing, material balance calculations will yield lower water saturations at breakthrough. The ultimate recovery would not change, as the oil bypassed in the tubing would eventually be flushed. The importance of the bypassing of the oil depends on the relative volumes of the core and the exit tubing dead volume.

The second and more important result of the study is the viscous fingering within the core. Relative permeabilty curves are calculated based on linear Buckley-Leverett displacement. Viscous fingering leads to a violation of the assumption of linear one dimensional flow. The relative permeabilities calculated in such a situation represent psuedo-

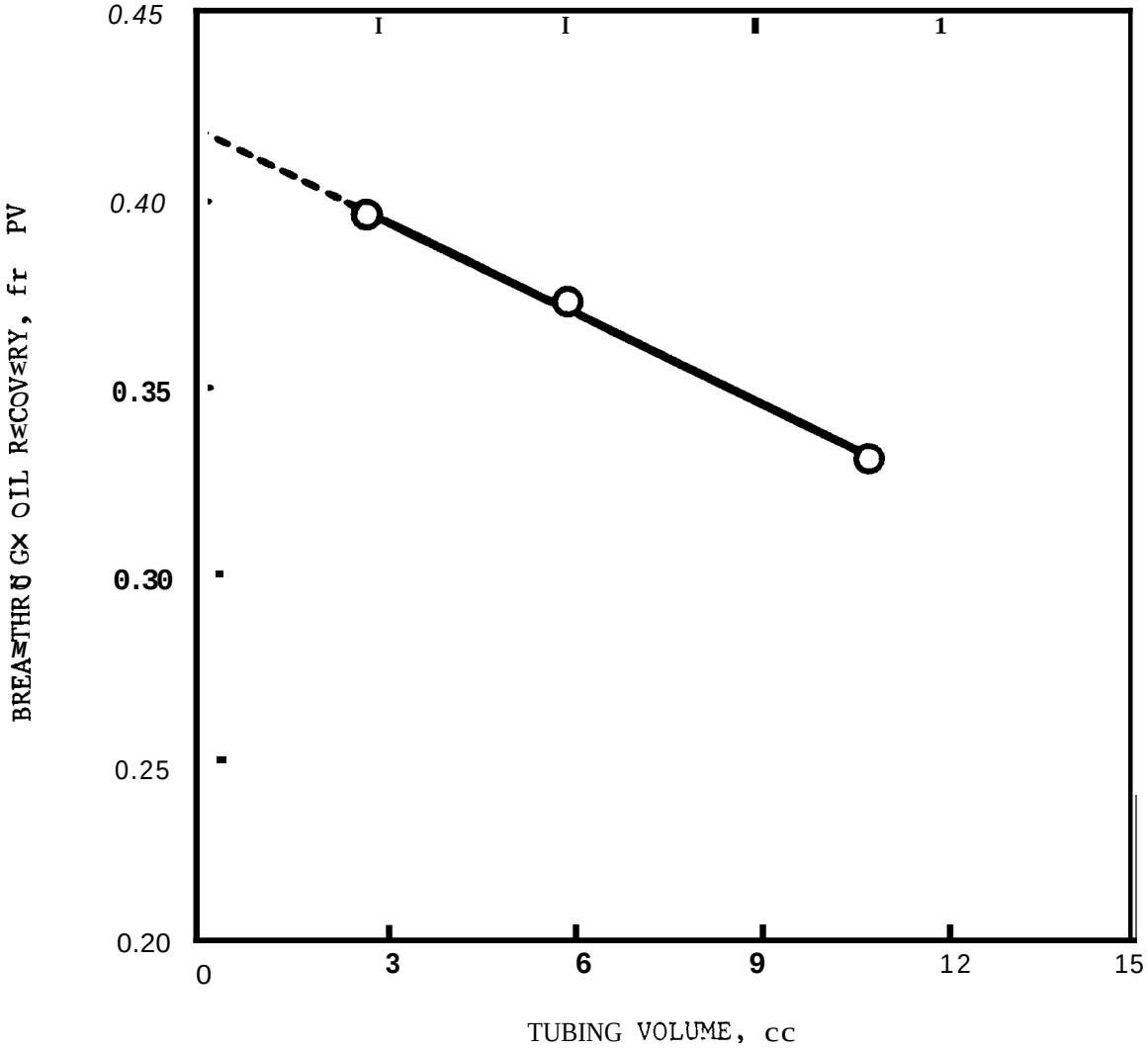

Fig. 6.9 BREAKTHROUGH OIL RECOVERY VS EXIT TUBING VOLUME FOR A FLOWRATE FLOWRATE OF 60 cc/hr (TEMPERATURE = 70°F)

relative permeabilities for that run. However, the curves may not be applicable to other systems. In core floods aimed at determining relative permeabilities for particular reservoirs, experiments should be conducted at flowrates low enough to avoid viscous fingering.

These results can be used to re-analyze certain data presented in the literature. Mungan (September, 1966) conducted core floods to study breakthrough and ultimate recoveries as functions of viscosity ratios. His Figs. 9 and 10 are reproduced here as Figs. 6.10a and 6.10b. These fingers show a sharp increase in breakthrough recoveries for both oil-wet and water-wet cores when the viscosity ratio changes from unfavorable to favorable. Viscous fingering has been shown by Peters and Flock (1979) to be more severe when the displacing fluid is non-wetting. Figure 6.10b corresponds to displacement by a non-wetting phase, and shows a larger increase in breakthrough recovery.

Newcombe et al., (1955) show an increase in breakthrough recovery for an increasing scaling coefficient, given by $LV\mu_w \sigma/\mu_o \cos\Theta$ if Θ is less then 90° and $LV\mu_w/\sigma\mu_o \cos\Theta$ if Θ is greater then 90°. This suggests an interplay between viscous and capillary forces within the pores. However, a decrease in breakthrough recovery was observed when the oil being displaced had a high viscosity. Instabilities can be used to explain these reductions in breakthrough recovery for the viscous oils.

In the temperature study, a displacement rate of 400 cc/hr was used. Although this rate corresponds to conditions of viscous instability in the core, it is the minimum rate satisfying the Rapoport and Leas stability criterion at the highest temperature in this study. Due to the large decrease in the oil viscosity with temperature

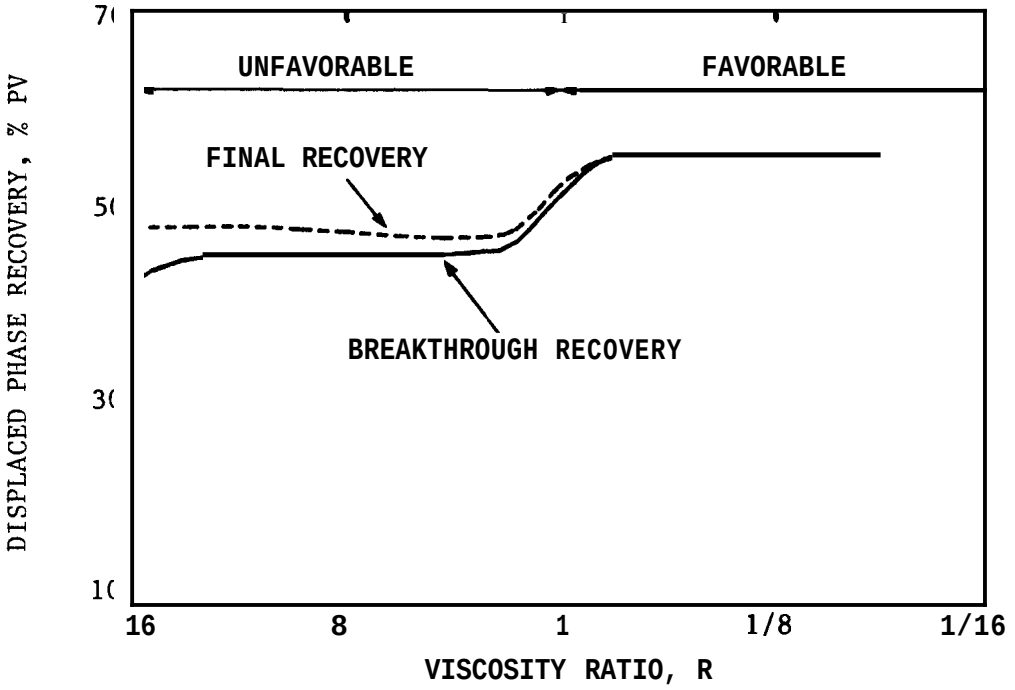

Fig. 6.10a WETTING PHASE DISPLACING NON-WETTING

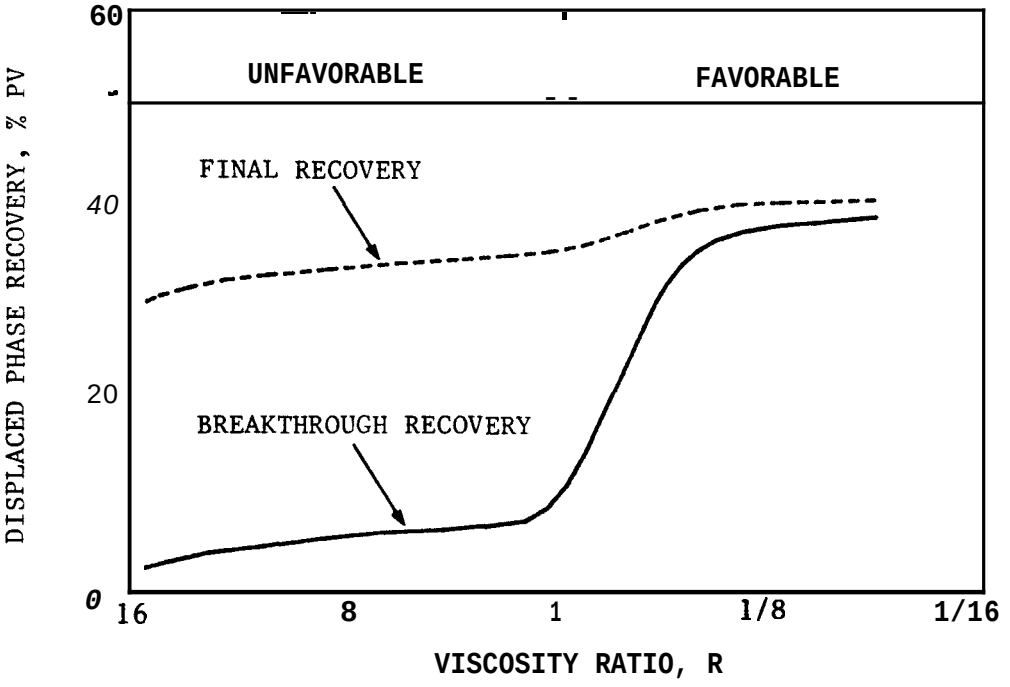

Fig. 6.10b NON-WETTING PHASE DISPLACING WETTING

Fig. 6.10 DISPLACED PHASE RECOVERY VS VISCOSITY RATIO
(MUNGAN, September 1966)

increase, viscous fingering was not anticipated above 100°F. With the dimensions of the core and the viscosity of the oil used in this study, it was not possible to operate room temperature core floods at rates which would simultaneously satisfy the Rapoport and Leas stability criterion and also avoid viscous fingering. This problem has been identified by Bentson and Saeedi **(1981)** for core floods with viscous oils.

6.3 Temperature Effects on Residual Oil Saturation

Residual oil saturations obtained at 400 cc/hr for three temperatures are shown in Fig. **6.11.** These results are for runs starting with an oil saturation of 100% PV. For each run, the initial state was reached by successively flushing the core at room temperature with acetone, iso-propyl alcohol, mineral spirits and refined oil. The value of residual oil saturation decreased from **31%** PV at room temperature **to 9%** PV at 250°F. The residual oil saturation was taken as the point corresponding to a water cut of **99+** percent. Once this set of runs was completed, another series of displacements were conducted which continued the water floods to completion. In the latter case, residual oil saturations showed little decrease with temperature. These results are shown in Fig. 6.12. There was a small decrease in residual oil saturation from room temperature to 120°F but there is some question as to whether the room-temperature floods were run to completion. The room temperature floods were terminated after **155** pore volumes of water had been injected. The oil analysis system used for these late runs is the one shown in Fig. 4.9.

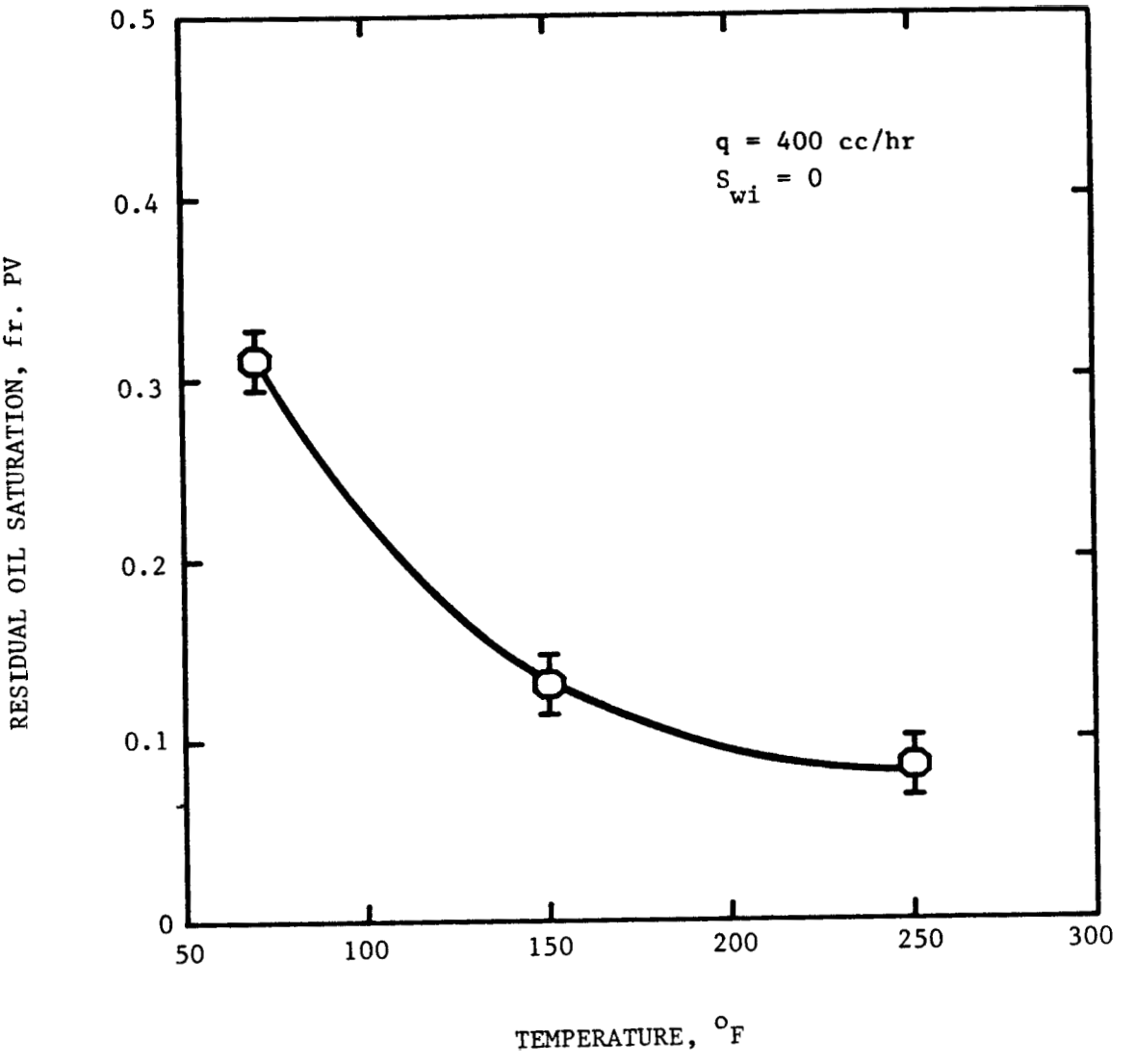

Fig. 6.11 RESIDUAL OIL SATURATION VS TEMPERATURE FOR WATERFLOODS TERMINATED AT 99^+ % WATER CUT

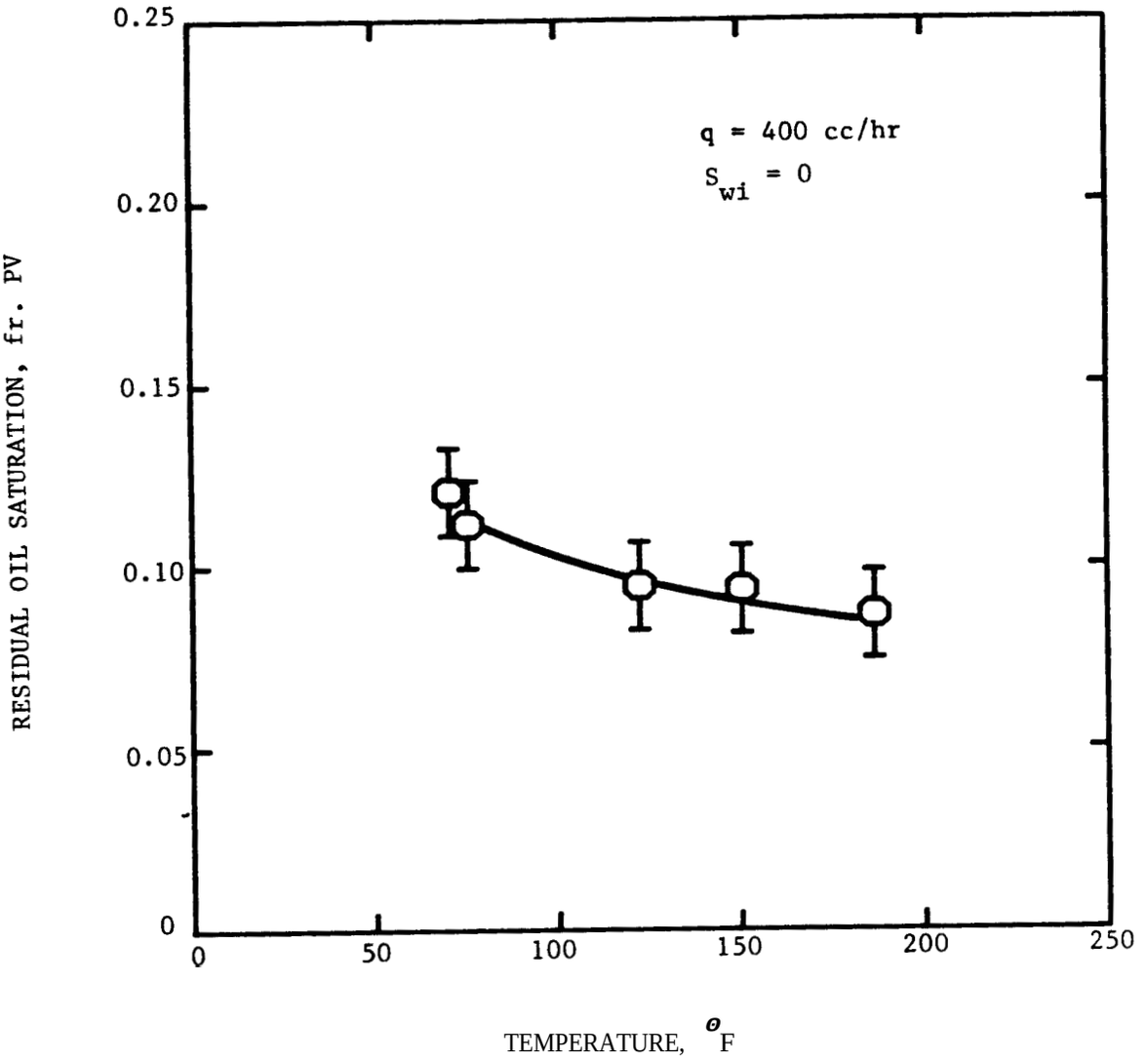

Fig. 6.12 **RESIDUAL** OIL SATURATION VS TEMPERATURE FOR WATERFLOODS CARRIED TO COMPLETION

The reason for the sensitivity of residual oil saturation to the water cut at which the run is terminated can be illustrated by Fig. 6.13. This is a graph of the fractional flows generated by complete core floods at different temperatures. (The data from which these curves were constructed is presented in Appendix B-6). As temperature increases, the viscosity ratio of the oil-water system decreases rapidly (220 cp at 70°F, 68 cp at 122°F and 28.5 cp at 186°F). Reduction in the viscosity ratio results in a change in shape of the fractional flow curves. For the three curves on Fig. 6.13, intersection with lines of constant f_w result in different saturations. If a line is drawn corresponding to f_w of 0.996, it intersects the 70°F, 122°F, and 186°F curves at water saturations of 70%, 80%, and 84%, respectively. If these saturations are assumed to correspond to residual oil saturations, an apparent reduction in S_{or} is observed with temperature increase, even though the actual residual oil saturation appears to be independent of temperature.

In reservoir performance, oil recovery is controlled by water cut at production wells. So, temperature may cause a change in the "practical" residual oil saturation. However, no change with temperature is evident in the terminal residual oil saturation found in this study.

These findings may explain some results of past researchers. Poston et al. (1970) terminated their waterfloods at a WOR of 100 and attempted to extrapolate residual saturations to a final value. For the viscous oils used, extrapolation to a terminal state was difficult. Thus a decrease in residual oil saturation with temperature increase is believed to be only an apparent increase. Similar reasoning could

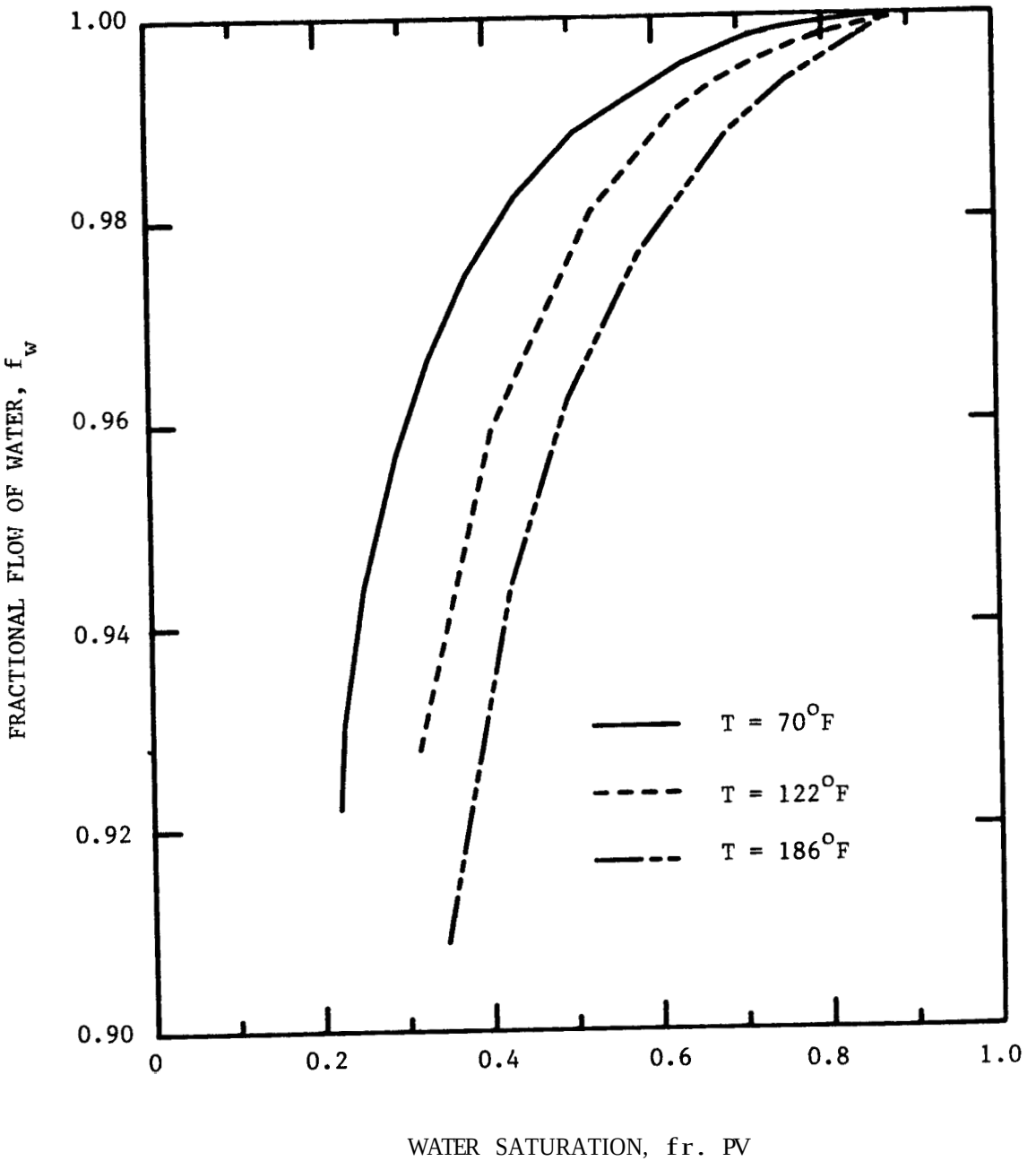

Fig. 6.13 WATER FRACTIONAL FLOW VS WATER SATURATION FOR WATERFLOODS AT SEVERAL TEMPERATURES

explain the work of Weinbrandt et al. (1975) and Lo and Mungan (1972) for viscous oils. Further, when Lo and Mungan used fluids showing no change in viscosity ratio with temperature, no temperature effects were observed on residual oil saturation. For a constant viscosity ratio, the f_w curves would not change in shape, resulting in the same apparent residual oil saturation at any temperature. Even the results of Sinnokrot, et al. (1971) giving residual oil saturations from capillary pressure measurements might be affected by a shift in fractional flow curves. In capillary pressure measurements, a shift in fractional flow curves would result in changing stabilizing times.

Runs were also made with cores initially containing oil at an irreducible water saturation. Within experimental error, the residual oil satuations were identical to ones obtained from core floods which started with 100% initial oil saturation. A comparison of two types of runs is presented in section 6.6.

It is concluded that observed changes in residual oil saturation with temperature change can be explained by changes in the fractional flow curve. Changes in wettability and interfacial tension, suggested by past researchers, are not required to explain temperature effects on oil recovery.

The next section presents results of experiments studying temperature effects on irreducible water saturation, S_{wi}.

6.4 Temperature Effects on Irreducible Water Saturation

A study of temperature level on irreducible water saturation was conducted by oil flooding a 100% PV water-saturated core. The floods

were conducted at various temperatures, and the results are presented on Fig. 6.14. (Data from oilfloods to determine S_{wi} are presented in Appendix B-7). The flowrate used was 400 cc/hr. Irreducible water saturation increased from 6.4% PV at 70°F to 8% PV at 186°F. This increase in S_{wi} has been considered by various researchers to be indicative of apparent increased water wetness of the core with increasing temperature. Figure 6.15 shows results of another study conducted in this part of the experiment. The water-saturated core was oil flooded at an initial low rate, 20 cc/hr, to irreducible water saturation. The oil flowrate was increased, and immediate water production was observed from the core. This early water production was followed by a period in which water flowed out as a fine suspension in the oil. This phenomenon was observed every time the oil flowrate was increased. Irreducible water saturation is graphed as a function of oil flow rate on Fig. 6.15. The decrease in irreducible water saturation corresponds to additional water produced from the core at higher flow rates. The decrease was apparently due to an increase only in viscous forces. Immediate water production indicates a saturation change near the outlet face of the core. An explanation could be provided by the presence of an outlet end effect, as shown by Fig 6.16a. As the flow rate is increased, increased viscous forces push the end effect closer to the outlet core face, thereby producing water as soon as the rate is increased. The saturation distribution would then be approximated by Fig. 6.16b. The production of a fine suspension of water in oil corresponds to mobilization of trapped water by an increase in viscous forces. This can be explained by the pore model shown in Fig. 6.17. Water, being the wetting phase, is trapped in a small pore channel. The

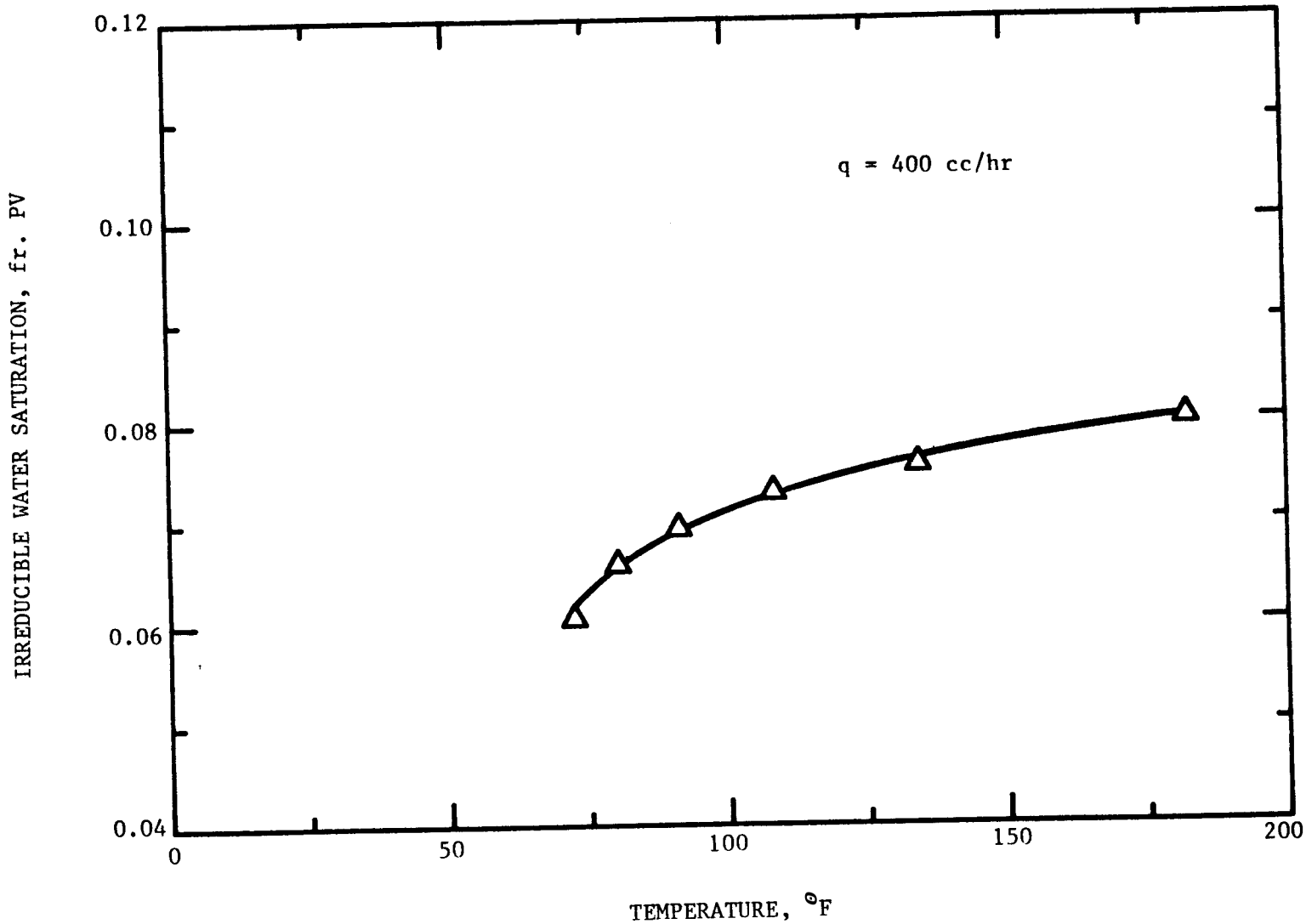

Fig. 6.14 APPARENT IRREDUCI: ≤ WATER SATURATION VS TEMPERATURE

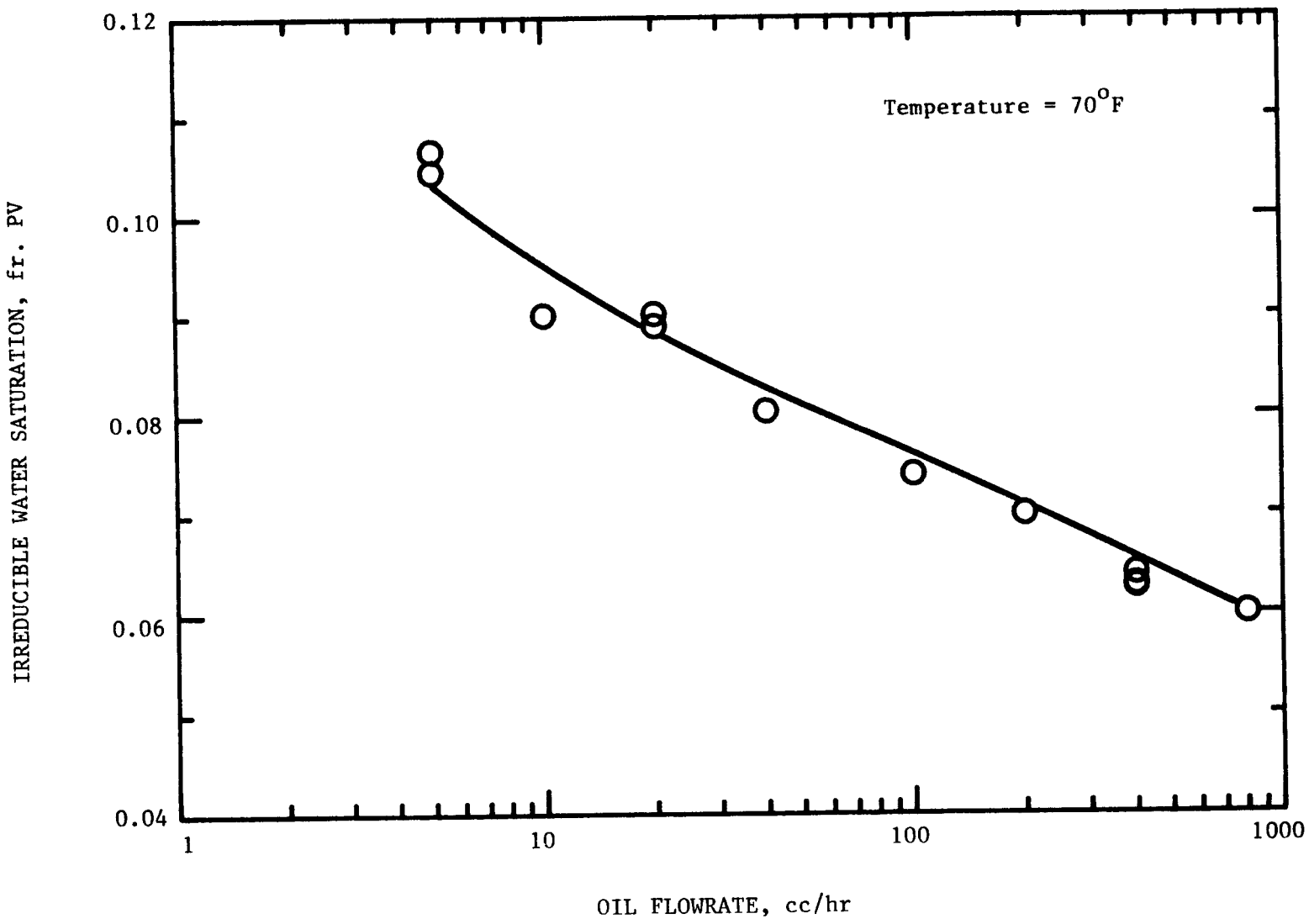

Fig. 6.15 IRREDUCIBLE WATER SATURATION VS OIL FLOWRATE AT ROOM TEMPERATURE

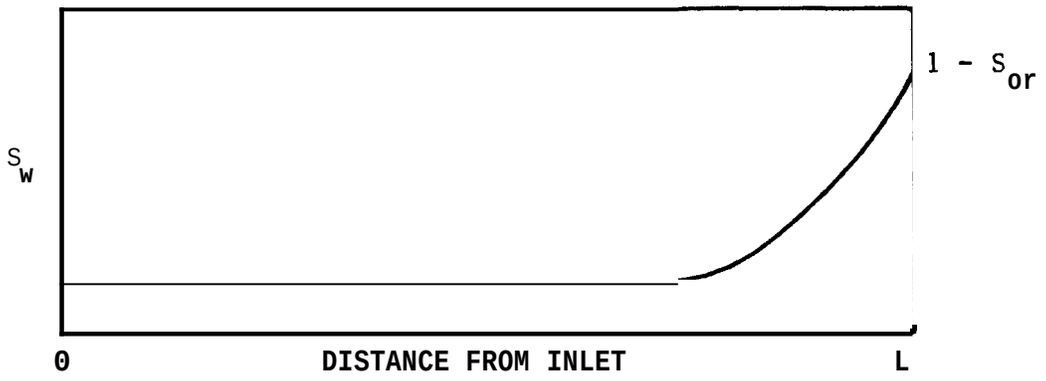

Fig. 6.16a OIL FLOODING AT LOW RATE

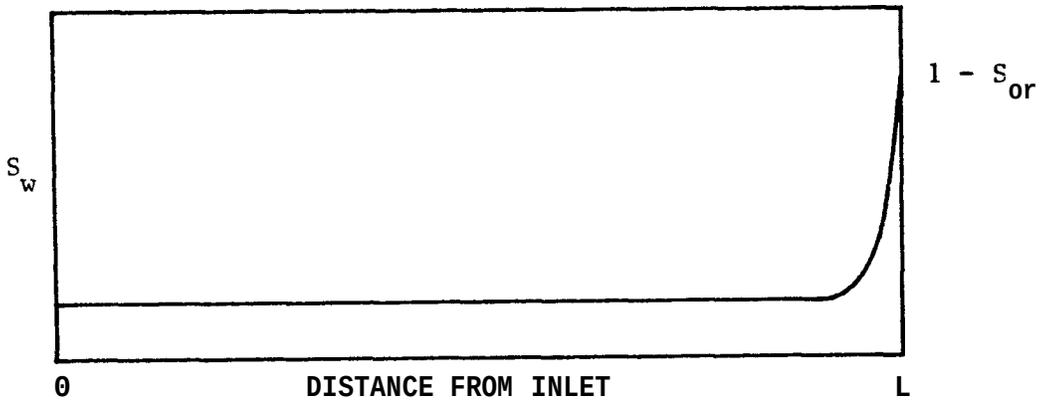

Fig. 6.16b OIL FLOODING AT HIGH RATE

Fig. 6.16 SATURATION PROFILE AT THE COMPLETION OF *AN* OIL FLOOD FOR TWO DIFFERENT FLOODING RATES, SHOWING THE EFFECT ON THE CAPILLARY END EFFECT

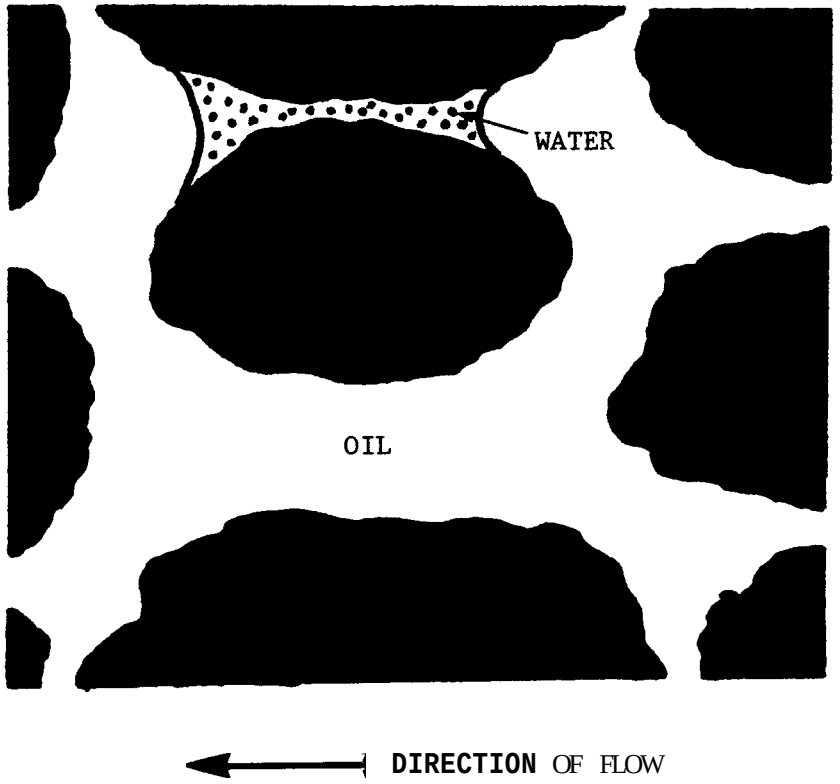

Fig. **6.17 TRAPPED WATER IN A WATER-WET POROUS MEDIUM**

amount trapped depends on a balance of capillary forces at the pore openings and the viscous pressure drop imposed by oil flow in the larger channels. As flow rate increases, so does the viscous pressure drop across the water filled pore, causing some trapped water to be mobilized. This mobil water is produced, and seen as a fine suspension in oil flow from the core.

The relative contributions of water production from capillary end effect, and production of trapped water caused by flowrate increases, could not be measured in this experiment. This inability was due to insufficient accuracy in material balance determination of the extra water produced from the core. Qualitatively, however, most of the saturation change occurred immediately upon increasing the flowrate, indicating a major portion of the decrease in S_{wi} was caused by a change in the capillary end effect.

To relate the results shown in Figs. 6.14 and 6.15, irreducible water saturation was graphed against the log of a viscous force term $q\mu_o$. The oil viscosity at flooding temperature was used. A graph of S_{wi} vs $q\mu_o$ is given on Fig. 6.18. Data points are coded as circles, triangles, and squares. The circles represent data generated by changing the flow rate, while the triangles correspond to results obtained by changing the temperature. The squares show results obtained by using refined oils having different viscosities to change the viscous force term.

As Fig. 6.18 shows, changes in irreducible water saturation appear to depend only on a change in the viscous force, whether caused by a temperature, fluid or rate change. This indicates that apparent changes in irreducible water saturation with temperature level are not caused by

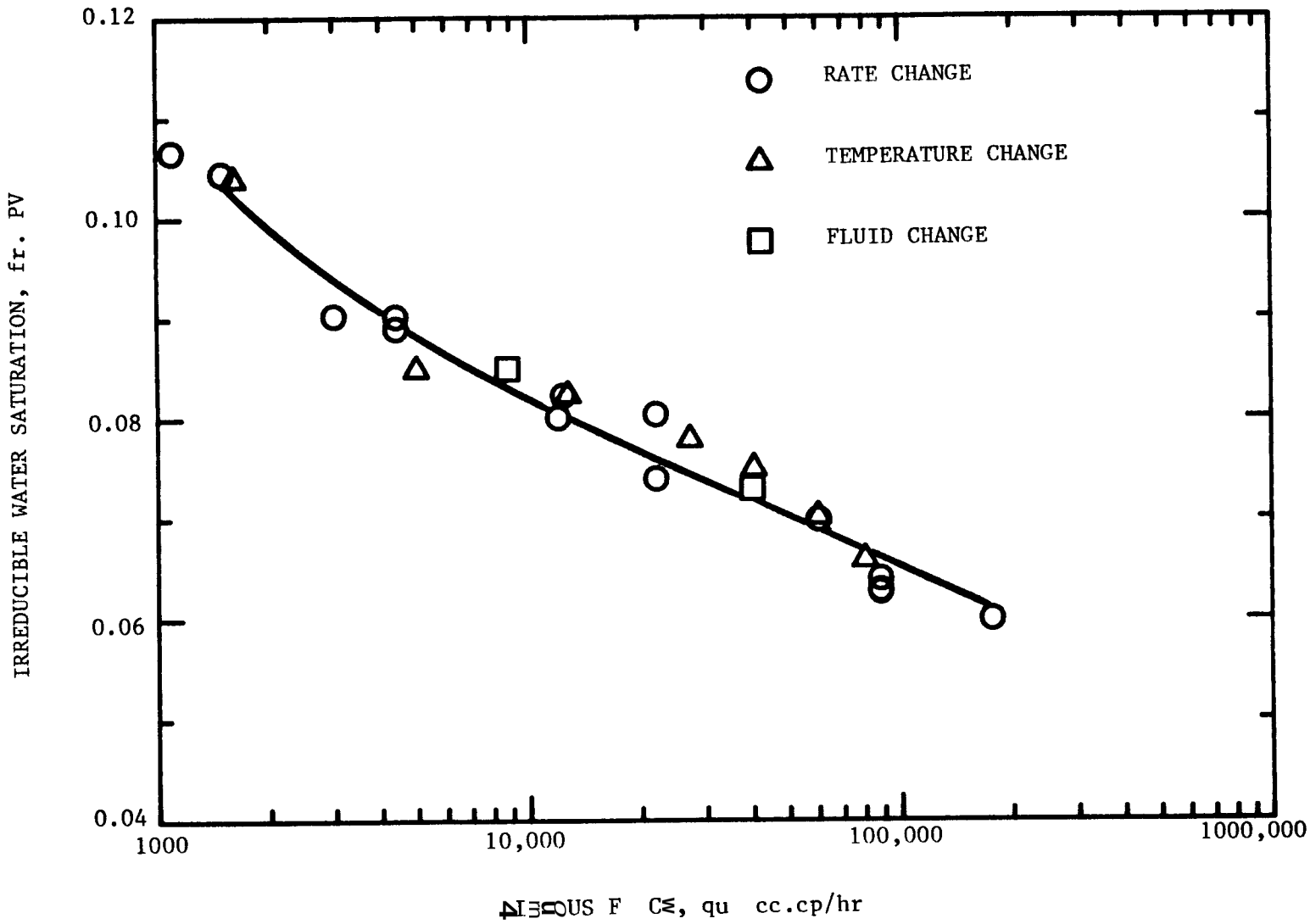

Fig. 6.18 IRREDUCIBLE WATER WS WISC S FORCE

wettability changes, but by changes in the viscous force. For heavy oils, the viscous force may decrease by two orders of magnitude for a temperature increase of 70°F to 350°F.

Similar oils were used by Poston et al. (1969), Weinbrandt et al. (1975) and Lo and Mungan (1972). It appears that their results can be explained on the basis of changes in viscous forces. In reservoirs, however, changes in viscous forces will cause only the production of some of the trapped water because the capillary end effect is usually believed to be negligible.

After indentifying the effects of temperature on end point saturations, the next section deals with temperature effects on relative permeability curves.

6.5 Temperature Effects on Relative Permeability Curves

The relative permeability curves generated from displacements on oil-saturated cores were shown to be rate sensitive below 240 cc/hr. Hence, floods were conducted at 400 cc/hr to determine relative permeability curves. Figure 6.19 shows relative permeabilities at 70°F and 122°F. Within experimental and computational error, the curves are identical. In section 6.2, it was determined that viscous fingering occurs at room temperature for rates higher than 100 cc/hr. However, due to a decrease in the viscosity ratio, viscous fingering does not present a problem at 122°F for a flowrate of 400 cc/hr. Figure 6.19 then, is a comparison between two cases: one stable, and the other with viscous fingering. The close agreement indicates the insensitivity of the curves to viscous fingering for these cases. (Data from the floods

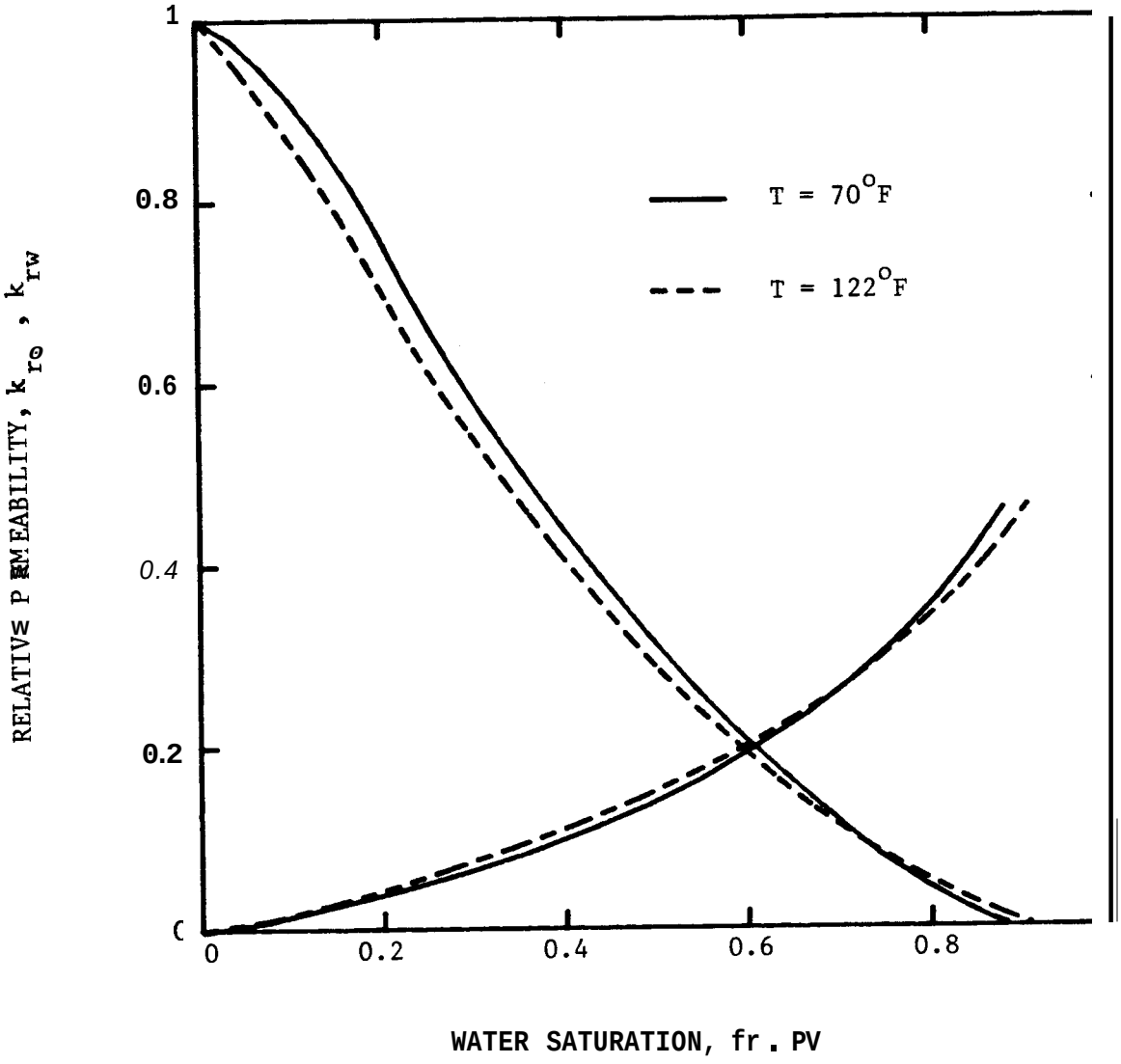

Fig. 6.19 OIL *AND* WATER RELATIVE PERMEABILITIES VS WATER SATURATION AT TWO DIFFERENT TEMPERATURES ($S_{wi} = 0$)

showing permeability ratio curves is presented in Appendix B-2).

The independence of relative permeabilities on temperature level provides a useful result for numerical simulation studies of thermal oil recovery processes. At present, complex empirical models are being used to consider changes in relative permeability curves caused by temperature level changes. The results presented in this section of the study appear to eliminate the need for models representing changes in relative permeability with temperature. However, this study considered only the effect of temperature on the flow dynamics within a porous medium, without accompanying rock-fluid interactions at elevated temperatures. Temperature level may have an effect on reservoir systems where such interactions exist.

6.6 Interdependence of End-point Saturations

It was mentioned in section 6.3 that the residual oil saturations were found to be independent of the water saturation at the start of the waterflood, for water saturations from zero to irreducible water saturation. The relative permeability curves from two waterfloods, one having no initial water saturation and the other initially at the irreducible water saturation, are shown in Fig. 6.20. The only significant difference between the curves occurs at low water saturations. Once sufficient water has been moved through the core, the flow characteristics of the two cases become identical. It had been suggested that the change in the residual oil saturation with temperature may be partly a result of a shift in the irreducible water saturation. The reasoning behind this has been presented in Section

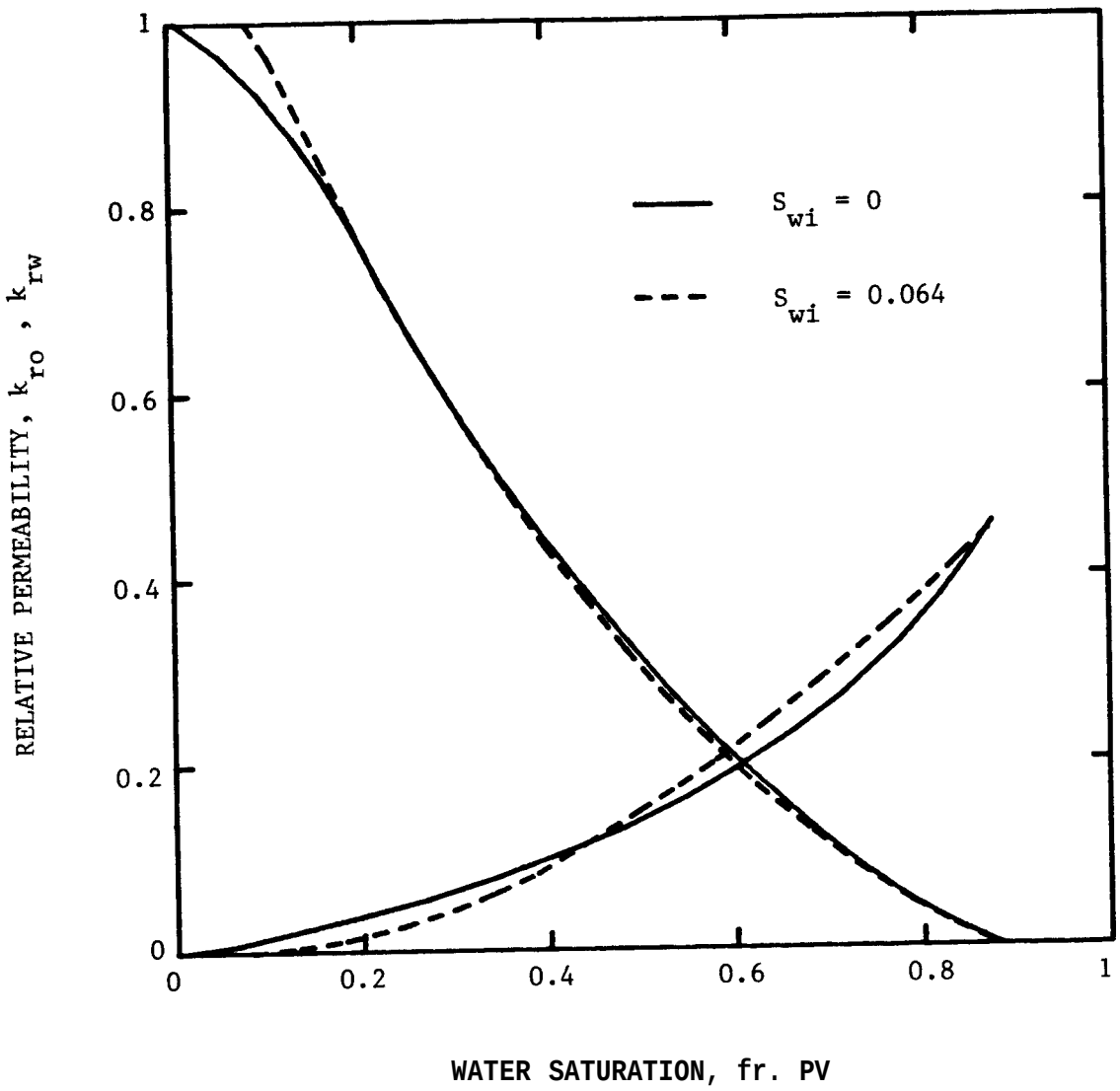

Fig. 6.20 OIL AND WATER RELATIVE PERMEABILITY CURVES VS WATER SATURATION FOR TWO DIFFERENT INITIAL WATER SATURATIONS (T = 70°F)

2. However, results of this study show no relation between the two end point saturations. This independence may be due to the homogeneous system used in this study. Further research is required with natural cores. Weinbrandt et al. (1975) used consolidated Berea cores and may have observed some relationship between the end point saturations. Other major studies on temperature effects have used clean unconsolidated cores which would result in systems wherein, as this study shows, the effects of changes in residual oil saturation on irreducible water saturation would be expected to be small.

7. CONCLUSIONS

As a result of this study, the following conclusions appear warranted. The results apply to flow of refined oil and distilled water through clean, unconsolidated sand.

1. Temperature level has no effect upon relative permeabilities to oil and water from 70°F to 186°F.

2. Residual oil saturation is independent of temperature level. There is a reduction in the "practical" residual oil saturation due to a change in shape of fractional flow curves. Fractional flow curves change shape because of a reduction in viscosity ratio with increasing temperature.

3. Irreducible water saturation, as determined by oilfloods on unconsolidated cores, increases with an increase in temperature. This increase in S_{wi} is caused by a reduction in the viscous force from the oil as temperature level is increased. A change in S_{wi} appears to be the sum of two changes, one in the outlet end effect and the other in the water trapped in smaller pores within the core. Qualitatively, the major contribution seems to be due to changes in the outlet end effect.

4. Apparent changes in the end point saturations need not be explained by expansion of the rock matrix, or changes in wettability and interfacial tension.

5. Fingering may present a problem in calculating true relative permeability curves for viscous oils. Bypassing of oil in the downstream tubing after a core can cause errors in the determination of true breakthrough recovery. This effect is in addition to the effect of viscous fingering in the porous medium.

6. A stability criterion, similar to that of Rapoport and Leas, can be determined by comparing relative permeability curves measured at different flowrates. The minimum rate required for a stable flood corresponds to the rate above which the relative permeability curves become rate independent. This appears to be an original result of this study.

7. A computer program was developed which calculates relative permeability curves from raw data using the Jones-Roszelle (1978) graphical technique.

8. A photoelectric cell was used to analyse fluids produced from the core during a waterflood. An electronic cut-off system was designed and built to enable continuous measurement of the produced oil as a function of time. This permitted a significant increase in accuracy of experimental results. In

addition, a high pressure oil collection system was developed which permitted direct measurement of cumulative oil produced during a run.

8. RECOMMENDATIONS FOR FURTHER WORK

This study of temperature effects on oil-water relative permeabilities has shown the curves to be temperature independent. The conclusion, however, applies to the flow of pure fluids through clean unconsolidated Ottawa sand. Future areas of research that can expand on the results of this study are as follows:

1. The equipment used in this study is rated to temperatures of 400°F. Experiments were not conducted above 200°F in the present study to prevent any solubility effects between the oil and water from interfering with temperature effects. Relative permeability curves can be generated for higher temperatures but the equipment must be modified slightly to pre-equilibrate the fluids before introducing them into the core.

2. A study of temperature effects on oil-water relative permeability curves for clean consolidated porous media can be initiated as a second step in the continuation of this study. The aim here would be to introduce greater heterogeneity into the system which, in turn, would result in larger variations in viscous and capillary forces within the porous medium. These variations may be more temperature sensitive and result in

possible temperature effects not present in multiphase flow through unconsolidated porous media.

3. After conducting experiments using pure fluids, another area of useful research is the use of reservoir fluids, (live oil and brine). The main interest in these experiments would be the effect of the interaction between the fluids at elevated temperatures on flow characteristics within a porous medium. For these fluids, the photocell assembly may not work effectively due to emulsification. A capacitance probe designed and built during the early part of the present study may be substituted for the photocell. A schematic of this probe is presented in Appendix C-5.

4. Another interesting study would be the effect of clay swelling on relative permeability curves. BY using water-wet cores containing clay. the amount of swelling could be controlled by varying the salinity of the aqueous phase. Fresh water would result in maximum clay swelling and hence, lowest permeability to water. Comparison of results of displacements conducted with water having different brine concentrations could be used to provide insight into the fundamental nature of multiphase flow through porous media.

5. Experiments to determine relative permeability curves are generally conducted at high flowrates to eliminate capillary end effects. High flowrates, however, can result in viscous

fingering as was observed in the present study. Another phenomenon that could occur is turbulent flow of the fluids through the pore channels. Turbulent flow of a single phase flowing through a porous medium has been studied. However, little is known about conditions which would result in turbulent flow when more than one phase is present. This provides an interesting and useful area of research.

6. By changing the interfacial tension between the fluids, the equipment can be used to study effects of capillary number on residual saturations at different temperatures. This can provide useful information to predict recoveries from steamflooding with additives where low tension flooding will occur at elevated temperatures.

7. Finally, the equipment can be used to conduct both steady-state and dynamic displacement experiments. If there are differences in the results from the two types of experiments, possible explanations may be provided to account for them.

NOMENCLATURE

A	area, cm^2
f_o	fractional flow of oil, dimensionless
f_{o2}	fractional flow of oil at outlet face of core, dimensionless
f_w	fractional flow of water, dimensionless
f_w'	derivative of f_w with respect to S_w, dimensionless
fw2	fractional flow of water at outlet face of core, dimensionless
f_{w2}'	derivative of f_w with respect to S_w at S_{w2}, dimensionless
I_r	relative injectivity, dimensionless
I_r^*	apparent relative injectivity at intersection of tangent to $1/I_r$ vs $1/W_i$ curve and y-axis, dimensionless
I_0	relative injectivity at intersection of tangent to $1/I_r$ vs W_i curve and y-axis, dimensionless
k	absolute permeability, darcys
k_i	effective permeability to fluid i, darcys
k_{ri}	relative permeability to fluid i, dimensionless
k_{ro}	relative permeability to oil, dimensionless
k_{rw}	relative permeability to water, dimensionless
k_o/k_w	oil-water permeability ratio, dimensionless
L	length of core, cm

N_{ca}	capillary number, $\Delta p/L\sigma$, (psi/ft)/(dynes/cm)
N_p	volume of oil recovered, cm^3
P	pressure, psi
p_o	pressure in oil phase, psi
p_w	pressure in water phase, psi
p_c	capillary pressure, equal to $(p_o - p_w)$, psi
q	volumetric flowrate, cc/hr
r	radius of flow tube, cm
S_{or}	residual oil saturation, fraction of pore volume
S_w	water saturation, fraction of pore volume
$\bar{S}_w$	average water saturation, fraction of pore volume
S_{wi}	irreducible water saturation, fraction of pore volume
S_{w2}	water saturation at the outlet face, fraction of pore volume
S_w^*	water saturation given by intersection of tangent to ΔS_w vs $1/W_i$ curve and y-axis, dimensionless
v	total fluid velocity, cm/hr
v_s	total fluid velocity at start of waterflood, cm/hr
W_i	pore volumes of water injected, dimensionless
x	distance, cm
θ	contact angle, degrees
μ	viscosity, cp
μ_o	oil viscosity, cp
μ_w	water viscosity, cp
Δp	pressure drop, psi
Δp_s	pressure drop at start of waterflood, psi
$\Delta p/q$	injectivity, psi/(cc/hr)

σ	surface or interfacial tension, dynes/cm
ϕ	porosity, fraction

SUBSCRIPTS

o	oil
ab	water-oi1
as	water-solid
bs	oil-solid
w	water
2	producing end

REFERENCES

1. Abrams, A.: "The Influence of Fluid Viscosity, Interfacial Tension, and Flow Velocity on Residual Oil Saturation Left by Waterflood," Soc. Pet. Eng. J. (October 1975) 437.

2. Batycky, J. P., McCaffery, F. G., Hodgins, P. K., and Fisher, D. B.: "Interpreting Relative Permeability and Wettability From Unsteady-State Displacement Measurements," Soc. Pet. Eng. J. (June 1981) 296.

3. Bentsen, R. G., and Saeedi, J.: "Liquid-liquid Immiscible Displacement in Unconsolidated Porous Media," J. Can. Pet. Tech. (January-March 1981), 93.

4. Bobek, J. E., Mattax, C. C., and Denekas, M. O.: "Reservoir Rock Wettability - Its Significance and Evaluation," Trans. AIME (1958) 213, p. 155.

5. Botset, H. G.: "Flow of Gas-Liquid Mixtures through Consolidated Sands," Trans. AIME (1940) 136, p. 91

6. Buckley, S. E., and Leverett, M. C.: "Mechanism of Fluid Displacement in Sands," Trans. AIME (1941) 142, p. 107

7. Cardwell, W. T.: "The Meaning of the Triple Value in Noncapillary Buckley-Leverett Theory," Trans. AIME (1959) 216, p. 271.

8. Chuoke, R. L., van Meurs, P., and van der Poel, C.: "The Instability of Slow, Immiscible, Viscous Liquid-Liquid Displacement in Permeable Media," Trans. AIME (1959) 216, p. 188.

9. Combarnous, M. and Pavan, J.: "Deplacement par Eau Chaude d'Huiles en place dans un Millieu Poreux," IIIe Colloque ARTFP (1968) No. 6, Pau, France.

10. Counsil, J. R.: "Steam-Water Relative Permeability," Ph.D dissertation, Department of Petroleum Engineering, Stanford University, Stanford, California (1979)

11. Croissant, R: "Developpement des Instabilite's en Millieu poreux, Influence de la Pression Capillaire," Revue IFP (1970) Vol.25,227.

12. Davidson, L. B.: "The Effect of Temperature on Relative on the Relative Permeability Ratio of Different Fluid Pairs in Two Phase

Systems," J. Pet. Tech. (August 1969) 1037.

13. Donaldson, E. C., Lorenz, P. B., and Thomas, R. D.: "The Effects of Viscosity and Wettability on Oil and Water Relative Permeabilities," SPE 1562, paper presented at the 41st. Annual Fall Meeting, Dallas, Tex., Oct. 2-5, 1966.

14. Douglas, J., and Wagner, R. J.: "Calculation of Linear Waterflood Behavior Including the Effects of Capillary Pressure," Trans. AIME (1958) 213, p. 96.

15. Du Prey, L. E. J.: "Factors Affecting Liquid Liquid Relative Permeabilities of a Consolidated Medium," Soc. Pet. Eng. J. (January 1973) 39.

16. Edmmondson, T. A: "Effect of Temperature on Waterflooding," J. Can. Pet. Tech. (April 1965) 236.

17. Fayers, F. J., and Sheldon, J. W: "The Effect of Capillary Pressure and Gravity on Two-Phase Flow in a Porous Medium," Trans. AIME (1959) 216, p.147.

18. Geffen, T. M., Owens, W. W., Parish, D. R., and Morse, R. A.: "Experimental Investigations of Factors Affecting Laboratory Relative Permeability Measurements," Trans. AIME (1951) 192, p. 99.

19. Hadley G. F., and Handy L. L: "A Theoretical and Experimental Study of the Steady State Capillary End Effect," SPE 707-G, paper presented at the 31st Annual Fall Meeting, Los Angeles, Calif., Oct. 14-17, 1956.

20. Hagoort, J.: "Displacement Stability of Water Drives in Water-Wet Connate -Water-Bearing Reservoirs," Soc. Pet. Eng. J. (February 1974) 63.

21. Hassler, G. L., et. al : "Investigations on the Recovery of Oil from Sandstones by Gas Drive," Trans. AIME (1936) 118, p. 116.

22. Hovanessian, S. A., and Fayers, F. J.: "Linear Water Flood with Gravity and Capillary Effects," Soc. Pet. Eng. J. (March 1961) 32.

23. Jones-Parra, J., and Calhoun, J. C: "Computation of a Linear Flood by the Stabalized Zone Method," Trans.AIME (1953) 198, p. 335.

24. Jones, S. C., and Roszelle, W. O.: "Graphical Techniques for Determining Relative Permeability From Displacement Experiments," Trans. AIME (1978) 265, p. 807.

25. Johnson, E. F., Bossler, D. P., and Naumann, V. O.: "Calculation of Relative Permeability from Displacement Experiments," Trans. AIME (1959) 216, p. 370.

26. Kyte, J. R., Naumann, V. O., and Mattax, C. C: "Effect of Reservoir Environment on Water-Oil Displacements," J. Pet. Tech, (June 1961) 579.

27. Kyte, J. R., and Rapoport, L. A: "Linear Waterflood Behavior and End Effects in Water-Wet Porous Medium," Trans. AIME (1958) 213, p. 423.

28. Labastie, A., Guy, M., Delclaud, Jean P., and Iffly, R: "Effect of Flow Rate and Wettability on Water-Oil Relative Permeabilities and Capillary Pressure," SPE 9236, paper presented at the 55th Annual Fall Technical Meeting, Dallas, Texas, September 21-24, 1980.

29. Leverett, M. C.: "Capillary Behavior in Porous Solids," Trans. AIME (1940) 136, p. 152.

30. Leverett, M. C., and Lewis, W. B: "Steady Flow of Gas-oil-water Mixtures through Unconsolidated Sands,'' Trans. AIME (1940) 136, p. 107.

31. Levine, J. S.: "Displacement Experiments in a Consolidated Porous System," Trans. AIME (1954) 201, p. 57.

32. Lo, H. Y., and Mungan, N: "Effect of Temperature on Water-Oil Relative Permeabilities in Oil-Wet and Water-Wet systems," SPE 4505, paper presented at the 48th Annual Fall Meeting, Las Vegas, Sept. 30 - Oct. 3, 1973

33. Merliss, F. E., Doane, J. D., and Rzasa, M. J.: "Influence of Rock and Fluid Properties On Immiscible Fluid-Flow Behavior In Porous Media," SPE 510-G, paper presented at the 30th Annual Fall Meeting, New Orleans, October 2-5, 1955.

34. Mungan, N: "Role of Wettability and Interfacial Tension in Water Flooding," Soc. Pet. Eng. J. (June 1964) 115.

35. Mungan, N: "Certain Wettability Effects in Laboratory Waterfloods," J. Pet. Tech, (Feb. 1966) 247.

36. Mungan, N: "Interfacial Effects in Immiscible Liquid-Liquid Displacement in Porous Media," Soc. Pet. Eng. J. (Sept. 1966) 247.

37. Naar, J., Wygal, R. J., and Henderson, J. H: "Imbibition Relative Permeability in Unconsolidated Porous Media," Soc. Pet. Eng. J. (March 1962) 13

38. Newcombe, J., Mcghee, J., and Rzasa, M. J.: "Wettability versus Displacement in Water Flooding in Unconsolidated Sand Columns," Trans. AIME (1955) 204, p. 227.

39. Osoba, J. S., Richardson, J. G., Kerver, J. K., Hafford, J. A., and Blair, P. M: "Laboratory Measurements of Relative Permeability," Trans. AIME (1951) 192, p. 47.

40. Owens, W. W., Parish, D. R., and Lamoreaux, W. E.: "An Evaluation of a Gas Drive Method for Determining Relative Permeability Relationships," Trans. AIME (1956) 207, p. 275.

41. Perkins, T. K., and Johnston, O. C.: "A Study of Immiscible Fingering in Linear Models," Soc. Pet. Eng. J. (March 1969) 39.

42. Peters, E. J., and Flock, D. L.: "The Onset of Instability During Two-Phase Immiscible Displacement in Porous Media," SPE 8371, paper presented at the 54th Annual Fall Meeting, Las Vegas, Nevada, September 23-26, 1979

43. Plateau, J. A. F.: "Experimental and Theoretical Research on the Figures of Equilibrium of a Liquid Mass withdrawn from the Action of Gravity," Smith Inst. Ann. Repts, 1863-1866

44. Poston S. W., Ysrael, S., Hossain, A. K. M. S., Montgomery 111, E. F., and Ramey, H. J. Jr.: "The Effect of Temperature on Irreducible Water Saturation and Relative Permeability of Unconsolidated Sands," Soc. Pet. Eng. J. (June 1970) 171.

45. Rachford, H. H.: "Instability in Water Flooding Oil from Water-Wet Porous Media Containing Connate Water," Sot.-Pet. Eng. J. (June 1964) 133.

46. Rapoport, L. A., and Leas, W. J.: "Properties of Linear Waterfloods," Trans AIME (1953) 198, p. 139.

47. Richardson, J. G., Kerver, J. K., Hafford, J. A., and Osoba, J. S.: "Laboratory Determination of Relative Permeability," Trans. AIME (1952) 195, p. 187.

48. Sandberg, C. R., Gourney, L. S., and Sippel, R. F.: "The Effect of Fluid-Flow Rate and Viscosity on Laboratory Determination of Oil-Water Relative Permeabilities," Trans AIME (1958) 213, p. 36.

49. Sanyal, S. K., Marsden, S. S. Jr. and Ramey, H. J. Jr.: "Effect of Temperature on Petrophysical Properties of Reservoir Rocks," SPE 4819, paper presented at the 49th Annual Fall Meeting, Houston, Texas, Oct. 1974

50. Sinnokrot, A. A., Ramey, H. J. Jr., and Marsden, S. S.: "Effect of Temperature Level upon Capillary Pressure Curves," Soc. Pet. Eng. J. (March 1971) 13.

51. Taber, J. J.: "Dynamic and Static Forces Required To Remove a Discontiouous Oil Phase from Porous Media Containing Both Oil and Water," Soc. Pet. Eng. J. (March 1969) 3

52. Treiber, L. E., Archer, D. L., and Owens, W. W.: "A Laboratory Evaluation of the Wettability of Fifty Oil-Producing Reservoirs," Soc. Pet. Eng. J. (Dec. 1972) 531.

53. Van Meurs, P.: "The Use of Transparent Three-Dimensional Models for Studying the Mechanism of Flow Processes in Oil Reservoirs," Trans. AIME (1957) 210, p. 295.

54. Van Meurs. P.. and van der Poel, C.: "A Theoretical Description of Water-Drive Processes Involving Viscous Fingering," Trans. AIME (1958) 213, p. 103.

55. Wagner, O. R., and Leach, R. O.: "Effect of Interfacial Tension on Displacement Efficiency," Soc. Pet. Eng. J. (Dec. 1966) 335.

56. Welge, H. J.: "A Simplified Method for Computing Oil Recovery by Gas or Water Drive," Trans. AIME (1952) 195, p. 91.

57. Wilson, J. W: "Determination of Relative Permeabilities under Simulated Reservoir Conditions," AIChE J. (1956) 2, No. 1, 94

58. Weinbrandt, R. M., Ramey, H. J. Jr., and Casse, F. J.: "The Effect of Temperature on Relative and Absolute Permeability of Sandstones," Soc. Pet. Eng. J., (Oct. 1975), 376-384

APPENDICES

APPENDIX A-1

DERIVATION AND APPLICATION OF THE JONES-ROSZELLE GRAPHICAL TECHNIQUE TO CALCULATE RELATIVE PERMEABILITIES BY THE DYNAMIC DISPLACEMENT METHOD.

Relative permeability curves are used together with viscosity ratio to obtain fractional flow curves for immiscible two-phase flow of fluids through a porous medium. Conversely, relative permeability curves can be obtained if the fractional flow curve, viscosity ratio and pressure history are available. To understand the technique involved, first consider the fractional flow curve shown in Fig. A-1.1. Buckley-Leverett theory predicts that the slope of the fractional flow curve, at any outflow face saturation S_{w2}, equals $1/W_i$, where W_i is the pore volumes of water injected to achieve that saturation. The intercept of the tangent with a fractional flow of one corresponds to the average water saturation within the core, $\bar{S}_w$. The relationship can he expressed mathematically by Eq. A-1.1 as follows:

$$W_i = \frac{(\bar{S}_w - S_{w2})}{(1 - f_{w2})} \qquad \text{(A-1.1)}$$

where f_{w2} is the fractional flow of water at the outlet face saturation of S_{w2}. This equation can be expressed in terms of the oil fractional flow at the outlet face, f_{o2}, to yield Eq. A-1.2

$$\bar{S}_w - S_{w2} = W_i f_{o2} \qquad \text{(A-1.2)}$$

During a waterflood, the amount of oil recovered, N_p, is obtained as a function of cumulative water injected into the core. In the Jones-Roszelle technique, the oil produced is expressed as a change in the average water saturation within the core. Graphing this change in saturation versus the pore volumes of water injected results in an

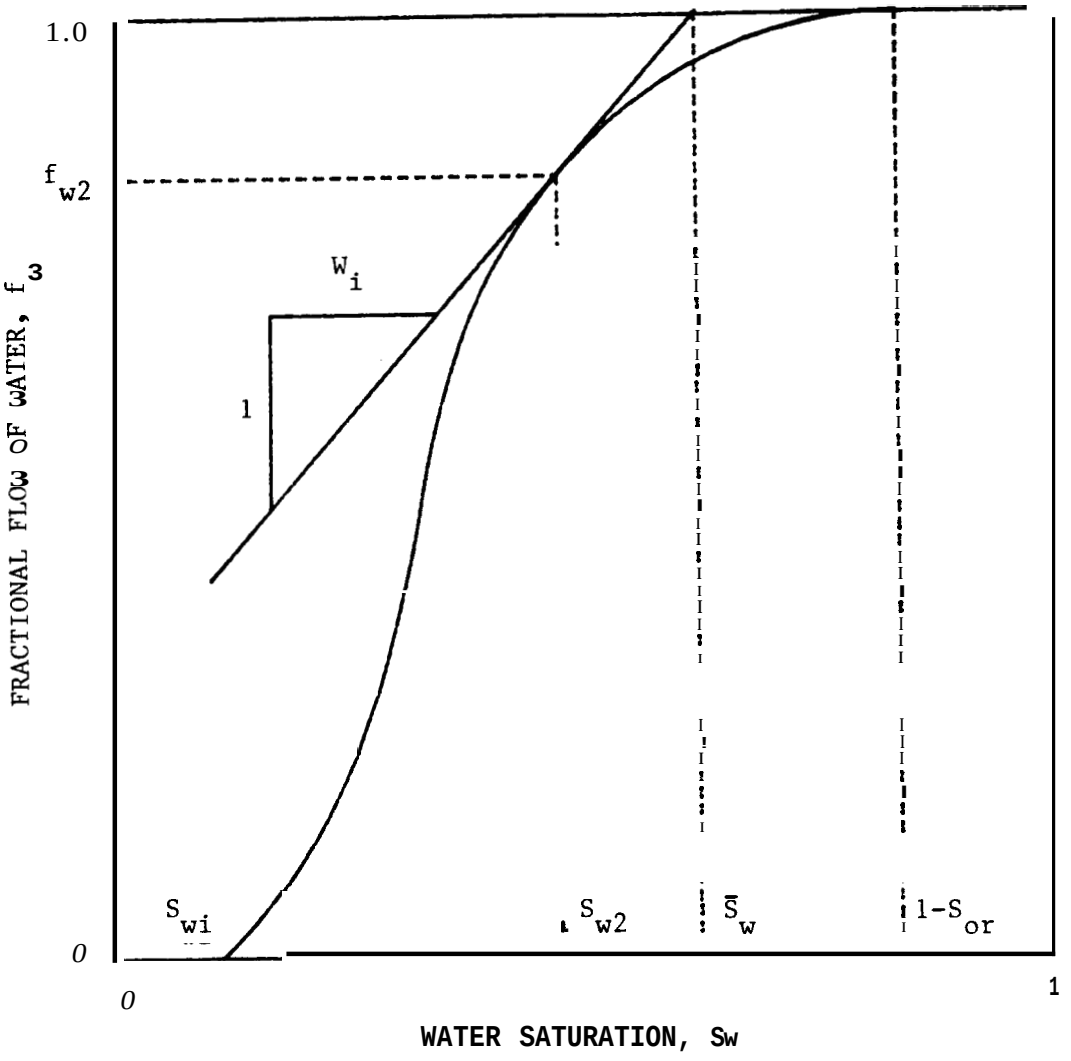

Fig. A-1.1 TYPICAL FRACTIONAL FLOW CURVE FOR WATER-OIL SYSTEM

effective graphical technique to calculate permeability ratios as a function of water saturation. A typical plot of production data is shown in Fig. A–1.2. As shown in the figure, a tangent to the curve at point A intersects the recovery axis at point C. The slope of this tangent is equal to the fractional flow of oil at the outlet face, f_{o2}. Since the horizontal distance to point A is W_i, and the slope is f_{o2}, the vertical distance (BC) must equal $W_i f_{o2}$. Eq. A–1.2 can be written as the difference of two terms as follows:

$$W_i f_{o2} = (\bar{S}_w - S_{wi}) - (S_{w2} - S_{wi}) \qquad \text{(A–1.3)}$$

Point B equals $\bar{S}_w - S_{wi}$, so point C, the intercept must be $S_{w2} - S_{wi}$. Thus the outflow saturation can be obtained by drawing tangents back to the y–axis and reading the intercept. At this outflow face saturation, the oil fractional flow can be obtained from Eq. A–1.2. Then, the permeability ratio at S_{w2} can be obtained from Eq. A–1.4 which is as follows:

$$\frac{k_{ro}}{k_{rw}} = \frac{\mu_o}{\mu_w} \frac{f_{o2}}{1 - f_{o2}} \qquad \text{(A–1.4)}$$

Late in the life of a waterflood, the oil recovery graph tends to become nearly horizontal. As a result, it is difficult to draw an accurate tangent and determine the correct intercept. The problem can be handled by plotting recovery versus $1/W_i$ on the x–axis instead of W_i. In their paper, Jones and Roszelle (1978) claim two advantages of using the $1/W_i$ approach. First, long extrapolations of tangents back to the y–axis are avoided, resulting in greater accuracy in the calculations.

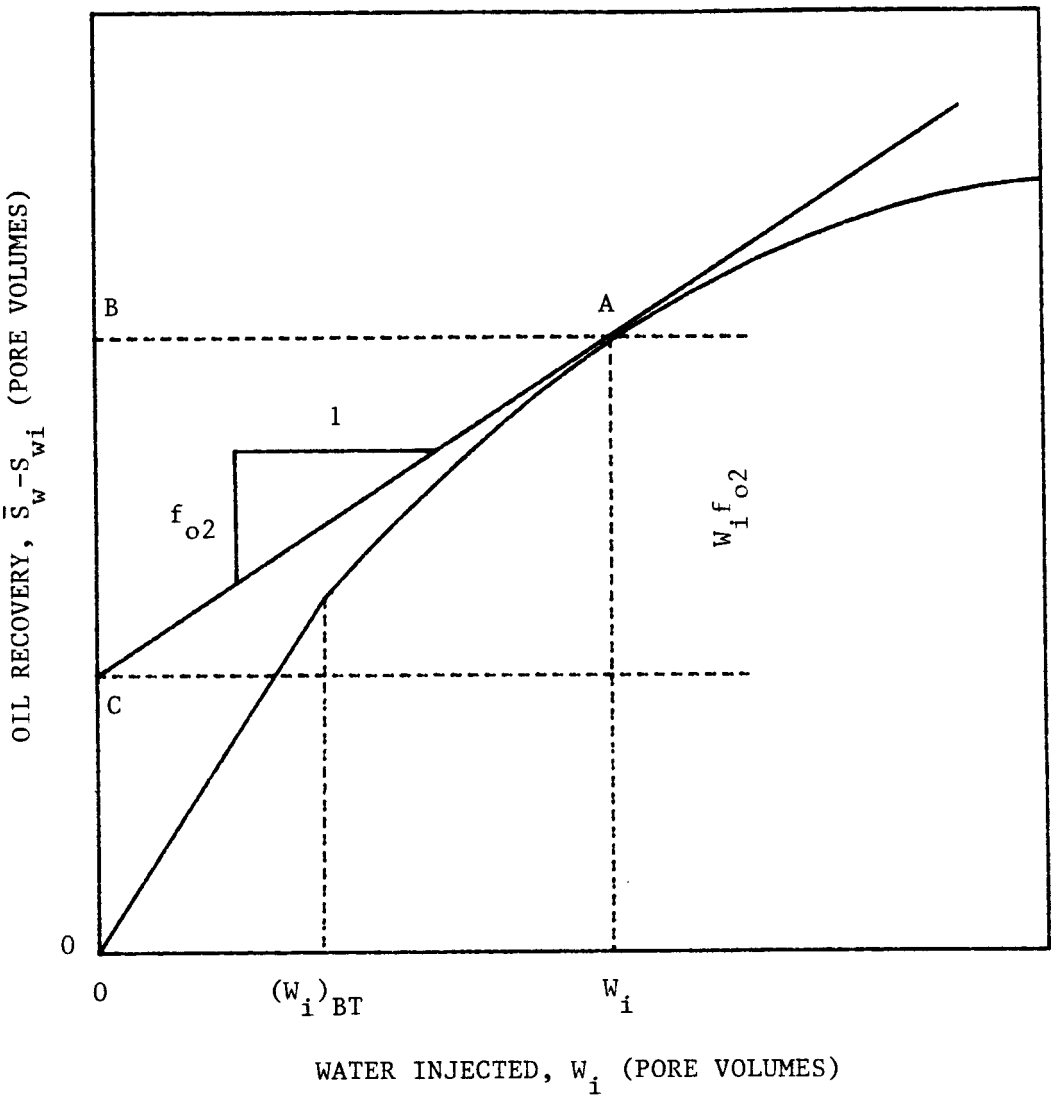

Fig. A-1.2 TYPICAL OIL RECOVERY VS WATER INJECTED CURVE FOR WATER DISPLACING OIL

Second, the data can be extrapolated back to the y-axis. This corresponds to the saturation change for an infinite amount of water injection into the core and can, therefore, yield true residual oil saturations. The validity of the second advantage, however, is questionable due to an inability to correctly predict the extrapolated shape of the production curve. In most cases, the data is extrapolated linearly back to the y-axis although there is no mathematical justification for it. This may result in erroneous permeability curves in the extrapolated region and wrong values of residual oil saturations.

The $1/W_i$ approach does have the advantage of higher accuracy in analyzing production data late in the life of a waterflood. Fig. A-1.3 shows typical production data graphed as ΔS_w versus $1/W_i$. A tangent is drawn to the curve at point A which intersects the y-axis at point C. Let point C correspond to a recovery given by $S_w^* - S_{wi}$. The slope of the tangent to the curve at point A is then given by the following equation:

$$\frac{d(\bar{S}_w - S_{wi})}{d(1/W_i)} = \frac{(\bar{S}_w - S_{wi}) - (S_w^* - S_{wi})}{1/W_i} \qquad \text{(A-1.5)}$$

This equation can be written as

$$- W_i \, (S_w^* - S_w) = - W_i^2 \frac{d\bar{S}_w}{dW_i} \qquad \text{(A-1.6)}$$

However, as mentioned before, dS_w/dW_i equals f_{o2} and from Eq. A-1.2, $W_i f_{o2}$ equals $S_w - S_{w2}$. Substituting these definitions into Eq. A-1.6 results in the following relationship between the saturations:

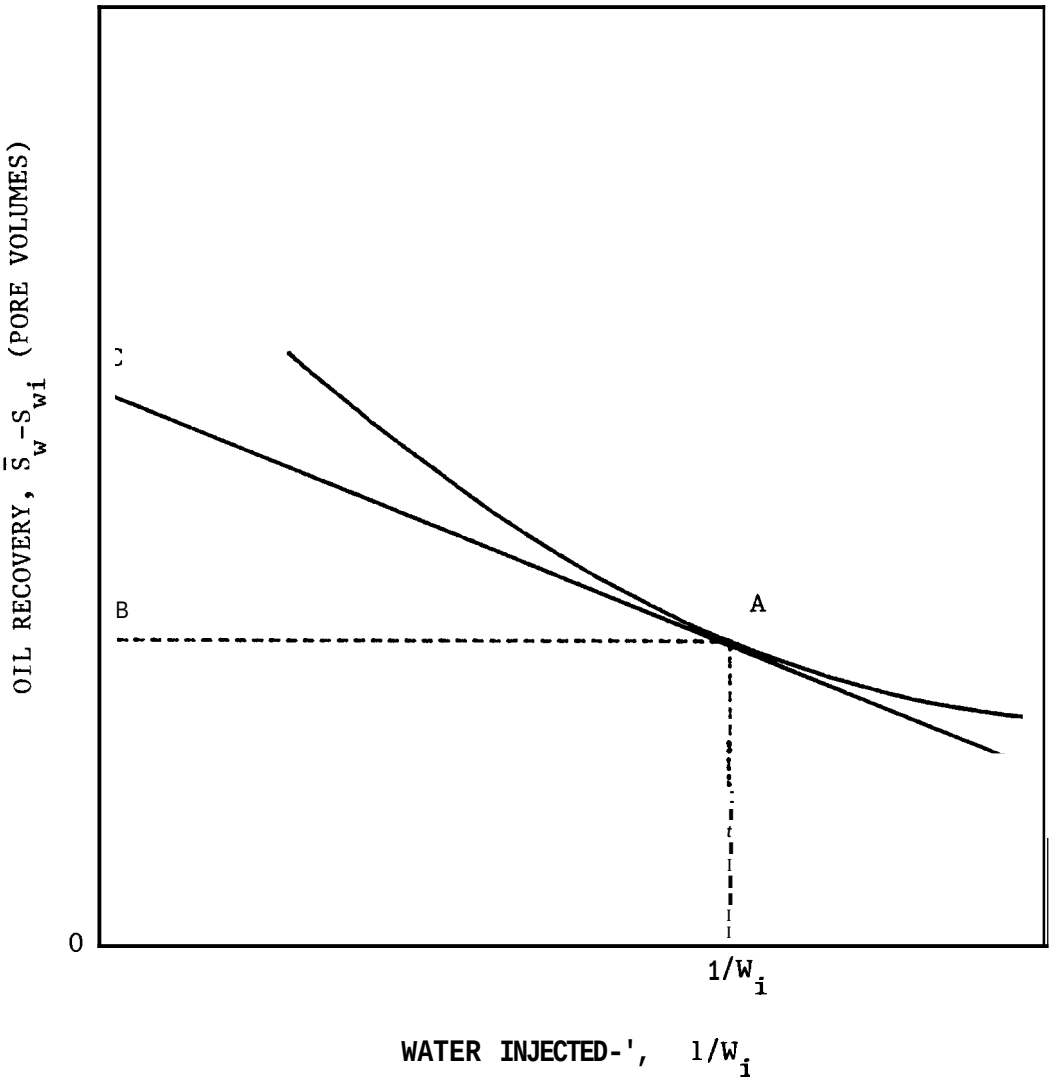

Fig. **A-1.3 TYPICAL OIL RECOVERY VS $1/W_i$ CURVE** FOR **WATER DISPLACING OIL (LARGE THROUGHPUT CASE)**

$$S_w^* = 2\,\bar{S}_w - S_{w2} \qquad \text{(A-1.7a)}$$

$$S_{w2} = 2\,\bar{S}_w - S_w^* \qquad \text{(A-1.7b)}$$

Once S_w^* is known, the outflow face saturation, S_{w2} can be determined using Eq. A-1.7b. The fractional flow of oil at that saturation is obtained using Eq. A-1.2 and the permeability ratio is then found from Eq. A-1.4.

The continuation of this method to obtain individual relative permeability curves requires pressure drop and rate as a function of water injected into the core. Neglecting capillary forces, Darcy's law, for flow of oil in the presence of another immiscible phase, is given by the following equation:

$$f_o v = -\frac{k\,k_{ro}}{\mu_o}\frac{dp}{dx} \qquad \text{(A-1.8)}$$

where v is the total fluid velocity defined as total volumetric flowrate divided by the cross-sectional area. In the equation, f_o is the fractional flow of oil, μ_o the oil viscosity, k_{ro} the relative permeability to oil and k the absolute permeability of the porous medium. The term dp/dx is the pressure gradient causing flow and, in the absence of capillary forces, is the same in both the oil and water phase. The pressure drop across the core, Ap, can be obtained by integrating the pressure gradient over the length of the core as shown in Eq. A-1.9.

$$\Delta p = \int_0^L \frac{dp}{dx}\, dx \qquad \text{(A-1.9)}$$

Substituting for dp/dx from Eq. A-1.8, gives the following equation for the pressure drop across the core:

$$\Delta p = \frac{v\,\mu_o}{k} \int_0^L \frac{f_o}{k_{ro}}\, dx \qquad \text{(A-1.10)}$$

From Buckley-Leverett theory, the relationship between any distance x, and the total distance L, can be written in terms of the derivitives of the fractional flow curve as follows:

$$\frac{x}{L} = \frac{f_w'}{f_{w2}'} \qquad \text{(A-1.11)}$$

from which the following expression is obtained for dx:

$$dx = \frac{L}{f_{w2}'}\, df_w' \qquad \text{(A-1.12)}$$

Substituting for dx in Eq. A-1.10 results in the following expression:

$$\Delta p = \frac{L\,v\,\mu_o}{f_{w2}'\,k} \int_0^{f_{w2}'} \frac{f_o}{k_{ro}}\, df_w' \qquad \text{(A-1.13)}$$

At the start of a waterflood, only oil is flowing within the core with a velocity of v_s and a pressure drop of Δp_s. The resulting flow equation at that condition is given by:

$$\frac{v_s}{\Delta p_s} \qquad \frac{k_r}{\mu_o L} \qquad \text{(A-1.14)}$$

Substituting for $\frac{k}{\mu_o L}$, Eq. A-1.12 can be written as follows:

$$\int_0^{f_{w2}'} \frac{f_o}{k_{ro}} df_w' = \frac{f_{w2}'}{I_r} \qquad \text{(A-1.15)}$$

where the term I_r is the relative injectivity and is defined as follows:

$$I_r = \frac{v / \Delta p}{v_s / \Delta p_s} \qquad \text{(A-1.16)}$$

Differentiating Eq. A-1.15 with respect to f_{w2}' gives the following equation:

$$\frac{d\left(\frac{f_{w2}'}{I_r}\right)}{df_{w2}} = \frac{f_{o2}}{k_{ro2}} \qquad \text{(A-1.17)}$$

However, as mentioned before, f_{w2}' equals $1/W_i$. Substituting for f_{w2}' in Eq. A-1.17 gives the following equation:

$$\frac{d\left(\frac{1}{W_i I_r}\right)}{d\ 1/W_i} = \frac{f_{o2}}{k_{ro2}} \qquad \text{(A-1.18)}$$

To calculate the relative permeability curves, $1/I_r$ is graphed versus W_i as shown in Fig. A-1.4. A tangent to this curve at point A

will intersect the y-axis at some point C. To see the graphical significance of this tangent, Eq. A-1.18 can be re-arranged to suit Fig. A-1.4 as follows:

$$\frac{f_{o2}}{k_{ro2}} = \frac{\left(\frac{1}{W_i^2 \; I_r^2}\right)(W_i dI_r + I_r dW_i)}{1 \; / \; W_i \quad dW_i} \qquad \text{(A-1.19)}$$

which can be simplified to give

$$\frac{f_{02}}{k_{ro2}} = \frac{W_i}{I_r^2} \frac{dI_r}{dW_i} + \frac{1}{I_r} \qquad \text{(A-1.20)}$$

or

$$\frac{f_{02}}{k_{ro2}} = \frac{-W_i \; d(1/I_r)}{dW_i} + \frac{1}{I_r} \qquad \text{(A-1.21)}$$

The slope of the tangent at point A in Fig. A-1.4 is $d(1/I_r)/dW_i$. Since the horizontal distance from B to A is W_i, the vertical distance from B to C must be $-W_i \; d(1/I_r)/dW_i$ as indicated in the diagram. This is the first term on the right-hand side of Eq. A-1.21. Further, point B equals $1/I_r$ at the time when W_i pore volumes of water have been injected. Hence, point C must equal the left-hand side of Eq. A-1.21; that is, f_{o2}/k_{ro2}. From the production curve, f_{o2} is known for any W_i which enables the determination of k_{ro2}. Then, the relative permeability to water, k_{rw2}, is calculated by dividing k_{ro2} by the permeability ratio calculated from the recovery curve.

The same problem that occurred for the saturation data occurs for the injectivity data late in the life of the flood. Again, it can be handled by graphing $1/I_r$ versus $1/W_i$. The resulting graph will have a

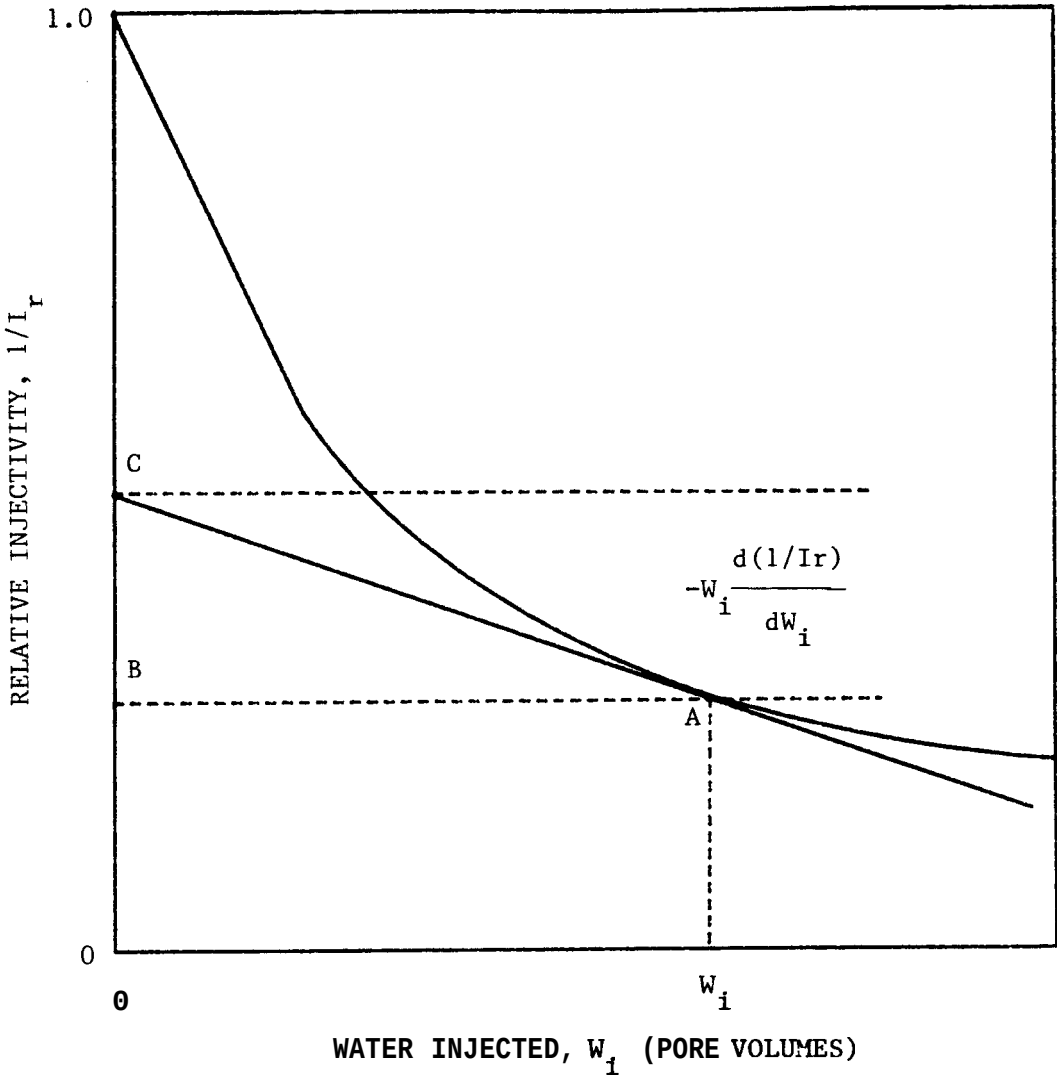

Fig. A-1.4 TYPICAL RELATIVE INJECTIVITY VS WATER INJECTED CURVE FOR WATER DISPLACING OIL

shape similar to that shown in Fig. A-1.5. Let the tangent to this curve at point A intersect the y-axis at a "false injectivity", $1/I_r^*$, given by point C in the diagram. The slope from the geometric construction can be equated to that defined by differentiating the variables resulting in the following equation:

$$\frac{(1/I_r) - (1/I_r^*)}{1/W_i} = \frac{d(1/I_r)}{d(1/W_i)} \qquad \text{(A-1.22)}$$

Re-arranging and substituting Eq. A-1.21, the following equation is obtained in terms of $1/I_r$ and $1/I_r^*$

$$\frac{f_{o2}}{k_{ro2}} = 2\left(\frac{1}{I_r}\right) - \frac{1}{I_r^*} \qquad \text{(A-1.23)}$$

where $1/I_r$ corresponds to the value at point B shown in Fig. A-1.5. Drawing tangents at various values of $1/W_i$ gives the oil relative permeabilities from Eq. A-1.23. The water relative permeabilities are then calculated by the procedure described previously.

The graphical technique is an accurate though time consuming method of determining relative permeability curves from displacement experiments. A computer program was developed to perform the graphical calculations. This program is described and presented in Appendix A-2.

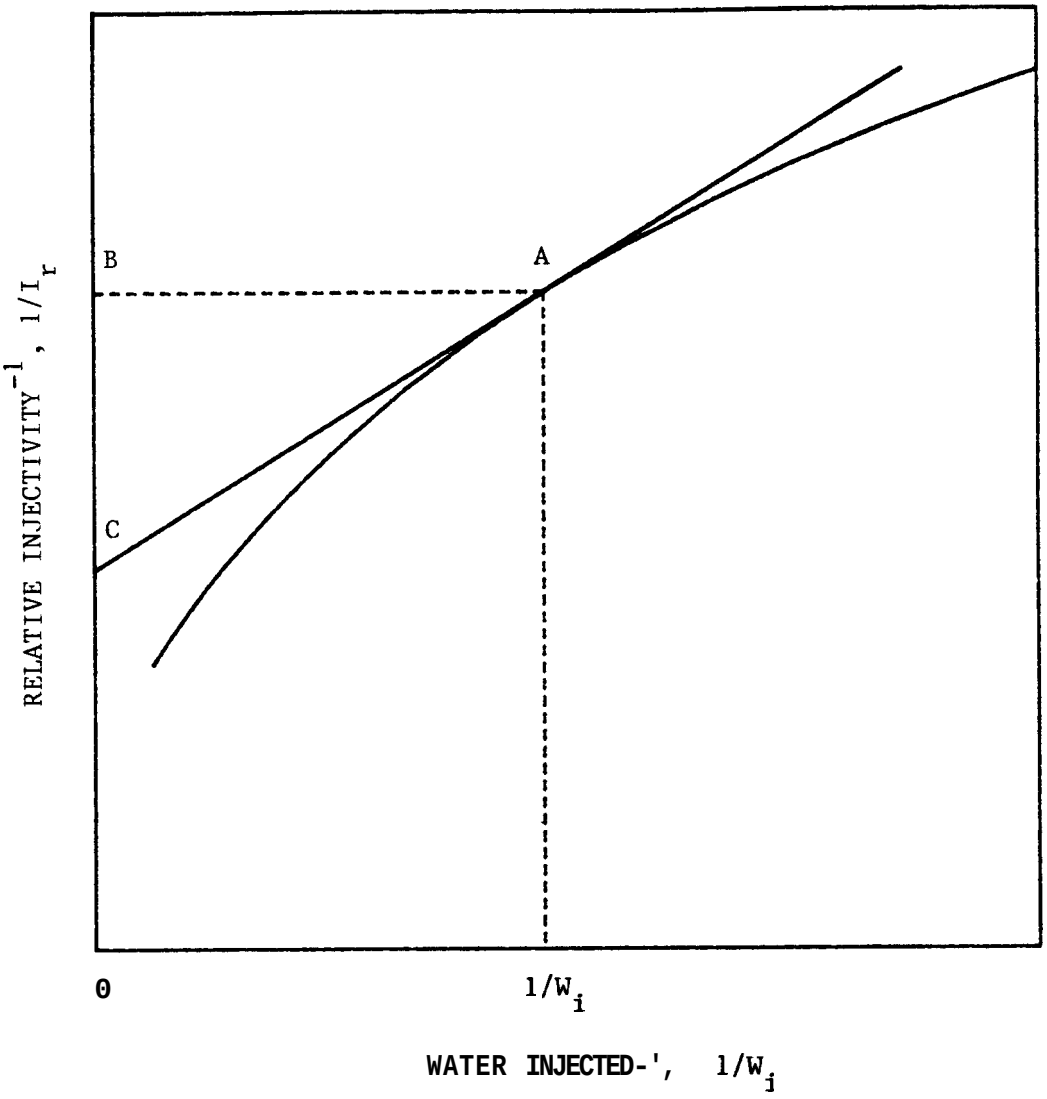

Fig. A-1·5 TYPICAL RELATIVE INJECTIVITY^{-1} VS 1/W CURVE FOR WATER DISPLACING OIL (LARGE THROUGHPUT CASE)

APPENDIX A–2

LISTING OF COMPUTER PROGRAM TO CALCULATE RELATIVE PERMEABILITY CURVES BY THE JONES–ROSZELLE GRAPHICAL TECHNIQUE

This program has been written in BASIC for use on a Hewlett-Packard 9845B mini computer. A Hewlett-Packard 9847A digitizer is used to read data from the experiment. The permeability curves are plotted by a Hewlett-Packard 9872B plotter.

To digitize either the production data or the injectivity data, the origin and axes of the graph are determined by using the "axis-align'' key on the digitizer. Following this, digitizing is accomplished by using the "single" key on the digitizer.

For the production data, the first point digitized is the corner diagonally across from the origin. The plot should be scaled such that this first digitized point corresponds to 50 cc of total oil recovered (including oil from the dead or tubing volume). The second point digitized is the origin, followed by the point corresponding to water breakthrough. From there, points are digitized randomly on the curve but with increasing distance fron the origin. (Digitizing points about 3-5 mm apart along the curve is generally accurate enough. Once the trace becomes less curved, this distance can be increased to 1–1.5 cm). The digitizing mode is terminated by digitizing a point at least 0.5 cm below the x-axis.

The program then averages the data by combining five consecutive points into one starting with the third digitized point. This process eliminates the sensitivity of the program to any one digitized point. Slopes are determined by the difference between two consecutive points. The program uses the S_w versus W_i approach until ten pore volumes of water have been injected after which it switches to the S_w versus $1/W_i$

technique. Output from this part of the program gives permeability ratio at different outflow face saturations.

The pressure data is digitized by first using the "axis-align" key as before. Next, digitizing of the pressure curve is done by using the "single" key on the digitizer. (The same distance along the curve as for the production curve is sufficient). For the pressure data, the corner diagonally across from the origin is not digitized. The curve is digitized by entering random points along the curve with an increasing x-axis. Termination of the digitizing mode is accomplished in the same way as with the production data.

To combine the results from the pressure drop response and production data, the program does a semi-log interpolation to obtain permeability ratios and relative permeabilities at the same saturation. These results are tabulated and plotted on the plotter after which they are stored in the appropriate data file.

Due to the small slope towards the end of the floods, the calculated relative permeability points (one or two) may become unstable near residual oil saturation. Hence, after the results have been tabulated, the program asks for the number of unstable points. These points are then eliminated from plots of relative permeabilities.

```
18    PRINT " ",PAGE
20    PRINT "     THIS PROGRAM CALCULATES RELATIVE PERMERBILITY AND PERMEABILITY"
38    PRINT "RATIO CURVES USING THE JONES TECHNIQUE.  IT HAS BEEN WRITTEN TO"
40    PRINT "WORK IN CONJUNCTION WITH THE RELATIVE PERMEAMETER IN THE SUPRI"
50    PRINT "LAB.  BE SURE THAT THE DIGITIZER IS SWITCHED ON AND YOU HAVE "
60    PRINT "CREATED A DATA FILE.  IF NOT,  PLEASE DO SO."
70    PRINT "                                                GOOD LUCK"
80    PAUSE
98    DIM U(500),V(500),W(500),X(500),Y(500),Xp(500),Yp(500),F1(500),F2(500)
91    DIM Xii(500),Yii(500)
95    DIM Sat(500),Krkw(500),Kro(500),Krw(500),Fok(500),Yi(500),Xi(500)
100   PRINT " ",PAGE
110   INPUT "WHRT IS THE NAME OF YOUR DATA FILE?",A$
128   INPUT "WHAT IS THE INITIAL WATER SATURATION?",Swi
138   INPUT "WHAT IS THE VISCOSITY RATIO?",R
140   INPUT "WHAT IS THE INITIAL PRESSURE DROP(PSI)?",Dpi
150   INPUT "WHAT IS THE TEMPERATURE DURING THE FLOOD(F)?",T
151   INPUT "ENTER OIL EXPANSION FACTOR",E
152   INPUT "ENTER WATER EXPANSION FACTOR", Ew
160   INPUT "WHAT TRANSDUCER PLATE RESPONSE ARE YOU USING?",P1
170   INPUT "WHAT IS THE SYSTEM PORE VOLUME(c.c/s)?",Pv
188   INPUT "WHAT IS THE FLOODING RATE (cc/hr)?",Q
198   INPUT "WHAT IS THE TOTAL OIL PRODUCED?",Nfc
218   INPUT "ENTER THE CHART SPEED ",Cs
220   ASSIGN #1 TO AS
230   OUTPUT 786; "IN"
248   PRINT " ",PAGE
258   PRINT "LOCATE THE ORIGON ON THE DIGITIZER BY USING THE AXIS ALIGN"
268   PRINT "KEY.  PRESS CONTINUE WHEN READY."
270   PAUSE
288   PRINT " ",PAGE
281   OUTPUT 706; "OS"
282   ENTER 706;Status
283   IF BIT(Status,2)=0 THEN 281
284   OUTPUT 706; "OD"
285   ENTER 786; Xb, Yb
298   FOR I=1 TO 200
308   OUTPUT 706;"OS"                    !SET OUTPUT STATUS MODE OH DIGITIZER
318   ENTER 706;Stat.us                        !GET DIGITIZER STATUS
328   IF BIT(Status,2)=0 THEN 300
338   OUTPUT 706; "OD"
340   ENTER 706;X(I),Y(I)
360   X(I)=(X(I)*Q*Ew/(400*Cs)-7.9)/Pv       [CALCULATE WATER INJECTED (PV)
365   IF Y(I)/Yb<-.02 THEN 425               !TO EXIT DIGITIZE MODE
378   Y(I)=((Y(I)*50/Yb-5.4)*E-2.5)/Pv       'CALCULATE SATURATION CHANGE (PV·
391   PRINT USING 400;I,X(I),Y(I)            !SHOW DIGITIZED DATA ON SCREEN
400   IMAGE 2X,DDD,2X,DDD.DD,2X,.DDD
411   BEEP
428   NEXT I
425   Y(I)=0
426   X(I)=0
430   J=I-1
431   BEEP
432   Yyy=Y(J)/Nfc
433   0=3
434   Oo=O+4
435   FOR 1=3 TO J           !THIS LOOP AVERAGES FIVE DATA POINTS INTO ONE
436   Sum=0
437   Sum1=0
438   FOR K=O TO Oo
439   Sum=Sum+Y(K)
440   Sum1=Sum1+X(K)
441   NEXT K
442   IF Oo>J THEN 458
443   IF Oo=J THEN 450
444   O=O+5
445   Oo=Oo+5
446   Y(I)=Sum'5
447   X(I)=Sum1/5
448   NEXT I                    !END OF DATA AVERAGING LOOP
450   Y(I)=Sum/(5-Oo+J)         !ANALYSIS OF LAST AVERAGE POINT
```

```
451   X(I)=Sum1/(5-Oo+J)        !ANALYSIS OF LAST AVERAGE POINT
452   J=I
465   Np1=Y(2)
467   Wi1=X(2)
46%   FOR K=3 TO J  !THIS LOOP DRAWS TANGENTS TO THE RECOVERY CURVE
470   LEK-1         !AND EXTRAPOLATES BACK TO THE Y-AXIS
480   Wi 2=X(K)
490   Np2=Y(K)
500   IF Wi2>10 THEN 700    !IF Wi IS GREATER THEN 10, USE 1/Wi APPROACH
510   S2a=Np1-Wi1*(Np2-Np1)/(Wi2-Wi1)  !INTERCEPT OF TANGENT WITH Y-AXIS
520   Wifo=.5*(Np2+Np1)-S2a
530   Fo=2*Wifo/(Wi1+Wi2)
531   IF Fo>0 THEN 540
532   Fo=.0000001     !IF Fo IS NEGATIVE, REPLACE BY SMALL POSITIVE NUMBER
540   Ratio=(1/(1-Fo)-1)*R   !EQUATION TO CALCULATE PERMEABILITY RATIO
550   Ratiol=LGT(Ratio)
560   S2=S2a+Swi          !OUTFLOW FACE SATURATION, Sw2
565   F1(K)=Fo            !FRACTIONAL FLOW OF OIL AT Sw2
570   U(K)=S2             !OUTFLOW FACE SATURATION
580   V(K)=Ratio          !PERMEABILITY RATIO
590   W(K)=Ratiol
610   Wi1=Wi2
620   Npl=Np2
630   NEXT K
640   GOTO 886
700   Np1=Y(L)          !START OF 1/Wi APPROACH
710   Wi1=1/X(L)
720   L=L+1
736   FOR M=L TO J
748   Np2=Y(M)
750   Wi2=1/X(M)
766   S2a=Np1-Wi1*(Np2-Np1)/(Wi2-Wi1)
770   Wifo=S2a-(Np1+Np2)/2
780   Fo=Wifo*2*Wi1*Wi2/(Wi1+Wi2)
790   S2=Np1+Np2-S2a+Swi
7%1   IF Fo>0 THEN 800
792   Fo=.0000001
806   Ratio=(1/(1-Fo)-1)*R
810   Rat iol=LGT(Ratio)
811   F1(M)=Fo
820   U(M)=S2
830   V(M)=Rat io
840   W(M)=Ratiol
850   Wi1=Wi2
860   Np1=Np2
870   NEXT M            !END OF 1/Wi APPROACH
886   BEEP
890   PRINTER IS 16
906   FOR K=2 TO J
910   PRINT USING 920;K,X(K),Y(K),U(K),V(K),W(K)
920   IMAGE DDD,4X,DDD.D,4X,DDD.D,4X,D.DDD,4X,DDD.DDD,4X,DDD.DDD
930   NEXT K
931   PAUSE
933   Sor=1-((Nfc-5.4)*E-2.5)/Pv-Swi
934   Sor=Sor*1000
935   Sor=INT(Sor)
936   Sor=Sor/1000
940   PRINTER IS 16
941   GOTO 2200
950   PRINT " ",PAGE         !PLOTTING ROUTINE
960   PRINT "PRESS CONTINUE IF YOU WANT THE CURVE PLOTTED"
961   PAUSE
963   PRINTER IS 7,5
967   Zz=0
1305  PRINT USING "K";"SI.2,.4"
1306  INTEGER P
1307  INTEGER Ql
1310  FOR I=3 TO J-1
1320  P=1000*W(I)+6000
1330  Q1=1900+5000*U(I)
1350  PRINT USING "K";"PA",Q1,",",P
```

```
1360  PRINT USING "K";"LBo"
1361  NEXT I                          !END OF PLOTTING ROUTINE
1362  GOTO 3962
2200  PRINT "",PAGE
2210  PRINT "  YOU CAN START DIGITIZING THE PRESSURE DATA NOW.  REMEMBER"
2220  PRINT "TO USE THE AXIS ALIGN KEY FIRST.  TO EXIT THE DIGITIZE MODE"
2230  PRINT "ENTER A POINT WITH A NEGATIVE Y-COORDINATE.   PRESS CONTINUE"
2240  PRINT "WHEN READY TO DIGITIZE."
2300  PAUSE
2310  PRINT "",PAGE
2311  N=1
2450  L-3
2461  OUTPUT 706;"IN"
2470  FOR I=L TO 200       !START DIGITIZE LOOP
2480  OUTPUT 706;"OS"
2490  ENTER 706;Status
2500  IF BIT(Status,2)=0 THEN 2480
2510  OUTPUT 706;"OD"
2520  ENTER 706;Xp(I),Yp(I)
2530  Yp(I)=Yp(I)*P1/(Yb*Dpi)        !CALCULATE 1/(RELATIVE INJECTIVITY)
2540  Xp(I)=Xp(I)*Q/(400*Cs*Pv)      !CALCULETE WATER INJECTED (PV)
2541  BEEP
2550  L=I-1
2570  IF Yp(I)<0 THEN 2585           !EXIT LOOP IF Y IS NEGATIVE
2580  NEXT I
2585  Sc=0    !OPTION TO CHANGE TO NEW SCALE WITH ANOTHER TRANSDUCER PLATE
2590  INPUT "ENTER 1 IF YOU WANT A NEW SCALE",Sc
2591  IF Sc=1 THEN 2600
2592  GOTO 2724
2608  INPUT "ENTER NEW SCALE OF TRANSDUCER",P1
2601  GOTO 2470
2724  Yp(I)=0
2725  Xp(I)=0
2726  O=3
2727  Oo=O+4
2728  FOR I=3 TO L       !DATA AVERAGING ROUTINE
2729  Sum=0
2730  Sum1=0
2731  FOR k=O TO 00
2732  Sum=Sum+Yp(K)
2733  Sum1=Sum1+Xp(K)
2734  NEXT K
2735  IF Oo>L THEN 2745
2736  IF Oo=L THEN 2745
2737  O=O+5
2738  Oo=Oo+5
2739  Yp(I)=Sum/5
2740  Xp(I)=Sum1/5
2741  NEXT I
2745  Yp(I)=Sum/(5-Oo+L)
2746  Xp(I)=Sum1/(5-Oo+L)       !END OF DATH AVERACING ROUTINE
2747  L=I
2756  Pp1=Yp(3)
2758  Wi1=Xp(3)
2760  FOR I=4 TO L        !GRAPHICAL DETERMINATION OF INDIVIDUAL PERMEABILITIES
2770  Pp2=Yp(I)
2780  Wi2=Xp(I)
2790  IF Wi2>10 THEN 2960    !FOR Wi > 10, USE 1/Wi APPROACH
2800  Fok(I)=Pp2-Wi2*(Pp2-Pp1)/(Wi2-Wi1)   !INTERCEPT TO OBTAIN Kro
2810  FOR K=2 TO L        !LINEAR INTERPOLATION WITH RECOVERY DATA
2820  IF Wi2>X(K) THEN 2840
2830  GOTO 2850
2840  NEXT K
2850  COSUB Inter
2920  M=I+1
2930  Pp1=Pp2
2940  Wi1=Wi2
2950  NEXT I
2960  M=I        !1/Wi ROUTINE
2965  Pp1=Yp(M-1)
2970  Wi1=1/Xp(M-1)
```

```
2980  FOR I=M TO L
2990  Pp2=Yp( I)
3000  Wi2=1/Xp( I)
3010  Fok.II)=Yp(I)+Yp( I-1)-(Pp1- W1*(Pp2-Pp1)/(Wi2-Wi1))
3020  FOR K=2 TO L
3030  IF 1/Wi2>X(K) THEN 3056
3040  GOTO 3060
3050  NEXT K
3060  Wi2=1/Wi2
3070  GOSUB Inter
3080  Wi1=1/Wi2
3090  Ppl=Pp2
3100  NEXT I
3110  GOTO 3925
3840  ! THIS ROUTINE INTERPOLATES BETWEEN DHTH FROM THE RECOVERY ANALYSIS
3850 Inter:Foo=F1(K)+(F1(K-1)-F1(K))*(Wi2-X(K))/(X(K-1)-X(K))
3860  Uu=U(K)+(U(K-1)-U(K))*(Wi2-X(K))/(X(K-1)-X(K))
3870  Rr=W(K)+(W(K-1)-W(K))*(Wi2-X(K))/(X(K-1)-X(K))
3871  F21I)=Foo
3880  Sat( I)=Uu
3890  Krkw( I)=10^Rr
3900  Kro( I)=Foo/Fok(I)
3910  Krw( I)=Kro(I)/Krkw( I)
3920  RETURN
3925  PPINTER IS 16
3930  FOR 1=4 TO L
3940  PRINT USING 3950;I,Sat(I),Krkw(I),Kro(I),Krw(I)
3950  IMAGE DDD,2X,D.DDD,4X,DDD.DD,4X. D.DDD,4X,D.DDD
3953  NEXT I
3954  PAUSE
3961  GOTO 956
3962  PRINTER IS 7,5        !PLOTTING ROUTINE
3982  PRINT USING "K";"SP1"
3984  PRINT USING "K";"PA1900,4000;PD;VS6"
3950  PRINT USING "K";"PR0,5000,5000,0,0,-5000,-5080,0;PU;VS36"
3991  INPUT "ENTEP THE NU. OF UNSTABLE POINTS",Nus
4000  PRINT USING "K";"SI.2,.4"
4081  INTEGER P11
4082  INTEGER Q11
4008  P11=Swi*5000+1900
4009  Q11=4000
4010  PRINT USING "K";"PA",P11,",",Q11
4011  GOSUB Kwdot.
4030  FOR I=4 TO L-Nus
4040  P11=Sat(I)*5000+1900
4050  Q11=Krw(I)*5000+4000
4052  L11=I
4060  PRINT USING "K";"PA",P11,",",Q11
4070  GOSUB Kwdot.
4080  NEXT I
4081  Q11=1/(Yp(L)*R)*5000+4000
4082  P11=(1-Sor)*5000+1900
4083  PRINT USING "K";"PH",P11,",",Q11
4084  GOSUB Kwdot
4090  INTEGER Q111
4091  P11=Swi*5000+1900
4092  Q111=9000
4093  PRINT USING "K";"PA",P11,",",Q111
4096  GOSUB Kodot
4100  FOR I=4 TO L-Nus
4110  P11=Sat( I)*5000+1900
4120  Q111=Kro(I)*5000+4000
4130  PRINT USING "K";"PA",P11,",",Q111
4140  GOSUB Kodot
4142  NEXT I
4143  P11=(1-Sor)*5000+1900
4144  Q111=4000
4145  PRINT USING "K";"PA",P11,",",Q111
4146  GOSUB Kodot
442%  GOTO 4480
4440 Kwdot:PRINT USING "K";"PR-35,-35;PD;PR0,70,70,0,0,-70,-70,0;PU"
```

```
4450  RETURN
4460 Kodot:PRINT USING "K";"PR-35,-35;LBo"
4470  RETURN
4480  PRINT USING "K";"SP0;IN"
4510  PRINTER IS 16     !DATA STORAGE
4515  PRINT #1;Nus,Q,T,Pv,Swi,R,Sor,Dpi,Nfc,Cs,Pl,J,L
4520  FOR I=1 TO J
4530  PRINT #1;X(I), Y(I)
4540  NEXT I
4556  FOR 1=1 TO L
4560  PRINT #1;Xp(I),Yp(I),Sat(I),Krkw(I),Kro(I),Krw(I),F2(I)
4570  NEXT I
5520  PRINTER IS 16
5530  END
```

APPENDIX B-1

PLOTS OF OIL AND WATER RELATIVE PERMEABILITY CURVES

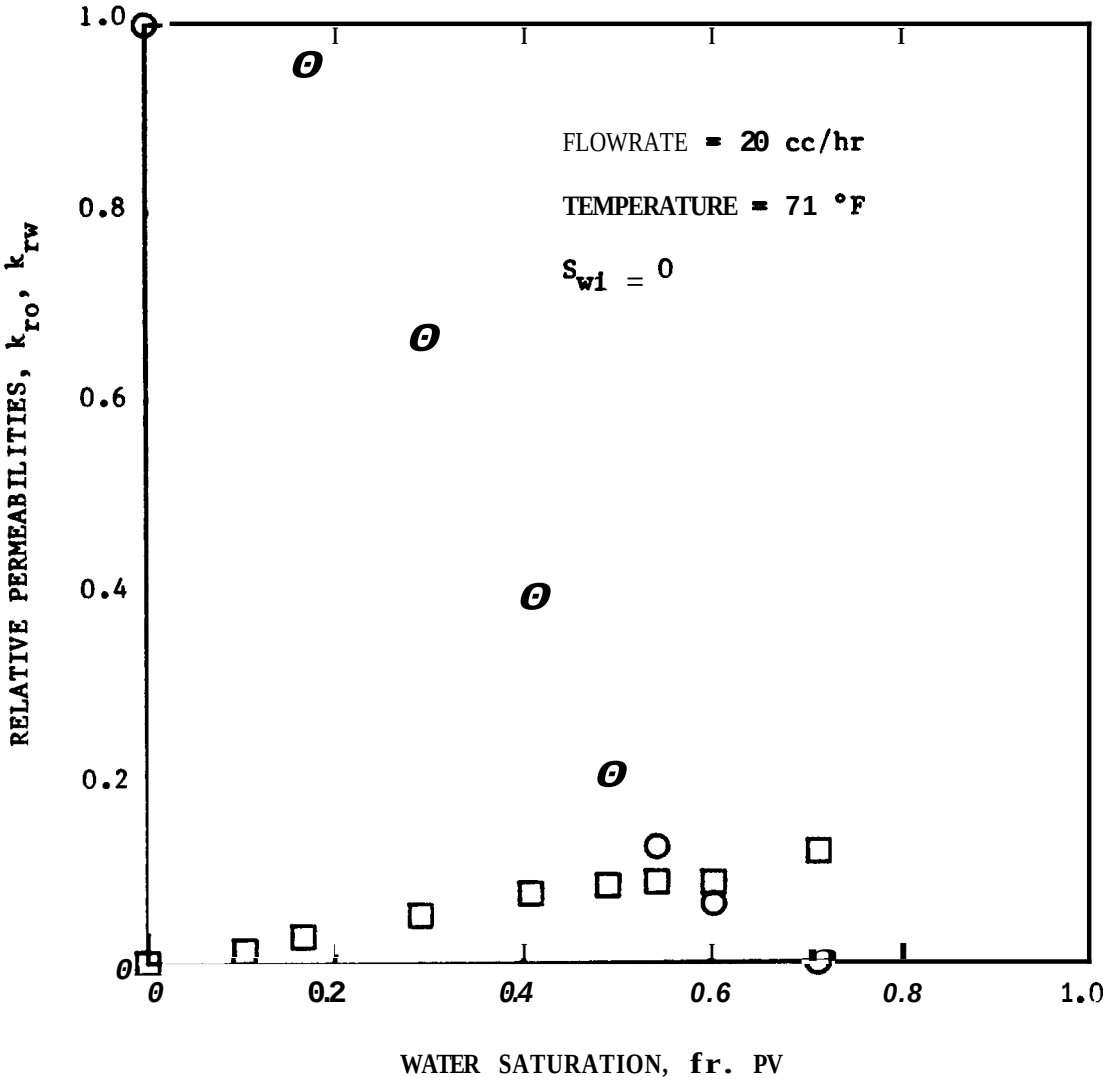

Fig. B-1.1 RELATIVE PERMEABILITIES VS WATER SATURATION (PV) FOR WATER DISPLACING OIL

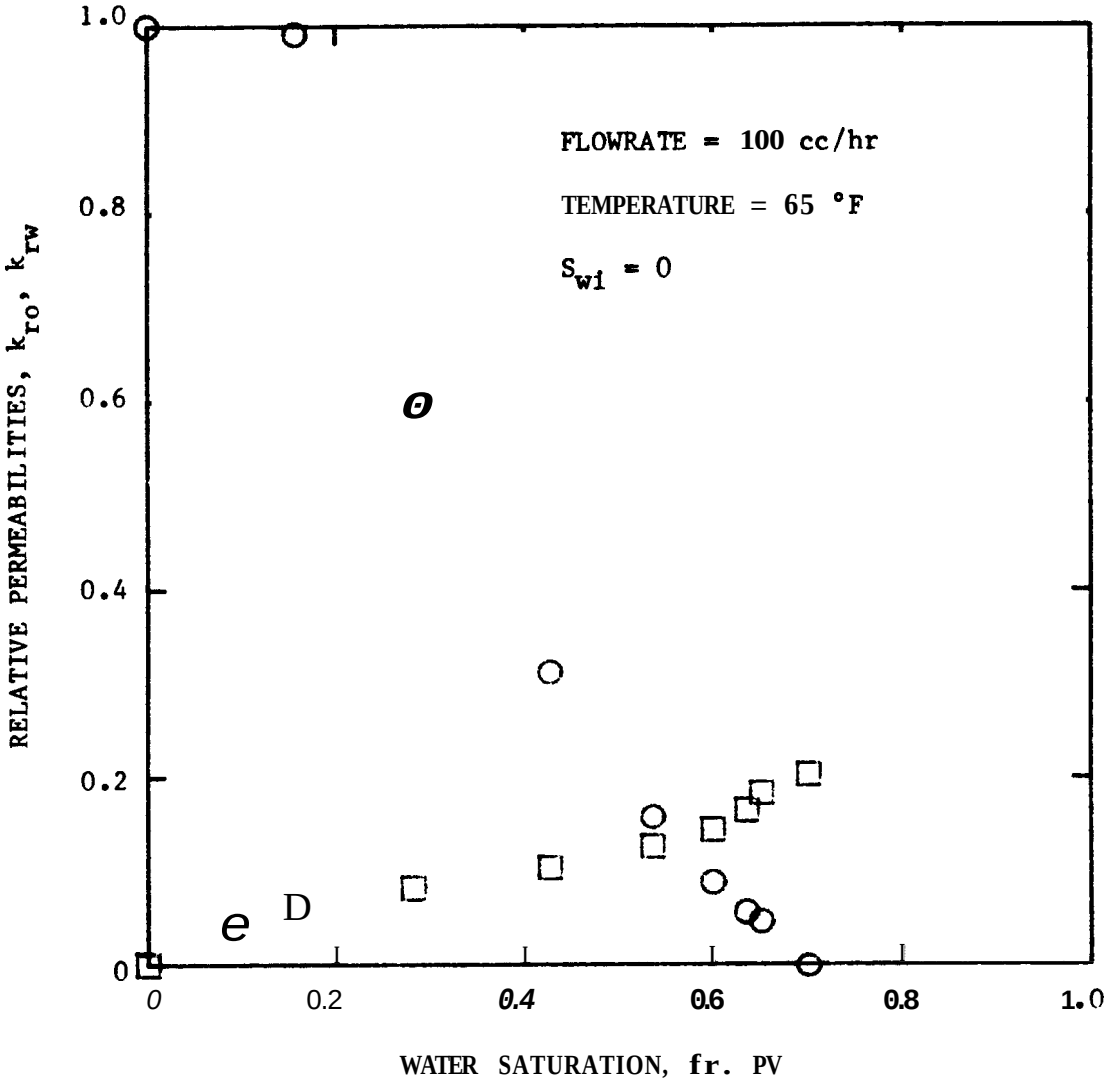

Fig. B-1.2 RELATIVE PERMEABILITIES VS WATER SATURATION (PV) FOR WATER DISPLACING OIL

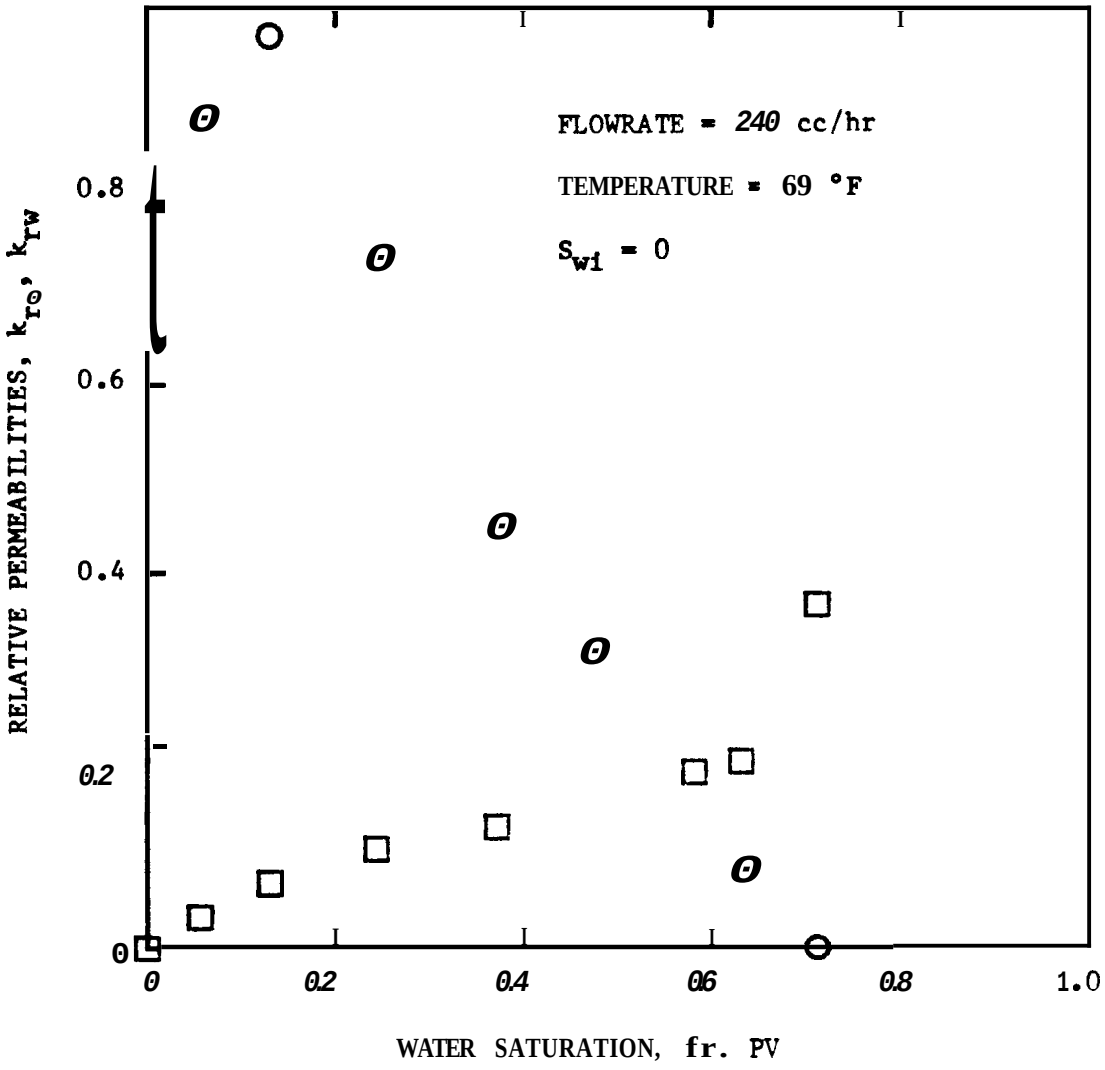

Fig. B-1.3 RELATIVE PERMEABILITIES VS WATER SATURATION (PV) FOR WATER DISPLACING OIL

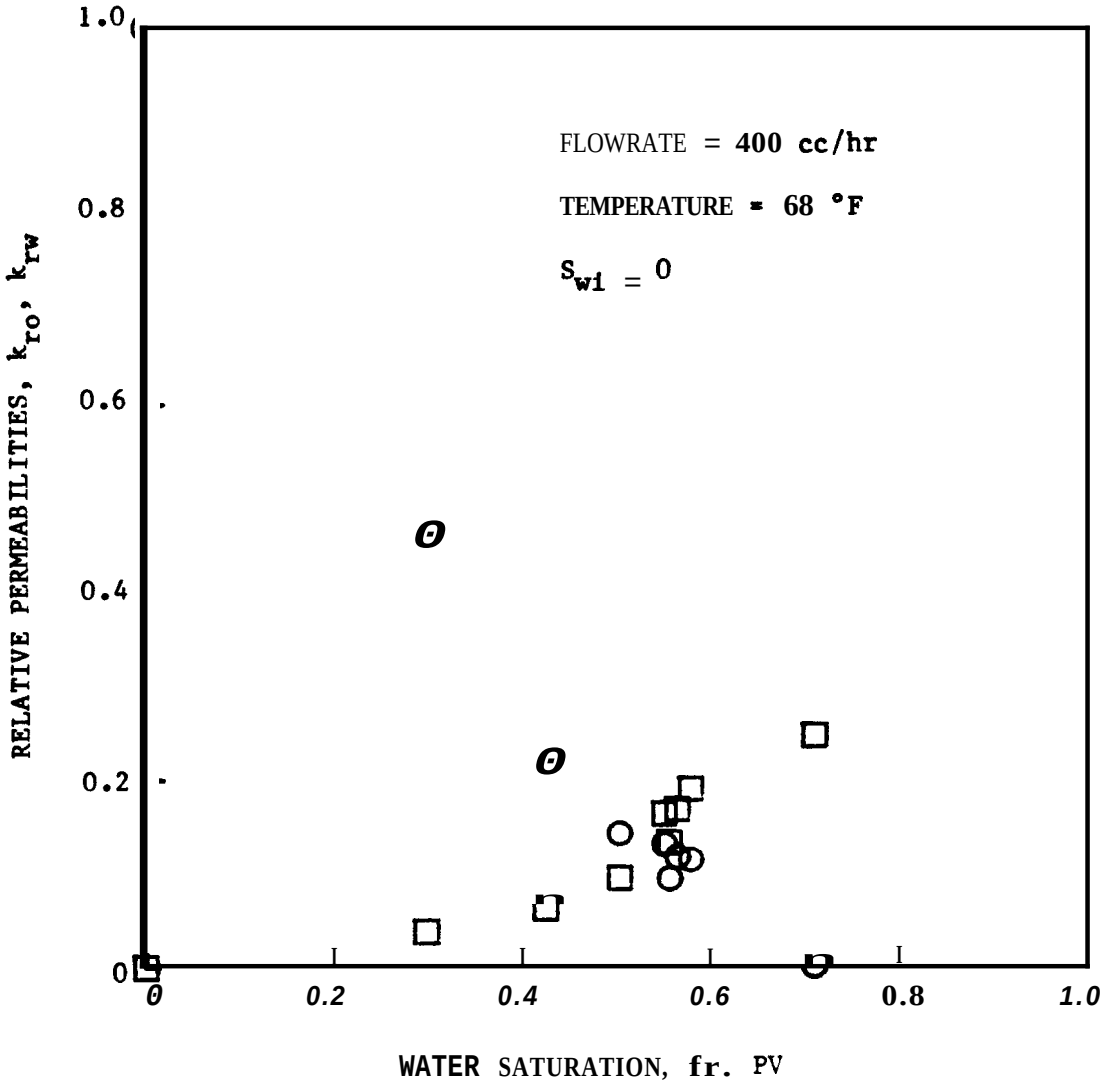

Fig. B-1.4 RELATIVE PERMEABILITIES VS WATER SATURATION (PV) FOR WATER DISPLACING OIL

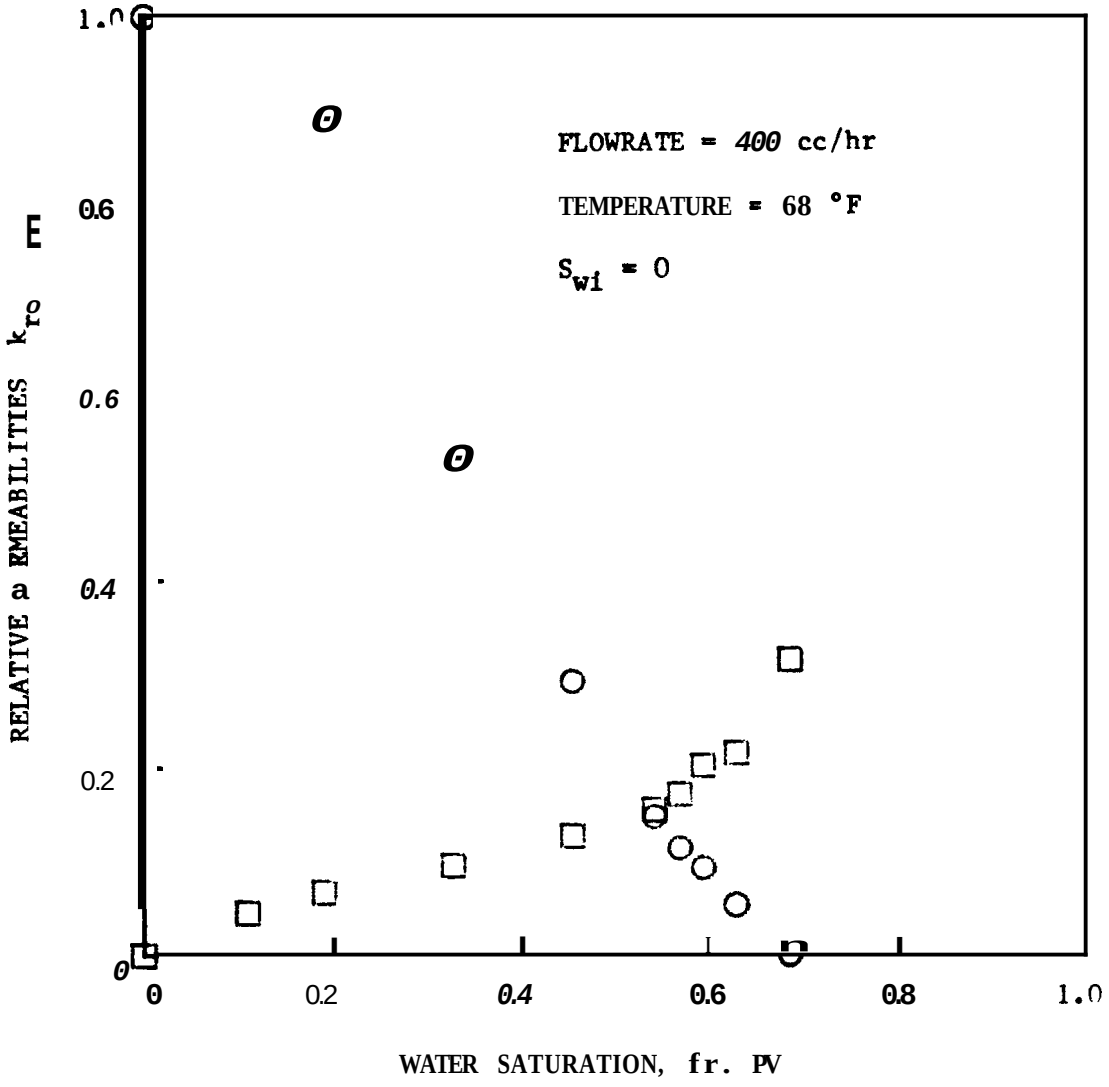

Fig. B-1.5 RELATIVE PERMEABILITIES VS WATER SATURATION (PV) FOR WATER DISPLACING OIL

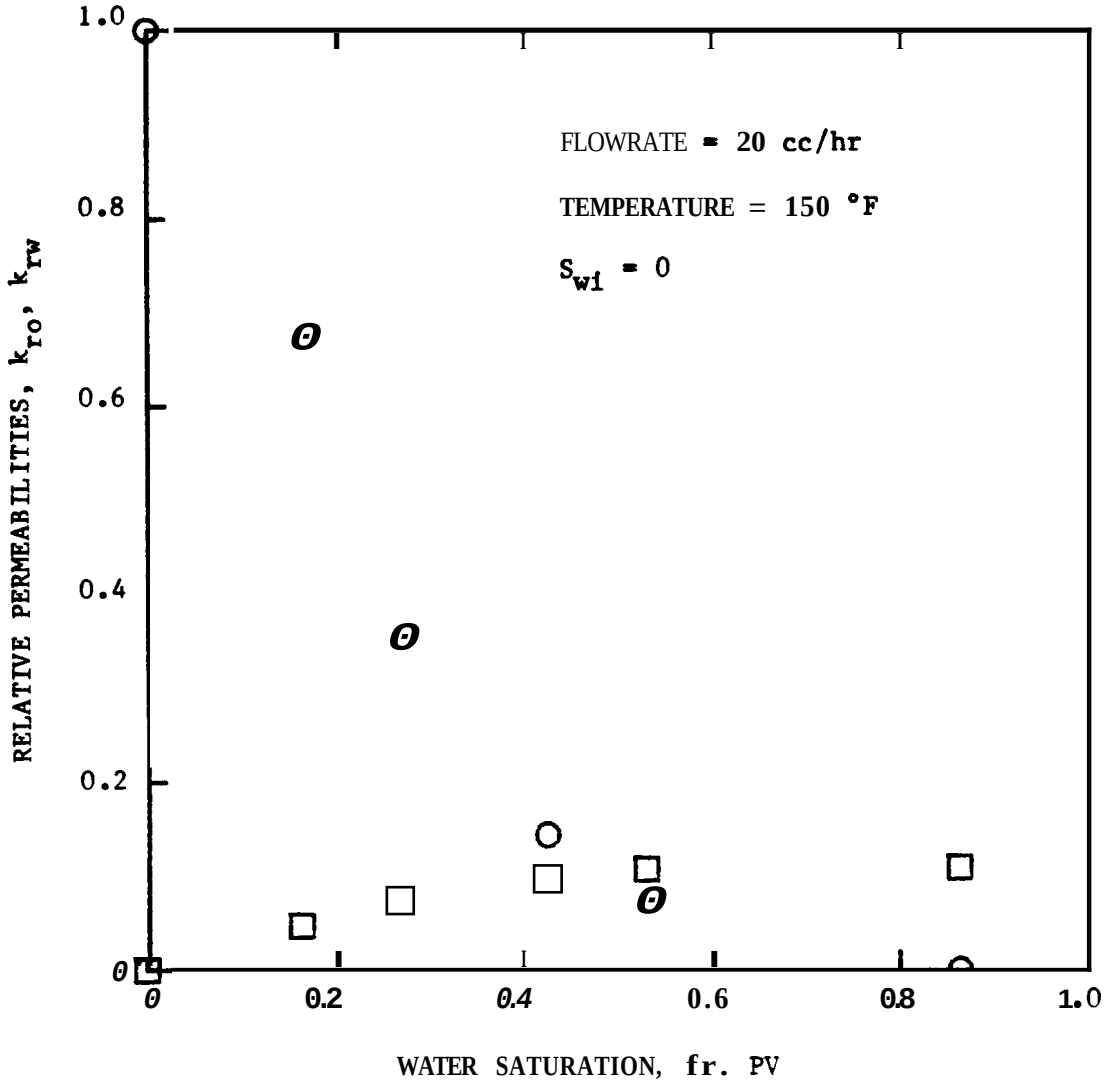

Fig. B-1.6 RELATIVE PERMEABILITIES VS WATER SATURATION (PV) FOR WATER DISPLACING OIL

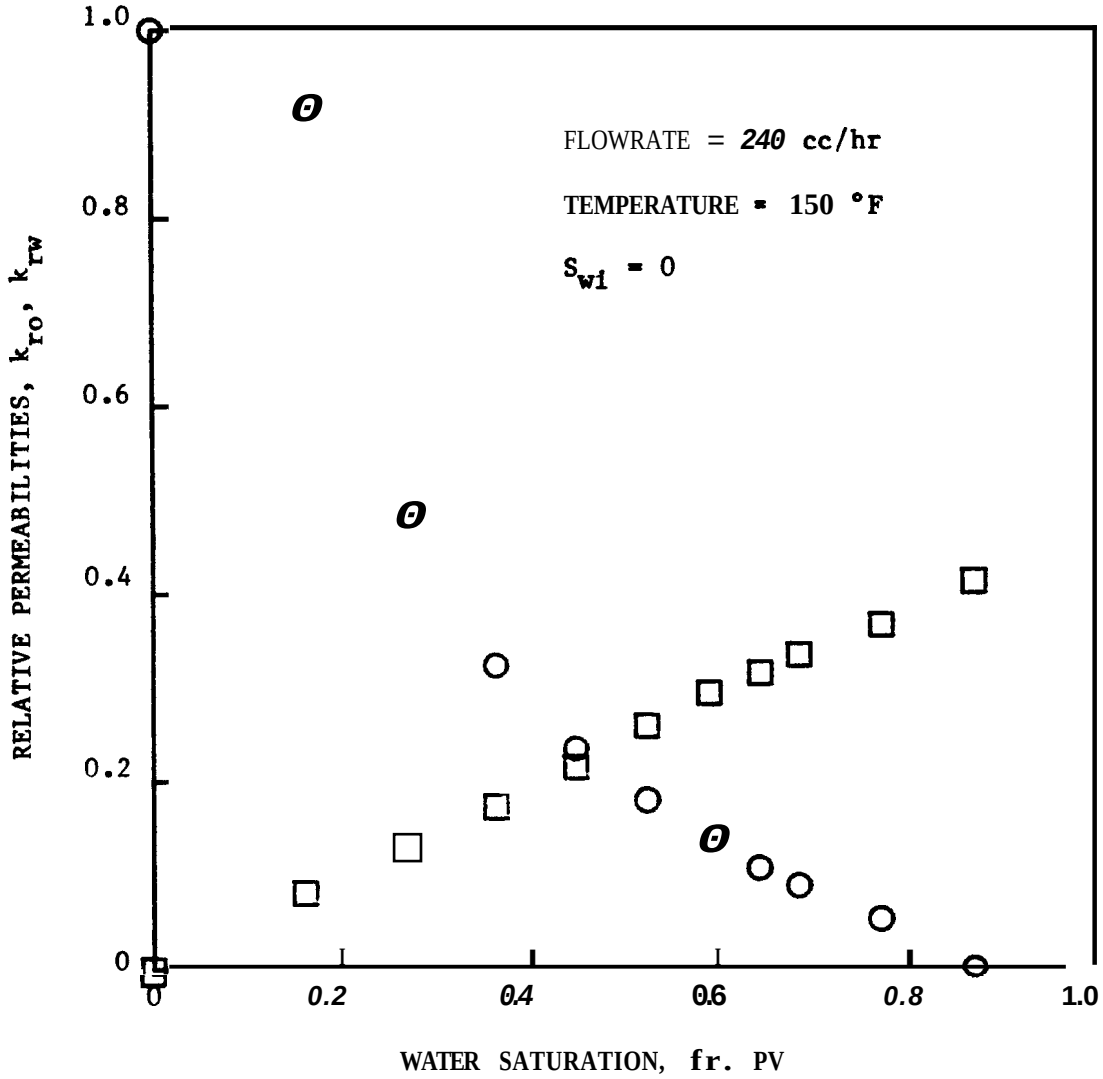

Fig. B-1.7 RELATIVE PERMEABILITIES VS WATER SATURATION (PV) FOR WATER DISPLACING OIL

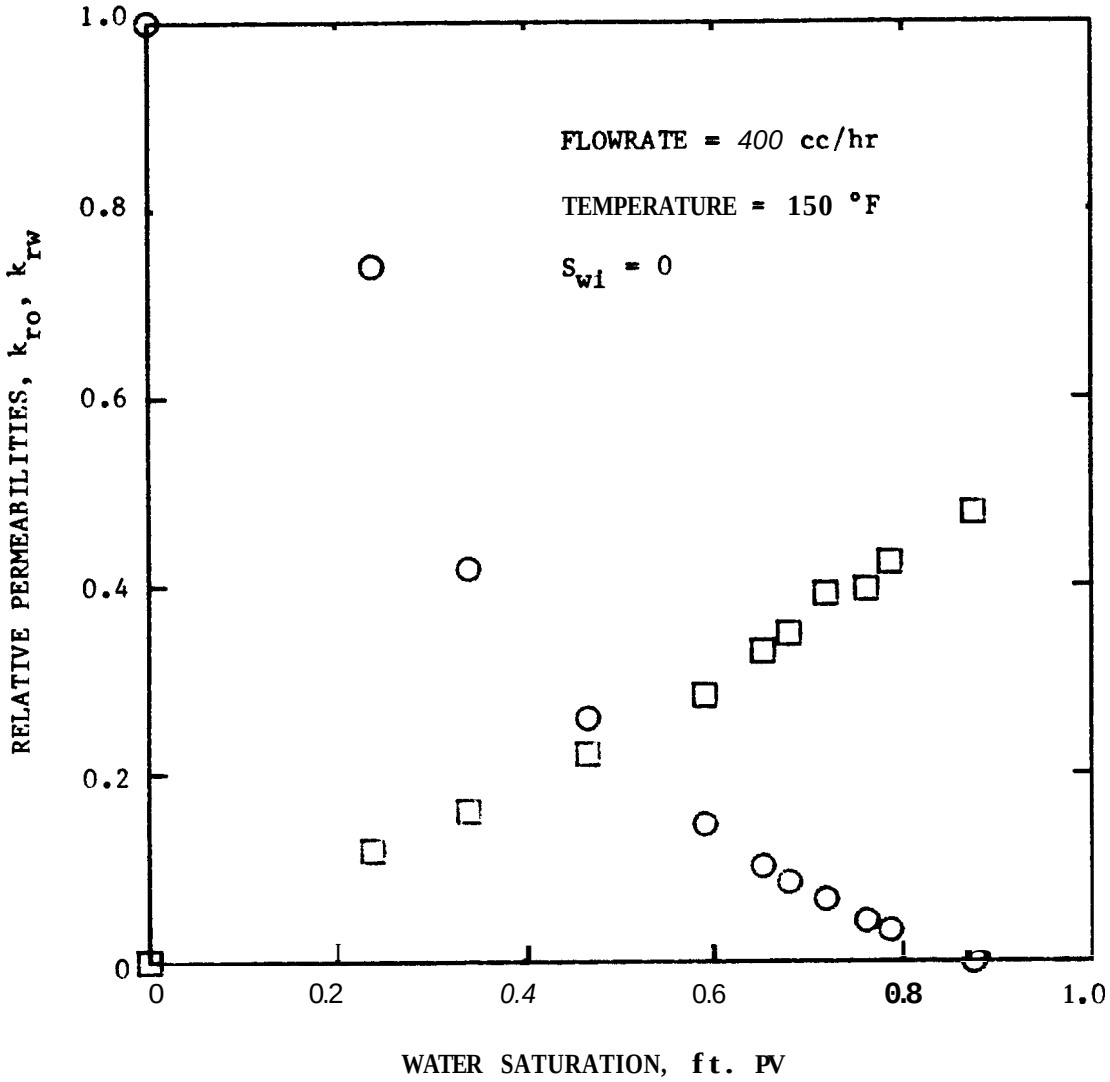

Fig. B-1.8 RELATIVE PERMEABILITIES VS WATER SATURATION (PV) FOR WATER DISPLACING OIL

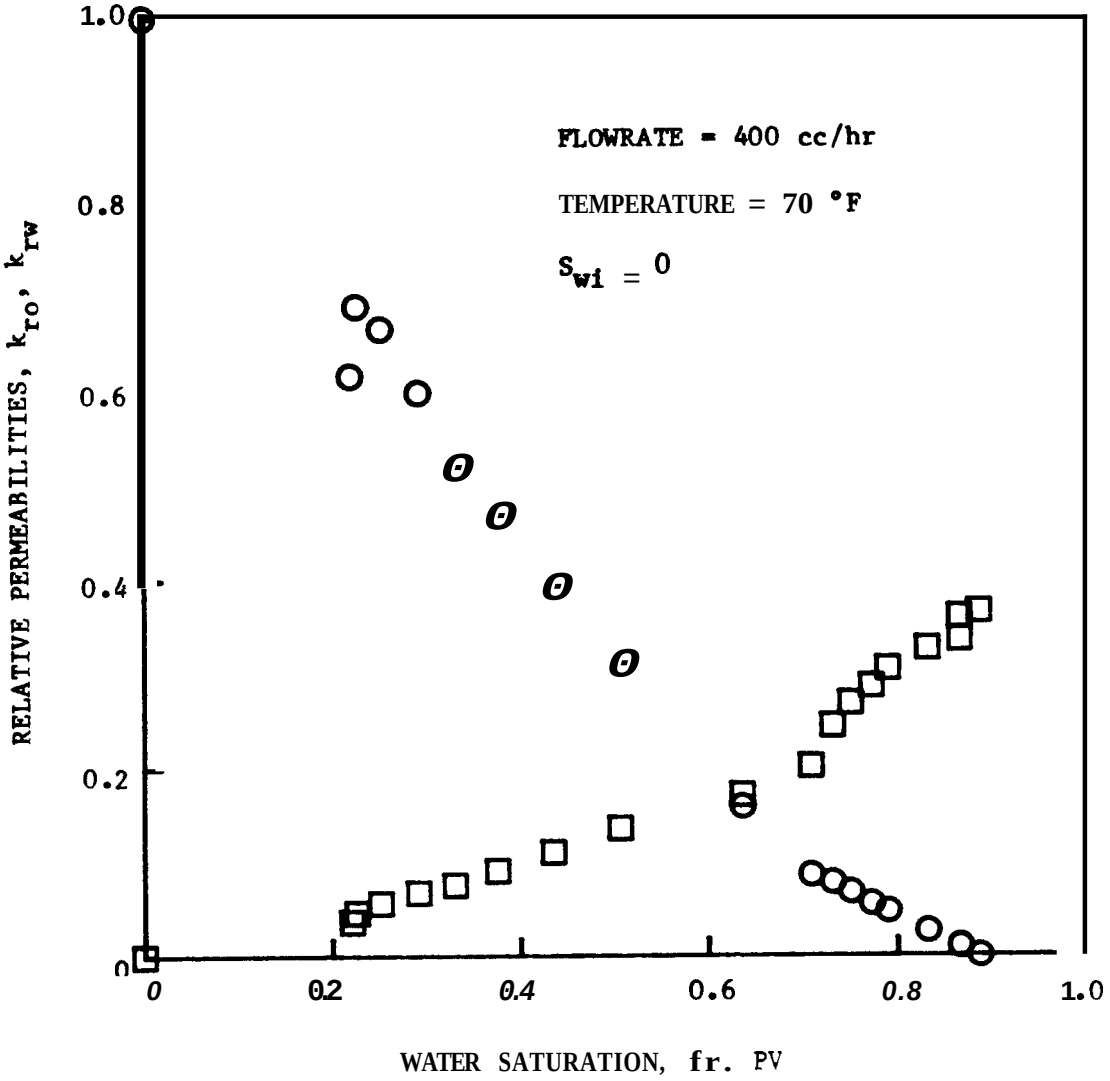

Fig. B-1.9 RELATIVE PERMEABILITIES VS WATER SATURATION (PV) FOR WATER DISPLACING OIL

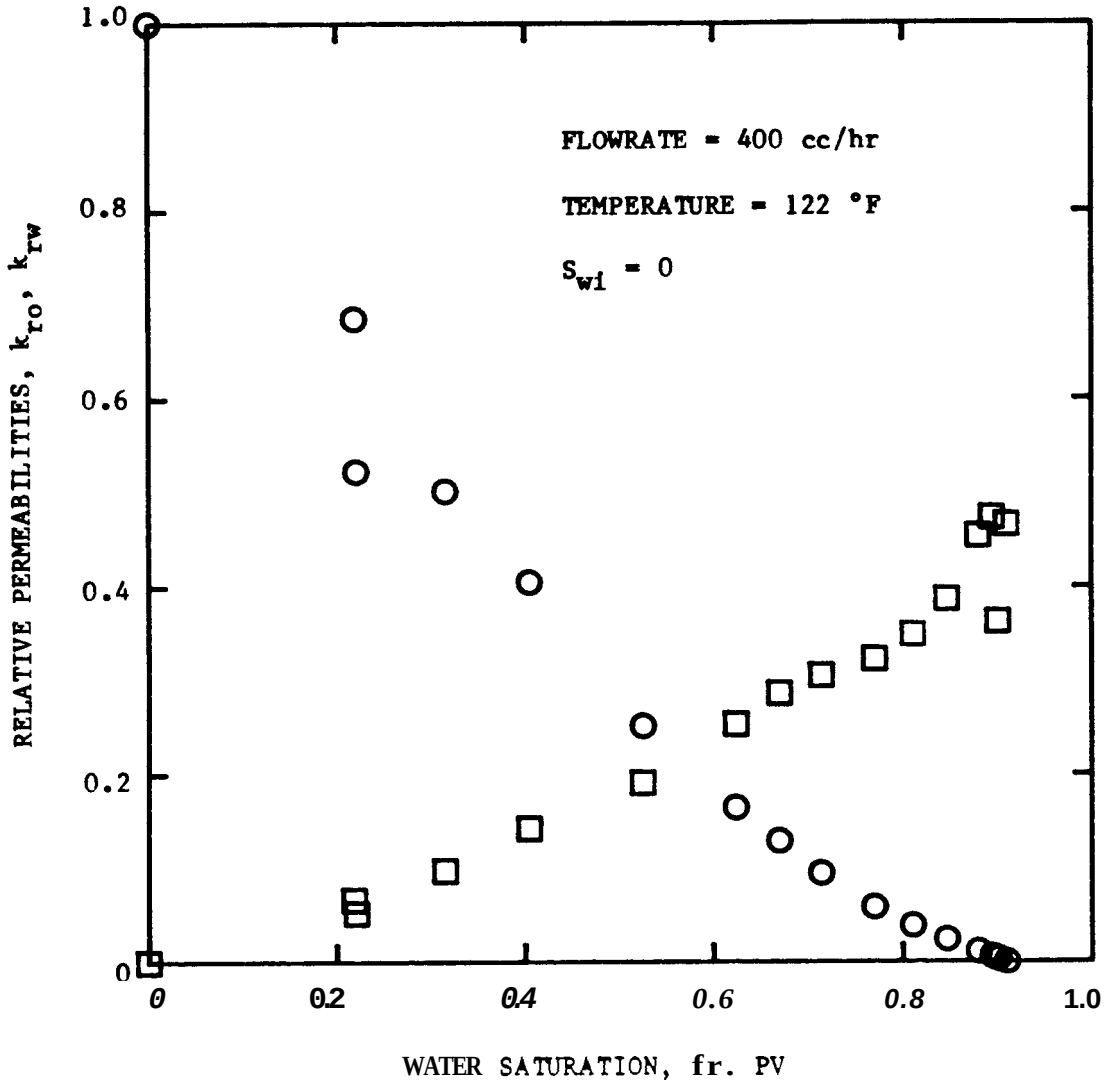

Fig. B-1.10 RELATIVE PERMEABILITIES VS WATER SATURATION (PV) FOR WATER DISPLACING OIL

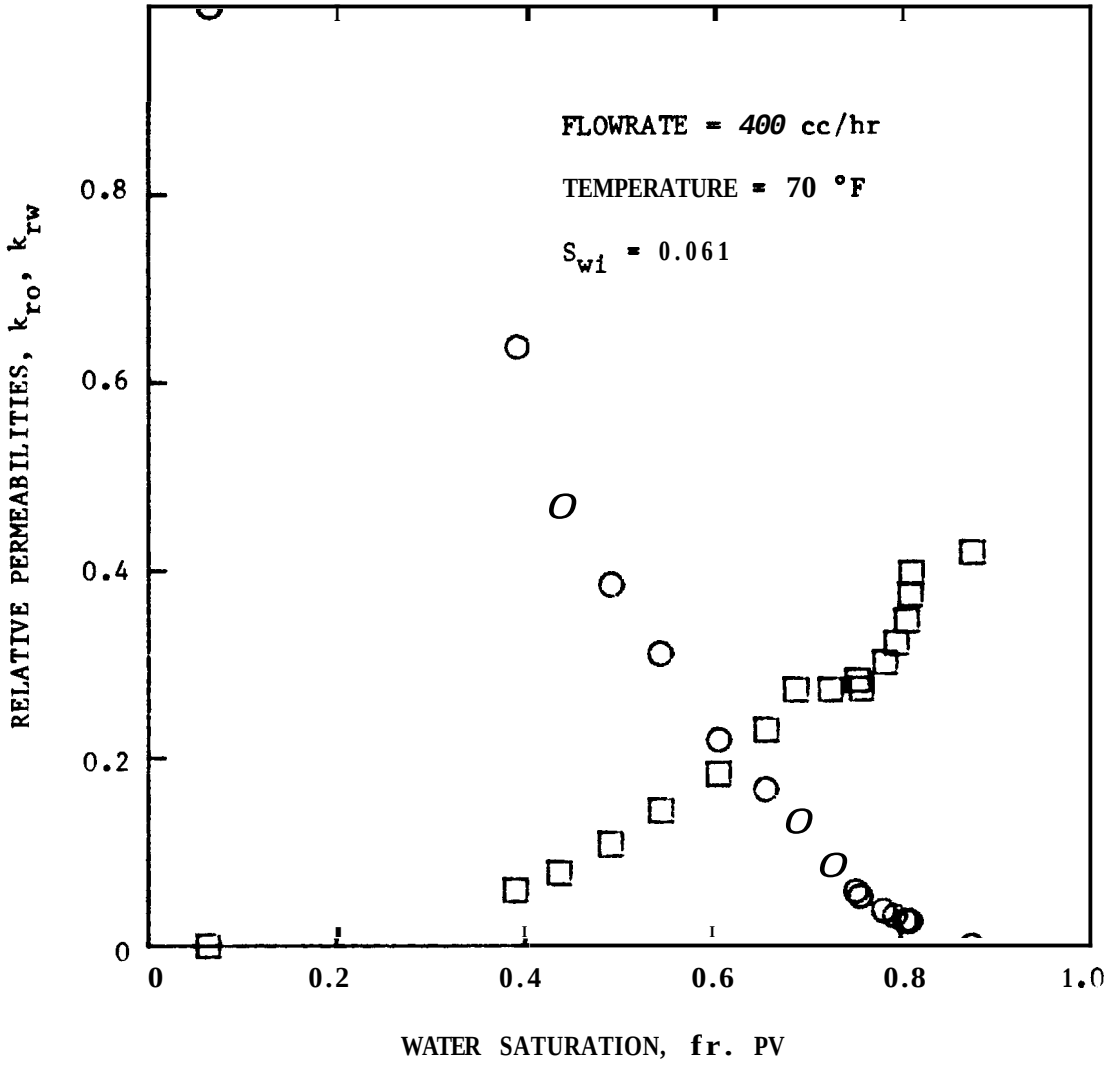

Fig. B-1.11 RELATIVE PERMEABILITIES VS WATER SATURATION (PV) FOR WATER DISPLACING OIL

APPENDIX B-2

PLOTS OF OIL AND WATER PERMEABILITY RATIO CURVES

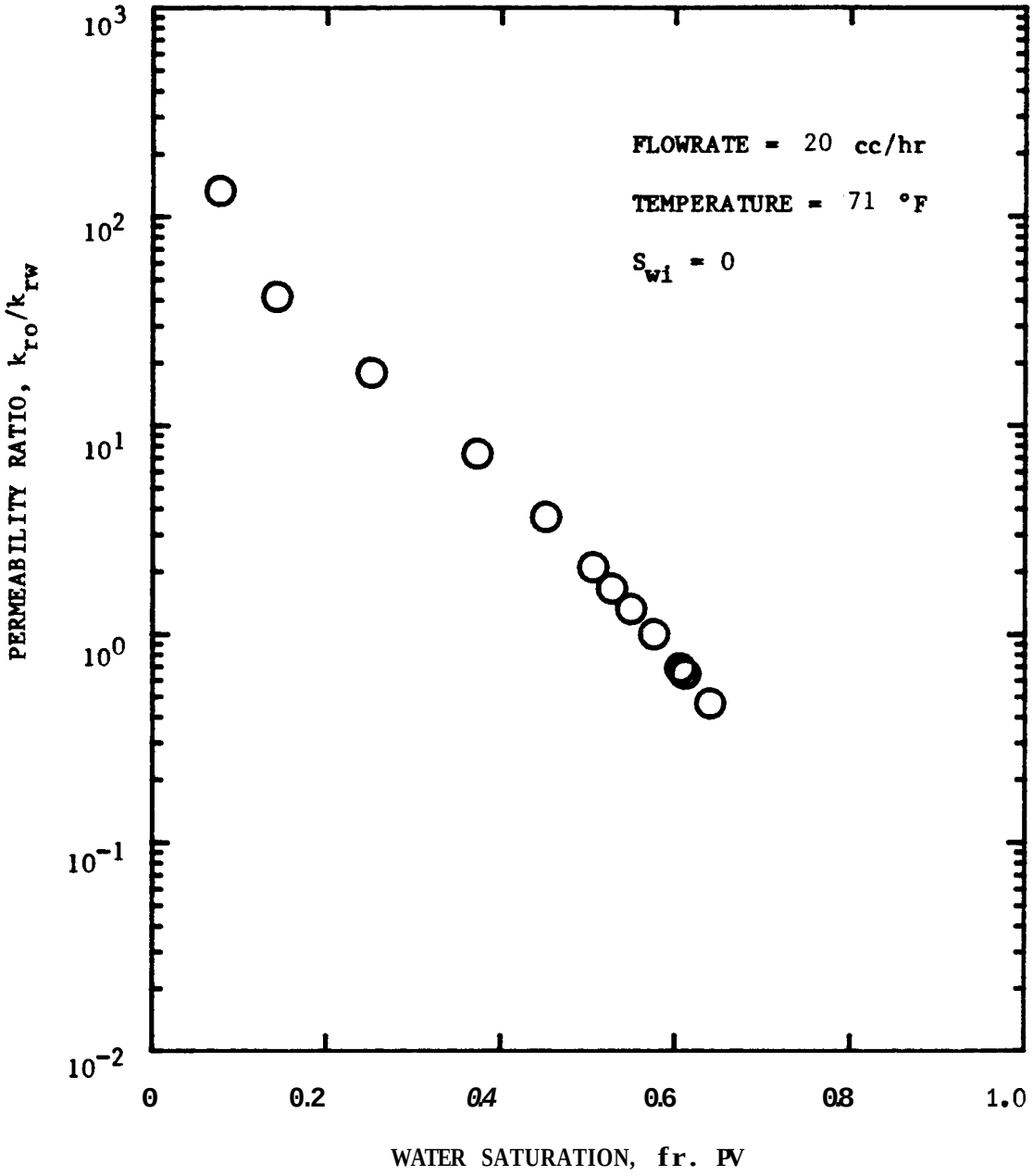

Fig. B-2.1 PERMEABILITY RATIO VS WATER SATURATION FOR WATER DISPLACING OIL

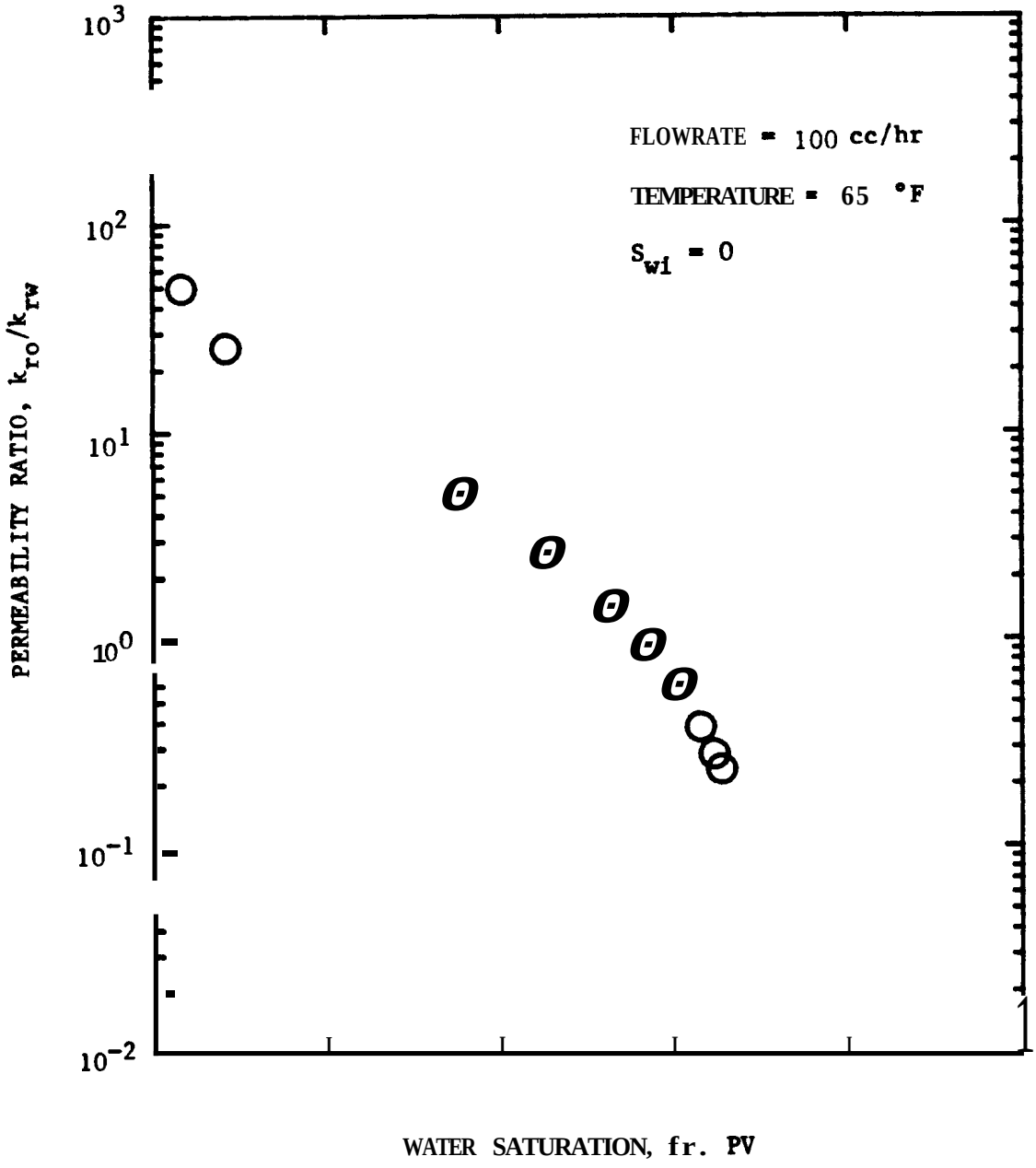

Fig. B-2.2 PERMEABILITY RATIO VS WATER SATURATION FOR WATER DISPLACING OIL

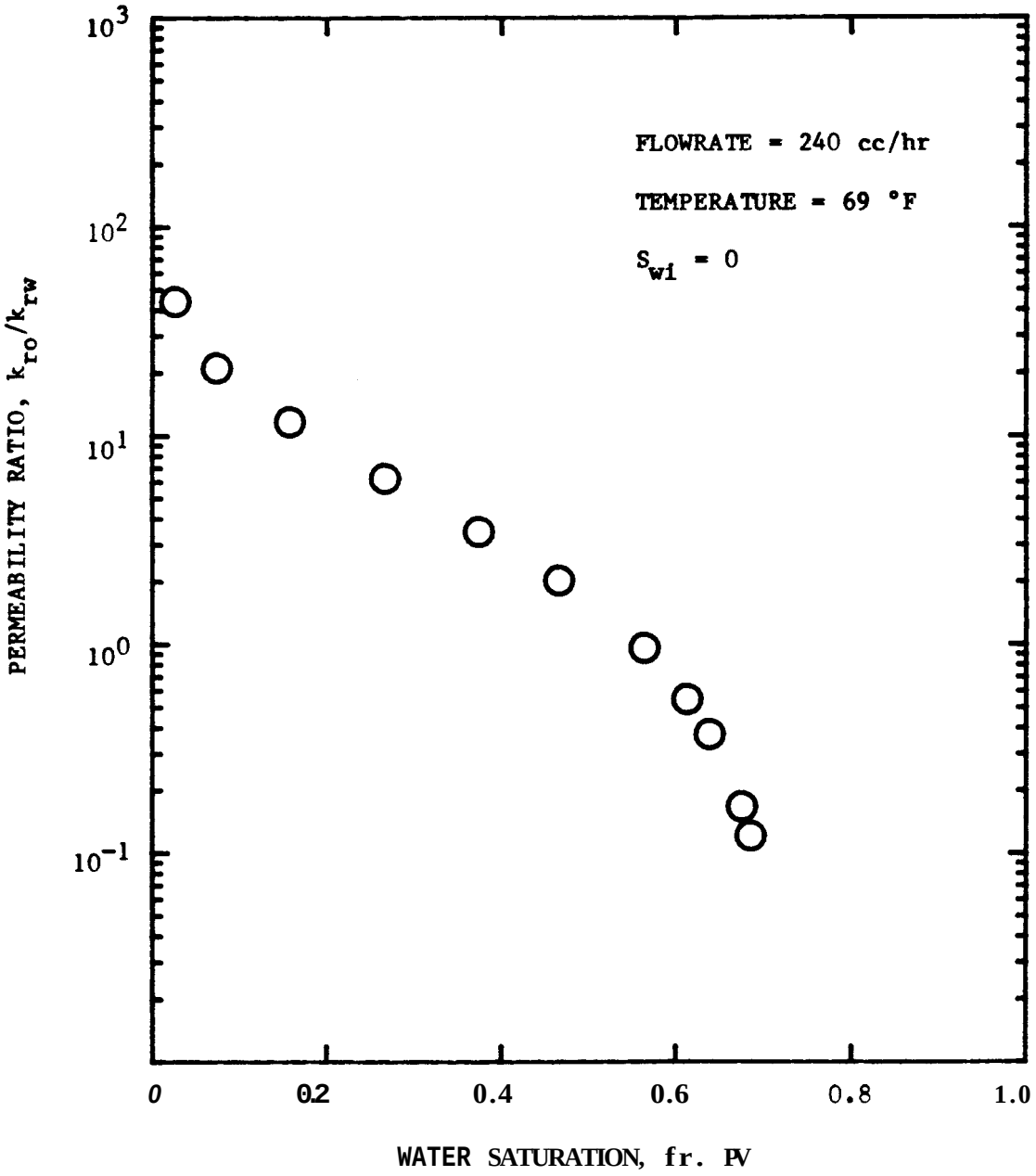

Fig. B-2.3 PERMEABILITY RATIO VS WATER SATURATION FOR WATER DISPLACING OIL

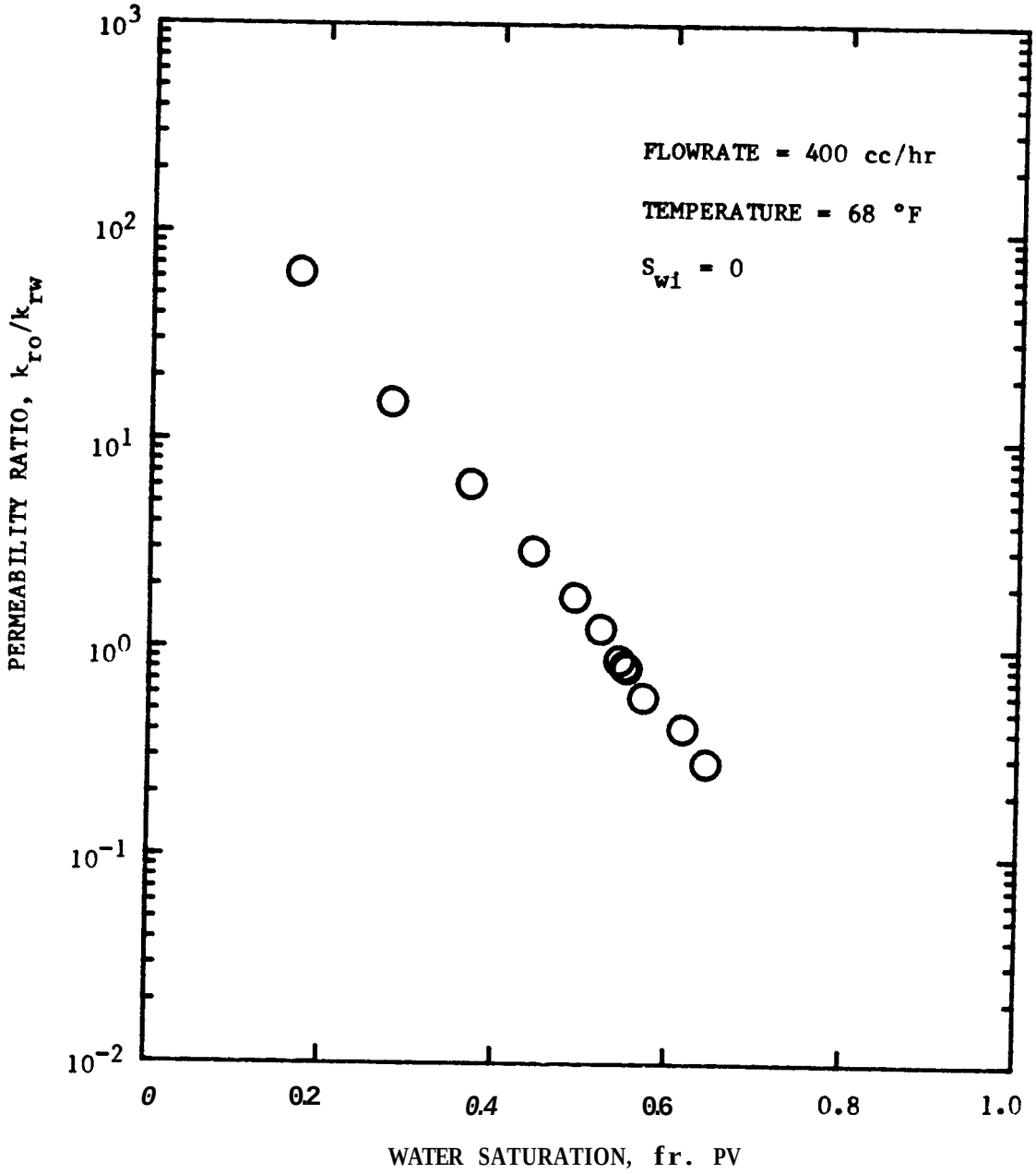

Fig. B-2.4 PERMEABILITY RATIO VS WATER SATURATION FOR WATER DISPLACING OIL

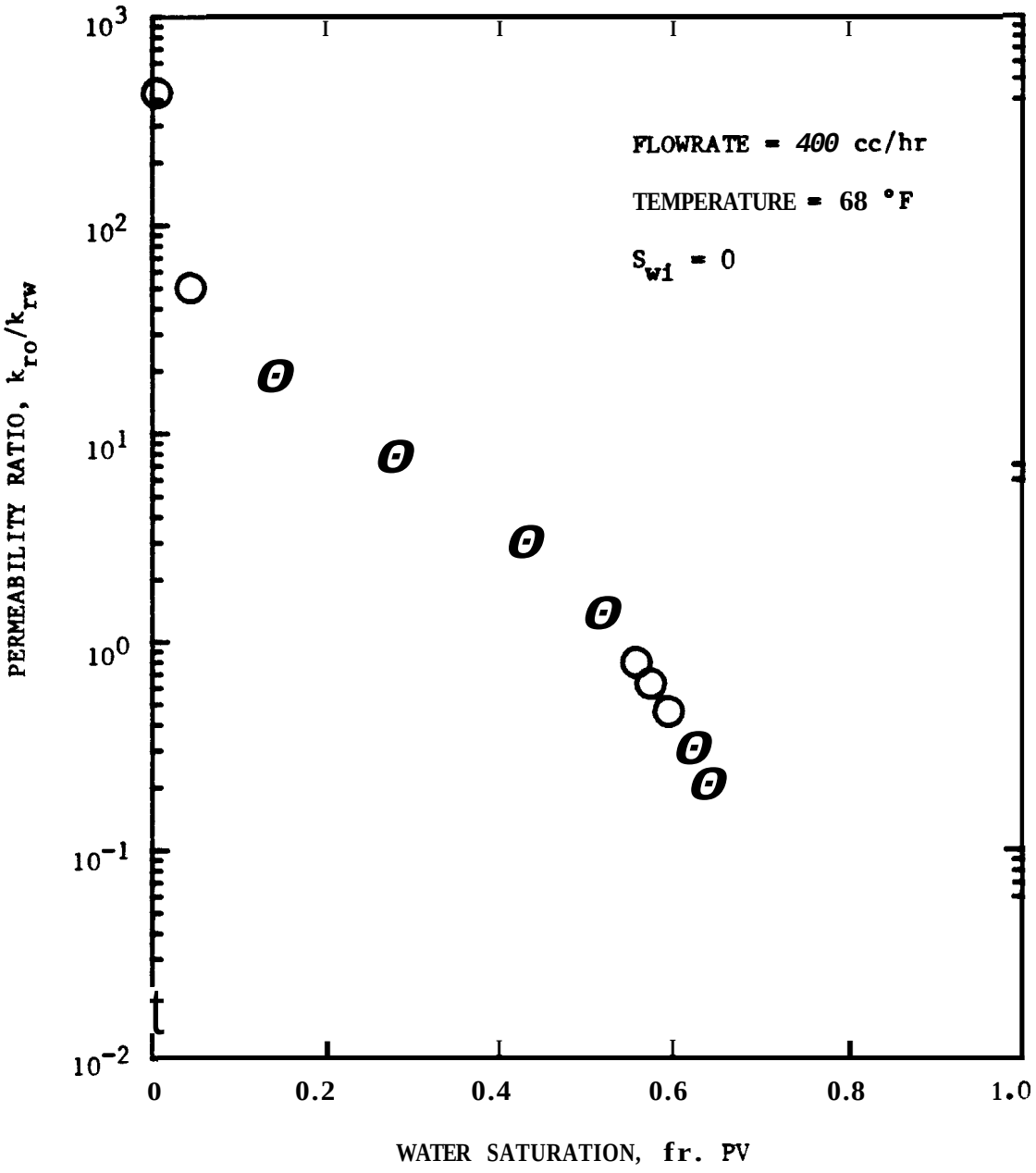

Fig. B–2.5 PERMEABILITY RATIO VS WATER SATURATION FOR WATER DISPLACING OIL

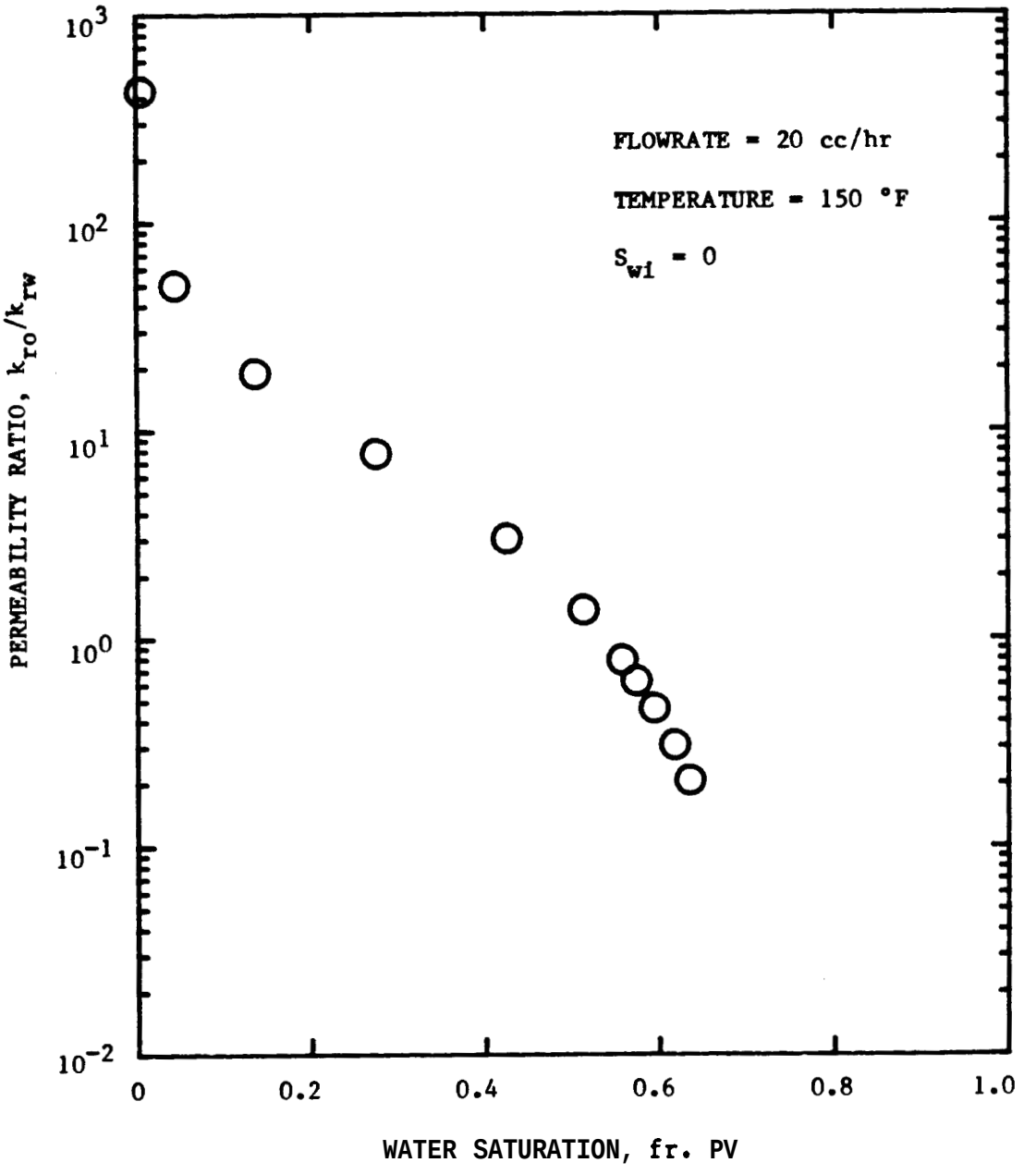

Fig. B-2.6 PERMEABILITY RATIO VS WATER SATURATION FOR WATER DISPLACING OIL

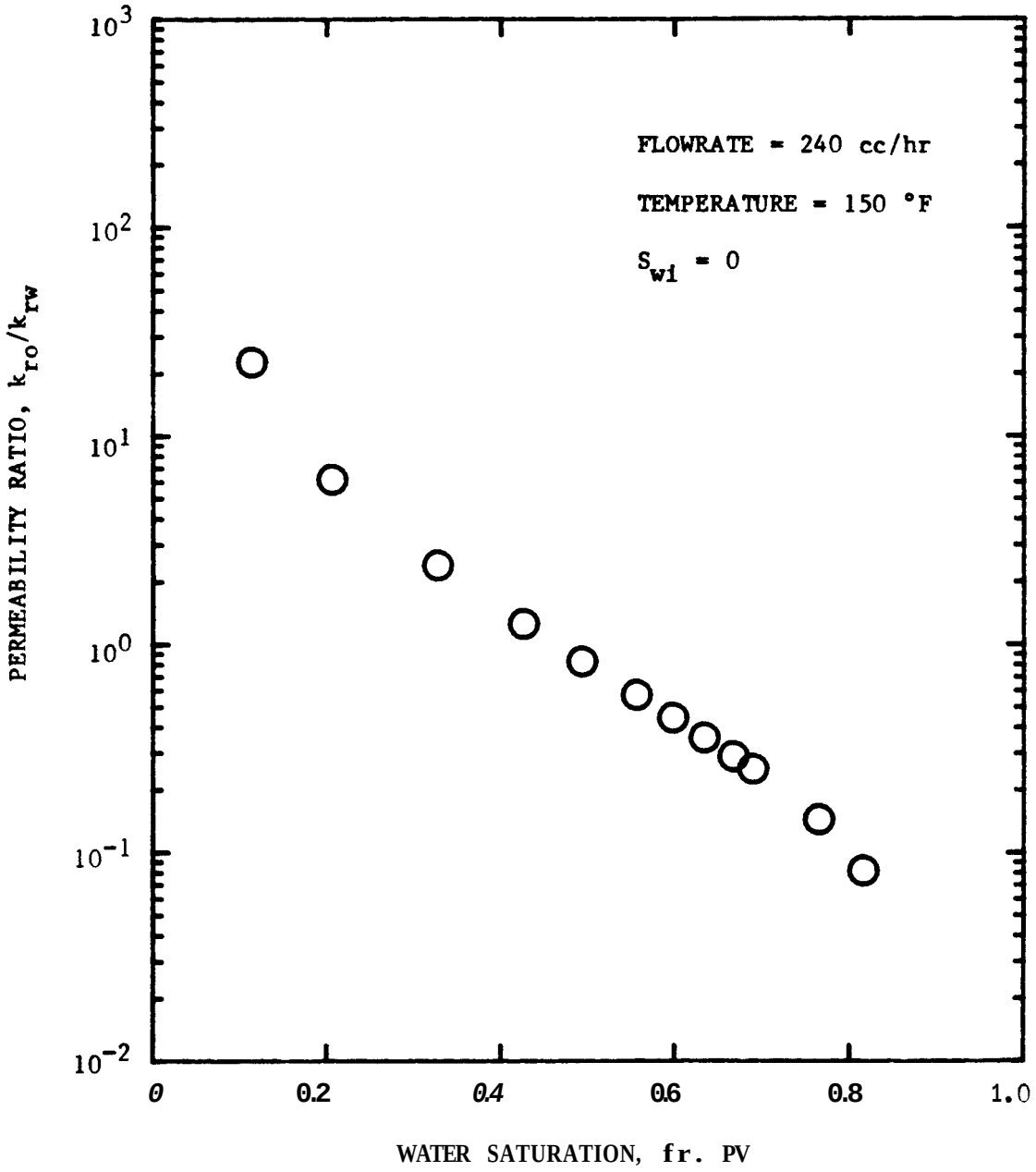

Fig. B–2.7 PERMEABILITY RATIO VS WATER SATURATION FOR WATER DISPLACING OIL

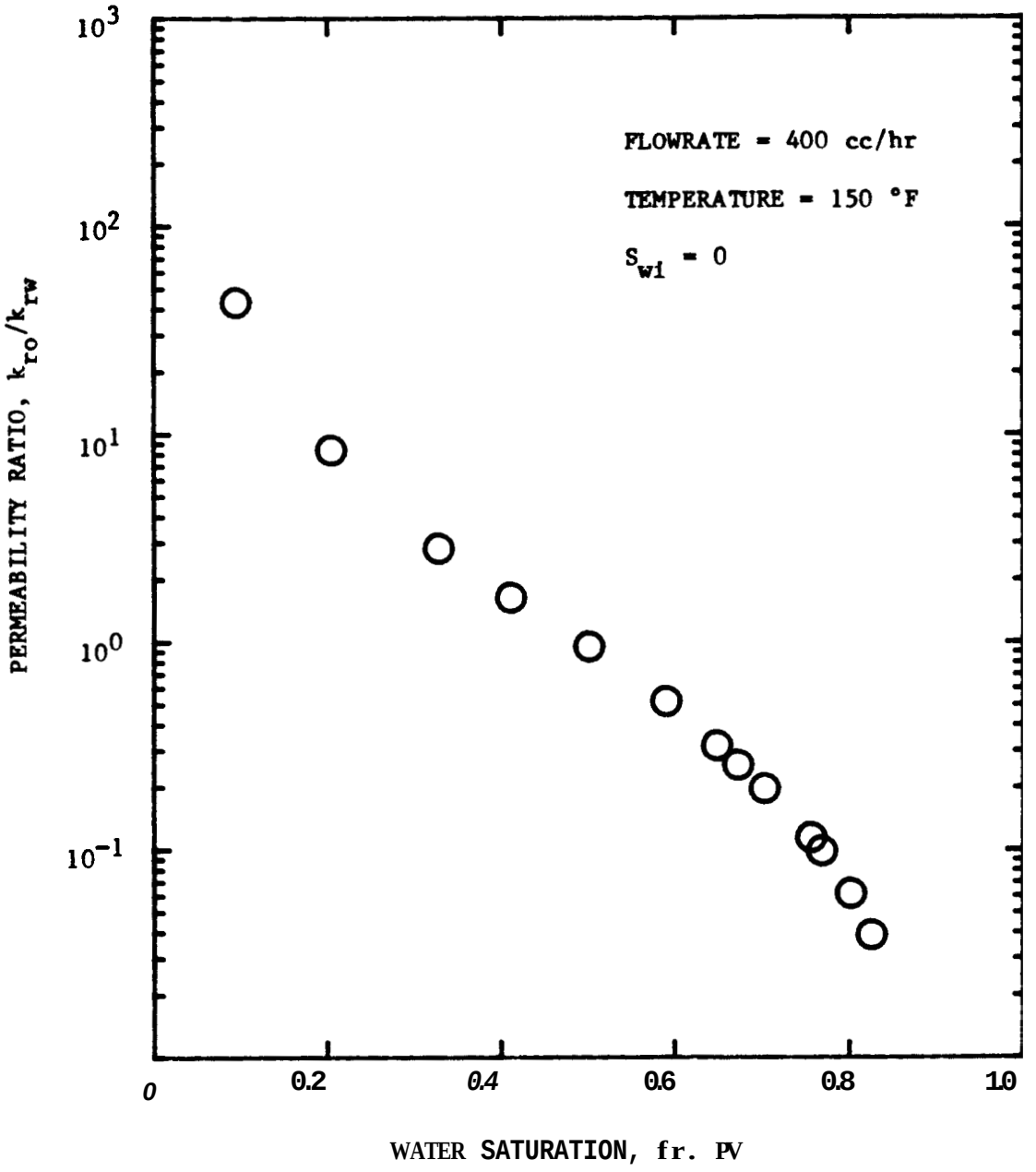

Fig. B-2.8 PERMEABILITY RATIO VS WATER SATURATION FOR WATER DISPLACING OIL

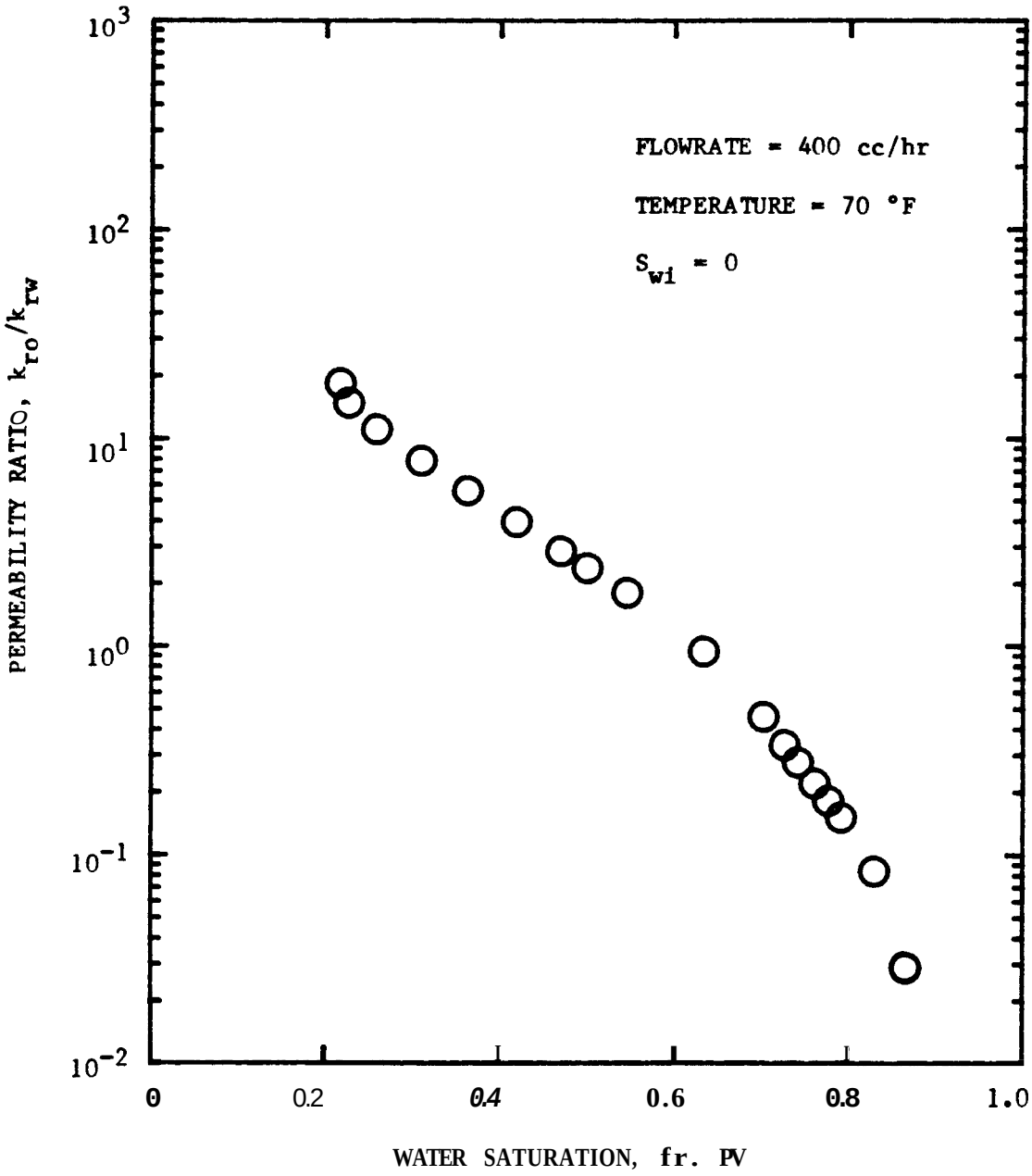

Fig. B-2.9 PERMEABILITY RATIO VS WATER SATURATION FOR WATER DISPLACING OIL

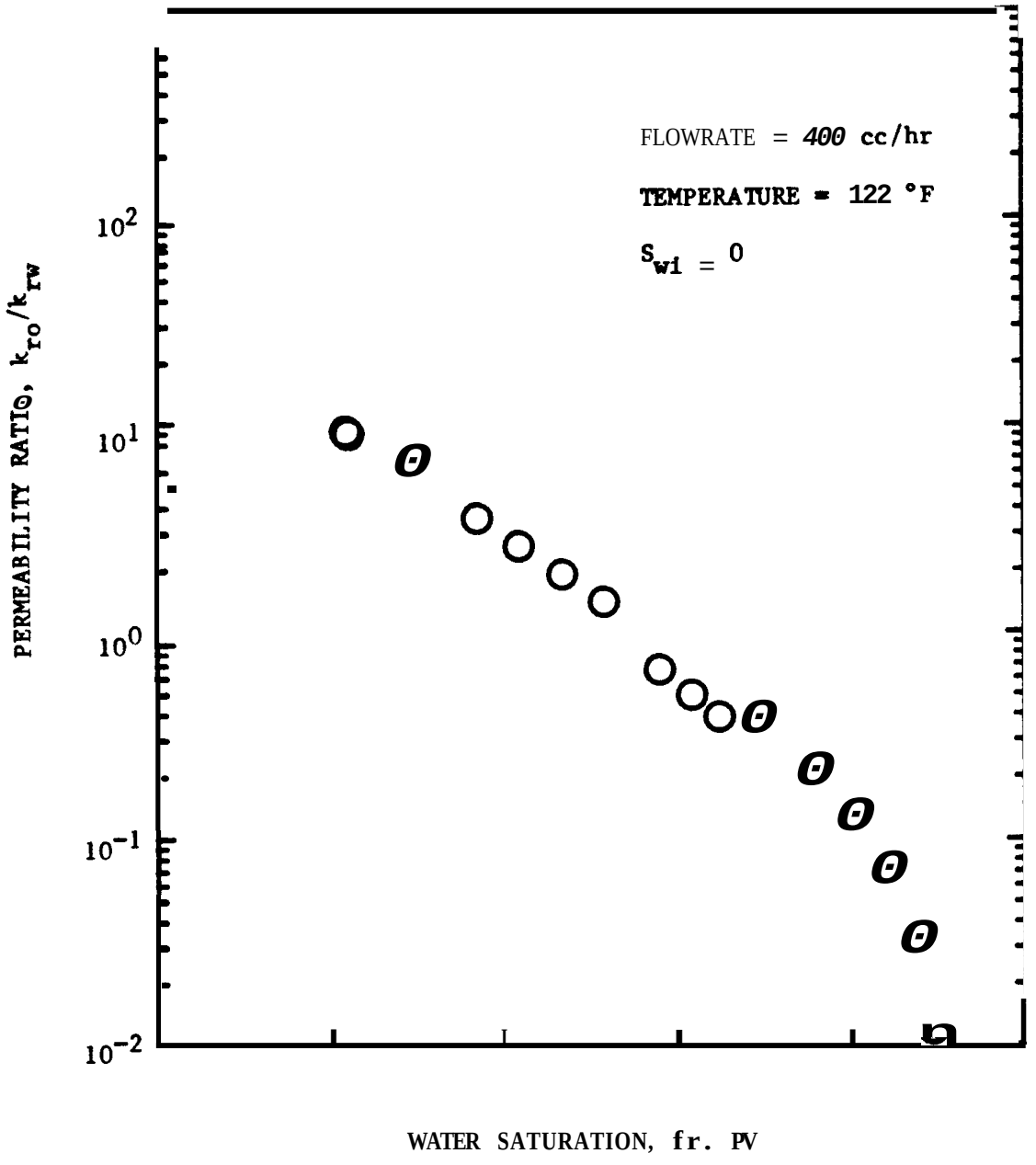

Fig. E-2.10 PERMEABILITY RATIO VS WATER SATURATION FOR WATER DISPLACING OIL

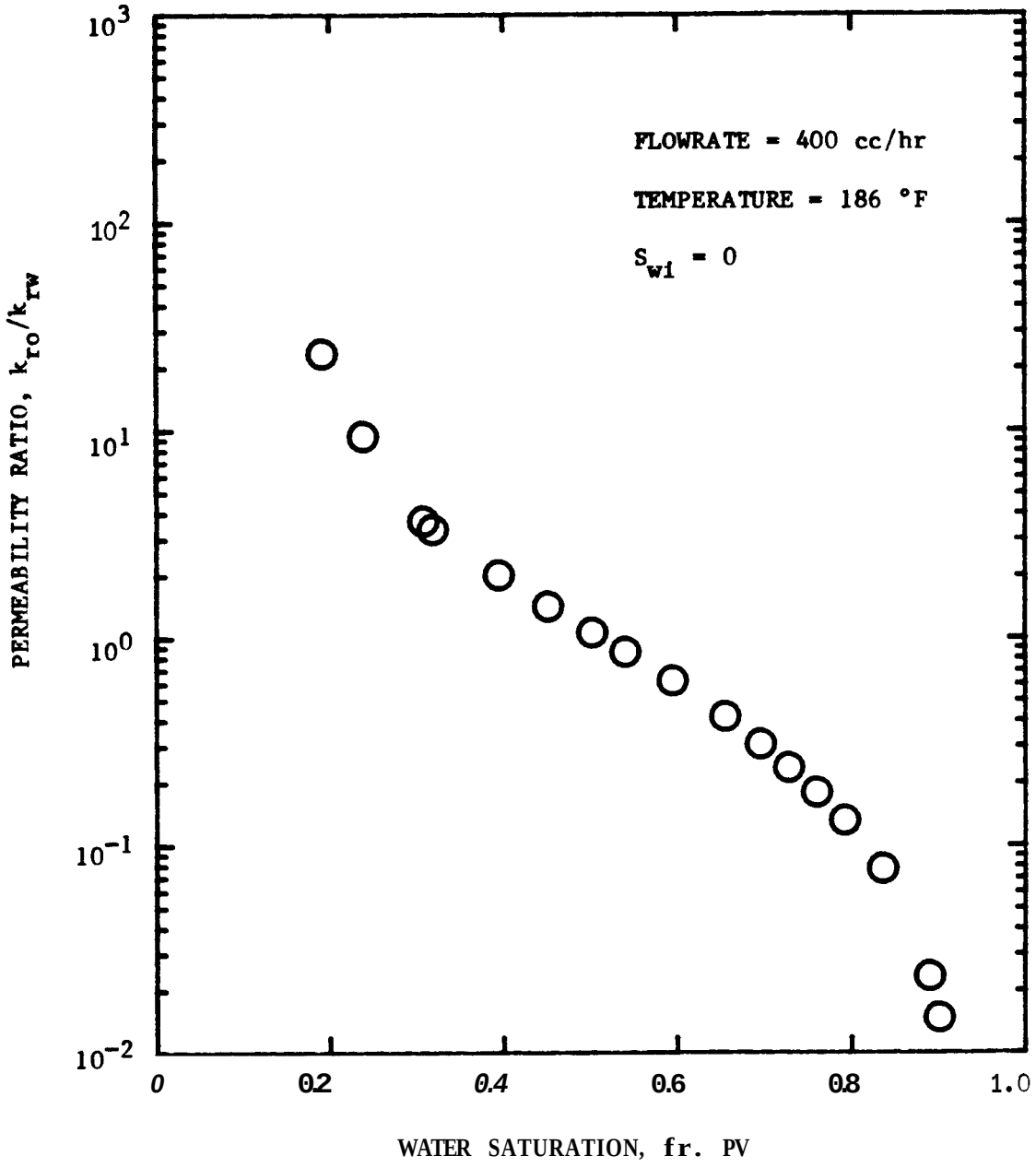

Fig. B-2.11 PERMEABILITY RATIO VS WATER SATURATION FOR WATER DISPLACING OIL

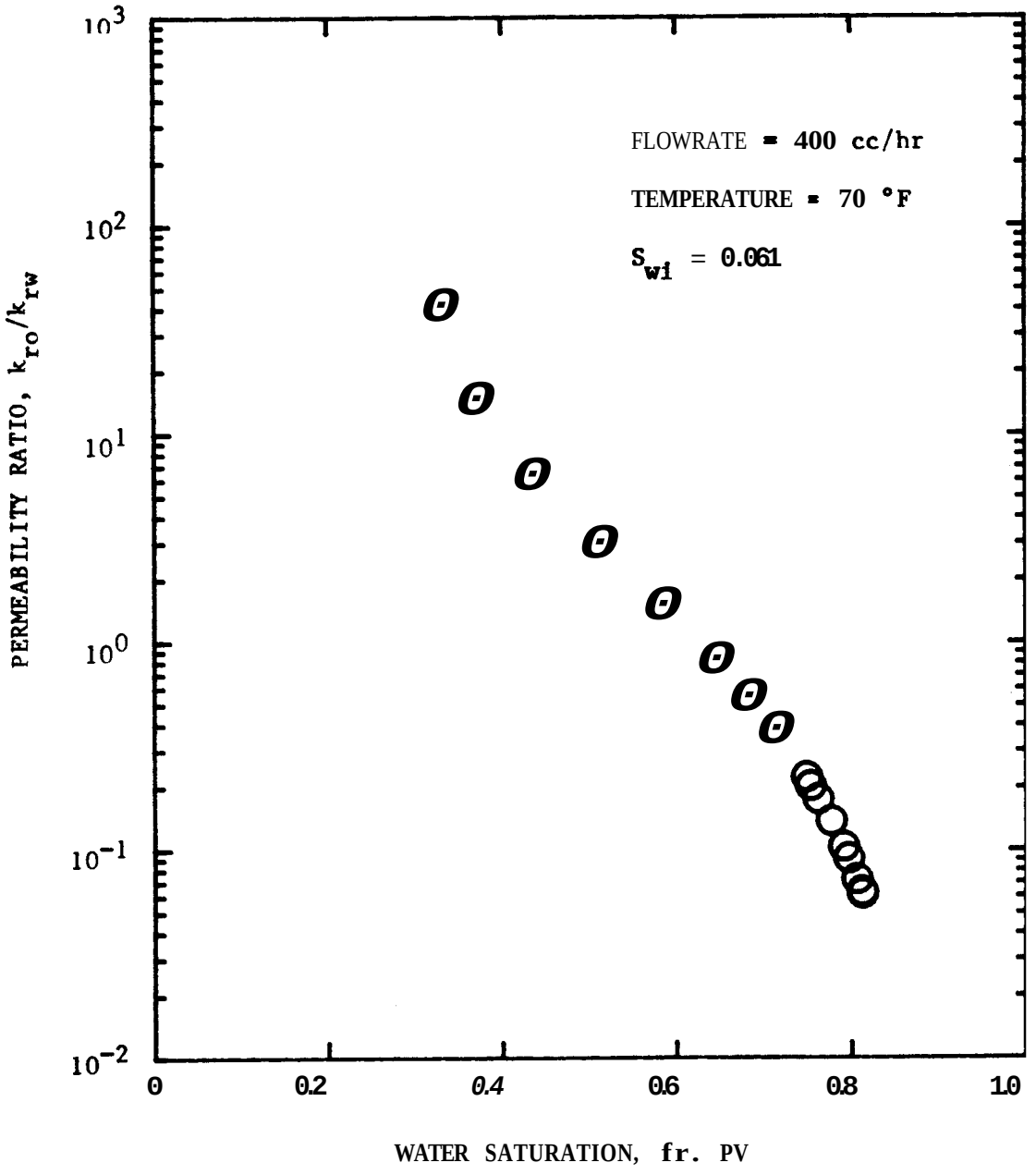

Fig. B-2.12 PERMEABILITY RATIO VS WATER SATURATION FOR WATER DISPLACING OIL

APPENDIX B-3

TABLES OF RELATIVE PERMEABILITIES AND PERMEABILITY RATIOS

SW	Kro/Krw	Kro	Krw
0.000		1.008	0.000
.104	83.458	1.069	.013
.165	34.924	.958	.027
.290	13.470	.667	.049
.407	5.401	.390	.072
.713	0.000	0.000	.086

SYSTEM PORE VOLUME	=	34.30	cc
FLOODING RATE	=	20	cc/hr
TEMPERATURE	=	71	F
INITIAL PRESSURE DROP	=	12	PSI
INITIAL WRTER SATURRTION	=	0.000	fr. PV
RESIDUAL OIL SATURATION	=	.287	fr-. PV
VISCOSITY RATIO	=	228.0	

Table B-3.1

PERMEABILITY DATA VS WATER SATURATION FOR
WATERFLOOD (q = 20 cc/hr, T = 71.0 F)

SW	Kro/Krw	Kro	Krw
0.008		1.000	8.008
.057	27.577	.899	.033
.131	14.100	.971	.069
.244	7.114	.747	.105
.372	3.493	.449	.129
.712	0.800	0.000	.210

SYSTEM PORE VOLUME	=	34.38	cc
FLOODING RATE	=	240	cc/hr
TEMPERATURE	=	69	F
INITIAL PRESSURE DROP	=	157	PSI
INITIAL WATER SATUPHTION	=	0.000	fr. PV
RESIDUAL OIL SATURATION	=	.288	fr. PV
VISCOSITY RATIO	=	230.0	

Table E-3.3

PERMEABILITY DHTA VS WHTEP SATURATION FOP
WATERFLOOD (q = 248 cc hr, T = 69.0 F)

Sw	Kro/Krw	Kro	Krw
0.000		1.000	0.000
.298	12.25%	.462	.038
.425	3.501	.219	.063
.505	1.49%	.142	.095
.557	.711	.094	.132
.711	0.000	0.000	.197

SYSTEM PORE VOLUME	=	34.48	cc
FLOODING RATE	=	400	cc/hr
TEMPERATURE	=	68	F
INITIAL PRESSURE DROP	=	227	PSI
INITIAL WATER SATURATION	=	0.000	fr. PV
RESIDUAL OIL SATURATION	=	.289	fr. PV
VISCOSITY RATIO	=	240.0	

Table B-3.4

PERMEABILITY DATA VS WATER SATURATION FOR
WATERFLOOD (q = 400 cc/hr, T = 68.0 F)

SW	Kro/Krw	Kro	Krw
0.000		1.000	0.006
.110	25.138	1.140	.045
.191	13.386	.891	.067
.330	5.525	.530	.096
.456	2.299	.291	.127
,543	.952	.147	.154
.687	0.000	0.000	.236

SYSTEM PORE VOLUME	=	34.30	cc
FLOODING RATE	=	400	cc/hr
TEMPERATURE	=	68	F
INITIAL PRESSURE DROP	=	232	PSI
INITIAL WRTEP SATURATION	=	0.000	fr. PV
RESIDUAL OIL SATURATION	=	.313	fr. PV
VISCOSITY RATIO	=	240.0	

Table **B-3.5**

PERMEAEILITY DATA VS WATER SATURATION FOR
WATERFLOOD (q = 400 cc/hr, T = 68.0 F)

SW	Kro/Krw	Kro	Krw
0.000		1.008	0.008
.165	14.377	.675	.047
.863	0.000	0.000	.084

SYSTEM PORE VOLUME	=	34.36	cc
FLOODING RATE	=	20	cc/hr
TEMPERATURE	=	156	F
INITIAL PRESSURE DROP	=	2	PSI
INITIAL WATER SATURATION	=	0.006	fr. PV
RESIDUAL OIL SATURATION	=	.137	fr. PV
VISCOSITY RATIO	=	43.5	

Table B-3.6

PERMEABILITY DATH VS WATER SATURATION FOR
WATERFLOOD (q = 20 cc/hr, T = 150.0 F)

SW	Kro/Krw	Kro	Krw
0.000		1.800	0.000
.163	11.509	.916	.080
.270	3.767	.483	.128
.365	1.884	.322	.171
.450	1.092	.233	.214
.525	.690	.177	.257
.591	.465	.135	.291
.872	0.000	0.800	.363

SYSTEM PORE VOLUME	=	34.36	cc
FLOODING RATE	=	240	cc/hr
TEMPERATURE	=	150	F
INITIRL PRESSURE DROP	=	16	PSI
INITIAL WATER SATURATION	=	0.000	fr. PV
RESIDUAL OIL SRTURHTION	=	.128	fr. PV
VISCOSITY RATIO	=	43.5	

Table B-3.7

PERMEABILITY DATR VS WATER SRTURATION FOR
WATERFLOOD (q = 240 cc/hr, T = 150.0 F)

[redacted]

SW	Kro/Krw	Kro	Krw
8.080		1.000	0.080
,238	6.263	.740	.118
.340	2.613	.419	.160
.467	1.174	.259	.221
.591	.516	.146	.283
.652	.307	.101	.330
.680	.241	.084	.349
.875	0.800	0.000	.434

SYSTEM PORE VOLUME = 34.30 cc
FLOODING RATE = 490 cc/hr
TEMPERATURE = 150 F
INITIAL PRESSURE DROP = 30 PSI
INITIAL WATER SATURATION = 0.000 fr. PV
RESIDUAL OIL SATURHTION = .125 fr. PV
VISCOSITY RATIO = 43.5

Table **B-3.8**

PERMEABILITY DATA VS MATER SATURATION FOR
WATERFLOOD (q = 400 cc/hr, T = 150.9 F)

[redacted]

Sw	Kro/Krw	Kro	Krw
0.008		1.000	e.000
.221	16.818	.617	.037
.226	14.981	.69 1	.046
,252	11.823	.668	.056
.292	8.861	.599	.068
.331	6.880	.520	.076
.376	5.173	.469	.091
.435	3.565	.393	.110
.507	2.291	.311	.136
.636	.929	.159	.171
.709	.428	.086	.202
.732	.320	.078	.244
.751	.253	.068	.268
.773	.193	.055	.287
.790	.156	.047	.305
.887	0.008	0.000	.354

SYSTEM PORE VOLUME	=	34.30	cc
FLOODING RATE	=	400	cc/hr
TEMPERATURE	=	70	F
INITIAL PRESSURE DROP	=	235	PSI
INITIAL WATEP SATURATION	=	0.000	fr. PV
RESIDUHL OIL SATURATION	=	.113	fr. PV
VISCOSITY RATIO	=	200.0	

Table **B-3.9**

PERMEAPILITY DATA VS WATER SHTURATION FOR
WATERFLOOD (q = 400 cc/hr, T = 70.0 F)

Sw	Kro/Krw	Kro	Krw
0.000		1.000	0.008
.221	10.029	.523	.052
.219	10.286	.686	,067
.315	5.153	.502	.097
.405	2.852	.405	.142
.525	1.319	.252	.191
.624	.650	.165	.253
.670	.452	.129	.286
.714	.311	.095	.305
.770	.182	.059	.322
.811	.111	.039	.349
.847	.062	.024	.386
.910	0.008	0.000	.452

SYSTEM PORE VOLUME	=	34.30 cc
FLOODING RATE	=	400 cc/hr
TEMPERATURE	=	122 F
INITIAL PRESSURE DROP	=	60 PSI
INITIAL WATER SATURATION	=	0.000 fr. PV
RESIDUAL OIL SATURATION	=	.090 fr. PV
VISCOSITY RATIO		68.0

Table B-3.10

PERMEABILITY DATA VS WATER SATURATION FOR WATERFLOOD (q = 400 cc/hr, T = 122.0 F)

SW	Kro/Krw	Kro	Krw
.064		1.000	0.000
.391	10.838	.637	.059
,437	6.101	.469	.077
.492	3.576	.385	.108
.545	2.166	.310	.143
.607	1.200	.219	.182
.657	.726	.166	.229
.689	.508	.133	.261
.726	.316	.086	.273
.758	.189	.052	.273
.754	.202	.057	.282
.783	.123	.037	.301
,794	.097	.031	.322
.875	0.000	0.000	.401

SYSTEM FORE VOLUME = 34.30 cc
FLOODING RATE = 400 cc/hr
TEMPERATURE = 70 F
INITIAL PRESSURE DROP = 282 PSI
INITIAL WATER SATURATION = .064 fr. PV
RESIDUAL OIL SATURATION = .125 fr. PV
VISCOSITY RATIO = 220.0

Table B-3.11

PERMEABILITY DATA VS WATER SATURATION FOR
WATERFLOOD (q = 400 cc/hr, T = 70.0 F)

APPENDIX B-4

TABLES AND PLOTS OF RECOVERY DATA FROM THE EXPERIMENTS

WATER INJ. (PV)	OIL RECOVERED (PV)
0	0
.08	.108
.30	.191
1.30	.350
2.80	.463
4.96	.533
7.92	.581
11.05	.611
14.60	.637
18.24	.659
21.69	.675
25.47	.686
29.90	.700
34.51	.713
37.74	.720

Table B-4.1

AMOUNT OF OIL RECOVERED (PV) VS WHTEP INJECTED (PV)
FOR WATER FLOODING OIL AT A RATE OF 28 cc/hr
AND TEMPERATURE OF 71.8 F (Swi = 0.000)

WATER INJ. (PV)	IL RECOVERED (PV)
0	0
.13	.053
.77	.148
2.70	.310
6.80	.469
11.84	.558
17.81	.614
23.80	.644
30.35	.666
37.18	.681
45.25	.692
54.39	.701
60.19	.706

Table B-4.2

AMOUNT OF OIL RECOVERED (PV) VS WATER INJECTED (PV)
FOR WATER FLOODING OIL AT A RATE OF 100 cc/hr
AND TEMPERATURE OF 65.0 F (Swi = 0.000)

WATER INJ. (PV)	OIL RECOVERED (PV)
0	0
.13	,047
.63	.127
2.34	.271
5.01	.399
9.28	.512
15.06	,597
21.58	.654
27.49	.678
33.99	.694
41.56	.706
49.87	.712
58.15	.716

Table B-4.3

AMOUNT OF OIL RECOVERED (PV) VS WATER INJECTED (PV)
FOR WATER FLOODING OIL AT A RATE OF 240 cc/hr
AND TEMPERATURE OF 69.0 F (Swi = 0.000)

WATER INJ. (PV)	OIL RECOVERED (PV)
0	0
.11	.192
.72	.319
2.70	.436
5.69	.511
9.97	.563
14.14	.594
18.16	.615
22.84	.626
27.87	.644
33.06	.662
39.79	.685
49.49	.702
59.23	.713

Table *B-4.4*

HMOUNT OF OIL RECOVERED (PV) VS WATER INJECTED (PV)
FOF WHTER FLOODING OIL HT A RATE OF 400 cc/hr
AND TEMPERATURE OF 68.8 F (Swi = 0.000)

WATER INJ. (PV)	OIL RECOVERED (PV)
0	0
.08	.059
.92	.204
3.30	.379
7.93	.524
13.00	.588
18.42	.618
23.91	.637
29.95	.652
36.01	.664
41.97	.672
47.92	.677

Table B-4.5

AMOUNT OF OIL RECOVERED (PV) VS WATER INJECTED (PV)
FOR WATER FLOODING OIL AT A RATE OF 400 cc/hr
AND TEMPERATURE OF 68.0 F (Swi = 0.000)

WATER INJ. (PV)	OIL RECOVERED (PV)
0	0
.15	.193
.57	.311
1.76	.453
3.64	.551
6.22	.624
9.14	.676
12.53	.719
16.37	.761
20.55	.800
25.30	.832
29.52	.846
34-76	.860
38.18	.868

Table B-4.6

AMOUNT OF OIL RECOVERED (PV) VS WATER INJECTED (PV)
FOR WATER FLOODING OIL AT A RATE OF 20 cc/hr
AND TEMPERATURE OF 150.0 F (Swi = 0.000)

WATER INJ. (PV)	OIL RECOVERED (PV)
0	0
.11	.153
.42	.259
1.68	.416
4.08	.541
7.18	.628
10.99	.700
14.54	.746
18.14	.782
21.95	.813
26.02	.840
30.63	.867
35.47	.883
38.35	.888

Table B-4.7

AMOUNT OF OIL RECOVERED (PV) VS WATEF INJECTED (PV)
FOR WHTEP FLOODING OIL AT H RHTE OF 240 cc/hr
AND TEMPERATURE OF 150.0 F (Sur = 0.000)

WATER INJ. (PV)	OIL RECOVERED (PV)
0	0
.14	.163
.33	.258
1.22	.403
3.38	.534
6.08	.632
9.23	.699
12.84	.742
17.42	.775
22.69	.806
28.30	.831
33.80	.845
39.17	.857
45.28	.866
49.58	.870

Table B-4.8

AMOUNT OF OIL RECOVERED (PV) VS WATER INJECTED (PV)
FOR WATER FLOODING OIL AT A RATE OF 400 cc/hr
AND TEMPERATURE OF 150.0 F (Swi = 0.000)

UATER INJ. (PV)	OIL RECOVERED (PV)
0	0
.17	.231
.65	.272
1.95	.361
3.47	.441
5.07	.501
7.16	.558
9.71	.607
12.96	.653
16.54	.695
20.80	.733
28.58	.769
39.60	.794
52.64	.816
66.55	.835
81.65	.852
95.84	.865
112.91	.878
130.17	.885
143.46	,887
155.38	.889

Table B-4.9

AMOUNT OF OIL RECOVERED (PV) VS WATER INJECTED (PV)
FOR WATER FLOODING OIL AT A RATE OF 400 cc/hr
AND TEMPERATURE OF 70.0 F (SWI = 0.000)

WATER INJ. (PV)	OIL RECOVERED (PV)
0	0
.41	.274
.75	.318
1.45	.410
2.45	.492
3.76	.557
5.16	.609
6.85	.655
9.12	.701
11.62	.733
14.80	.765
19.13	.798
26.10	.837
36.11	.869
46.59	.889
58.17	.901
70.55	.907
84.20	.910

Table **B-4.10**

AMOUNT OF OIL RECOVERED (PV) VS WATEP INJECTED (PV)
FOR WATER FLOODING OIL AT A RATE OF 400 cc/hr
AND TEMPERATURE OF 122.8 F (Swi = 0.000)

MATER INJ. (PV)	OIL RECOVERED (PV)
0	0
.13	.251
.23	.296
.52	,367
1.18	.443
1.95	.523
3.09	.599
4.42	.662
5.59	,704
6.95	.744
8.73	.782
10.71	.811
13.16	.837
16.32	.863
19.34	.882
22.98	.898
28.60	.913
35.63	.919
42.76	.923
49.01	.924

Table 5-4.11

AMOUNT OF OIL RECOVERED (PV) VS WATER INJECTED (PV)
FOR WATER FLOODING OIL AT A RATE OF 400 cc/hr
FIND TEMPERATURE OF 186.0 F (Swi = 0.000)

WATER INJ. (PV)	OIL RECOVERED (PV)
0	0
.10	.278
.42	.329
1.84	.420
5.20	.516
10.93	.594
19.42	.653
29.72	.693
40.16	.719
49.53	.736
59.05	.745
69.03	.753
79.81	.763
91.19	.770
102.38	,775
117.37	.782
131.25	.786
143.09	.789
153.93	.793

Table B-4.12

AMOUNT OF OIL RECOVERED (PV) VS WATER INJECTED (PV)
FOR WATER FLOODING OIL AT A RATE OF 400 cc/hr
AND TEMPERATURE OF 70.0 F (Swi = .064)

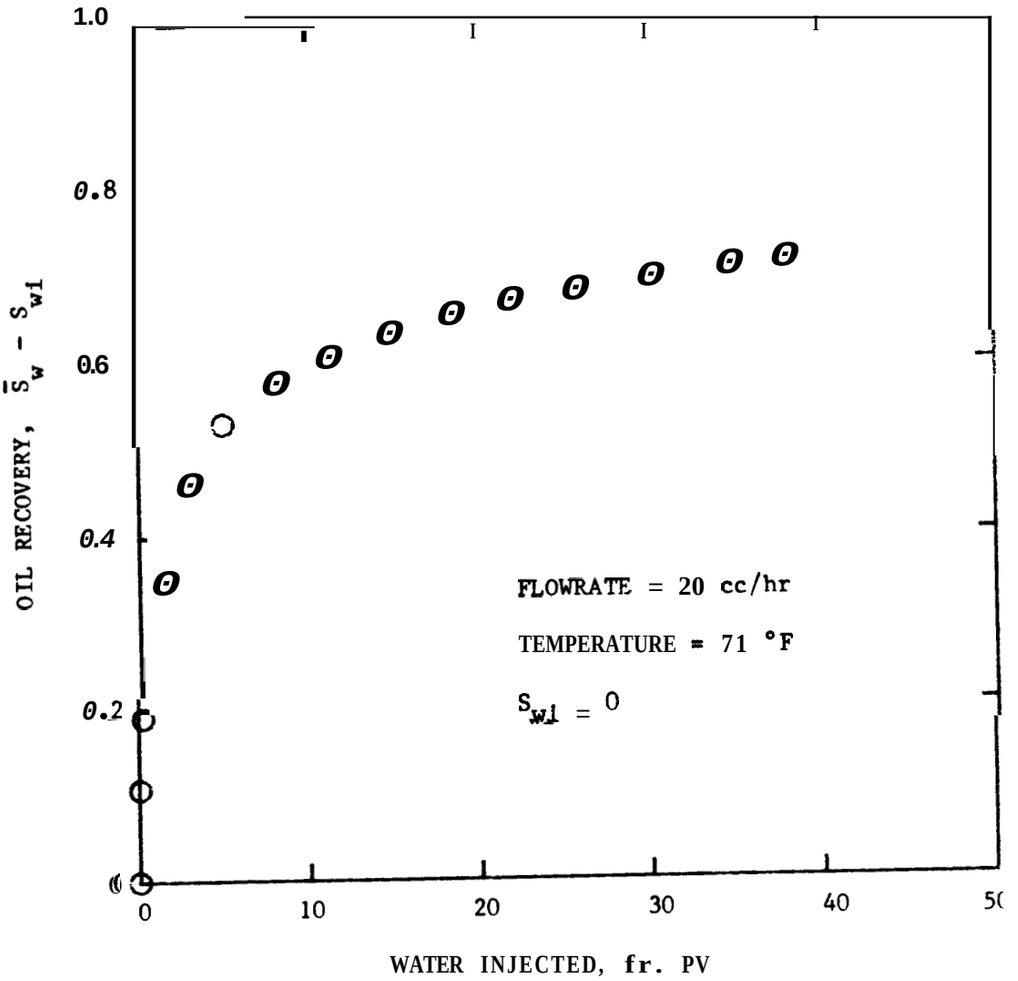

Fig. B-4.1 OIL RECOVERY (PV) VS WATER INJECTED (PV) FOR WATER DISPLACING OIL

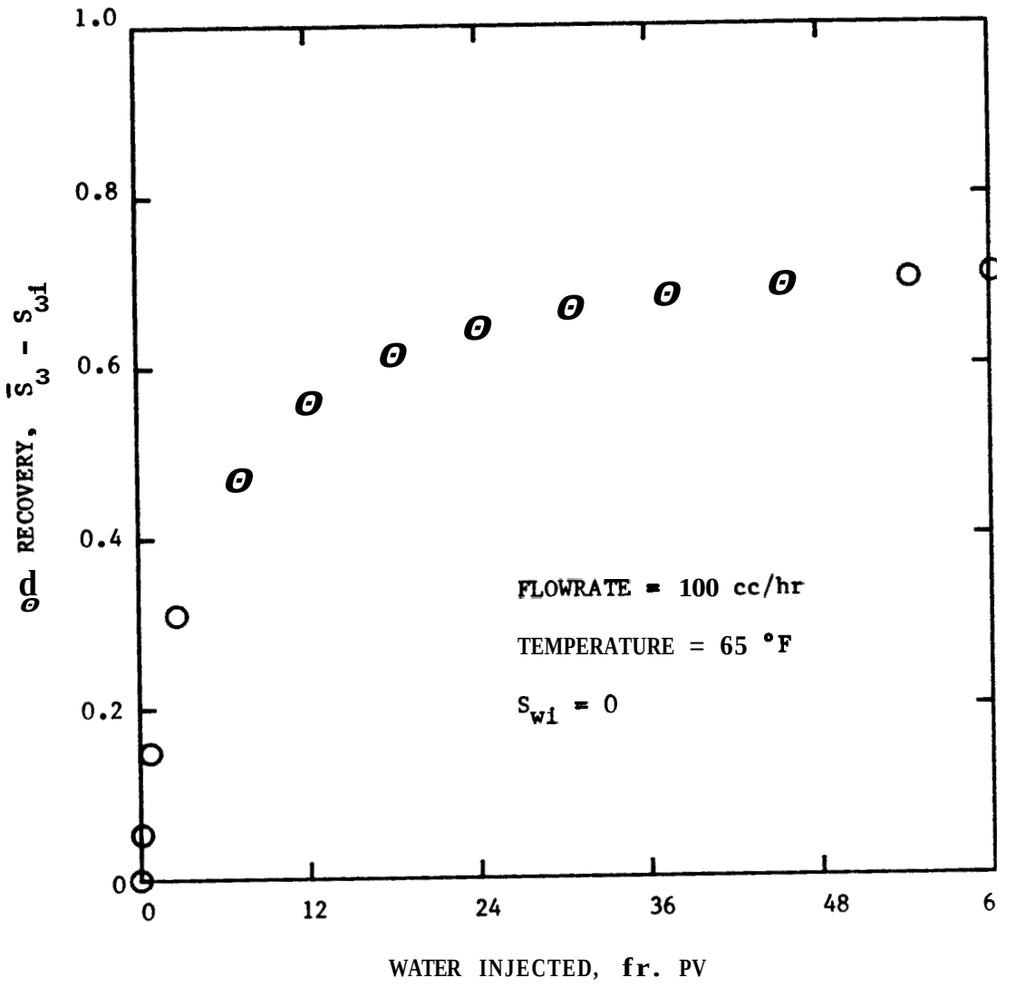

Fig. B-4.2 OIL RECOVERY (PV) VS WATER INJECTED (PV) FOR WATER DISPLACING OIL

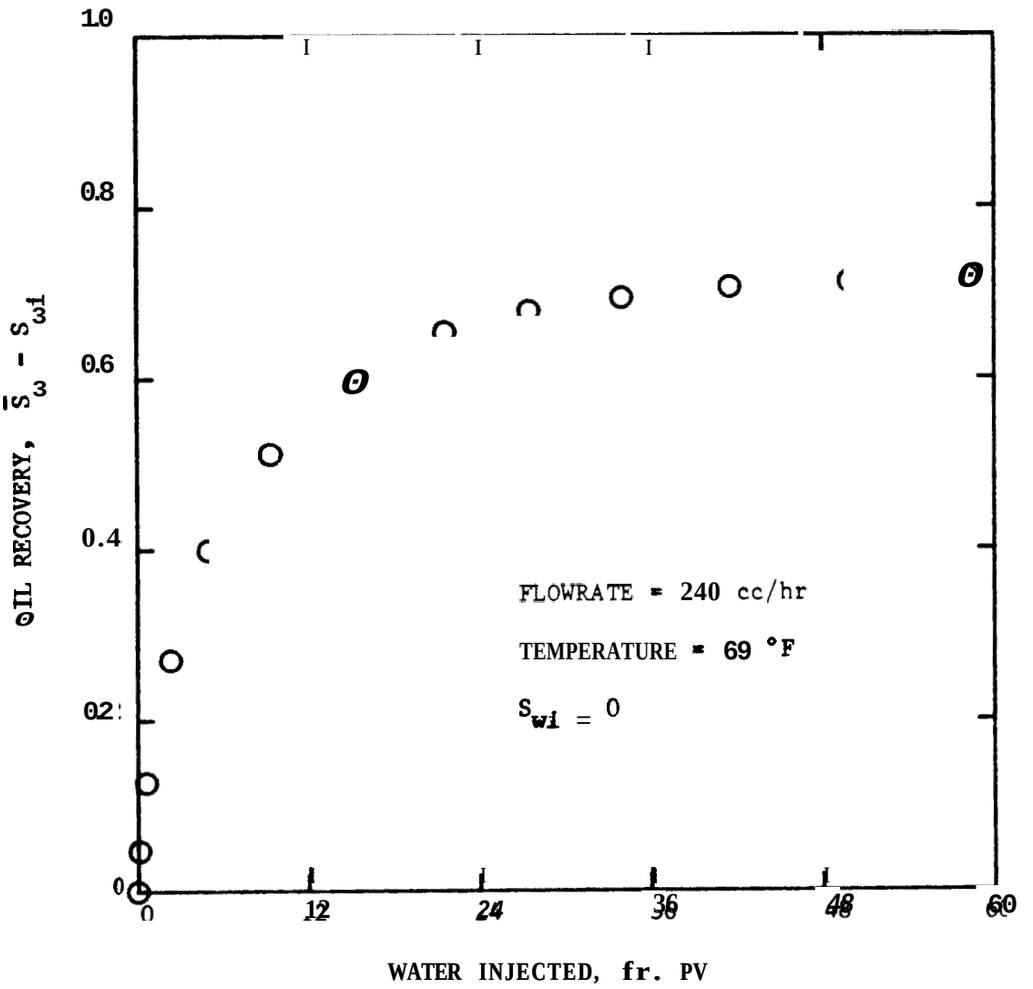

Fig. *B-4.3* OIL RECOVERY (PV) VS WATER INJECTED (PV) FOR WATER DISPLACING OIL

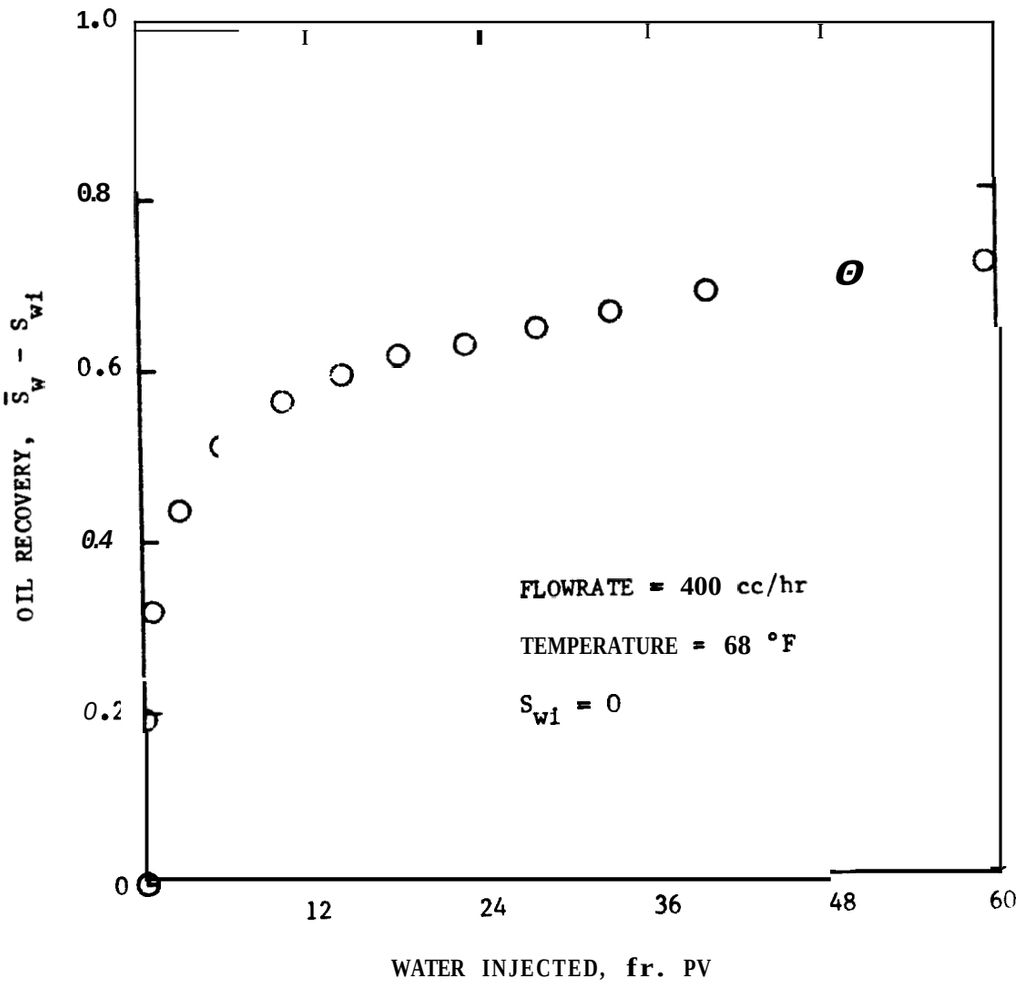

Fig. B-4.4 OIL RECOVERY (PV) VS WATER INJECTED (PV) FOR WATER DISPLACING OIL

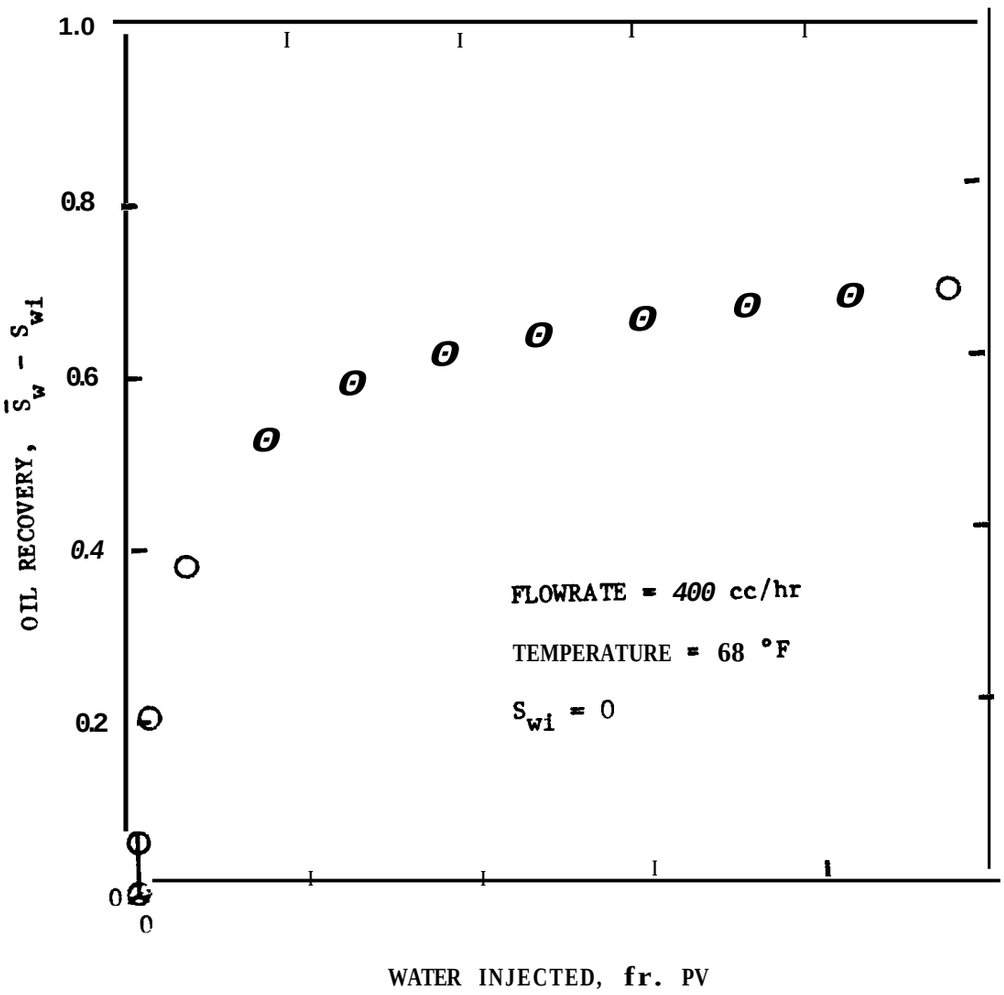

Fig. B-4.5 OIL RECOVERY (PV) VS WATER INJECTED (PV) FOR WATER DISPLACING OIL

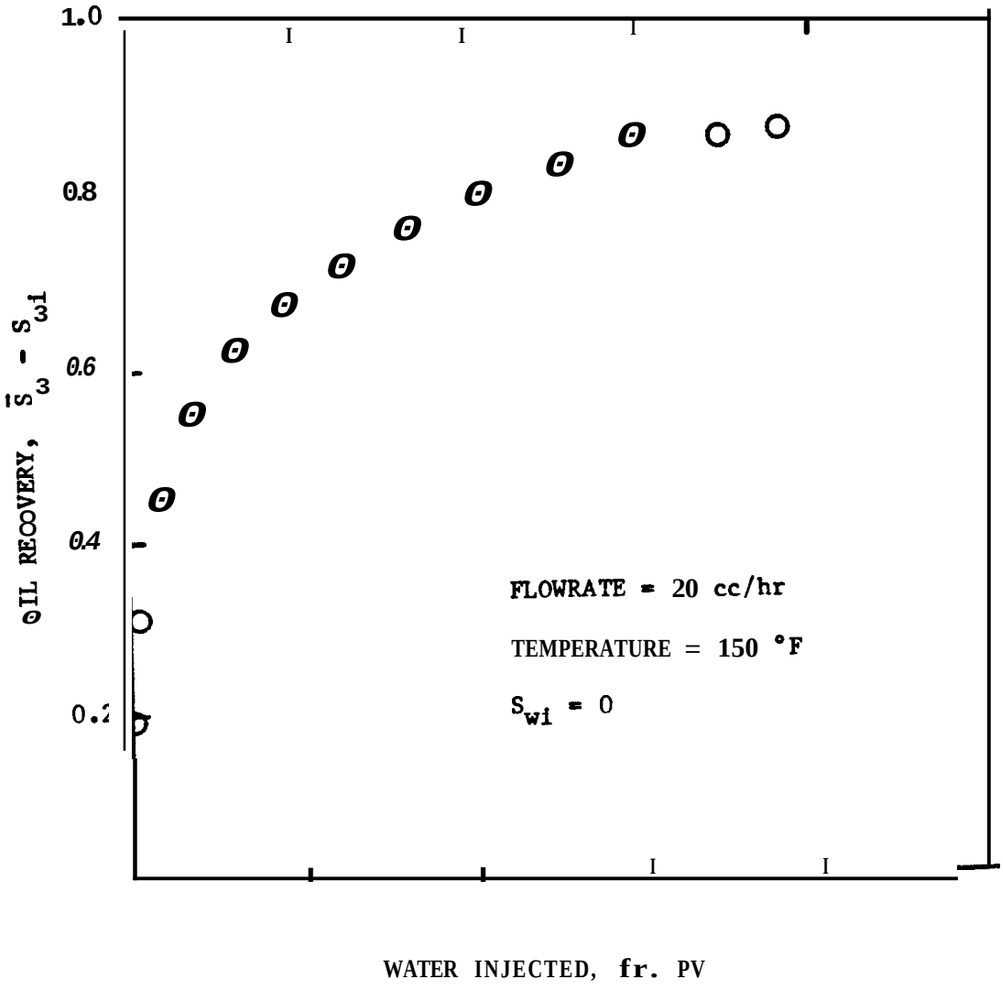

Fig. B-4.6 OIL RECOVERY (PV) VS WATER INJECTED (PV) FOR WATER DISPLACING OIL

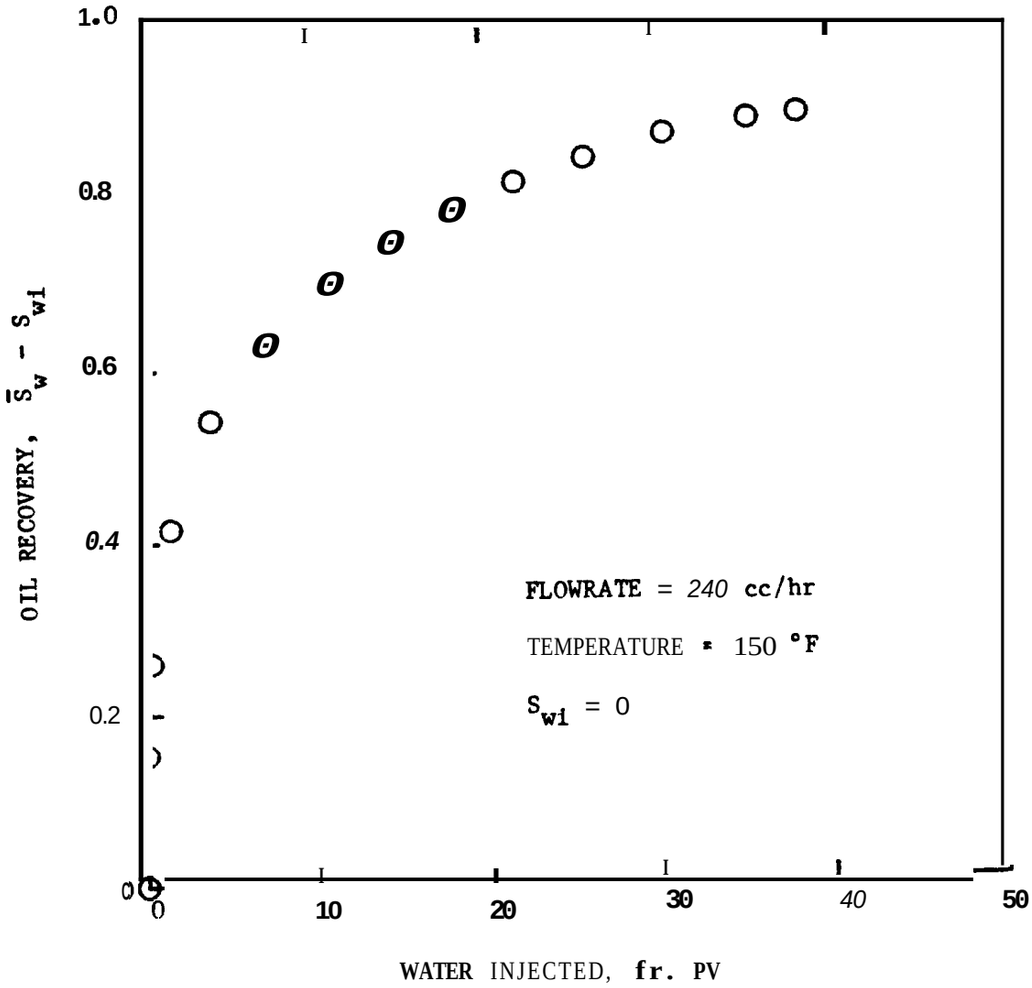

Fig. B-4.7 OIL RECOVERY (PV) VS WATER INJECTED (PV) FOR WATER DISPLACING OIL

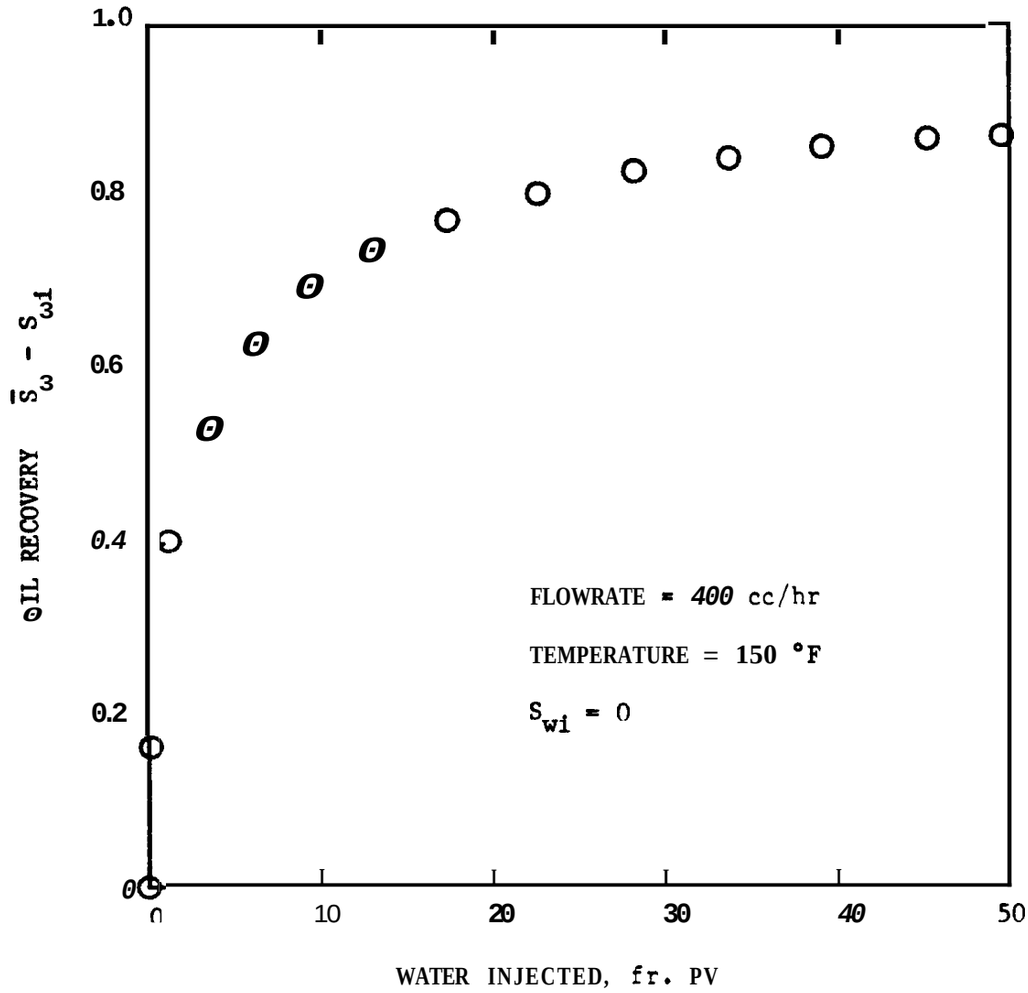

Fig. B-4.8 OIL RECOVERY (PV) VS WATER INJECTED (PV) FOR WATER DISPLACING OIL

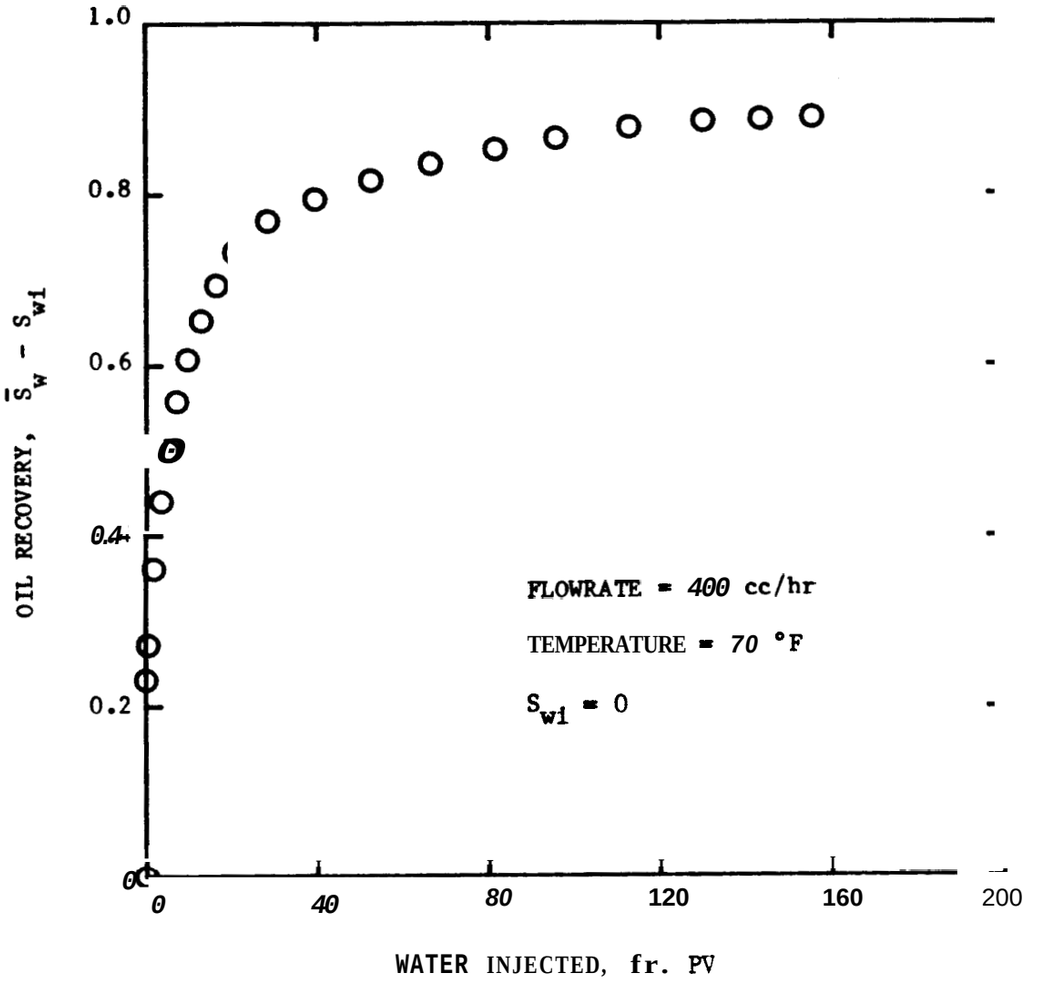

Pip;. B-4.9 OIL RECOVERY (PV) VS WATER INJECTED (PV) FOR WATER DISPLACING OIL

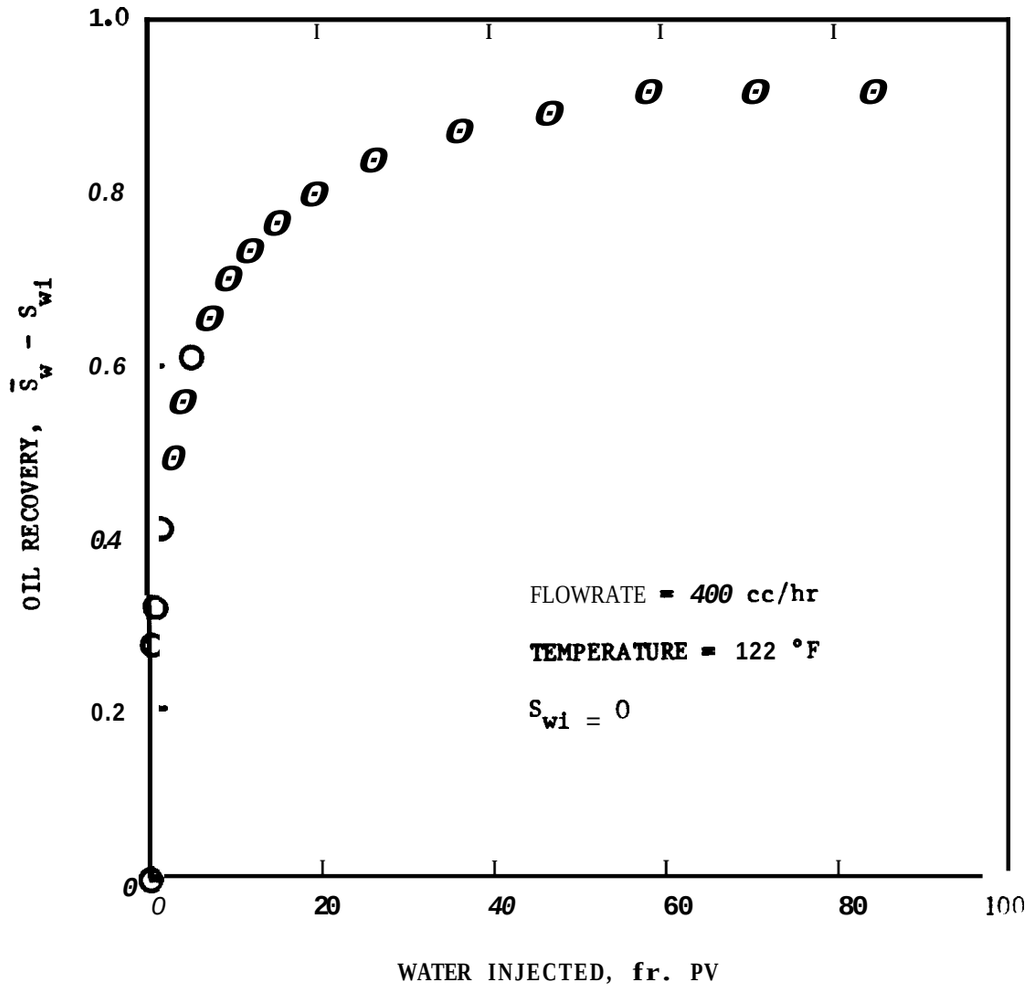

Fig. B-4.10 OIL RECOVERY (PV) VS WATER INJECTED (PV) FOR WATER DISPLACING OIL

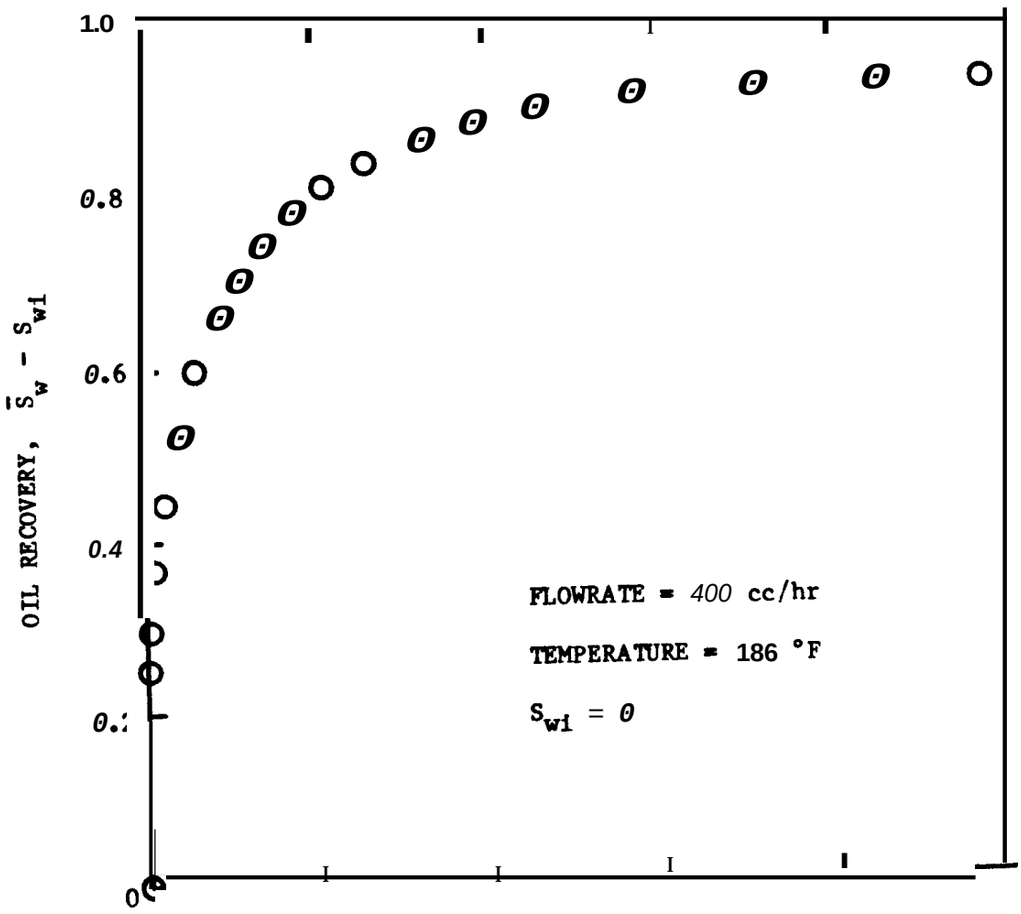

Fig. B-4.11 OIL RECOVERY (PV) VS WATER INJECTED (PV) FOR WATER DISPLACING OIL

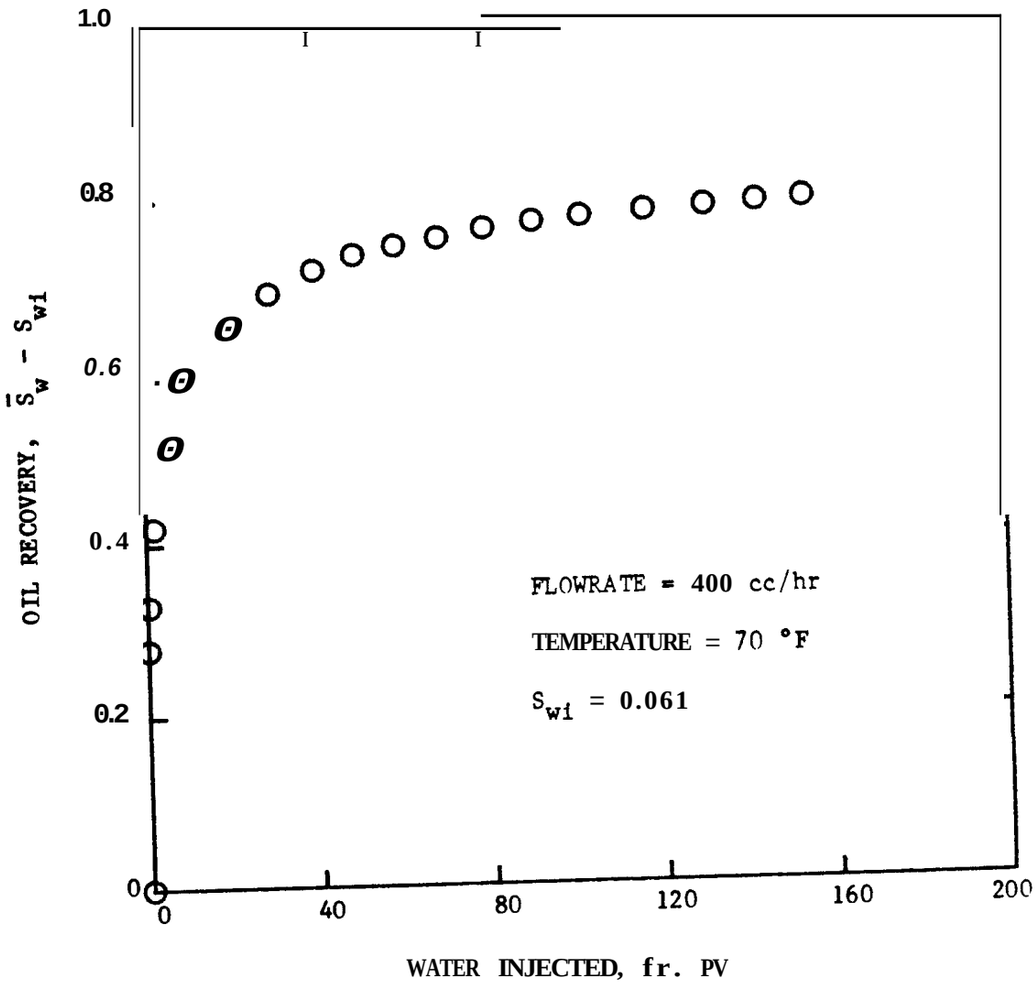

Fig. B-4.12 OIL RECOVERY (PV) VS WATER INJECTED (PV) FOR WATER DISPLACING OIL

APPENDIX B-5

TABLES AND PLOTS OF RELATIVE INJECTIVITY DATA FROM THE EXPERIMENTS

WATER INJ. (PV)	1/(RELATIVE INJECTIVITY)
0	1.000
.34	.195
.70	.117
1.61	.077
3.50	.058
6.26	.053

Table B-5.1

1/(RELATIVE INJECTIVITY) VS WATER INJECTED (PV)
FOR WATEF FLOODING OIL AT A RATE OF 20 cc/hr
AND TEMPERATURE OF 71.8 F (Swi = 0.000)

WATER INJ. (PV)	1/(RELATIVE INJECTIVITY)
0	1.800
1.63	.061
2.91	.046
5.16	.036
9.52	.029
16.55	.023
26.04	.021

Table **B-5.2**

1/(RELATIVE INJECTIVITY) VS WHTEK INJECTED (PV)
FOR WATER FLOODING OIL AT A RATE OF 100 cc/hr
AND TEMPERATURE OF 65.8 F (Swi = 0.000)

WATER INJ. (PV)	1/(RELATIVE INJECTIVITY)
0	1.000
.49	.103
1.72	.050
4.14	.034
8.37	.026
14.95	.021

Table **B-5.3**

1/(RELATIVE INJECTIVITY) VS WATER INJECTED (PV)
FOR WATER FLOODING OIL AT A RATE OF 240 cc/hr
AND TEMPERATURE OF 69.0 F ($Swi = 0.000)

WATER INJ. (PV)	1/(RELATIVE INJECTIVITY)
0	1.000
1.35	.089
3.40	.056
8.99	.034
16.07	.025
25.23	.021

Table B-5.4

1/(RELRTIVE INJECTIVITY) VS WRTEP INJECTED (PV)
FUR WATER FLOODING OIL AT A HATE OF 400 cc/hr
AND TEMPERATURE OF 68.8 F (Swi = 0.000)

[redacted]

WATER INJ. (PV)	1/(RELATIVE INJECTIVITY)
0	1.000
1.55	.066
2.62	.049
5.12	.036
9.78	.026
14.91	.021
22.08	.018

Table **B-5.5**

1/(RELATIVE INJECTIVITY) VS WATER INJECTED (PV)
FOR WATER FLOODING OIL AT A RATE OF 400 cc/hr
AND TEMPERATURE OF 68.0 F (Swi = 0.000)

WATER INJ. (PV)	1/(RELATIVE INJECTIVITY)
8	1.088
.17	.352
.74	.272

Table B-5.6

1/(RELATIVE INJECTIVITY) VS WATER INJECTED (PV)
FOR WHTER FLOODING OIL AT A RATE OF 28 cc/hr
AND TEMPERATURE OF 150.8 F (Swi = 0.000)

WATER INJ. (PV)	,/(RELATIVE INJECTIVITY)
0	1.000
.29	.224
1.08	.153
2.94	.108
5.24	.087
8.47	.075
12.75	.067
17.53	.063

Table **B-5.7**

1/(RELATIVE INJECTIVITY) VS WHTEP INJECTED (PV)
FOR WATER FLOODING OIL AT A RATE OF 240 cc/hr
AND TEMPERATURE OF 150.0 F (Swi = 0.000)

UATER INJ. (PV)	1/(RELATIVE INJECTIVITY)
0	1.000
1.00	.144
1.80	.113
3.76	.087
8.01	.068
12.89	.060
18.20	.056
23.97	.053

Table B-5.8

1/(RELATIVE INJECTIVITY) VS WATER INJECTED (PV)
FOR WATEP FLOODING OIL AT A RATE OF 400 cc/hr
AND TEMPERATURE OF 150.0 F (Swi = 0.000)

WATER INJ. (PV)	1/(RELATIVE INJECTIVITY)
0	1.000
.95	.088
1.19	.078
1.88	.065
3.13	.053
4.50	.044
5.87	.038
7.72	.033
10.70	.028
17.03	.024
28.73	.020
42.58	.017
56.24	.016
72.73	.015
91.36	.015
110.37	.014

Table B-5.9

1/(RELATIVE INJECTIVITY, VS WATER INJECTED (PV)
FOR WATER FLOODING OIL AT A RATE OF 400 cc/hr
AND TEMPERATURE OF 70.0 F (SWI = 0.000)

YRTER INJ. (PV)	1/(RELATIVE INJECTIVITY)
0	1.000
.56	.175
.78	.148
1.43	.111
2.86	.078
4.76	.063
9.45	.050
15.51	.045
22.60	.041
29.64	.038
39.73	.036
49.72	.034
60.73	.032

Table B-5.10

1/(RELATIVE INJECTIVITY) VS WATER INJECTED (PV)
FOR WATER FLOODING OIL RT A RATE OF 400 cc/hr
RND TEMPERRTURE OF 122.0 F (Swi = 0.000)

MATER INJ. (PV)	1/(RELATIVE INJECTIVITY)
0	1.000
1.77	.059
3.13	.044
5.66	.033
9.72	.025
15.21	.020
23.71	.017
33.49	.015
42.66	.014
53.09	.014
65.86	.013
79.82	.012
95.68	.012
110.36	.011

Table **B-5.11**

1/(RELATIVE INJECTIVITY) VS WATER INJECTED (PV)
FOR WATER FLOODING OIL AT A RATE OF 400 cc/hr
AND TEMPERATURE OF 70.0 F (Swi = .064)

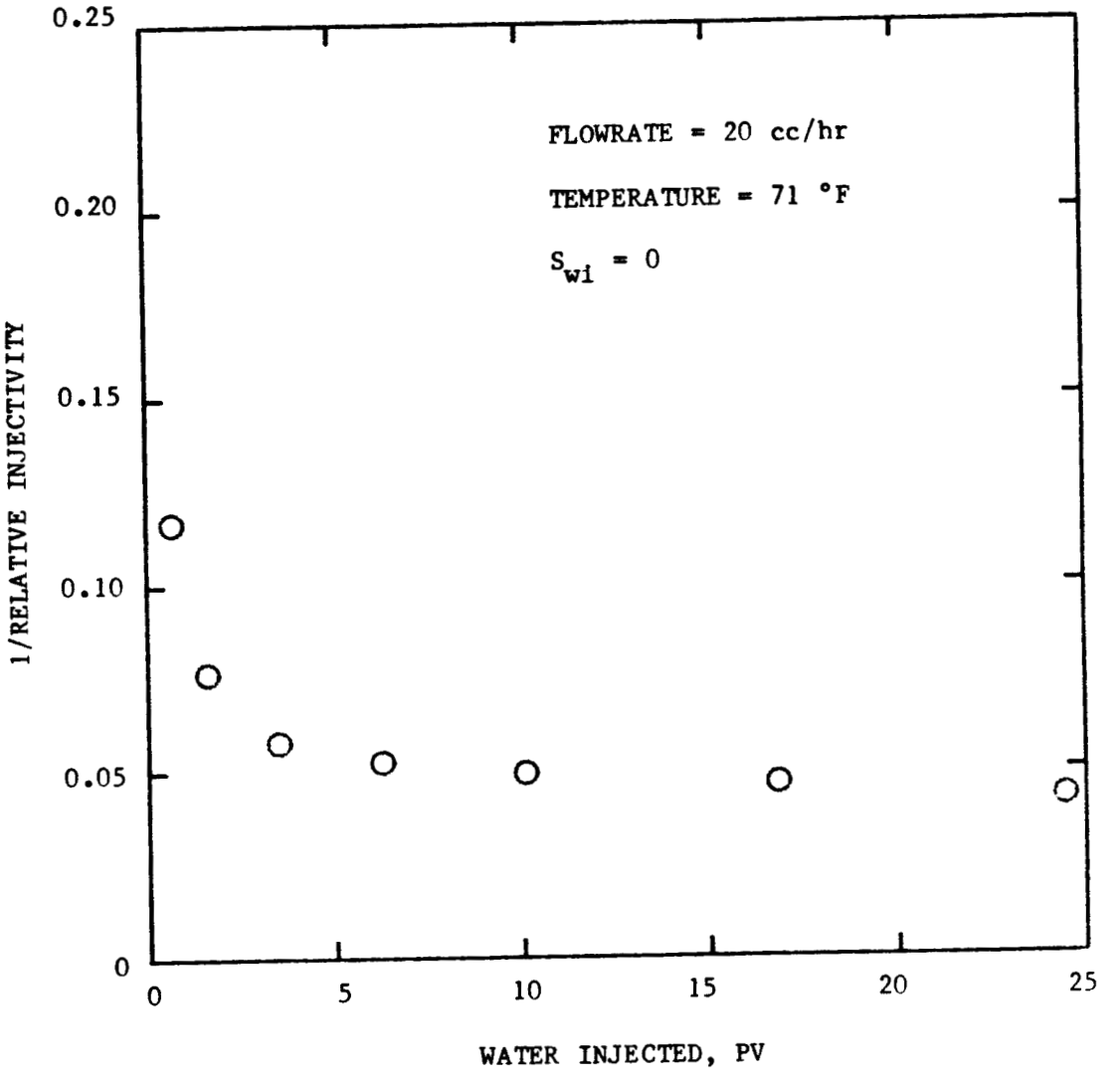

Fig. B–5.1 1/RELATIVE INJECTIVITY **VS WATER** INJECTED (PV) **FOR WATER** DISPLACING **OIL**

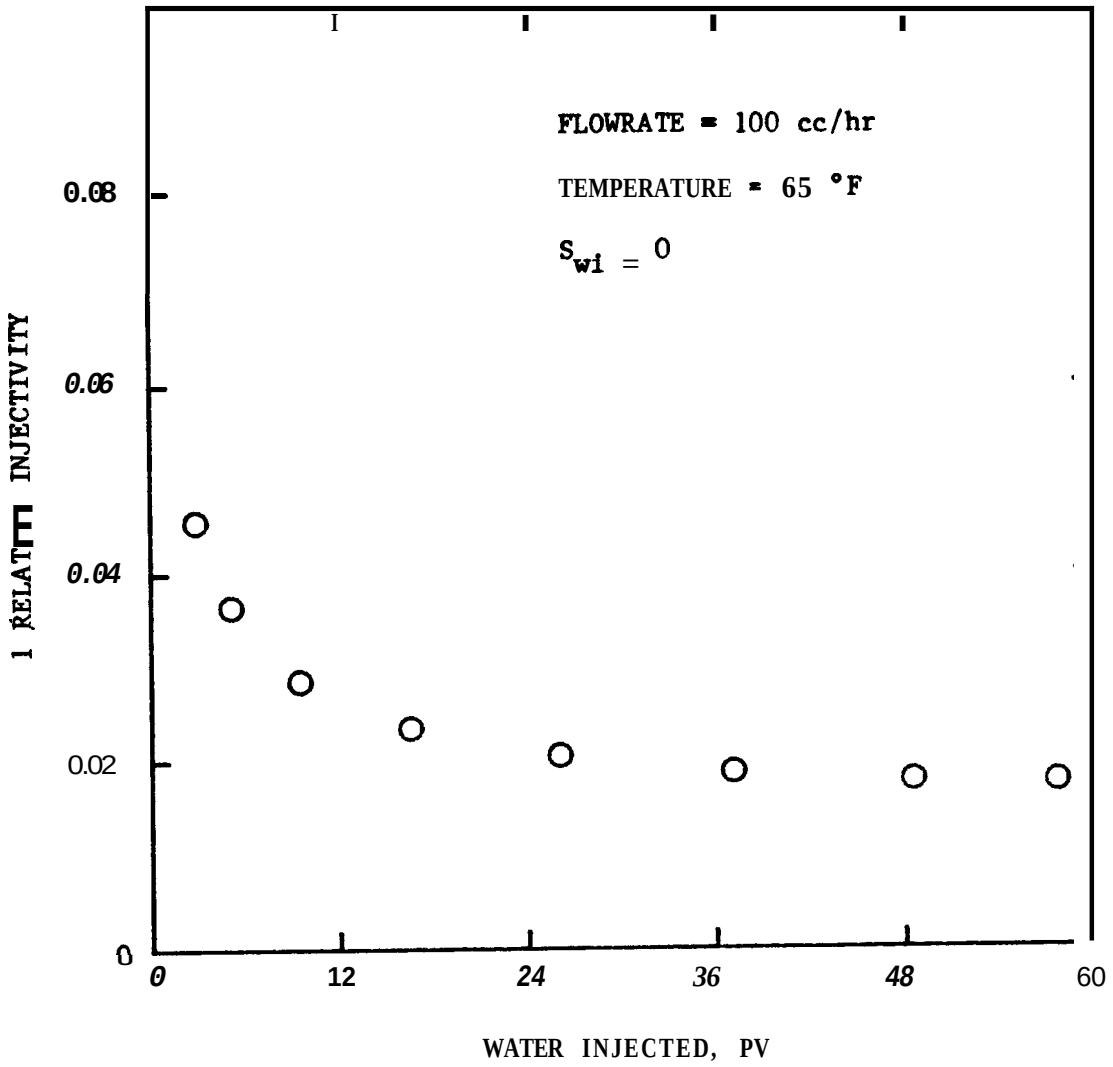

Fig. B-5.2 1/RELATIVE INJECTIVITY VS WATER INJECTED (PV) FOR WATER DISPLACING OIL

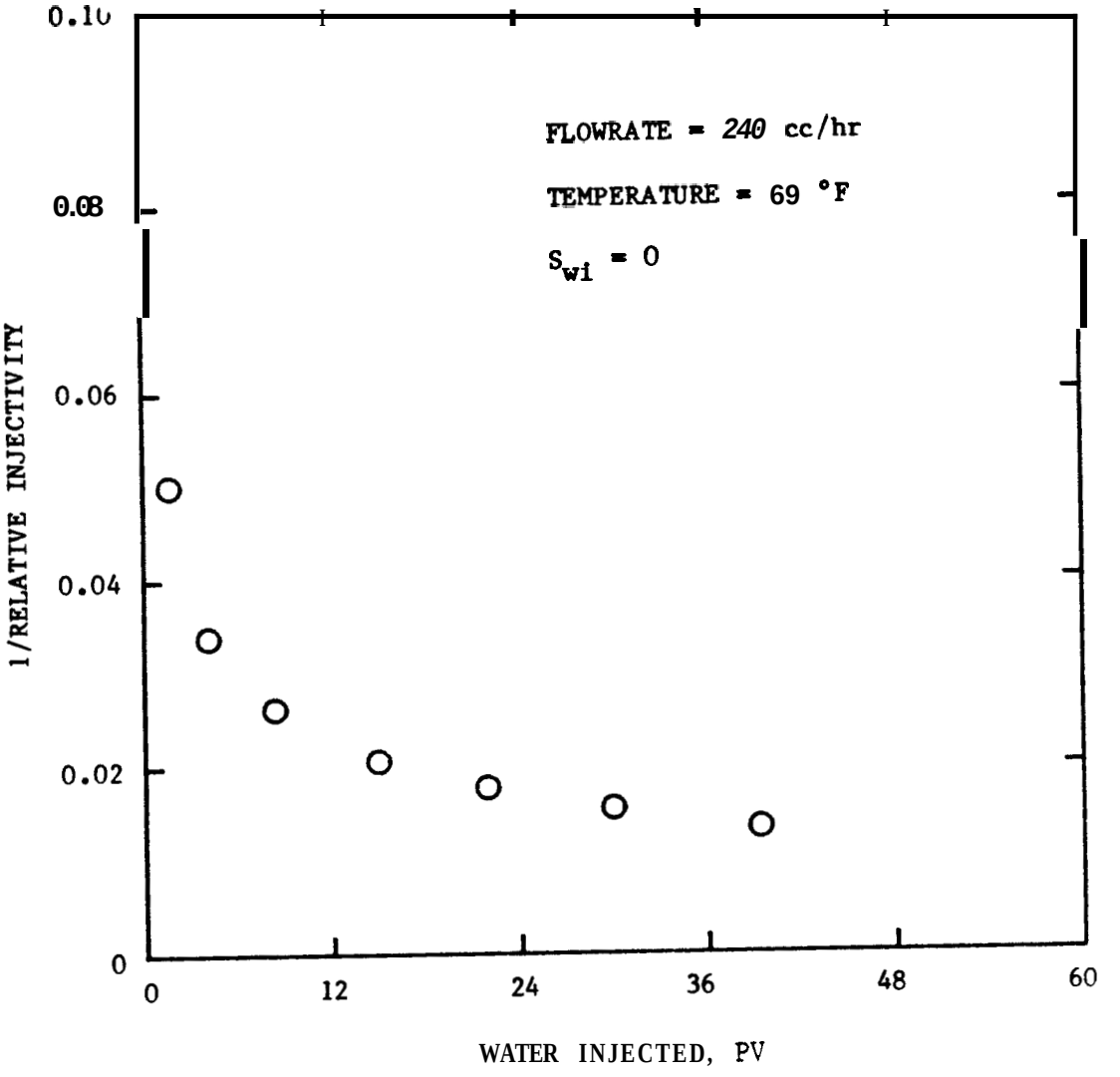

Fig. B-5.3 1/RELATIVE INJECTIVITY VS WATER INJECTED (PV) FOR WATER DISPLACING OIL

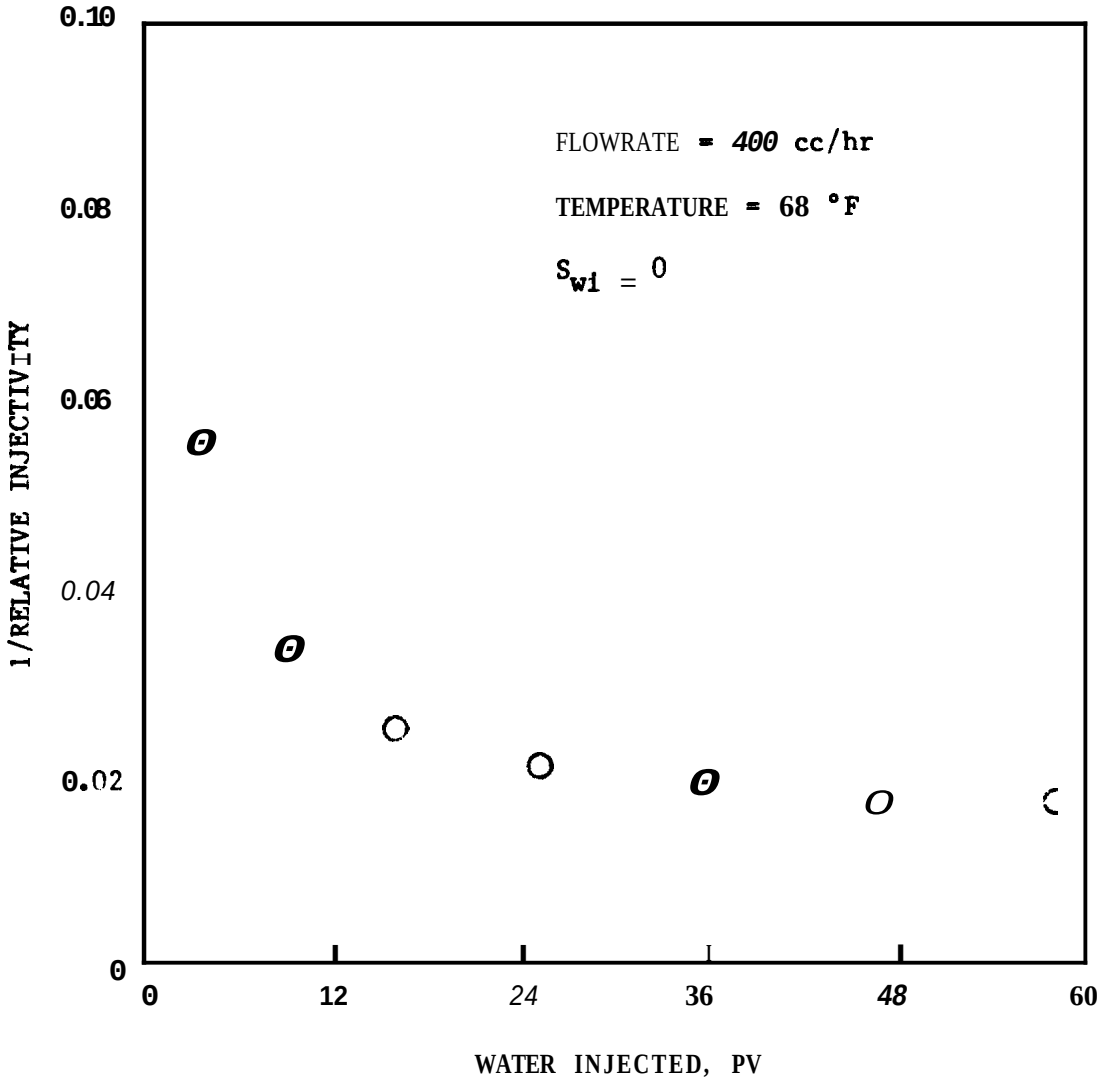

Fig. B-5.4 1/RELATIVE INJECTIVITY VS WATER INJECTED (PV) FOR WATER DISPLACING OIL

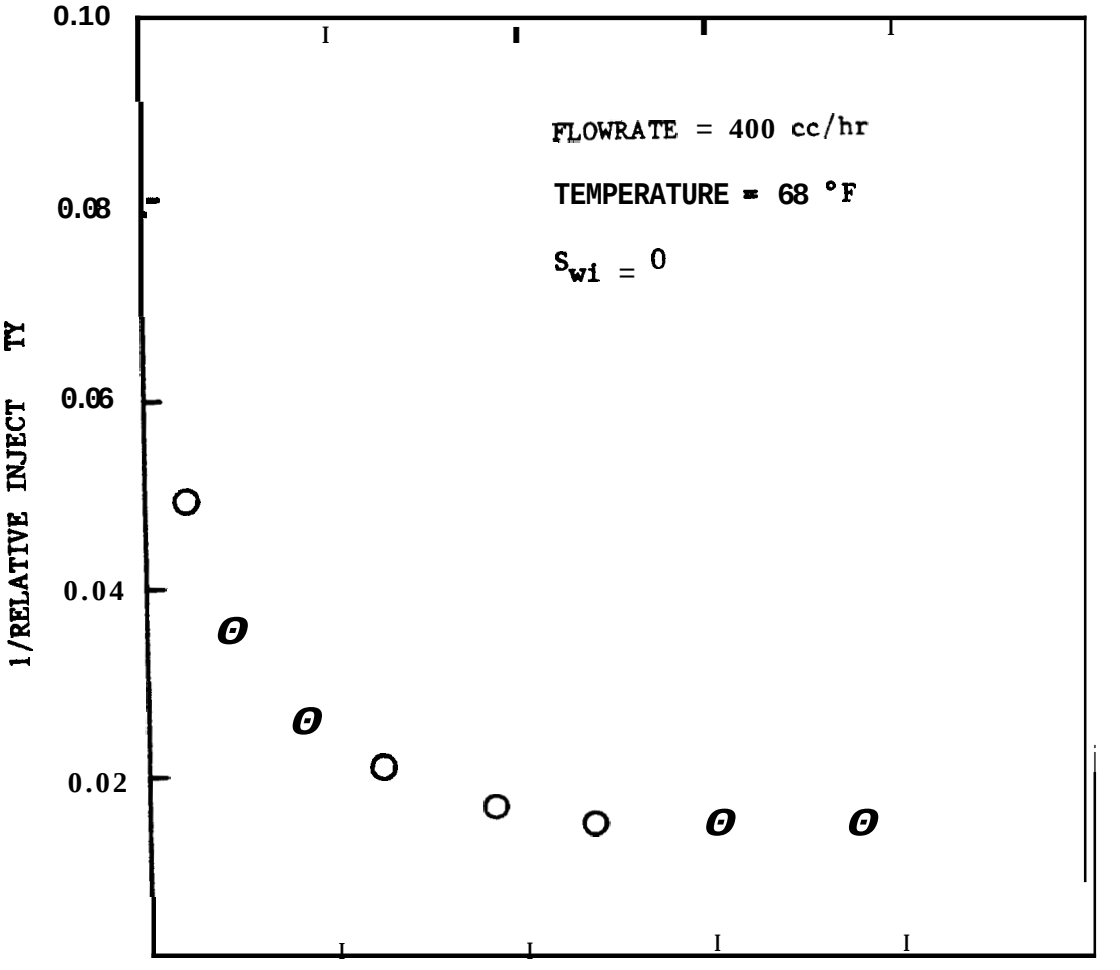

Fig. B-5.5 1/RELATIVE INJECTIVIW VS WATER INJECTED (PV) FOR WATER DISPLACING OIL

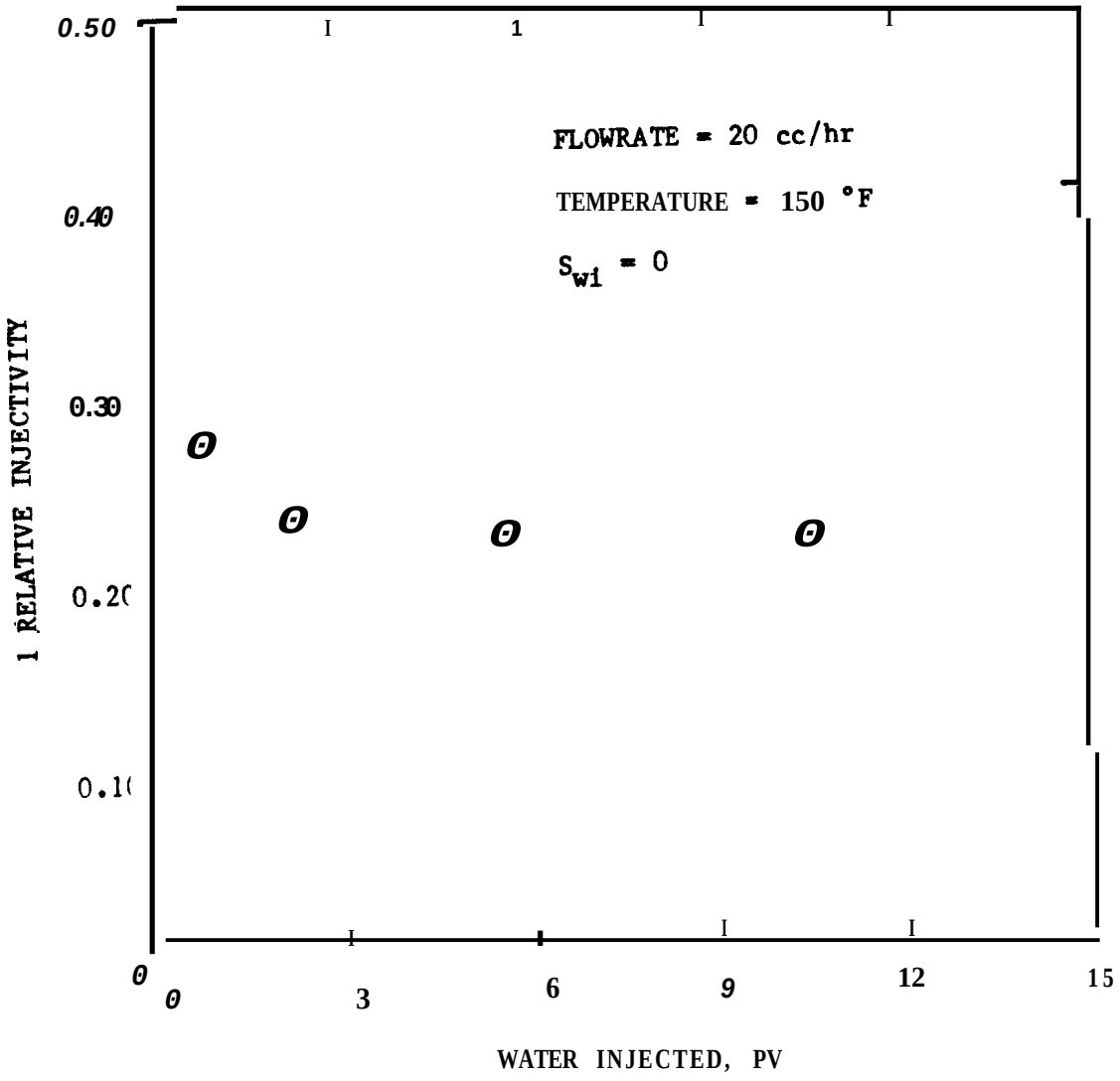

Fig. B-5.6 1/RELATIVE INJECTIVITY VS WATER INJECTED (PV) FOR WATER DISPLACING OIL

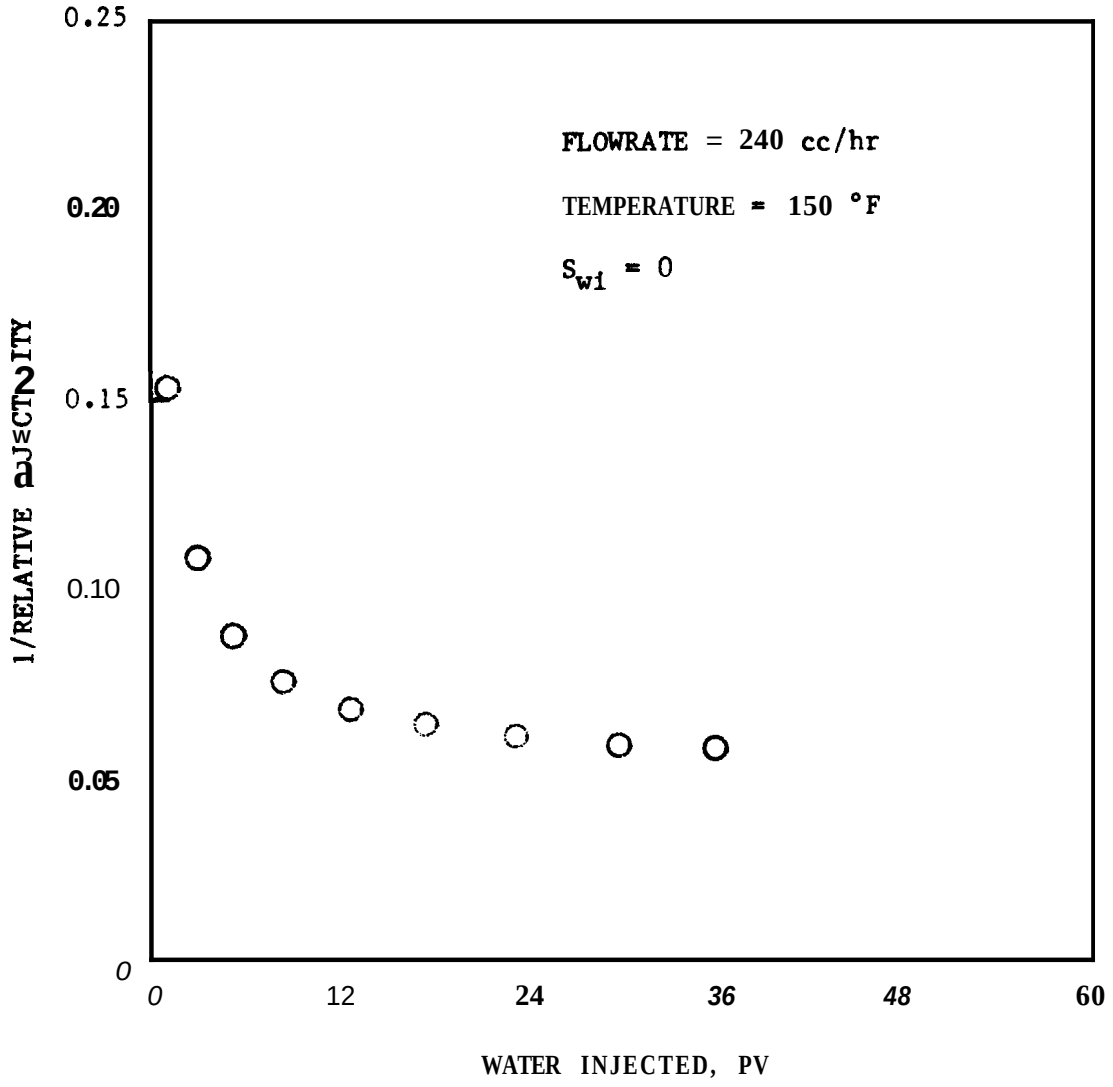

Fig. B-5.7 1/RELATIVE INJECTIVITY VS WATER INJECTED (PV) FOR WATER DISPLACING OIL

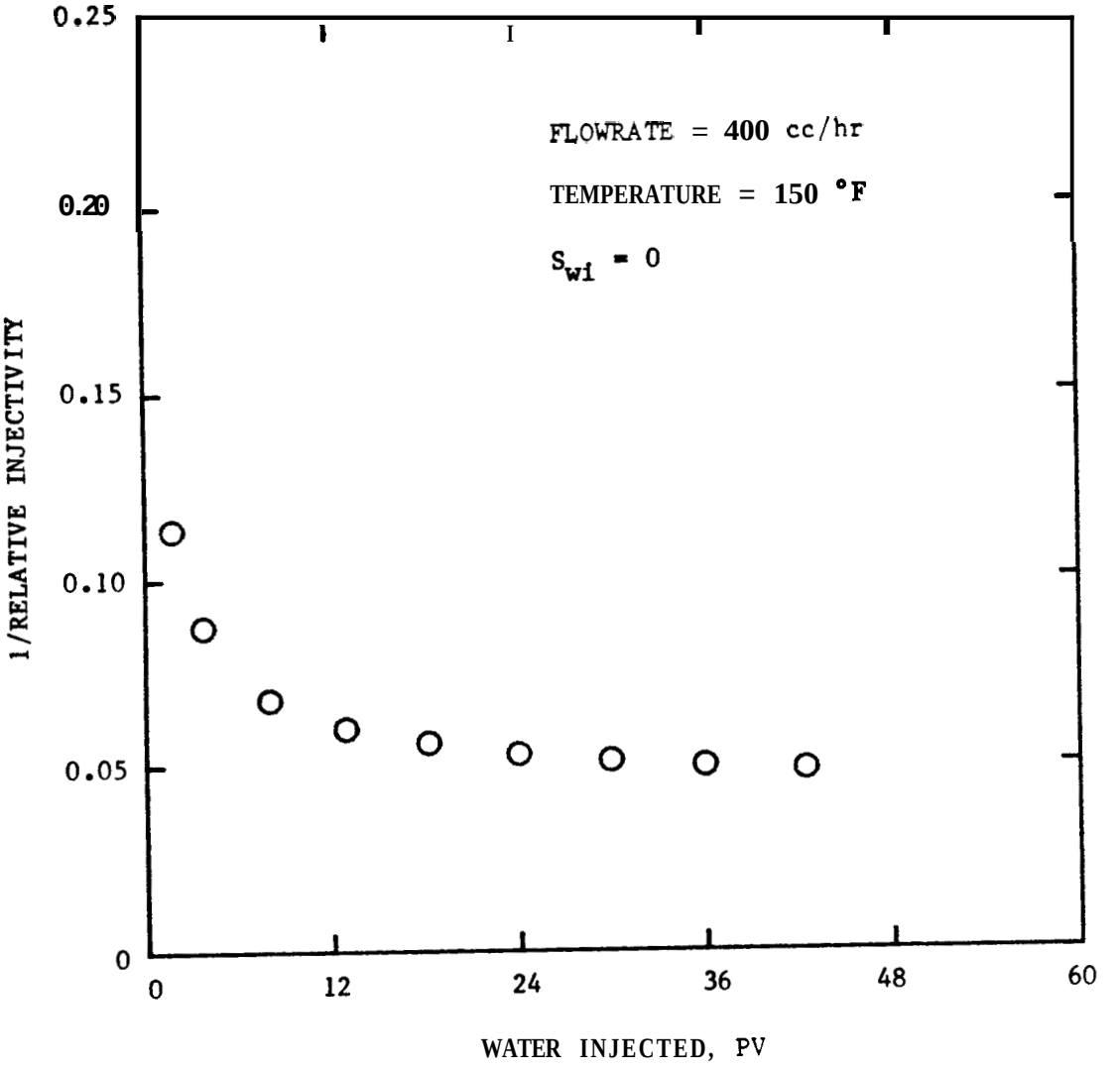

Fig. B-5.8 1/RELATIVE INJECTIVITY VS WATER INJECTED (PV) FOR WATER DISPLACING OIL

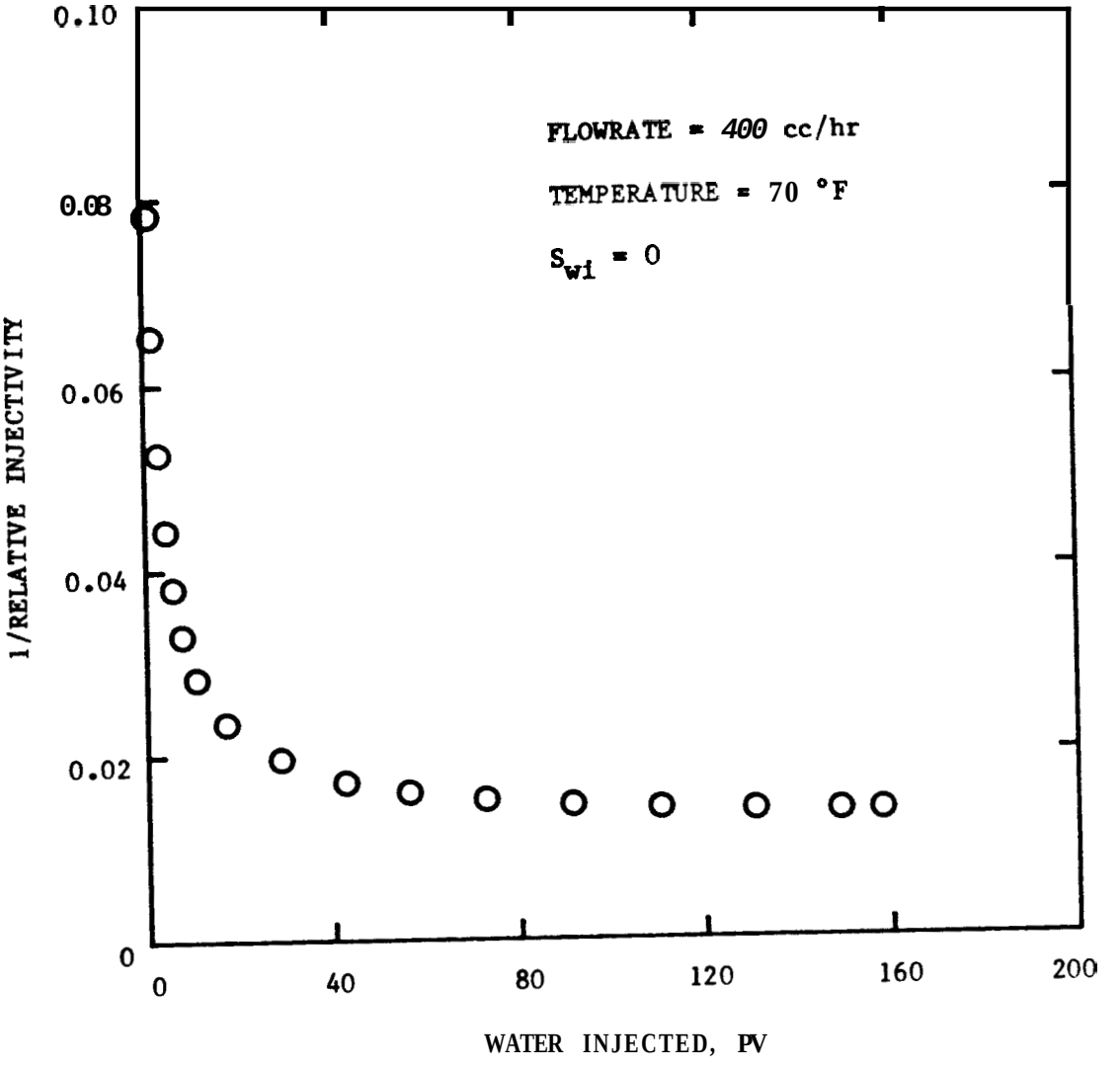

Fig. B-5.9 1/RELATIVE INJECTIVITY VS WATER INJECTED (PV) FOR WATER DISPLACING OIL

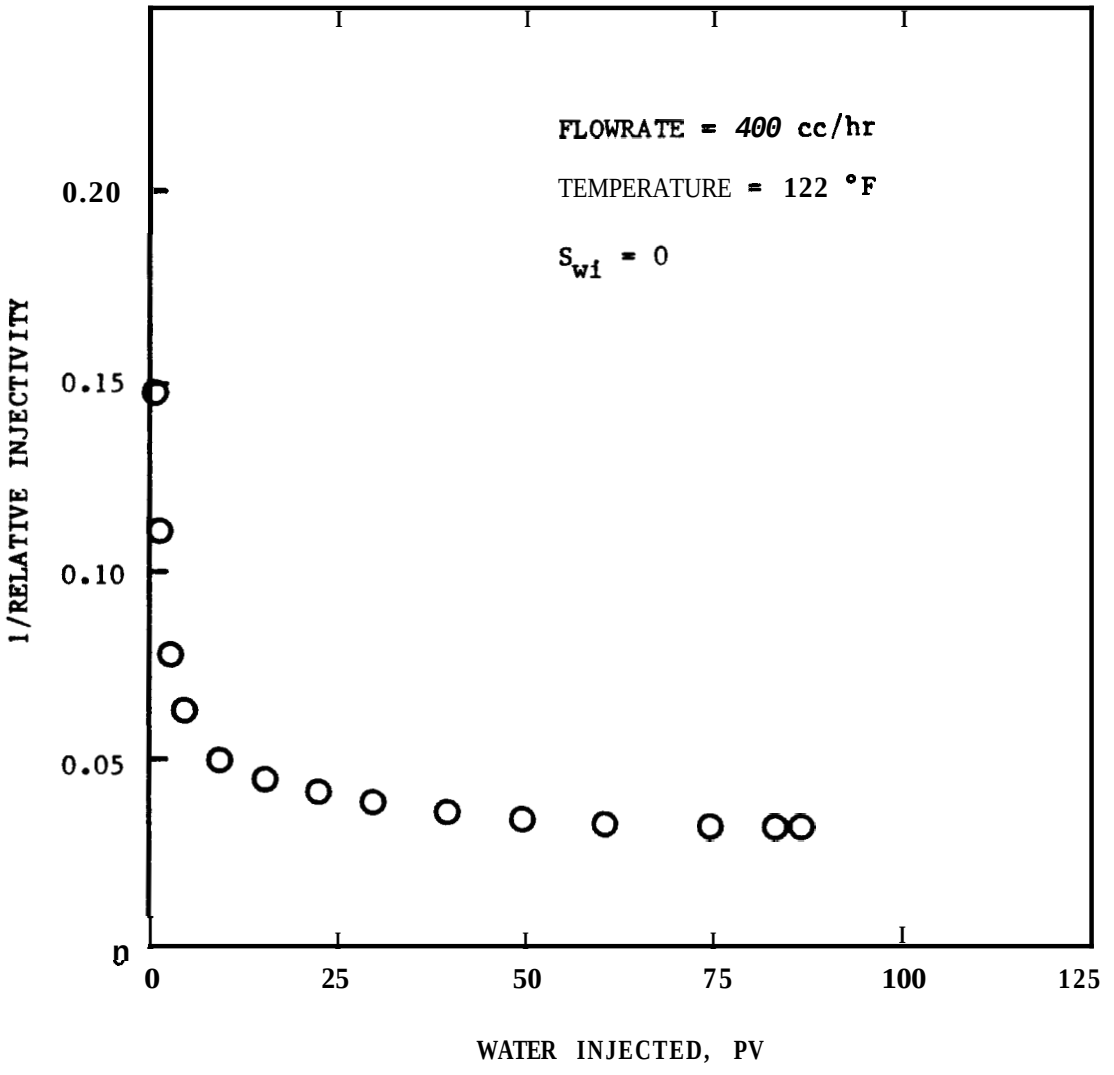

Fig. B-5.10 1/RELATIVE INJECTIVITY VS WATER INJECTED (PV) FOR WATER DISPLACING OIL

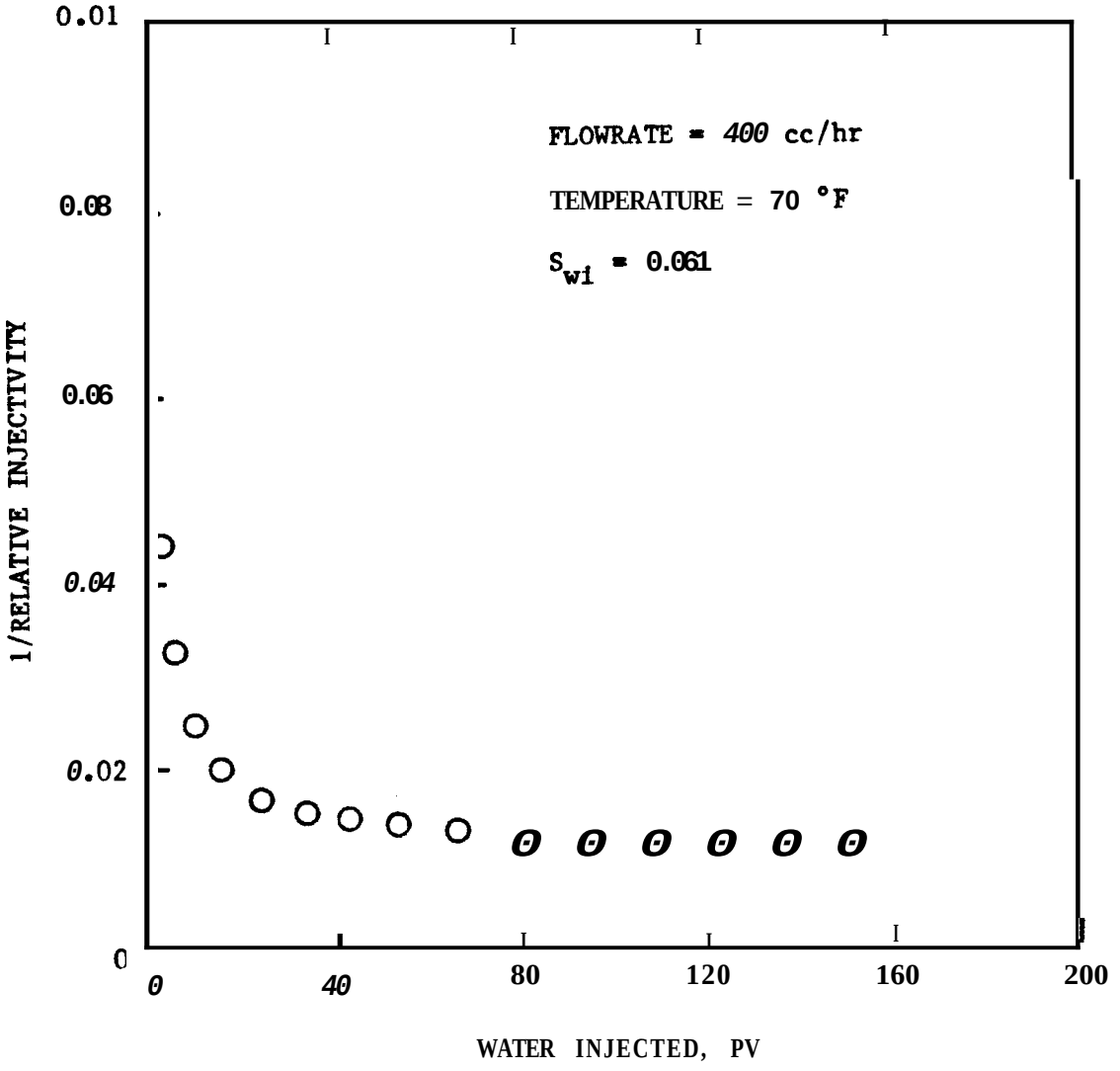

Fig. B-5.11 1/RELATIVE INJECTIVITY VS WATER INJECTED (PV) FOR WATER DISPLACING OIL

APPENDIX B-6

TABLES AND PLOTS OF FRACTIONAL FLOW DATA GENERATED FROM THE WATERFLOODS

WATER SATURATION	WATER FRACTIONAL FLOW
.077	.62325
.143	.84142
.251	.92449
.372	.96771
.452	.98365
.506	.99054
.528	.99250
.550	.99401
.576	.99546
.611	.99705
.606	.99688
.612	.99707
.640	.99789

FLOWRHTE = 20 cc/hr
TEMPERATURE = 71.0 F
Swi = 0.000

Table **B-6.1**

WATER FRACTIONAL FLOU VS WATER SATURATION
FOR WATER DISPLACING OIL

WATER SATURATION	WHTER FRACTIONAL FLOW
.033	.84970
.084	.91615
.206	.96137
.348	.98225
.449	.99073
.522	.99486
.565	.99665
.601	.99785
.631	.99866
.647	.99900
.655	.99916

FLOWRATE = 100 cc/hr
TEMPERATURE = 65.0 F
Swi = 0.000

Table B-6.2

WATER FRACTIONAL FLOW VS WATER SATURHTION
FOR WATER DISPLACING OIL

WATER SATURATION	WATER FRACTIONAL FLOW
.026	.83953
.074	.91605
,158	.9518%
.267	.97363
.374	.98521
.466	.99131
.564	.99585
.613	.99763
.639	.99839
.676	.99927
.686	.99947

FLOWRATE = 240 cc/hr
TEMPERATURE = 69.0 F
Swi = 0.000

Table **B–6.3**

WATER FRACTIONAL FLOW VS WATER SRTURATION
FOR WATER DISPLACING OIL

WATER SATURATION	WATER FRACTIONAL FLOW
.005	.35720
.044	.82646
.137	.92667
.275	.96859
.425	.98751
.513	.99430
.558	.99671
.574	,99739
.595	.99808
.618	.99872
.635	.99914

FLOWRATE = 400 cc/hr
TEMPERATURE = 68.0 F
Swi = 0.000

Table B-6.4

WATER FRACTIONAL FLOW VS WATER SHTURATION
FOR WATER DISPLACING OIL

WATER SATUKHTION	WATER FRACTIONAL FLOW
.169	.79157
.276	.94073
.369	.97495
.442	.98784
.490	.99267
.521	.99483
.570	.99757
.542	.99634
.549	.99657
.551	.99664
.616	.99827
.643	.99883

FLOWRATE = 406 cc/hr
TEMPERATURE = 68.0 F
Swi = 0.886

Table B-6.5

WATER FRACTIONAL FLOW VS WATER SATURATION
FOR WATER DISPLACING OIL

WATER SATURATION	WATER FRACTIONAL FLOW
.152	.72360
.243	.88082
.360	.94767
.448	.97169
.514	.98228
.559	.98723
.581	.98900
.610	.99073
.662	.99331
.748	.99669
.763	.99719
.784	.99781

FLOWRATE = 20 cc/hr
TEMPERATURE = 150.0 F
Swi = 0.000

Table **B-6.6**

WHTER FRACTIONAL FLOW VS WATER SATURHTION
FOR WATER DISPLACING OIL

WATER SATURATION	WATER FRRCTIONAL FLOW
.114	.65713
.206	.87534
.328	.94771
.427	.97191
.494	.98129
.557	.98700
,599	.98987
.635	.99186
.668	.99337
.690	.99424
,766	.99670
.816	.99813

FLOWRATE = 240 cc/hr
TEMPERATURE = 150.0 F
Swi = 0.000

Table B-6.7

UATER FRACTIONAL FLOW VS WATER SATURATION
FOR UATER DISPLRCING OIL

WATER SATURATION	WATER FRACTIONAL FLOW
.095	.50263
.205	.83829
.328	.93912
.412	.96378
.502	.97860
.590	.98822
.649	.99277
.673	.99416
.704	.99550
.757	.99738
.769	.99774
.802	.99859
.826	.99911

FLOWRATE = 400 cc/hr
TEMPERATURE = 150.0 F
Swi = 0.000

Table B-6.8

WATER FRACTIONAL FLOW VS WATER SATURATION
FOR WATER DISPLACING OIL

WATER SATURATION	WATER FRACTIONAL FLOW
.217	.91579
.227	.93113
.259	.94756
.310	.96237
.363	,97284
.420	.98071
.471	.98597
.501	.98832
.547	.99108
.635	.99531
.703	.99771
.728	.99832
.743	.99861
.762	.99890
.778	.99909
.792	.99924
.831	.99958
.866	.99986
.866	.99985

FLOWRATE = 400 cc/hr
TEMPERATURE = 70.0 F
Swi = *0.000*

Table **B-6.9**

WATER FRACTIONAL FLOW VS WATER SATURATION
FOR WATER DISPLACING OIL

WATER SATURATION	WATER FRACTIONAL FLOW
.221	.87158
.219	.86848
.290	.91749
.370	.95031
.418	.96299
.469	.97284
.517	.97983
.582	.98699
.619	.99016
.650	.99226
.690	.99436
.755	.99683
.800	.99809
.840	.99894
.873	.99951
.896	.99984

FLOWRATE = 400 cc/hr
TEMPERATURE = 122.0 F
Swi = 0.000

Table **B-6.10**

WATER FRACTIONHL FLOW VS WHTER SATURATION
FOR WATER DISPLACING OIL

ATER SATURATION	WATER FRACTIONAL FLOW
.192	.54812
.239	.75190
.308	.88581
.319	.89498
.395	.93403
.452	.95247
.503	.96400
.541	.97079
.595	.97863
.656	,98553
.696	.98933
.728	.99178
.760	.99374
.793	.99540
.836	.99730
.890	.99918
.901	.99948
.919	.99990

FLOWRATE = 400 cc/hr
TEMPERATURE = 186.0 F
Swi = 0.000

Table B-6.11

WATER FRACTIONAL FLOW VS WATER SATURATION
FOR WATER DISPLACING OIL

WATER SATURATION	WATER FRACTIONAL FLOW
.326	.83940
.367	.93642
.431	.97138
.509	.98634
.582	.99302
.643	.99619
.681	.99746
.712	.99824
.749	.99898
.762	.99920
.754	.99908
.777	.99937
.791	.99953
.797	.99959
.813	.99972
.806	.99967
.812	.99971

FLOWRHTE = 400 cc/hr
TEMPERATURE = 70.0 F
Swi = ,064

Table **B-6.12**

WATER FRACTIONAL FLOW VS WATER SATURHTION
FOR WATER DISPLACING OIL

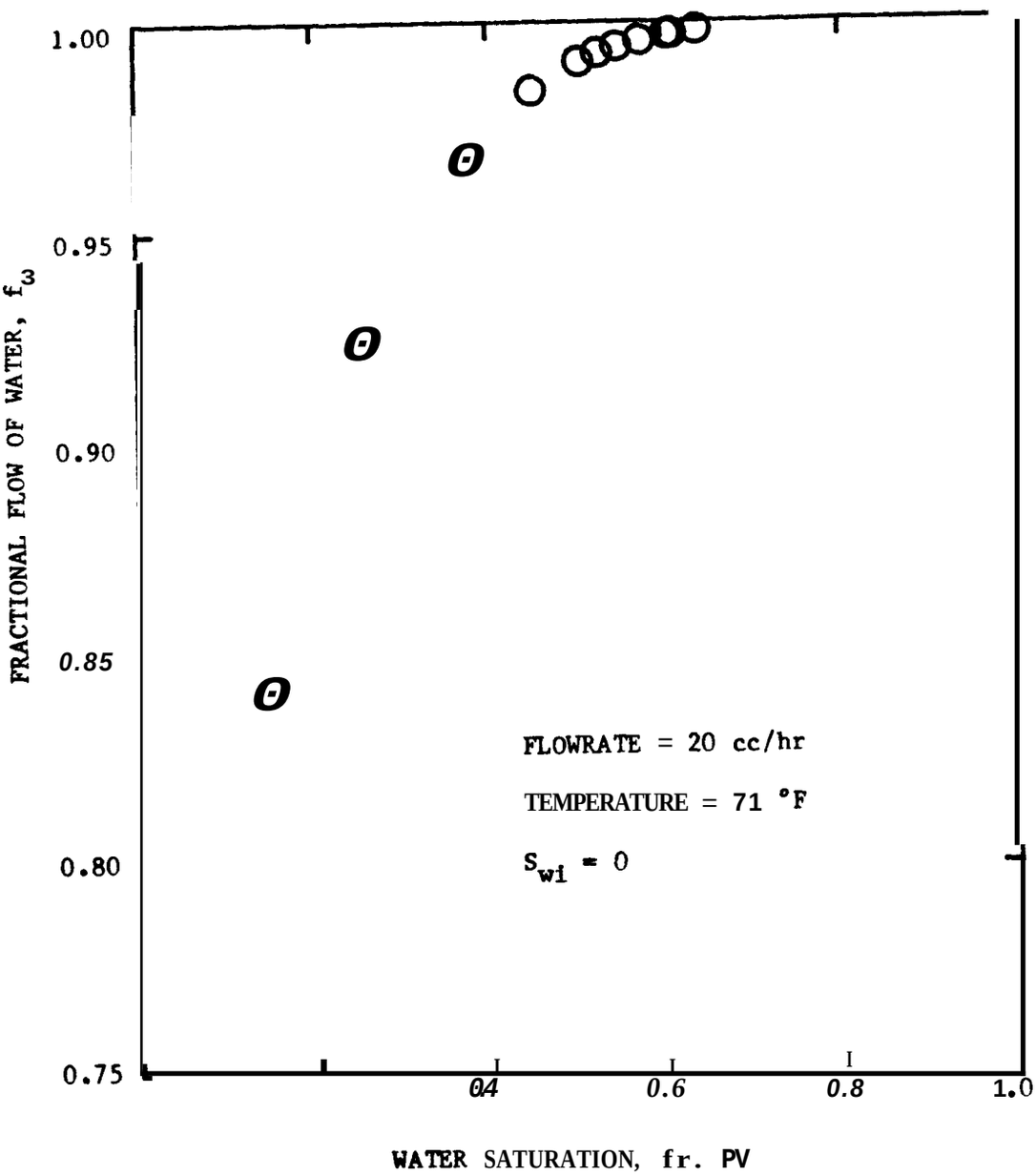

Fig. B-6.1 FRACTIONAL FLOW CURVE FOR WATERFLOOD

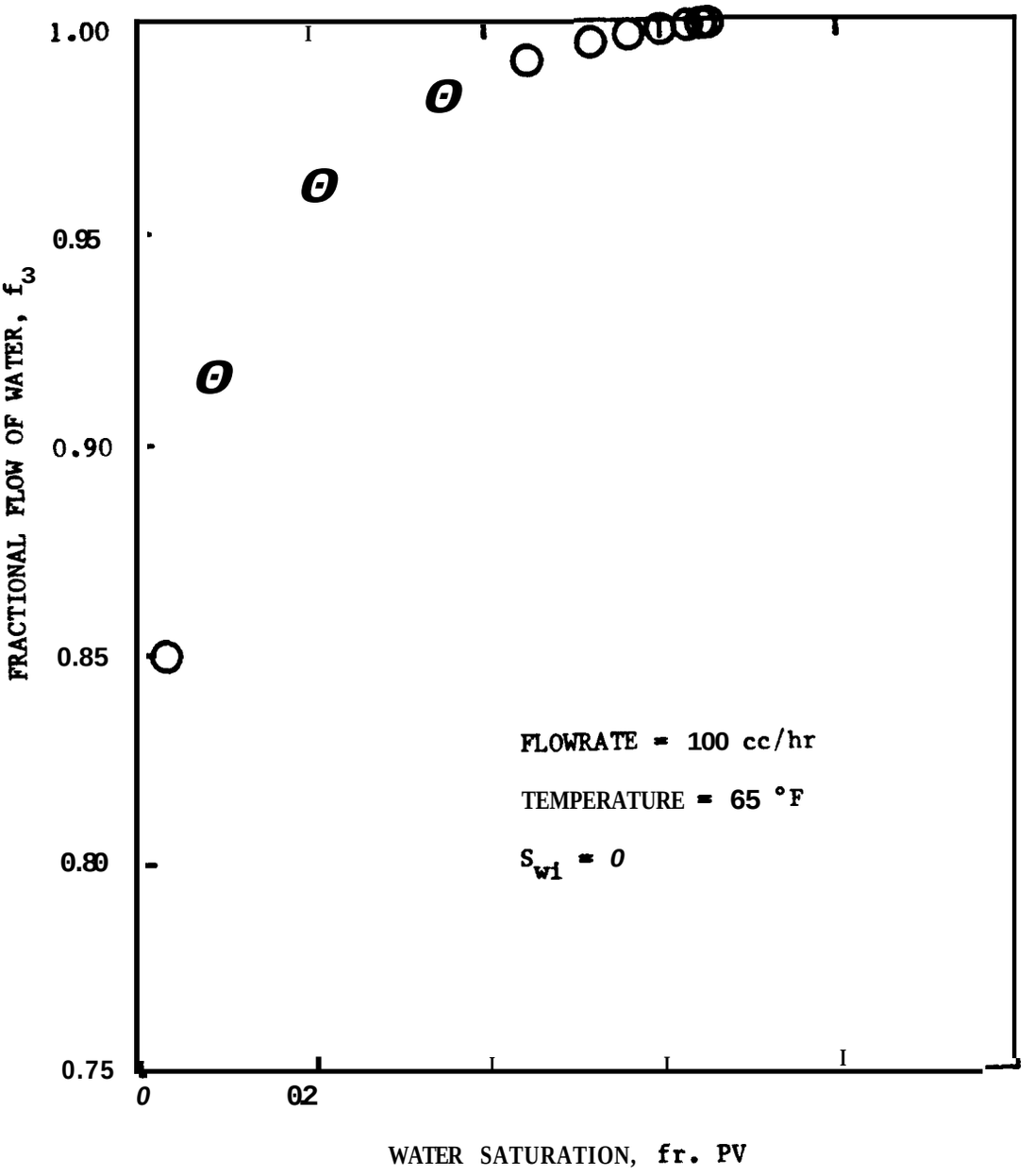

Fig. B-6.2 FRACTIONAL FLOW UJRVE FOR WATERFLOOD

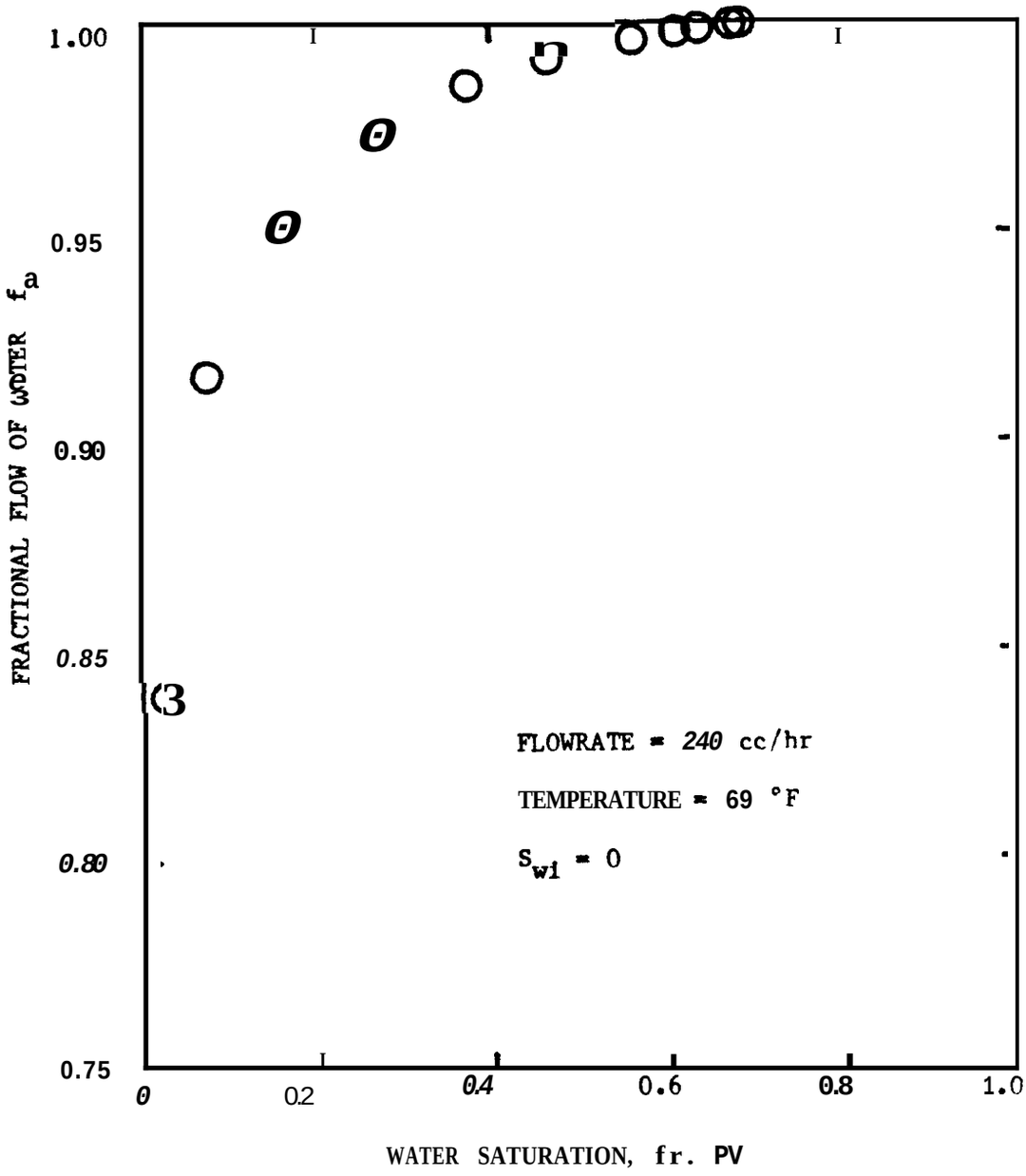

Fig. B-6.3 FRACTIONAL FLOW CURVE FOR WATERFLOOD

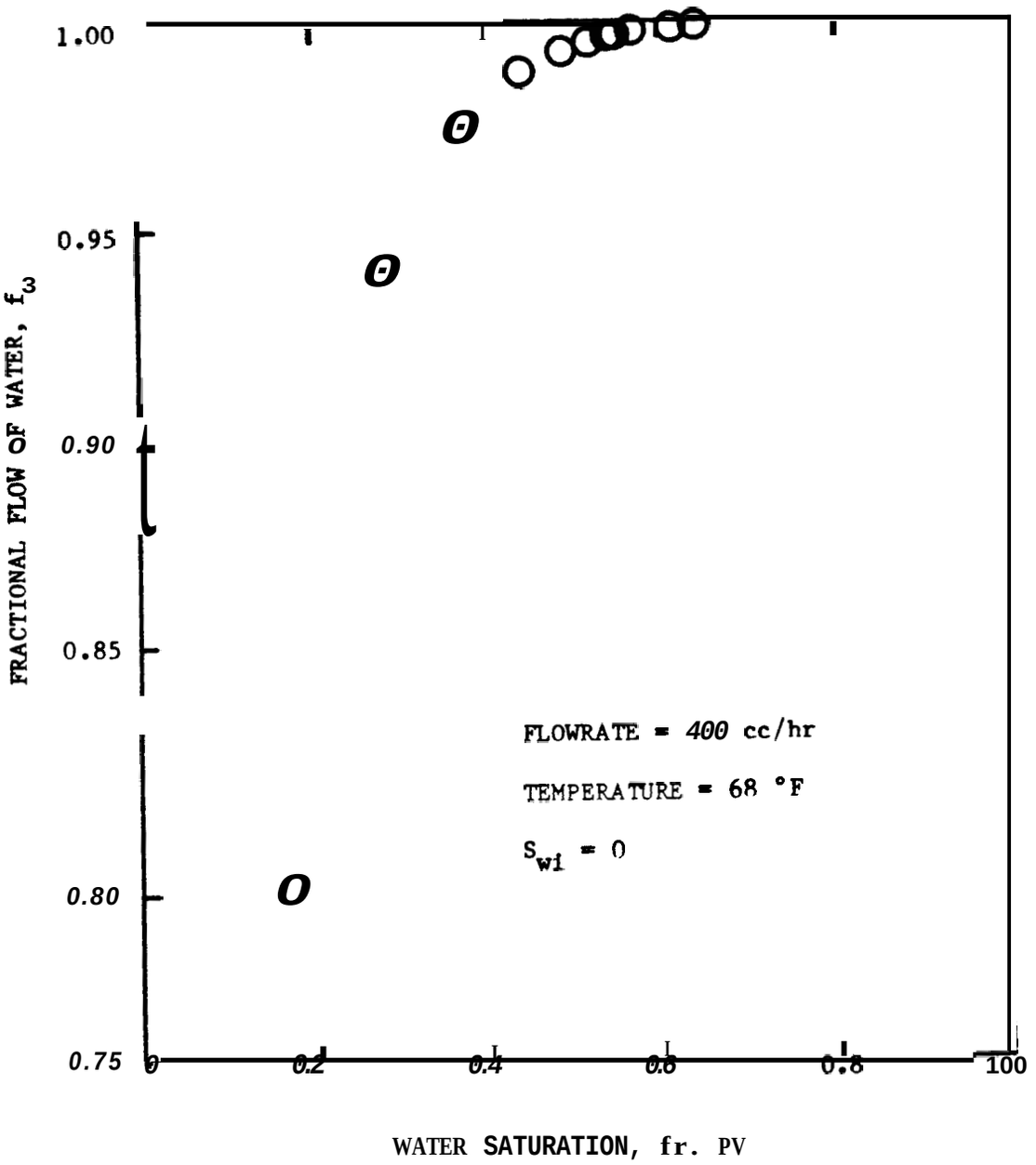

Fig. B-6.4 FRACTIONAL FLOW CURVE FOR WATERFLOOD

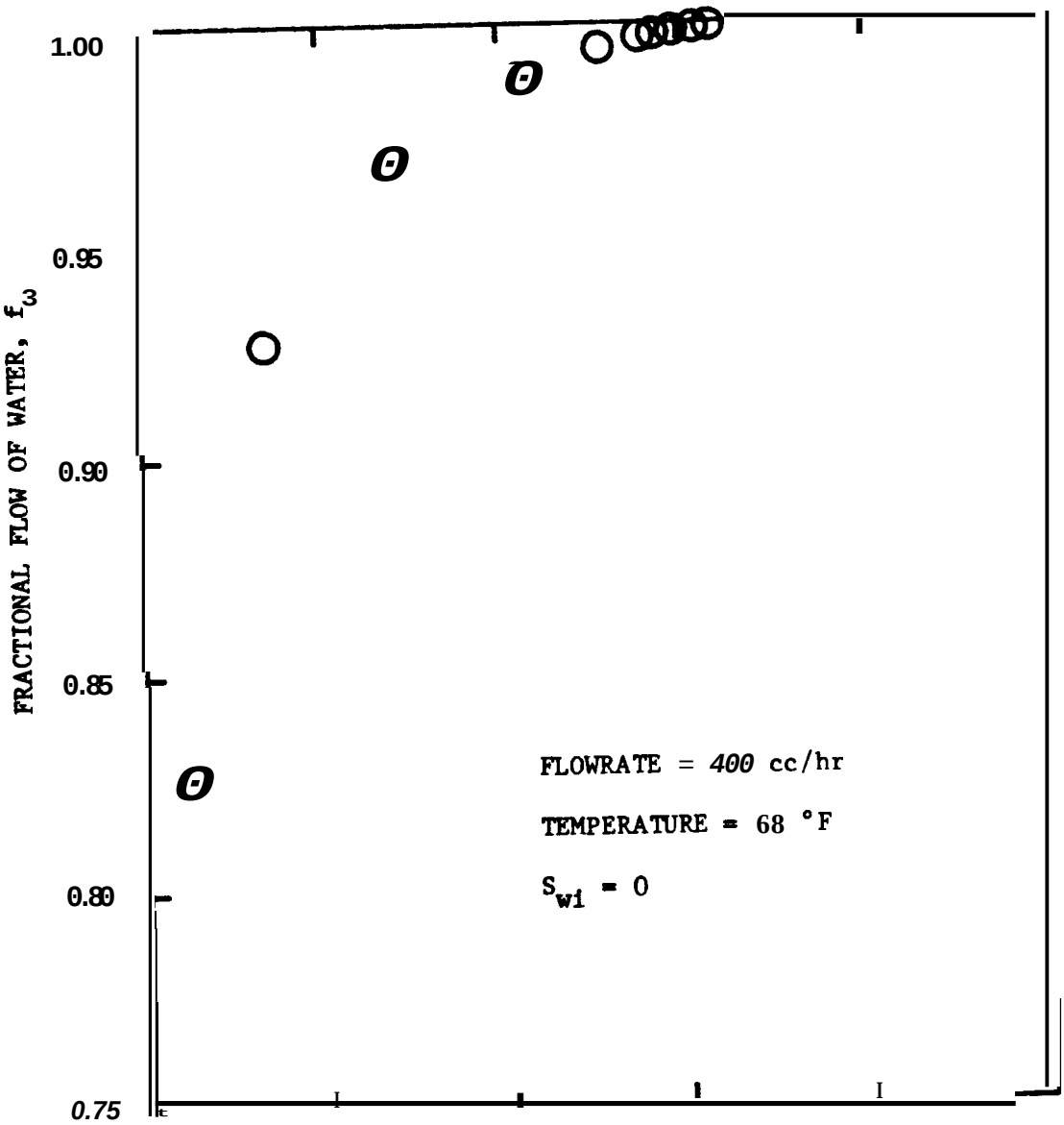
1.00
0.95
0.90
0.85
0.80
0.75
FRACTIONAL FLOW OF WATER, f_3
FLOWRATE = 400 cc/hr
TEMPERATURE = 68 °F
S_{wi} = 0

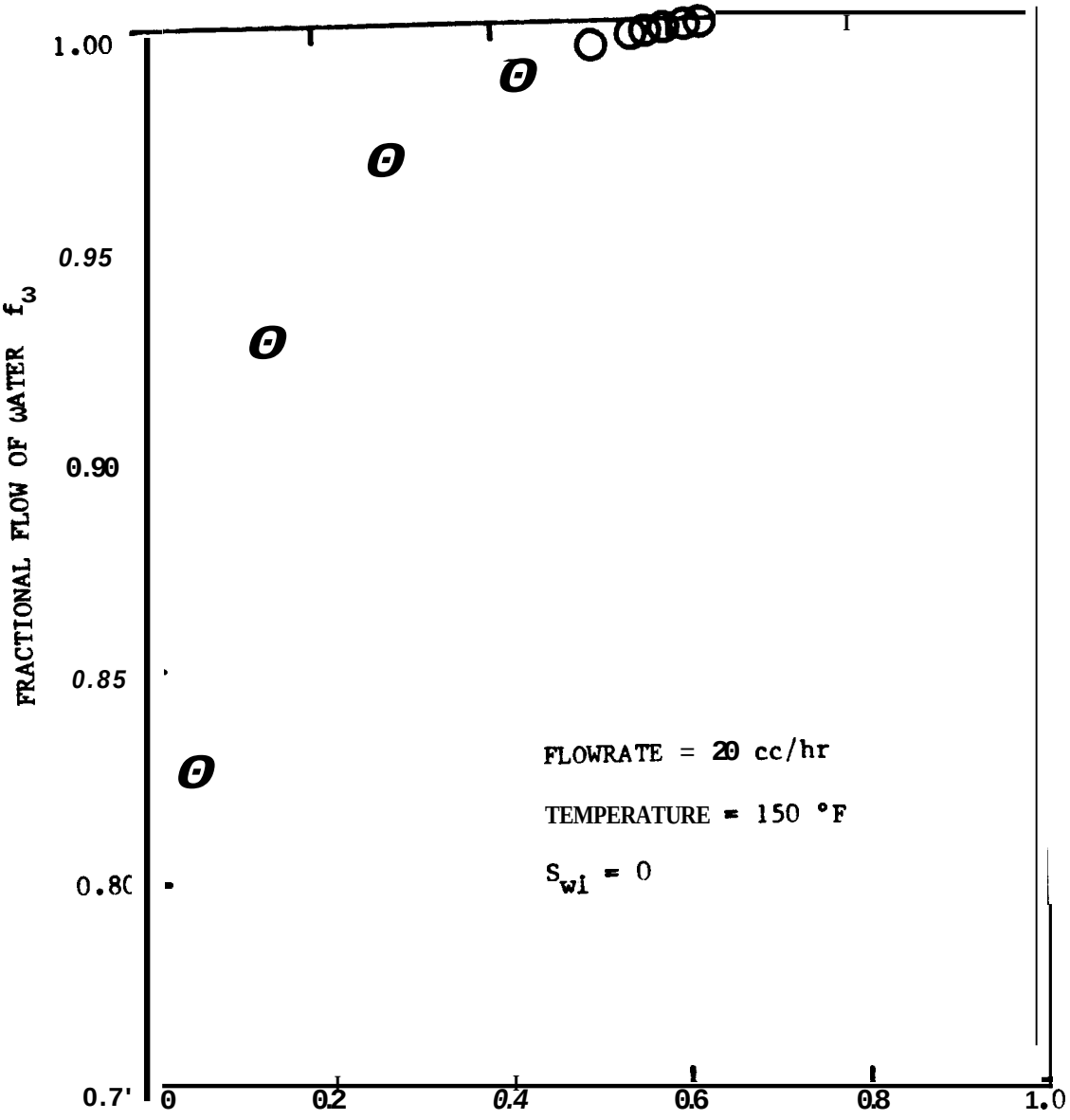
1.00
0.95
0.90
0.85
0.80
0.7'
FRACTIONAL FLOW OF WATER f_3
0
0.2
0.4
0.6
0.8
1.0
FLOWRATE = 20 cc/hr
TEMPERATURE = 150 °F
S_{wi} = 0

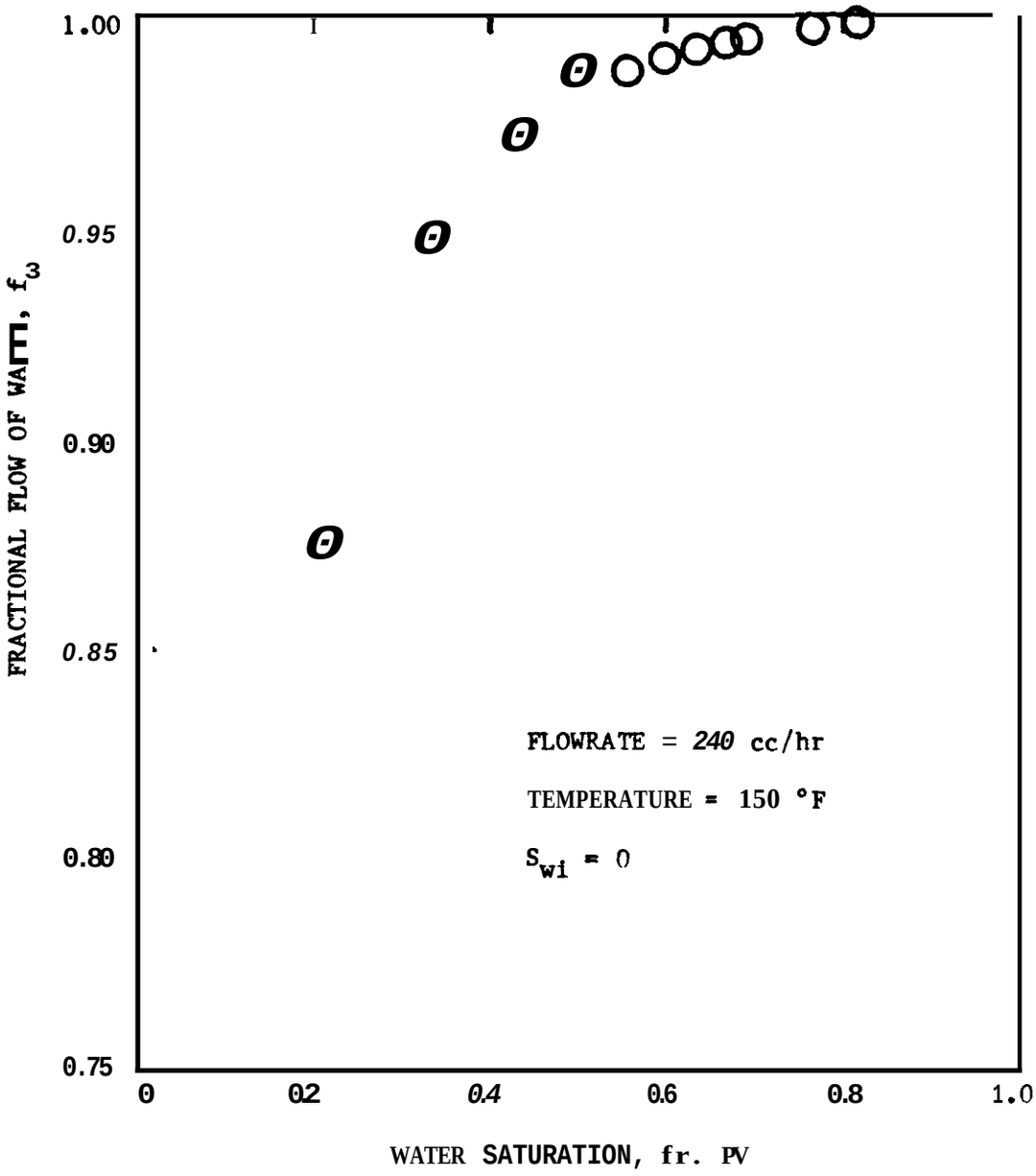

Fig. B-6.7 FRACTIONAL FLOW UJRVE FOR WATERFLOOD

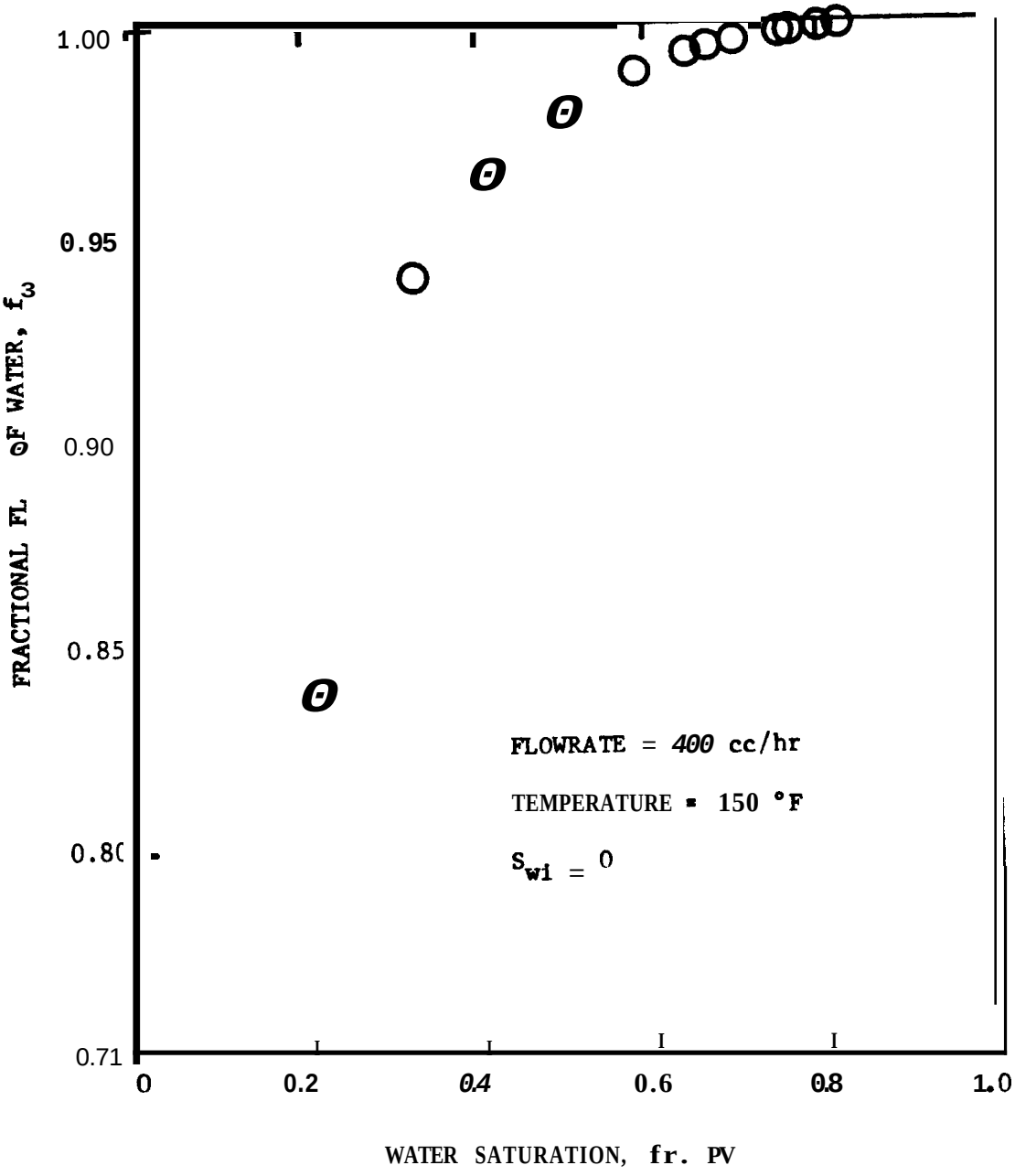

Fig. B-6.8 FRACTIONAL FLOW CURVE FOR WATERFLOOD

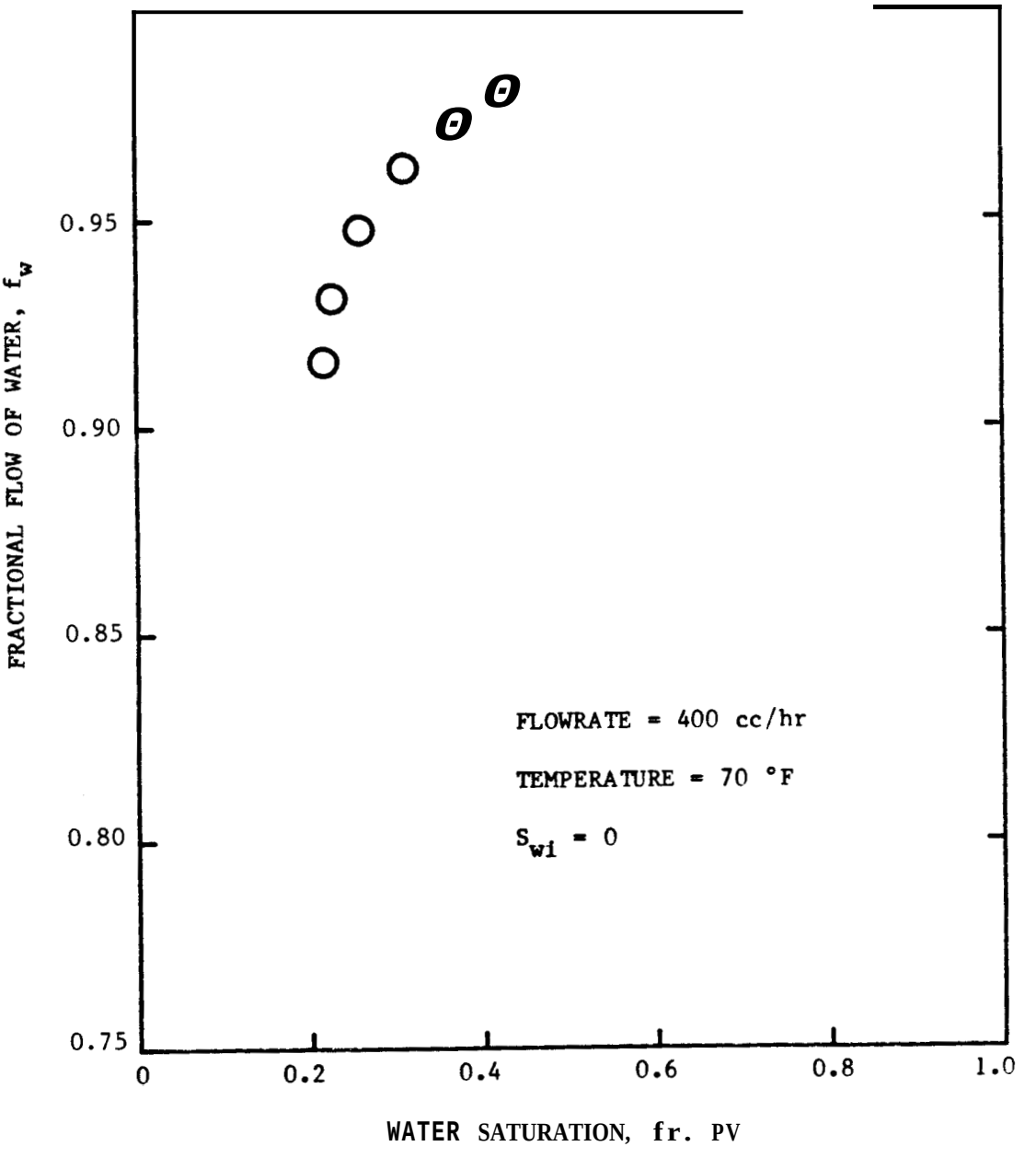

Fig. B-6.9 FRACTIONAL FLOW CURVE FOR WATERFLOOD

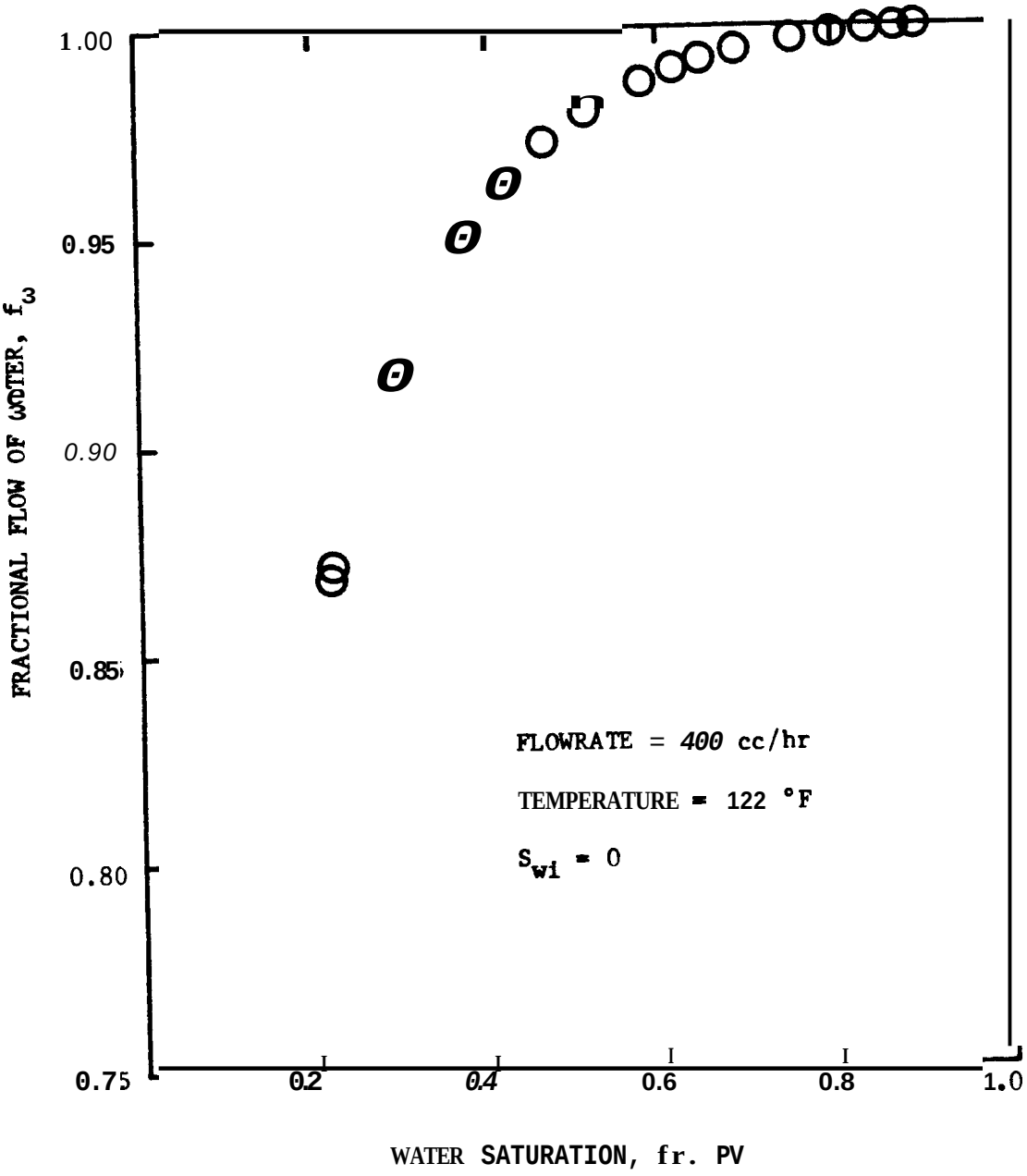

Fig. B-6.10 FRACTIONAL FLOW CURVE FOR WATERFLOOD

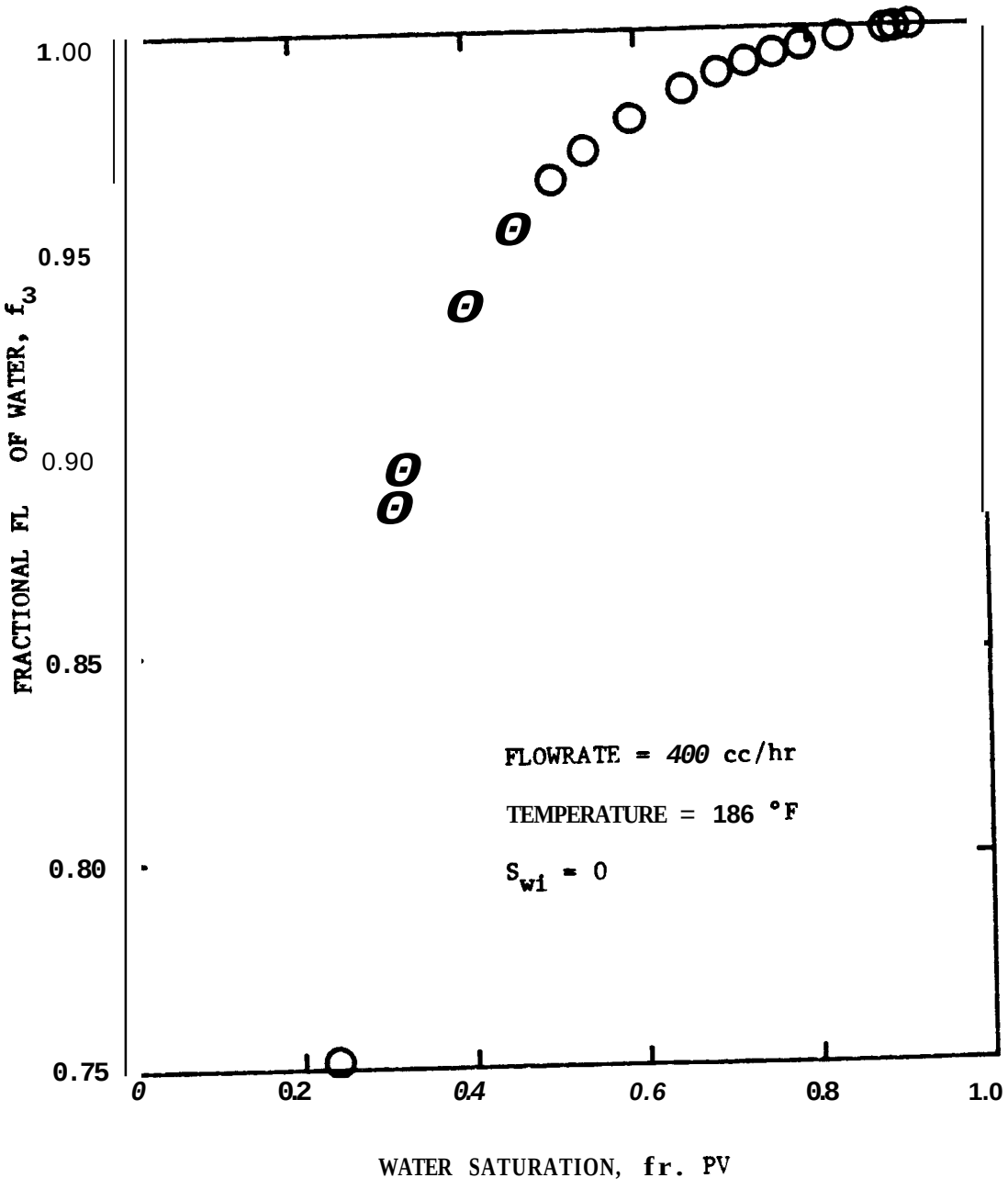

Fig. B-6.11 FRACTIONAL FLOW CURVE FOR WATERFLOOD

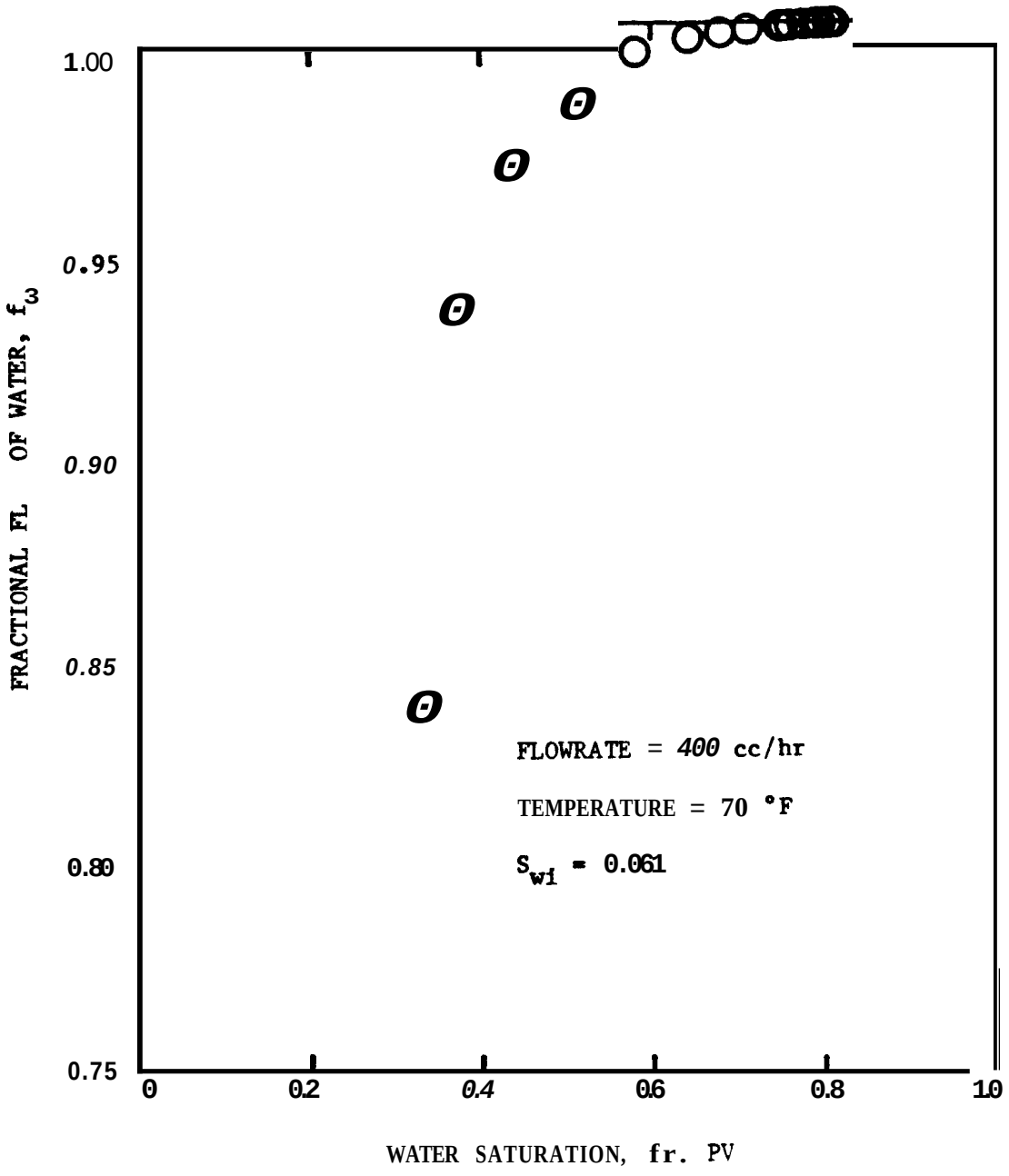

Fig. B-6.12 FRACTIONAL FLOW CURVE FOR WATERFLOOD

APPENDIX B-7

TABLES OF DATA FROM EXPERIMENTS STUDYING CHANGES IN IRREDUCIBLE WATER SATURATIONS

TEMPERRTURE (F)	Swi (fr. PV)
72	.061
80	,066
91	.070
108	.073
134	.076
182	.080

Table B-7.1

IRREDUCIBLE WATER SATURATION VS TEMPERATURE (FLOWRATE ≈ 400 cc/hr)

FLOWRATE (cc/hr)	Swi (fr. PV)
5	.105
5	.107
10	.090
20	.089
20	.091
40	.081
100	.074
200	.070
400	.064
400	.062
400	.063
800	.060

Table **B-7.2**

IRREDUCIBLE WATER SATURATION **VS** FLOWRATE (TEMPERATURE = 70°F)

VISCOUS FORCE (cc.cp/hr)	Swi (fr. PV)	MODE OF CHANGE
1100	.107	RATE
1500	.105	RATE
2900	.090	RATE
4488	.089	RATE
4518	.090	RATE
12898	.080	RATE
12588	.083	RATE
22028	.074	RATE
22518	.080	RATE
60590	.070	RATE
89578	.062	RATE
89570	.064	RATE
89480	.063	RATE
176386	.060	RATE
1648	.104	TEMPERATURE
5080	.085	TEMPERATURE
13060	.083	TEMPERATURE
27358	.078	TEMPERATURE
41280	.075	TEMPERATURE
60188	.070	TEMPERATURE
80818	.066	TEMPERRTURE
8708	.085	FLUID
48798	.073	FLUID

Table B-7.3

IRREDUCIBLE WATER SATURATION VS VISCOUS FORCE (cc.cp/hr)

APPENDIX B-8

TABLES OF DATA FROM EXPERIMENTS STUDYING VISCOUS FINGERING

Table B-8.1

OIL RECOVERY AT WATER BREAKTHROUGH VS FLOWRATE (TEMPERATURE = 70F)
(EXIT TUBING VOLUME = 2.4 cc)

FLOWRATE (cc/hr)	BREAKTHROUGH REC. (fr.PV)
30	.372
60	.398
120	.382
160	.333
280	.296
400	.248
800	.246
1120	.257

Table B-8.2

OIL RECOVERY AT WHTEP BREHKTHROUGH VS FLOWRHTE (TEMPERATURE = 70F)
(EXIT TUBING VOLUME = 10.2 cc)

FLOWRHTE (cc/hr)	BREAKTHROUGH REC. tfr·PV)
30	.301
60	.328
100	.323
120	.258
160	.204
240	.146
480	.098
800	.094
1120	.085

APPENDIX B-9

TABLES OF DATA FROM EXPERIMENTS STUDYING RESIDUAL OIL SATURATION

Table B-9.1

RESIDUAL OIL SATURATIONS AT DIFFERENT RATES FOR TWO TEMPERATURE LEVELS

FLOWRATE (cc/hr)	Sor (fr. PV)
20	.287
100	,298
240	.288
400	.313

FLOWRATE (cc/hr)	Sor (fr. PV)
20	.137
240	.128
400	.125

Table B-9.2

RESIDUAL OIL SATURATIONS AT DIFFERENT TEMPERATURES
FOR RUNS TERMINATED AT 99+ fw AND FOR COMPLETE FLOODS

CUTOFF AT fw = 99+

TEMPERATURE (F)	Sor (fr. PV)
70	.313
150	.137
250	.092

COMPLETE RUNS

TEMPERATURE (F)	Sor (fr. PV)
70	.113
73	.106
122	.090
150	.087
186	.075

APPENDIX C-1

DETAILED SCHEMATIC DIAGRAM OF THE EXPERIMENTAL EQUIPMENT

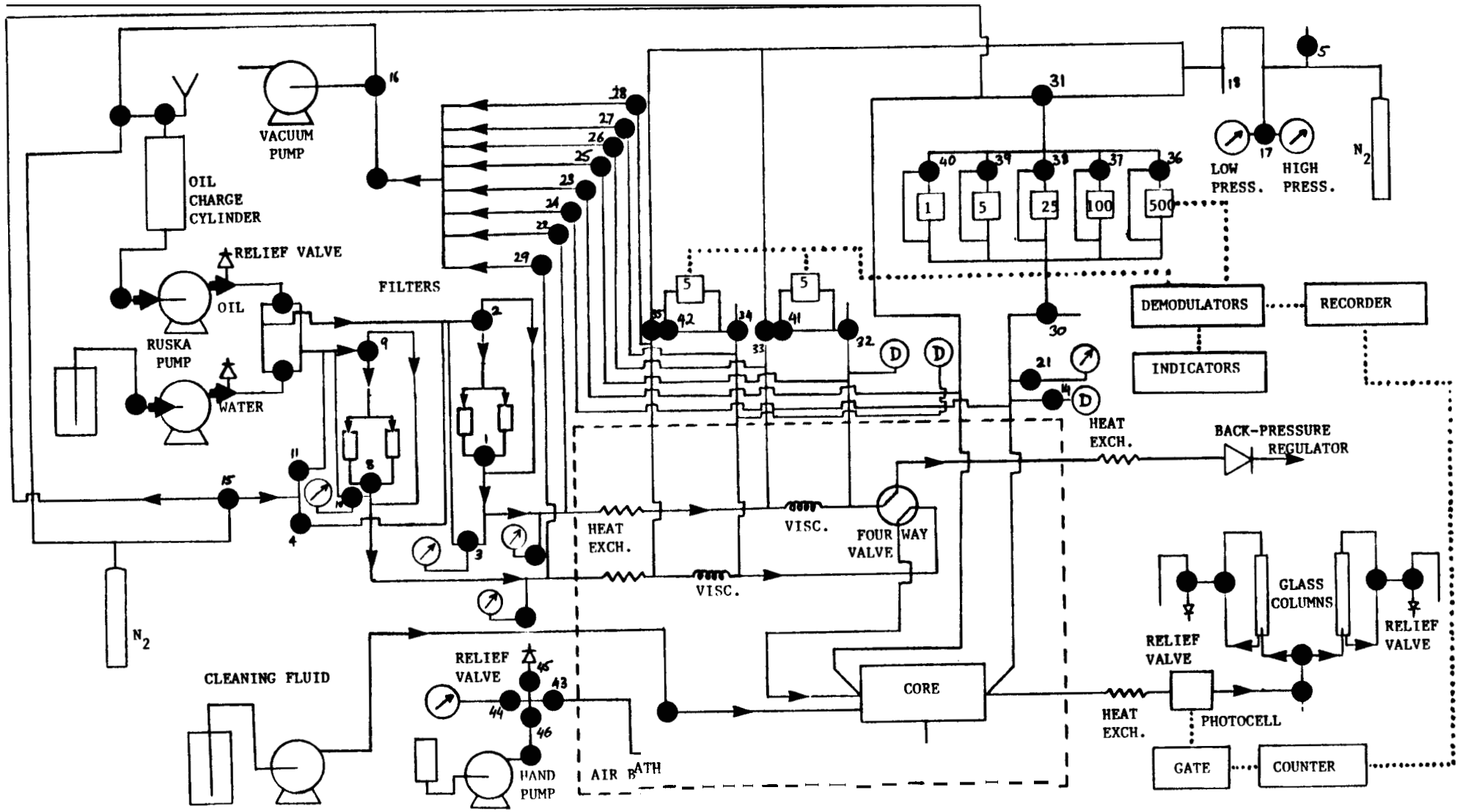

Fig. C.1.1. DETAILED SCHEMATIC OF RELATIVE PERMEAMETER

Fig. C-1.2 KEY OF VALVE PANELS (FOR USE WITH Fig. C-1.1)

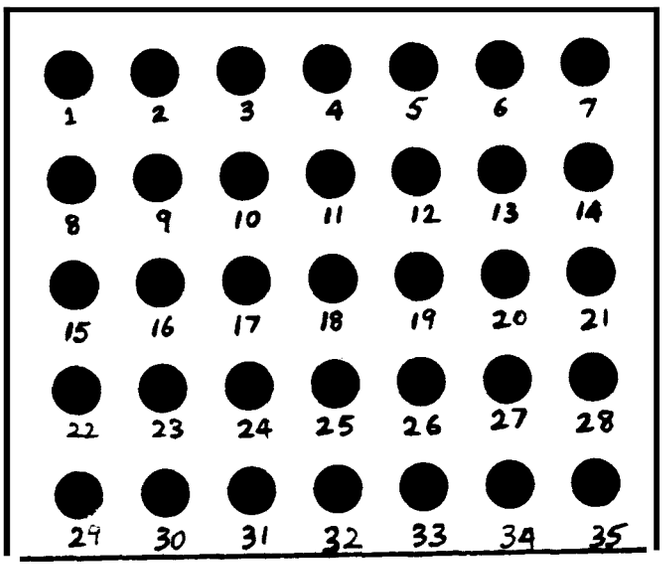

MAIN PANEL

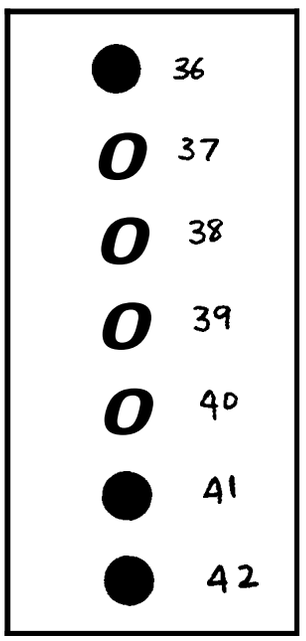

TRANSDUCER PANEL

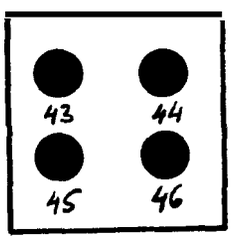

CONFINING PRESSURE PANEL

APPENDIX C-2

SCHEMATIC DIAGRAMS OF COMPONENTS OF THE CORE HOLDER

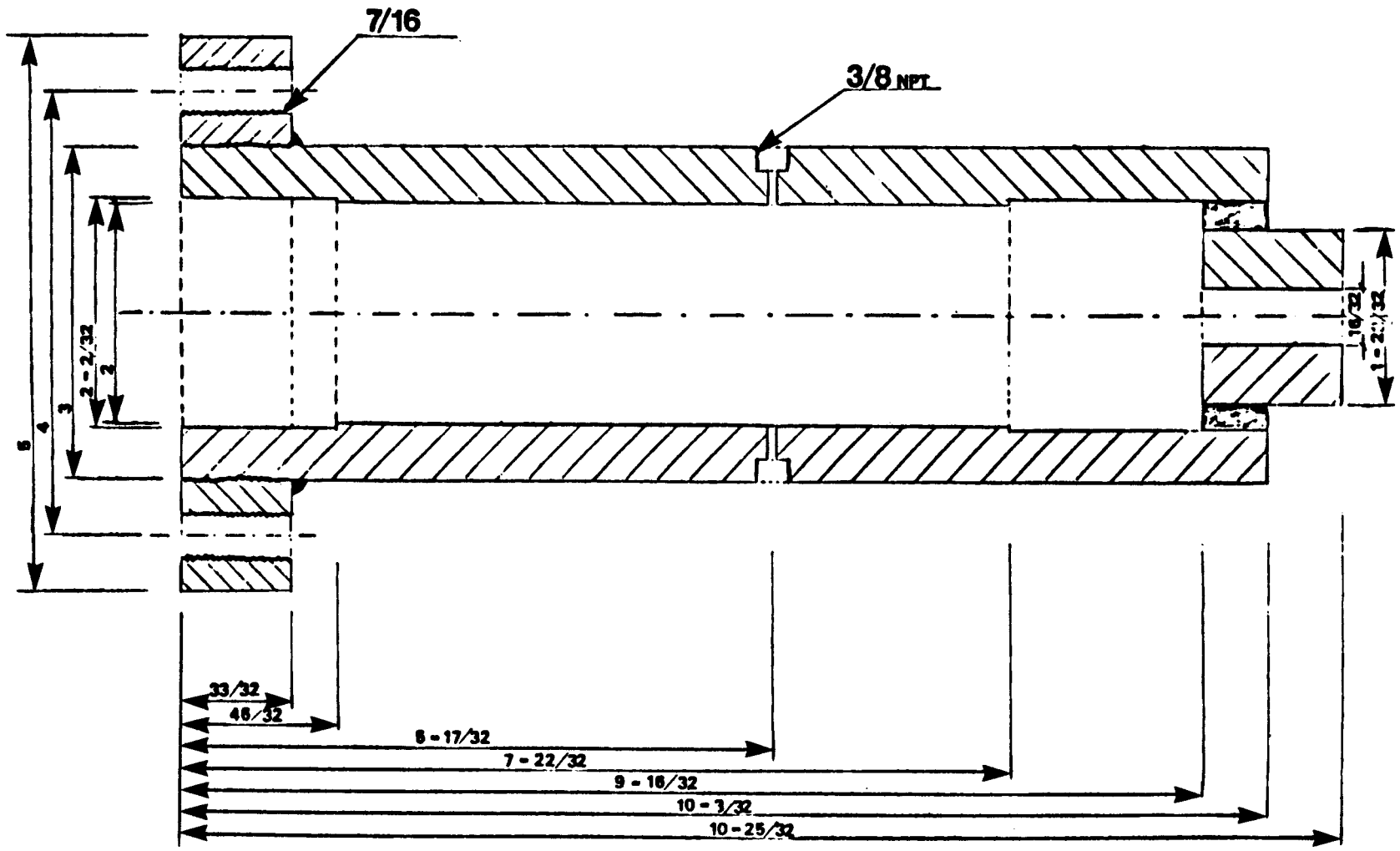

FIG. C-2.1 OUTER SHELL OF CORE HOLDER

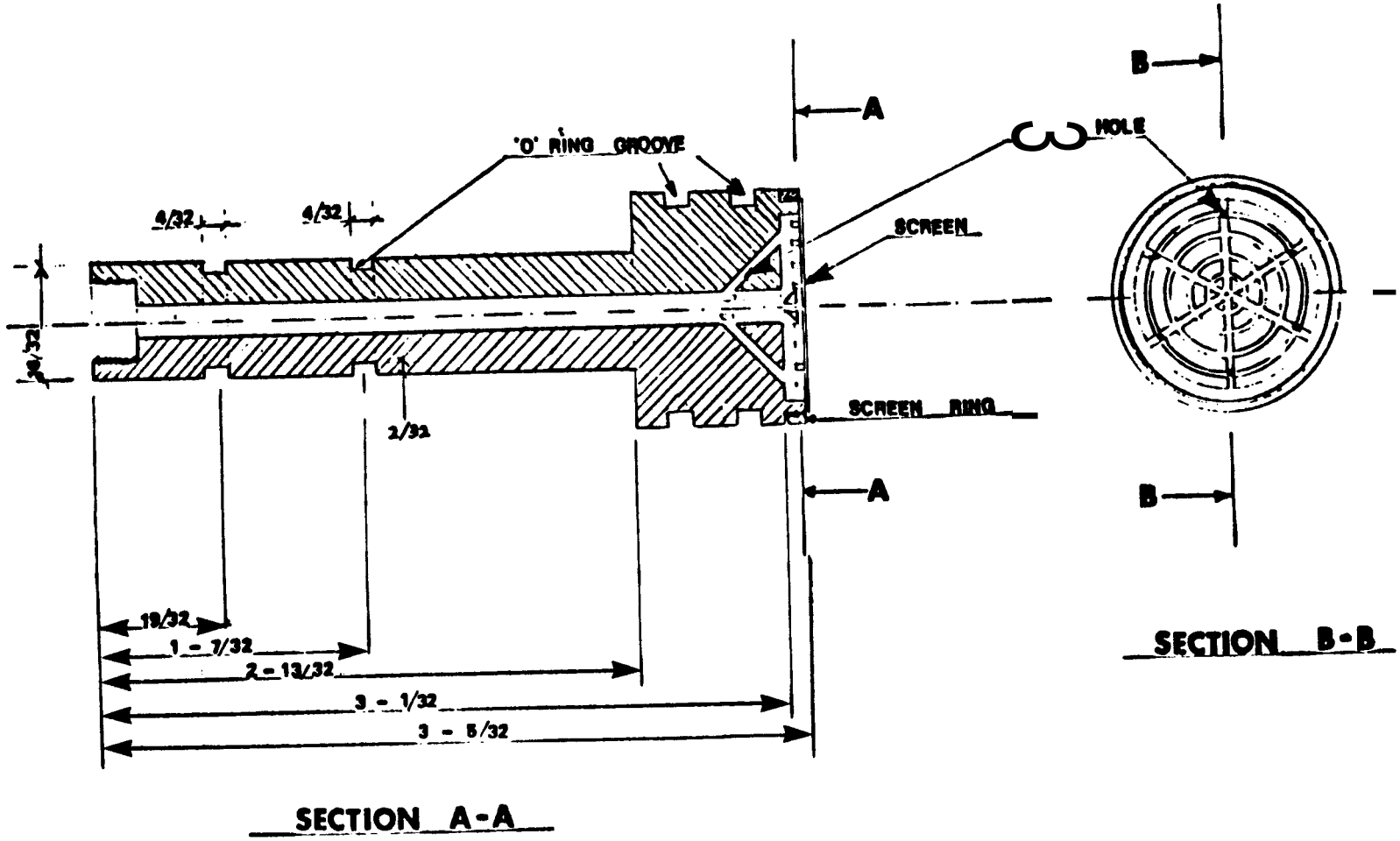

FIG. C-2.Z OUTLET END PLUG OF CORE HOLDER

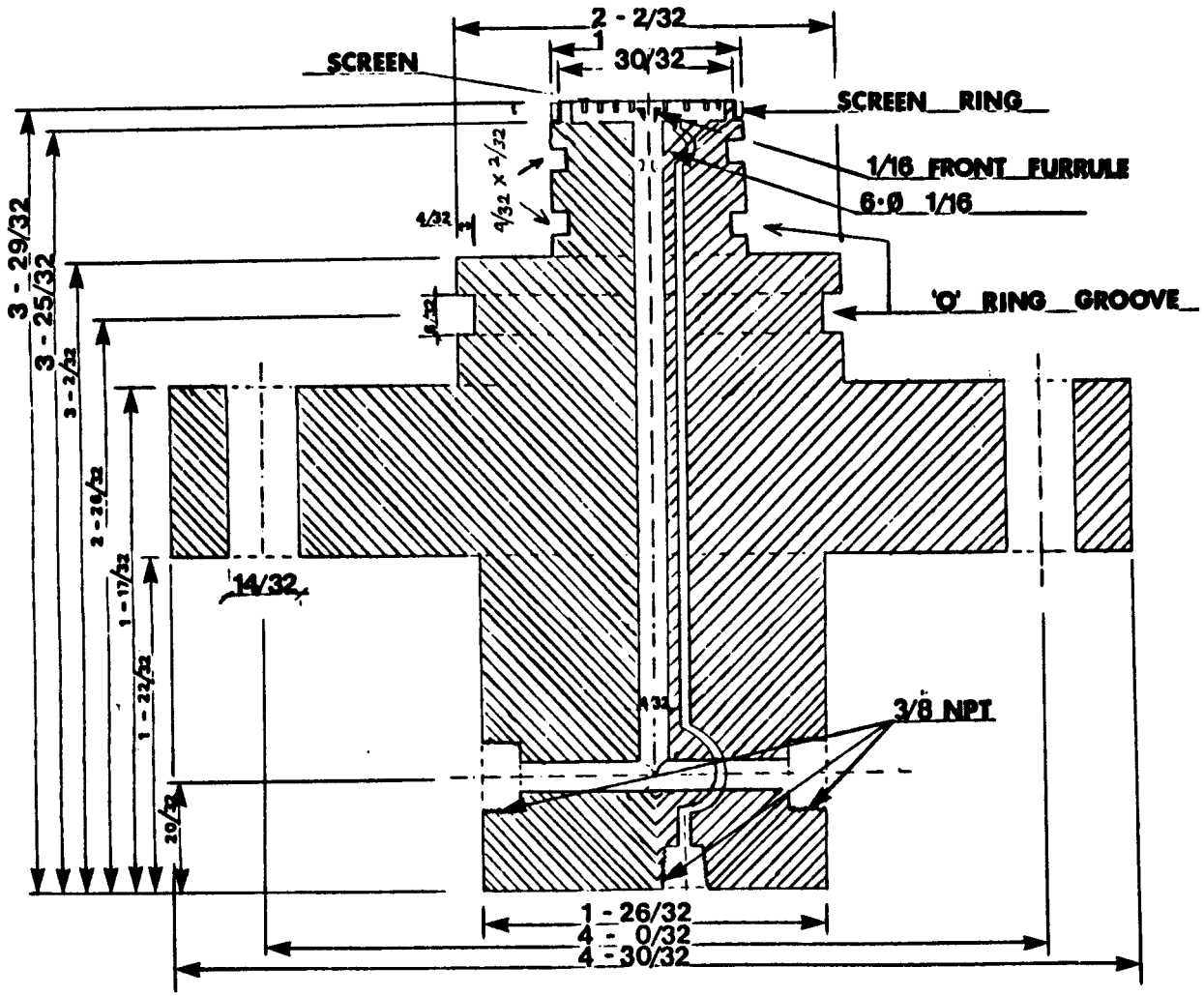

FIG. C-2.3 INLET END PLUG OF CORE HOLDER

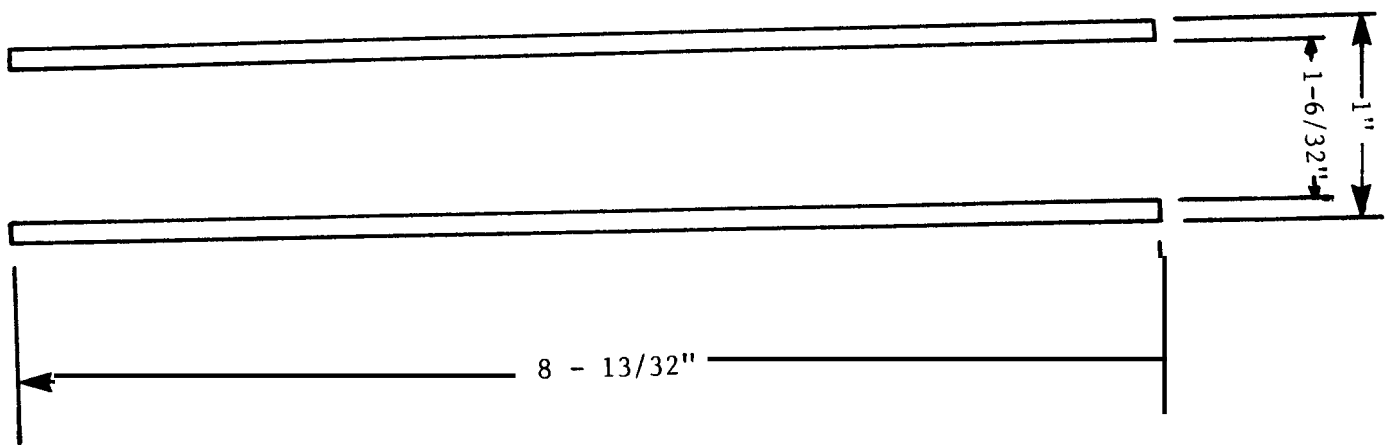

FIG. C-2.4 STAINLESS STEEL SLEEVE OF CORE HOLDER

APPENDIX C-3

SCHEMATIC DIAGRAM OF THE PHOTO-CELL ASSEMBLY

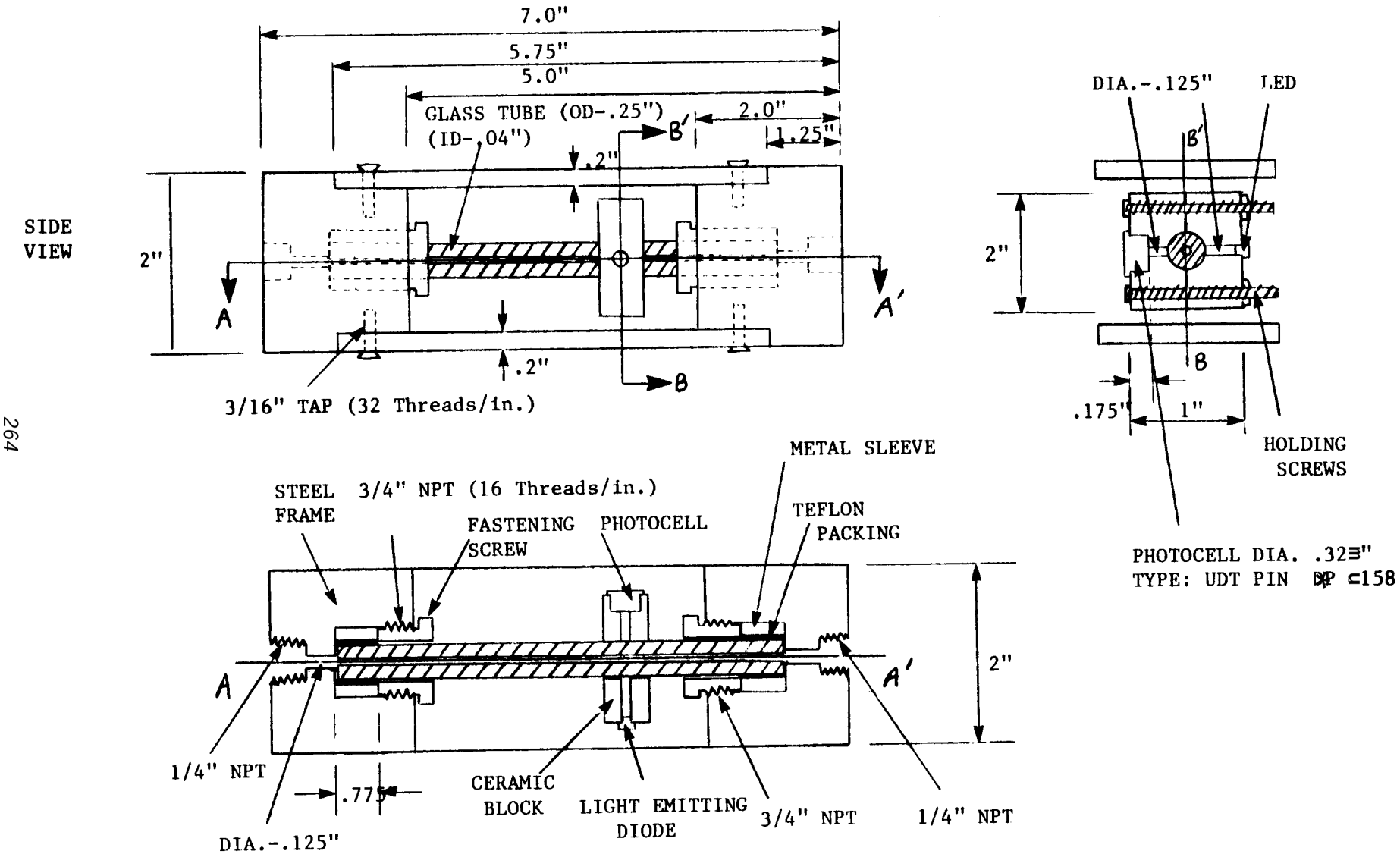

Fig. C-3.1 SCHEMATIC OF PHOTOELECTRIC CELL ASSEMBLY

APPENDIX C-4

WIRING DIAGRAM OF THE ELECTRONIC GATE

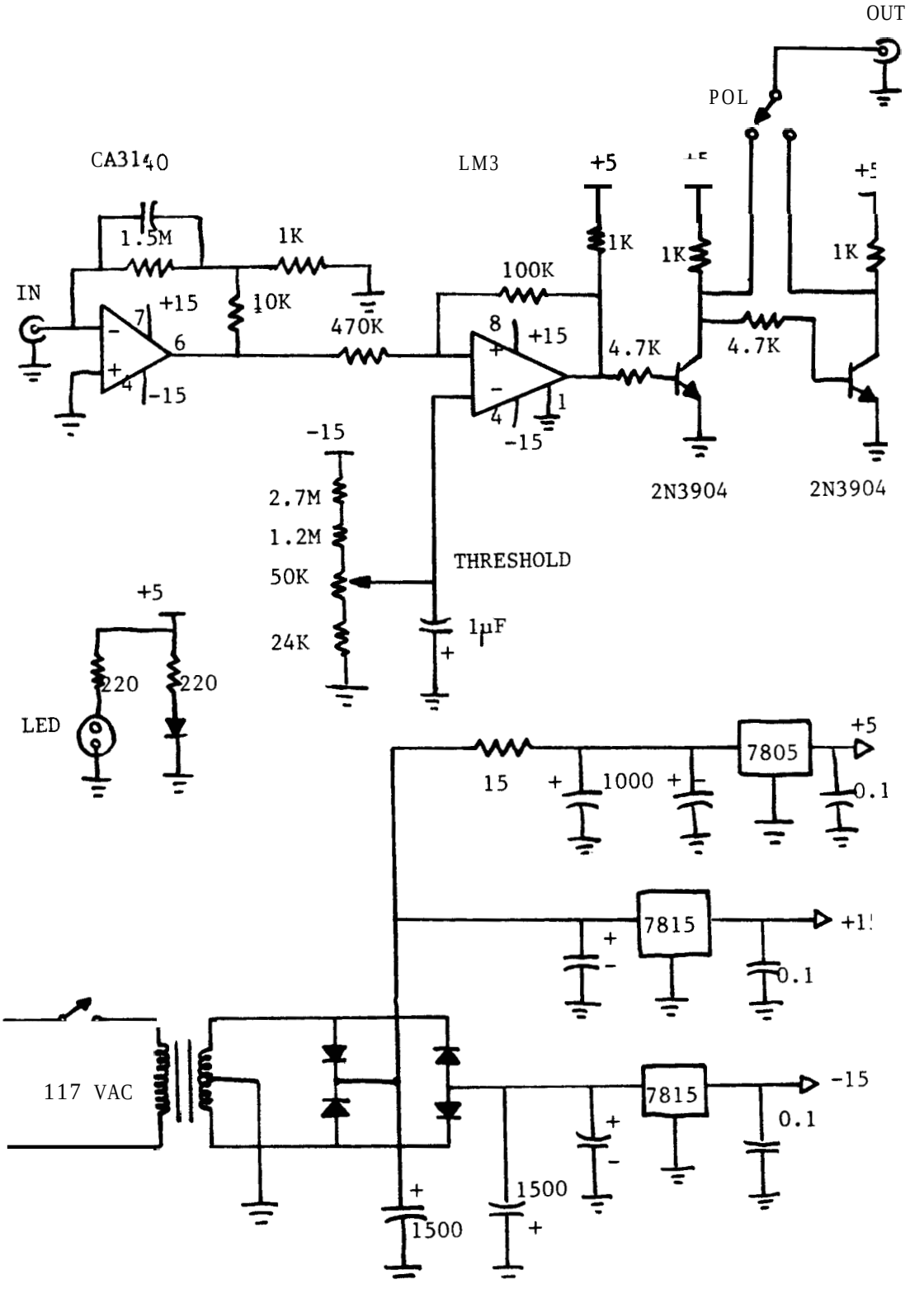

Fig. C-4.1 PHOTODIODE BOARD USED TO COMPARE VOLTAGE FROM PHOTOCELL AGAINST SET VOLTAGE AND ACTIVATE FREQUENCY COUNTER

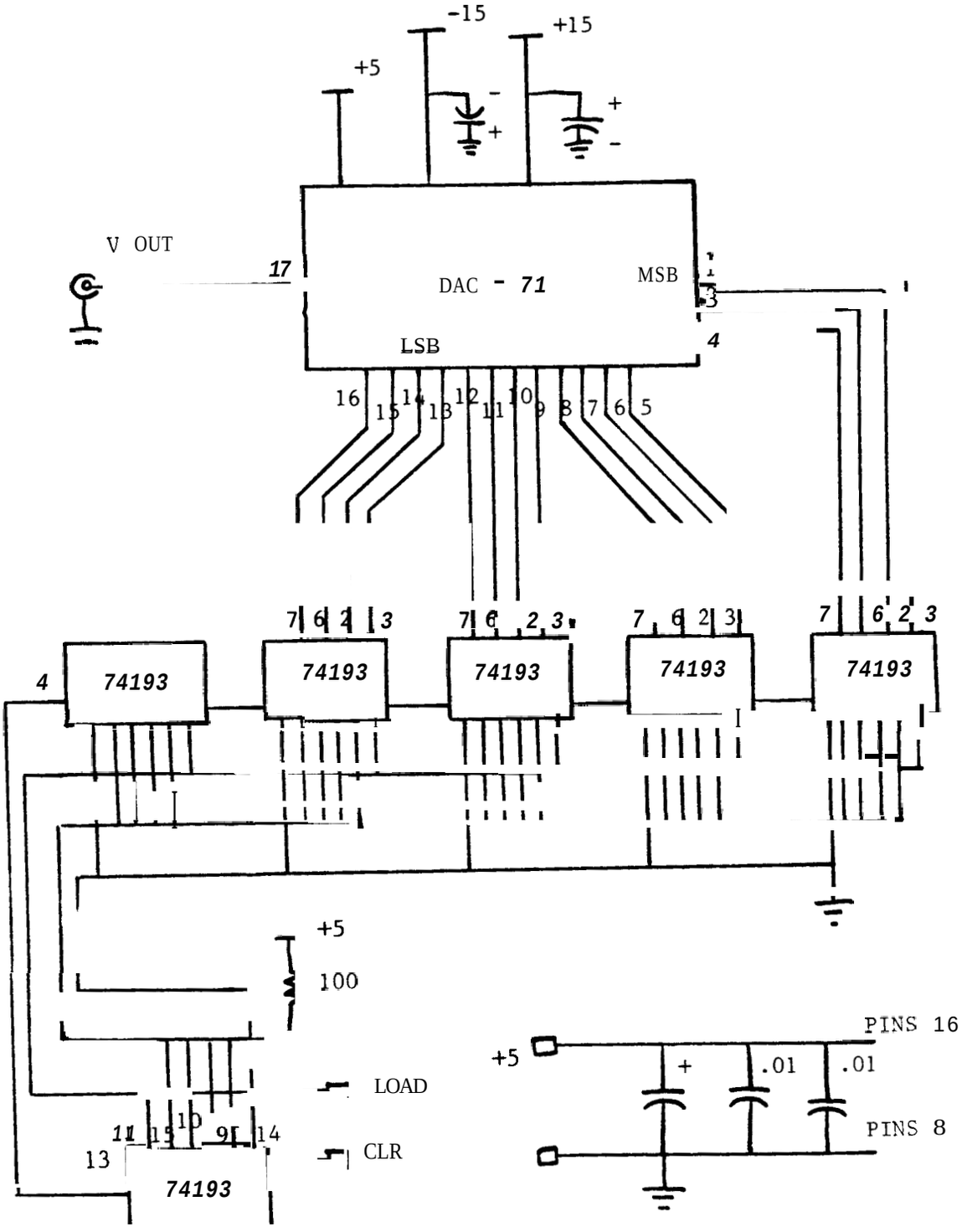

Fig. C-4.2 DIGITAL TO ANALOG BOARD USED TO CONVERT DIGITAL SIGNAL FROM FREQUENCY COUNTER TO ANALOG SIGNAL FOR CHART RECORDER

APPENDIX C-5

SCHEMATIC DIAGRAM OF CAPACITANCE PROBE

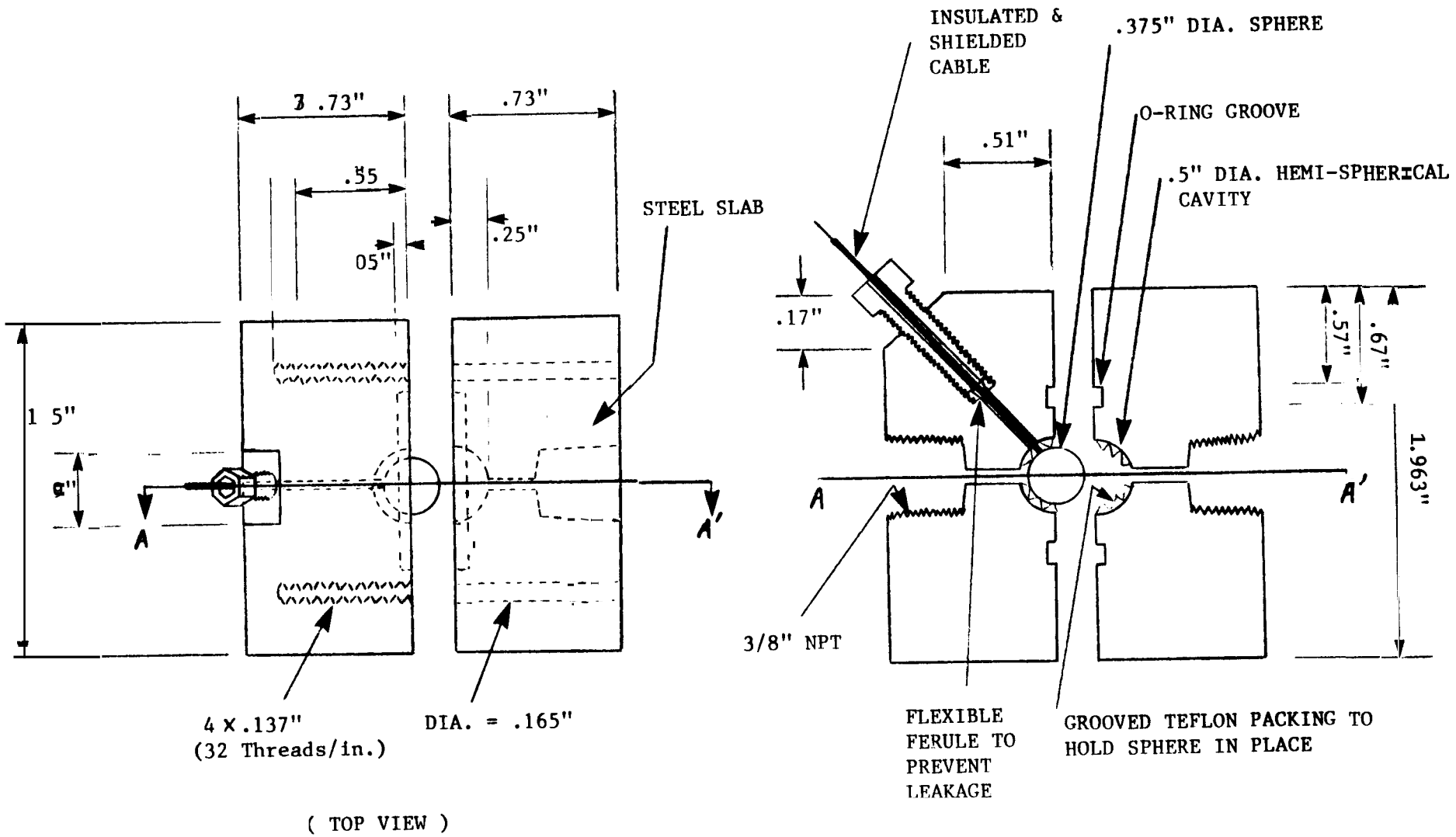

Fig C-5 1 SCHEMATIC OF SPHERICAL CAPACITANCE PROBE